Unclassified
SECURITY CLASSIFICATION OF THIS PAGE

REPORT DOCUMENTATION PAGE

Approved
OMB No. 0704-0188

AD-A229 964

1a. REPORT SECURITY CLASSIFICATION: Unclassified	1b.
2a. SECURITY CLASSIFICATION AUTHORITY: N/A since unclassified	3. AVAILABILITY OF REPORT: Approved for public release; distribution is unlimited
2b. DECLASSIFICATION / DOWNGRADING SCHEDULE: N/A since unclassified	
4. PERFORMING ORGANIZATION REPORT NUMBER(S): PU/CEOR/SM - 90 -9	5. MONITORING ORGANIZATION REPORT NUMBER(S): AFOSR-TR- 90 1182
6a. NAME OF PERFORMING ORGANIZATION: Princeton University	6b. OFFICE SYMBOL (If applicable):
6c. ADDRESS (City, State, and ZIP Code): Dept. of Civil Eng. & Oper. Research, Princeton University, Princeton, NJ 08544	7a. NAME OF MONITORING ORGANIZATION: Air Force Office of Scientific Res.
	7b. ADDRESS (City, State, and ZIP Code): Building 410, Bolling AFB, D.C. 20332-6448
8a. NAME OF FUNDING / SPONSORING ORGANIZATION: AFOSR/NA	8b. OFFICE SYMBOL (If applicable): NA
8c. ADDRESS (City, State, and ZIP Code): AFOSR/NA, Bolling AFB DC 20332-6448	9. PROCUREMENT INSTRUMENT IDENTIFICATION NUMBER: AFOSR - 88-0324
	10. SOURCE OF FUNDING NUMBERS: PROGRAM ELEMENT NO. 61102F; PROJECT NO. 2302; TASK NO C2; WORK UNIT ACCESSION NO.

11. TITLE (Include Security Classification)
Dynamic Rate-Dependent Elastoplastic Damage Modeling of Concrete Subject to Blast Loading: Formulation and Computational Aspects

12. PERSONAL AUTHOR(S)
Ju, Jiann-Wen

13a. TYPE OF REPORT	13b. TIME COVERED	14. DATE OF REPORT (Year, Month, Day)	15. PAGE COUNT
Final technical	FROM 880901 TO 900831	901031	261

16. SUPPLEMENTARY NOTATION
This work was sponsored by the AFOSR and Defense Nuclear Agency.

COSATI CODES		
FIELD	GROUP	SUB-GROUP
09	02	
11	02	

18. SUBJECT TERMS (Continue on reverse if necessary and identify by block number)
Damage Mechanics, Elastic-damage Models, Elastoplastic Damage Models, Constitutive Algorithms, Experimental Validation, Micro-mechanical Damage Theories, Rate-dependent Damage Models. (JN)

19. ABSTRACT (Continue on reverse if necessary and identify by block number)

dvanced elastic-damage and elastoplastic-damage models are presented within he frameworks of both continuum damage mechanics and micromechanical damage iechanics. Novel energy-based coupled elastoplastic continuum damage theories nd computational algorithms are proposed, including rate-dependent isotropic nd anisotropic damage models. Efficient constitutive algorithms and exten- ive experimental validation are also performed. In addition, novel finite leformation elastoplastic continuum damage models are developed to account or large strains and high rates. On the other hand, advanced and state-of- he-art two- and three-dimensional micromechanical anisotropic damage models re proposed to physically simulate micromechanical microcracking kinetics cleavage 1 and cleavage 2 processes) and damaged overall compliances for oncrete materials under tensile and compressive loadings. These results are nnovative, fundamental, and very useful in advanced damage modeling.

20. DISTRIBUTION / AVAILABILITY OF ABSTRACT	21. ABSTRACT SECURITY CLASSIFICATION
☐ UNCLASSIFIED/UNLIMITED ☒ SAME AS RPT ☐ DTIC USERS	Unclassified
22a. NAME OF RESPONSIBLE INDIVIDUAL: DR SPENCER Wu	22b. TELEPHONE (Include Area Code): 202-767-6962 / 22c. OFFICE SYMBOL: NA

Form 1473, JUN 86 — Previous editions are obsolete. — SECURITY CLASSIFICATION OF THIS PAGE: UNCLASSIFIED

DYNAMIC RATE DEPENDENT ELASTOPLASTIC DAMAGE MODELING OF CONCRETE SUBJECT TO BLAST LOADING: FORMULATION AND COMPUTATIONAL ASPECTS

J.W. JU

Department of Civil Engineering & Operations Research
Princeton University
Princeton, N.J. 08544

31 October 1990

Final Technical Report

Prepared for
Air Force Office of Scientific Research
Building 410
Bolling AFB, D.C. 20332-6448

PREFACE

This work was sponsored by the Air Force Office of Scientific Research and the Defense Nuclear Agency under Grant No. AFOSR-88-0324 and AFOSR-88-0324-A. This support and the interest and comments of Dr. Spencer Wu, Dr. Paul Senseny and Dr. Kent Goering are gratefully acknowledged.

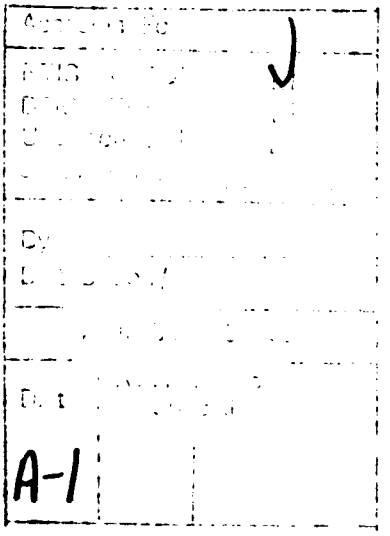

ABSTRACT

Advanced elastic-damage and elastoplastic-damage models are presented within the frameworks of both continuum damage mechanics and micromechanical damage mechanics. Novel energy-based coupled elastoplastic continuum damage theories and computational algorithms are proposed, including rate-dependent isotropic and anisotropic damage models. Efficient constitutive algorithms and extensive experimental validation are also performed. In addition, novel finite deformation elastoplastic continuum damage models are developed to account for large strains and high rates. On the other hand, advanced and state-of-the-art two- and three-dimensional micromechanical anisotropic damage models are proposed to physically simulate micromechanical microcracking kinetics (cleavage 1 and cleavage 2 processes) and damaged overall compliances for concrete materials under tensile and compressive loadings. These results are innovative, fundamental, and very useful in advanced damage modeling.

LIST OF PUBLICATIONS AND PRESENTATIONS

[1] J.W. Ju, "On Energy-Based Coupled Elastoplastic Damage Theories: Constitutive Modeling and Computational Aspects," *Int. J. Solids & Struct.*, Vol 25, No. 7, pp. 803-833, 1989.

[2] J.W. Ju, "On Energy-Based Coupled Elastoplastic Damage Models at Finite Strains," *J. of Eng. Mech.*, ASCE, Vol. 115, No. 11, pp. 2507-2525, 1989.

[3] J.W. Ju, "On Two-Dimensional Self-Consistent Micromechanical Damage Models for Brittle Solids," *Int. J. Solids & Struct.*, Vol. 27, No. 2, pp. 227-258, 1991.

[4] J.W. Ju and X. Lee, "On Three-Dimensional Self-Consistent Micromechanical Damage Models for Brittle Solids. Part I: Tensile Loadings", *J. of Eng. Mech.*, submitted for publication, June 1990.

[5] X. Lee and J.W. Ju, "On Three-Dimensional Self-Consistent Micromechanical Damage Models for Brittle Solids. Part II: Compressive Loadings", *J. of Eng. Mech.*, submitted for publication, June 1990.

[6] J.W. Ju, "On Novel Energy-Based Coupled Elastoplastic Damage Models," *Engineering Science Preprints*, Paper No. ESP25.99024, Joint Conference of ASME Applied Mechanics Division and Society of Engineering Science, June 20-22, 1988, Berkeley, California.

[7] J.W. Ju, "A Three-Dimensional Micromechanical Damage Model for Concrete in Tension", in *Developments in Theoretical and Applied Mechanics*, Proceedings of the 1990 XV Southeastern Conference on Theoretical and Applied Mechanics (SECTAM XV), pp. 911-917, 1990, Ed. S. Hanagud, M. Kamat, and C. Ueng, published by College of Engineering, Georgia Institute of Technology.

[8] J.W. Ju, "On Two-Dimensional Micromechanical Damage Models for Brittle Solids with Interacting Microcracks," in *Micromechanics of Failure of Quasi-Brittle Materials*, pp. 105-114, Ed. by S.P. Shah, S.E. Swartz, and M.L. Wang, Elsevier

Applied Science, London and New York, 1990.

[9] J.W. Ju, "On Two-Dimensional Micromechanical Damage Models for Brittle Solids," *Invited speaker,* ASCE/ASME Third Joint Mechanics Conference, University of California, San Diego, July 9-12, 1989.

[10] J.W. Ju, "On Two-Dimensional Micromechanical Damage Models for Brittle Solids," *Invited lecture,* Institute of Applied Mechanics, National Taiwan University, Taipei, Taiwan, July 25, 1989.

[11] J.W. Ju, "On Three-Dimensional Micromechanical Damage Models for Brittle Solids under Tension," *Invited lecture,* Department of Mechanics and Materials Science, Rutgers University, New Jersey, March 1, 1990.

[12] J.W. Ju, "On Three-Dimensional Micromechanical Damage Models for Brittle Solids under Tension and Compression," *Invited lecture,* Department of Materials Science and Mineral Engineering, University of California, Berkeley, March 13, 1990.

[13] J.W. Ju, "On Three-Dimensional Micromechanical Damage Models for Brittle Solids," *Invited speaker,* 1990 Southeastern Conference on Theoretical and Applied Mechanics (SECTAM XV), Atlanta, Georgia, March 22, 1990,

[14] J.W. Ju, "On Three-Dimensional Micromechanical Damage Models for Brittle Solids under Tensile and Compressive Loadings," *Invited speaker,* International Conference on Micromechanics of Failure of Quasi-Brittle Materials, Albuquerque, New Mexico, June 6, 1990.

[15] J.W. Ju, "On Three-Dimensional Micromechanical Damage Models for Brittle Solids under Tensile and Compressive Loadings," *Invited lecture,* Department of Mechanical Engineering, University of Pittsburgh, Pennsylvania, September 25, 1990.

[16] J.W. Ju, "On Energy-Based Elastoplastic Visco-Damage Models and Strain Softening," *Invited speaker,* DNA Conference on Computational Structural Dynamics, Menlo Park, California, October 11, 1990.

[17] J.W. Ju, "On Three-Dimensional Micromechanical Damage Models for Brittle Solids under Tensile and Compressive Loadings," *Invited lecture,* Department of Mechanical Engineering and Applied Mechanics, University of Pennsylvania, Philadelphia, October 18, 1990.

Table of Contents

PART I
On Energy-Based Coupled Elastoplastic Damage Theories: Constitutive Modeling and Computational Aspects

I.1. Introduction

The *inelastic* behavior of the mechanical constitutive responses of engineering materials is in general related to the irreversible thermodynamic processes involving energy dissipation and stiffness variation due to physical changes in the microstructure. Some commonly employed inelastic theories include, for instance, viscoelasticity, plasticity and damage mechanics. In the past two decades, in particular, the damage mechanics approach has emerged as a viable framework for the description of *distributed* material damage including material stiffness degradation, microcrack initiation, growth and coalescence, as well as damage-induced anisotropy, etc.. Damage mechanics has been applied to model creep damage (Hult [1974], Kachanov [1958][1981][1984], Krajcinovic [1983a], Leckie and Hayhurst [1974], Lemaitre [1984], Murakami [1981], Rabotnov [1963]), fatigue damage (Chaboche [1974], Lemaitre [1971][1984], Marigo [1985]), creep-fatigue interaction (Lemaitre [1984], Lemaitre and Chaboche [1974], Lemaitre and Plumtree [1979]), elasticity coupled with damage (Cordebois and Sidoroff [1979], Ju et al. [1989], Kachanov [1980][1987a][1987b], Krajcinovic and Fonseka [1981], Ortiz [1985], Wu [1985]), and ductile plastic damage (Cordebois and Sidoroff [1982], Dragon [1985], Dragon and Chihab [1985], Lemaitre and Dufailly [1977], Lemaitre [1984][1985][1986], Simo and Ju [1987a][1987b][1987c]). In addition, damage mechanics has been introduced to describe the inelastic behavior of brittle materials such as concrete and rock (Francois [1984], Ilankamban and Krajcinovic [1987], Kachanov [1982], Krajcinovic [1983b], Krajcinovic and Fonseka [1981], Loland [1980], Lorrain and Loland [1983], Mazars [1982][1986], Mazars and Lemaitre [1984], Resende and Martin [1984], Simo and Ju [1987a][1987b]).

Recently, *micromechanical* damage theories are proposed in the literature to model non-interacting microcrack growth in an originally *isotropic linear elastic* brittle solid; see, e.g., Wu [1985], Krajcinovic and Fanella [1986], Sumarac and Krajcinovic [1987] (which extends the work of Horii and Nemat-Nasser [1983] to a process model). In the case of *nonlinear* elastoplasticity coupled with many distributed *interacting* microcracks, nevertheless, such micromechanical derivation of microcrack kinetic laws presents tremendous difficulties and challenges, and is an objective for future research. Further, as was remarked by Krajcinovic [1985], a purely micromechanical theory may never replace a properly formulated phenomenological theory as a design tool.

Continuum damage mechanics is based on the thermodynamics of irreversible processes, the internal state variable theory and relevant physical considerations (e.g., the assumption of *distributed* microcracks, homogenization concept, the definition of micromechanical damage variable, kinetic law of damage growth, nonlocal damage characterization and plasticity-damage coupling mechanism, etc.). A scalar damage variable is suitable for characterizing (homogenized) *isotropic* damage processes. Nevertheless, a tensor-valued damage variable (fourth order) is necessary in order to account for *anisotropic* damage effects.

Many researchers in damage mechanics focused on the linear "elastic-damage" mechanics for brittle materials; i.e., *linear elastic* solids with distributed microcracks. For *nonlinearly* elastic solids and *elastoplastic* solids, nontheless, their methods are not applicable in general. By contrast, some elastoplastic damage theories have been proposed (e.g., Lemaitre [1984][1985][1986], Dragon [1985], Simo and Ju [1987a][1987b][1987c]). However, it appears that the thermodynamic free energy function and the "damage energy release rate" proposed by Lemaitre [1985] may not be physically appropriate. In fact, the theory advocated by Lemaitre implies that the thermodynamic force conjugate to elastoplastic microcrack evolution is simply the *elastic* strain energy, i.e., *plastic* strains do not contribute to the microcrack growth process. On the

other hand, the theory proposed by Dragon [1985] does not offer thermodynamic damage energy criteria, nor provide tangent moduli or numerical simulations or experimental validations. Hence, *coupled* elastoplastic damage mechanics warrants further study.

It is important to clarify the term "damage" employed in the current literature. As was pointed out by Krajcinovic, there are at least three different levels of scale of "damage" in material mechanical responses: (a) Atomic voids and crystal lattice defects, which require the use of *non-continuum* mechanics models at the atomic scale; (b) Microcracks and microvoids, which require micromechanical damage models (to model microstructural changes and *individual* microcracks grow) or phenomenological continuum damage models (to model *distributed* microcracks); and (c) Macrocracks, which warrant fracture mechanics models to model the growth of *discrete* macrocracks.

In this paper, novel energy-based (isotropic or anisotropic) coupled elastoplastic damage theories are presented to characterize distributed *microcracks* (not ductile microvoids) in brittle damage modes (including "Cleavage 1", "Cleavage 2" and "Cleavage 3" in the sense of Ashby [1979]). An outline of the paper is as follows. In Section 2, the definitions of "damage variable" are reviewed; the homogenization concept and alternative nonlocal damage definition are discussed; and the basic hypotheses of damage mechanics developed are summarized. In Section 3 energy-based isotropic elastoplastic damage theories are given, which are capable of accommodating *nonlinear* elastic response and general *plastic* response. The proposed theories can predict degradation in both elastic and plastic material properties (such as elastic moduli and plastic flow stresses). At variance with Lemaitre's formulation, a new free energy function and proper "damage energy release rate" are constructed.

In contrast to previous work by Simo and Ju [1987a][1987b][1987c] (which features an additive split of the *stress* tensor), this paper assumes an additive split of the *strain* tensor into the "elastic-damage" and "plastic-damage" parts from the outset. It is shown that the current "strain split" damage-plasticity formulation is physically more appealing

(analogous to the J-integral in nonlinear fracture mechanics) and results in more robust *tangent moduli* than the "stress split" formulation. In addition, the plastic flow rule and hardening law are characterized in terms of the *effective* stress quantities; namely, the **effective stress space plasticity**. A rate-dependent damage mechanism is subsequently developed to account for the microcrack retardation effects at higher strain rates. Rational mechanism is also proposed to simulate the "mode I" microcrack *opening* and *closing* operations.

The framework constructed in Section 3 is further extended in Section 4 to develop simple *energy-based* fourth-order *anisotropic* damage models for brittle materials. Recognizing the important role played by constitutive *algorithms* in constitutive theories and modeling, computational aspects of the proposed elastoplastic damage models are systematically explored in Section 5. In particular, new *three-step* operator split algorithms are developed within the present framework. Application is made to a class of inviscid and rate-dependent cap-damage models for concrete and mortar in Section 6. *Experimental validations* are also given to illustrate the applicability of proposed damage models and algorithms.

I.2. A framework for damage mechanics

Physically, degradation of material properties is related to the initiation, growth and coalescence of microcracks or microvoids. Some basic concepts pertaining to damage mechanics are reviewed in this section.

2.1. Damage variable and homogenization. "Damage" can be defined as a collection of *permanent* microstructural changes concerning material thermomechanical properties (e.g., stiffness, strength, anisotropy, etc.) brought about in a material by a set of *irreversible* physical microcracking processes resulting from the application of thermomechanical loadings (Talreja [1985]). The selection of a "damage" variable should be based on proper micromechanical considerations. For several types of material microstructure, microcracks develop in characteristic patterns and the microstructure can be assumed to be statistically homogeneous. These patterned damage are observed in fibrous composite laminates, concrete and ceramics (Weitsman [1987]). Several definitions of damage are possible for consideration. For example,

(i) Define the second-order damage tensor $\mathbf{D}$ as a spatial average:

$$\mathbf{D} \equiv \frac{1}{2V} \sum_{k} \int_{S^{(k)}} (\mathbf{b} \otimes \mathbf{n} + \mathbf{n} \otimes \mathbf{b})^{(k)} \, dS^{(k)} \ , \tag{2.1}$$

in which $\mathbf{b}$ and $\mathbf{n}$ denote the displacement discontinuity vector ($\mathbf{b} \equiv [\mathbf{u}]$) and the unit normal vector across the k-th microcrack surface $S^{(k)}$, respectively (Vakulenko and Kachanov [1971], Dragon [1985]). The *representative volume* V is a proper statistical and micromechanical measure for observing or computing an overall constitutive law. The minimum prescription for the representative unit cell is that the magnitude of local wave-like fluctuations about the expected (mean) values of phase variables should *not* depend on the *size* of the unit cell so that the system is macroscopically homogeneous (Hill [1967][1972]). At the macroscopic level, V plays the role of an infinitesimal material neighborhood with uniform state variables. At the microscale, however, V plays the role of a "micro-continuum" with nonuniform

spatial variables (Eringen [1968], Ortiz [1987a]). However, as pointed out by Krajcinovic [1985], the definition (2.1) is thermodynamically *incorrect* because it leads to energy dissipation during unloading. Eq. (2.1) is, nevertheless, a good index for "added flexibility" (damage-induced inelastic strain) due to open microcracks.

(ii) Define the damage variable $d_{\mathbf{n}}$ (in the normal direction $\mathbf{n}$) as

$$d_{\mathbf{n}} \equiv \frac{A_d}{A_T} \ , \tag{2.2}$$

where A_d is the *damaged* surface area (taking into account the microcrack area, the micro-stress concentration and the interaction between microcracks) and A_T is the total cross-sectional area of a surface of a unit cell along a normal direction $\mathbf{n}$ (see, e.g., Lemaitre [1984][1985]). The definition of a damage variable can also be anisotropic to signify different oriented geometry and micro-defects in material bonding; e.g., three changing principal normal directions of a three-dimensional oriented microcrack.

(iii) Define the damage measure d as (assuming only one single microcrack)

$$d \equiv \frac{a^3}{V} \ , \tag{2.3}$$

where a is the *radius* of an assumed single spherical microcrack and V is the volume of a *representative unit cell* in the mesostructure (see, e.g., Budiansky & O'Connell [1976], Wu [1985], Krajcinovic [1987]). This definition is related to the microcrack *porosity* (concentration ratio) within the unit cell. It is emphasized that Eq. (2.3) can lead to a fourth order damage tensor representation. □

The homogenization procedure can be applied not only to damage variables but also to stresses and strains. For instance, one may write:

$$\hat{\boldsymbol{\sigma}} \equiv \frac{1}{V} \int_V \boldsymbol{\sigma} \, dv \ ; \ \hat{\boldsymbol{\varepsilon}} \equiv \frac{1}{V} \int_V \boldsymbol{\varepsilon} \, dv \tag{2.4}$$

2.2. Alternative nonlocal damage characterization. As was noted earlier, the state variables display non-uniform spatial fluctuations at the microscale. Therefore, nonlocal continuum theory may be considered for damage mechanics; see, e.g., Bazant, Lin and Pijaudier-Cabot [1987], Eringen [1983], Eringen [1987], Eringen and Edelen [1972], Pijaudier-Cabot and Bazant [1987], Xia et al. [1987]. The essence of nonlocal theory includes the characteristic length (l) and the "attenuation" (weighting) function ($\omega(\mathbf{x})$). It is noted that nonlocal spatial averaging is fundamentally different from the homogenization concept, although nonlocal theory might provide a unified foundation for the homogenization concept. ω contains a crucial material parameter -- the characteristic length which is generally influenced by the spacing, size and shape of inclusions (or aggregates, fibers). In the event of inhomogeneous anisotropic materials, one could replace the homogeneous isotropic attenuation function $\omega(\mathbf{x})$ by a fourth-order attenuation tensor $\omega_{ijkl}(\mathbf{x})$.

2.3. Effective stress concept and hypothesis of strain equivalence. Let us denote by $\mathbf{M}$ a fourth-order tensor which characterizes the state of damage and transforms the homogenized stress tensor $\boldsymbol{\sigma}$ into the effective stress tensor $\bar{\boldsymbol{\sigma}}$; viz.,

$$\bar{\boldsymbol{\sigma}} \equiv \mathbf{M}^{-1} : \boldsymbol{\sigma} \tag{2.5}$$

For isotropic damage case, the mechanical behavior of microcracks is independent of their orientation and depends only on a scalar variable d. Accordingly, $\mathbf{M}$ simply reduces to $(1-d)\,\mathbf{I}$, where $\mathbf{I}$ is the rank four identity tensor, and (2.5) collapses to

$$\bar{\boldsymbol{\sigma}} \equiv \frac{\boldsymbol{\sigma}}{1-d} \tag{2.6}$$

The coefficient $(1-d)$ dividing the stress tensor in (2.6) is a *reduction factor* associated with the amount of damage in the material first introduced by Kachanov [1958]. The value $d = 0$ corresponds to the *undamaged* state, $d = d_c$ defines the *complete local rupture* ($d_c \in [0\,,\,1]$), and $d \in (0, d_c)$ corresponds to a partially *damaged* state. Local stresses are redistributed to the undamaged material micro-bonds and therefore the

effective stresses are higher than the nominal stresses. In addition, Lemaitre introduced the following hypothesis of strain equivalence:

> *"The strain associated with a damaged state under the applied stress is equivalent to the strain associated with its undamaged state under the effective stress."*

See Figure 1 for a schematic explanation.

Remark 2.1. Added flexibility. Due to the existence of microcracks, the flexibility of a material increases. To see this, consider for simplicity the elastic-damage case (see Figure 2). Let us denote by $\mathbf{C}^o$ the undamaged stiffness and $(1-d)\,\mathbf{C}^o$ the damaged unloading stiffness (as will be derived in Eq. (3.15) of Section 3.2). It is assumed that all microcracks *close* upon unloading and therefore no permanent deformation exists upon complete unloading. Accordingly, the truly reversible (elastic) strain is obtained by following the unloading slope $\mathbf{C}^o$ and is designated as $\hat{\boldsymbol{\varepsilon}}^e$. It is observed from Figure 2 that the gap between point O and point A is actually the inelastic strain $\boldsymbol{\varepsilon}^d$ due to microcrack opening during the loading process. See also Ortiz [1985]. □

I.3. Energy-based isotropic elastoplastic damage models

The underlying concept of the energy-based elastoplastic damage models presented in this section is that damage in a material is linked to the history of *both* elastic and plastic state variables. The framework constructed in this section will be extremely useful for the development of anisotropic damage models proposed in Section 4.

The fundamental problem of the ductile plastic damage formulation advocated by Lemaitre [1984][1985][1986] is the non-optimal choice of the locally averaged free energy potential. In particular, damage is associated only with the *elastic* strains and the damage energy release rate is shown to be the *elastic* strain energy in Lemaitre [1985]. This treatment amounts to *uncoupled* plasticity and damage processes, thus in a sense contradicting experimental evidence that plastic variables also contribute to the initiation and growth of microcracks. By contrast, a new free energy function and damage energy release rate are proposed in this section. The damage energy release rate (energy barrier) controls the microcrack propagation and arrest. The damage loading/unloading conditions are completely characterized by this energy barrier which is related to the local debonding energy required to initiate or propagate microcracks. The notion of effective stress and the hypothesis of strain equivalence are also utilized.

I.3.1. Thermodynamic basis. Strain split

The split of the total strain tensor into the "elastic-damage" and "plastic-damage" parts is assumed at the outset; i.e.,

$$\boldsymbol{\varepsilon} = \boldsymbol{\varepsilon}^e + \boldsymbol{\varepsilon}^p \tag{3.1}$$

It is emphasized that the "added flexibility" due to the existence of microcracks is already embedded in $\boldsymbol{\varepsilon}^e$ and $\boldsymbol{\varepsilon}^p$ implicitly (see Remark 2.1). That is, $\boldsymbol{\varepsilon}^e$ ($\boldsymbol{\varepsilon}^p$) includes not only the truly elastic (plastic) strain but also the added deformation due to active microcracks. Upon complete unloading, however, we assume that all microcracks are *closed* and no

residual strain is induced by micro-defects. To introduce both damage and plasticity mechanisms, let us consider the following locally averaged (homogenized) free energy function:

$$\Psi(\boldsymbol{\varepsilon}^e\ ,\mathbf{q}\ ,d)\ \equiv\ (1-d)\,\Psi^o(\boldsymbol{\varepsilon}^e\ ,\mathbf{q}) \tag{3.2}$$

where $\mathbf{q}$ denotes a suitable set of plastic variables and $\Psi^o(\boldsymbol{\varepsilon}^e\ ,\mathbf{q})$ signifies the total potential energy function of an *undamaged* (virgin) material. One often assumes (although unnecessary) that the elastic and plastic potential energy functions are uncoupled; i.e., $\Psi^o(\boldsymbol{\varepsilon}^e\ ,\mathbf{q}) \equiv \Psi^o_e(\boldsymbol{\varepsilon}^e) + \Psi^o_p(\mathbf{q})$.

Confining our attention to the purely mechanical theory, the Clausius-Duhem inequality takes the form

$$-\dot{\Psi} + \boldsymbol{\sigma} : \dot{\boldsymbol{\varepsilon}} \geq 0 \tag{3.3}$$

for any admissible process. Taking time derivative of Eq. (3.2), substituting into (3.3), and making use of standard arguments (Coleman and Gurtin [1967]) along with the additional assumption that damage and plastic unloading are *elastic* processes, we obtain

$$\boldsymbol{\sigma} = \frac{\partial \Psi}{\partial \boldsymbol{\varepsilon}^e} = (1-d)\,\frac{\partial \Psi^o}{\partial \boldsymbol{\varepsilon}^e}\ , \tag{3.4}$$

and the dissipative inequalities

$$\Psi^o(\boldsymbol{\varepsilon}^e\ ,\mathbf{q})\,\dot{d} \geq 0 \quad \text{and} \quad \frac{\partial \Psi^o}{\partial \boldsymbol{\varepsilon}^e} : \dot{\boldsymbol{\varepsilon}}^p - \frac{\partial \Psi^o}{\partial \mathbf{q}} \bullet \dot{\mathbf{q}} \geq 0\,. \tag{3.5}$$

It is clear from Eq. (3.4) and (3.5) that the present framework is capable of accommodating *nonlinear* elastic response and general plastic response. Moreover, it is noted that the effective stress is given by the expression

$$\bar{\boldsymbol{\sigma}} = \frac{\boldsymbol{\sigma}}{1-d} = \frac{\partial \Psi^o(\boldsymbol{\varepsilon}^e\ ,\mathbf{q})}{\partial \boldsymbol{\varepsilon}^e} \tag{3.6}$$

Remark 3.1. From Eq. (3.2) it follows that

$$-Y \equiv -\frac{\partial \Psi(\boldsymbol{\varepsilon}^e, \mathbf{q}, d)}{\partial d} = \Psi^o(\boldsymbol{\varepsilon}^e, \mathbf{q}) \tag{3.7}$$

Therefore, we conclude that the *undamaged* energy function $\Psi^o(\boldsymbol{\varepsilon}^e, \mathbf{q})$ is the thermodynamic force (damage energy release rate) *conjugate* to the damage variable d. This is at variance with Cordebois and Sidoroff [1982], Lemaitre [1984][1985][1986], who considered only the elastic part of the damage energy -- $\Psi_e^o(\boldsymbol{\varepsilon}^e)$. It is noted that by considering the elastic damage energy only is physically incorrect since plastic dissipation is not properly accounted for. See also Chow and Wang [1987a] for more anomalies of *elastic* damage energy release rate. □

Remark 3.2. A different formulation based on an additive split of the *stress* tensor was previously proposed by Simo and Ju [1987a][1987b]. In their work, the thermodynamic damage energy release rate was shown to be $\Psi^o(\boldsymbol{\varepsilon})$; i.e., the total undamaged stored energy function with the *total* strain tensor $\boldsymbol{\varepsilon}$ as its argument. By contrast, the damage energy release rate in the present formulation is $\Psi^o(\boldsymbol{\varepsilon}^e, \mathbf{q})$ which is *smaller* than $\Psi^o(\boldsymbol{\varepsilon})$. It is interesting to notice that $\Psi^o(\boldsymbol{\varepsilon}^e, \mathbf{q})$ is actually the local counterpart of the global J-integral fracture energy in nonlinear elastoplastic fracture mechanics. This is not the case for the alternative quantity $\Psi^o(\boldsymbol{\varepsilon})$ proposed by Simo and Ju [1987a][1987b]. □

I.3.2. Characterization of damage

A simple isotropic elastoplastic damage mechanism is characterized in this section to describe the progressive degradation of mechanical properties of materials. Motivated by Remark 3.1, we propose to employ the (locally averaged) *undamaged* energy function Ψ^o (the damage energy release rate) to characterize the damage loading/unloading conditions. For convenience, we define the notation ξ as

$$\xi \equiv \Psi^o(\boldsymbol{\varepsilon}^e, \mathbf{q}) \tag{3.8}$$

The state of damage in the material is then characterized by means of a *damage criterion* $g(\xi_t, r_t) \leq 0$ with the following functional form:

$$g(\xi_t, r_t) \equiv \xi_t - r_t \leq 0 \ , \quad t \in \mathbf{R}_+ \tag{3.9}$$

Here, the subscript t refers to the value at current time $t \in \mathbf{R}_+$, and r_t signifies the *damage threshold* (energy barrier) at current time t (i.e., the *radius* of the damage surface). If r_0 denotes the initial damage threshold before any loading is applied, a property characteristic of the material, we must have $r_t \geq r_0$. Condition (3.9) then states that damage in the material is *initiated* when the damage energy release rate (ξ_t) exceeds the initial damage threshold r_0. The above *energy*-based damage criterion is fundamentally linked to the history of both elastic and plastic variables. A large body of current literatures, however, adopts certain *stress*-based damage criteria; see, e.g., Chow and Wang [1987a][1987b] (which tried to remedy Cordebois and Sidoroff [1982]). It is noted that a stress-based damage criterion in the presence of significant plastic flows is inherently *inadequate* for predicting realistic plastic damage growth. To substantiate this statement, let us consider for simplicity the perfect plasticity coupled with damage. The effective stresses are constant and the homogenized stresses are decreasing; consequently, a stress-based criterion will not predict significant damage accumulation even under large plastic deformations.

To describe the growth of microcracks and the expansion of damage surfaces, it is necessary to specify the equations of evolution for d and r. As was mentioned earlier, micromechanical derivation of microcrack kinetic growth laws is currently achievable only in the case of originally homogeneous, linear isotropic elastic solids without microcrack interaction. In the case of general nonlinear elastoplasticity coupled with interacting microcracks, such micromechanical derivation is not available yet. Hence, in this section, a phenomenological description of the kinetics of microcrack growth is attempted. For the isotropic damage case, we define the evolution equations as

$$\begin{aligned} \dot{d}_t &= \dot{\mu}\, H(\xi_t\,, d_t\,; s\,, a\,, c\,, \rho) \\ \dot{r}_t &= \dot{\mu} \end{aligned} \tag{3.10}$$

where s is the spacing of inclusions (fibers or aggregates), a the grain size, c the micro-crack size, and ρ the porosity (e.g., water/cement ratio in concrete). In addition, $\dot{\mu} \geq 0$ is a *damage consistency* parameter which defines *damage loading/unloading* conditions according to the Kuhn-Tucker relations:

$$\dot{\mu} \geq 0\,, \quad g(\xi_t\,, r_t) \leq 0\,, \quad \dot{\mu}\, g(\xi_t\,, r_t) = 0\,. \tag{3.11}$$

Conditions (3.11) are standard for problems involving unilateral constraint. If $g(\xi_t\,, r_t) < 0$, the damage criterion is not satisfied and by condition $(3.11)_3$ we have $\dot{\mu} = 0$; hence, the damage rule (3.10) implies that $\dot{d} = 0$ and *no* further damage takes place. If, on the other hand, $\dot{\mu} > 0$; that is, further damage is taking place, condition $(3.11)_3$ now implies that $g(\xi_t\,, r_t) = 0$. In this event the value of $\dot{\mu}$ is determined by the "damage consistency condition"; i.e.,

$$g(\xi_t\,, r_t) = \dot{g}(\xi_t\,, r_t) = 0 \quad \Rightarrow \quad \dot{\mu} = \dot{\xi}_t\,. \tag{3.12}$$

So that r_t is given by the expression

$$r_t = \max\left\{ r_0\,, \max_{s \in (-\infty,\, t]} \xi_s \right\} \tag{3.13}$$

3.2.1. Elastic-damage tangent moduli. For isotropic ductile damage, the above characterization of damage results in *symmetric* elastic-damage tangent moduli. In the absence of *further* plastic flow, $\dot{\boldsymbol{\varepsilon}}^p \equiv \dot{\mathbf{q}} \equiv \mathbf{0}$. Time differentiation of (3.4) along with the damage rule (3.10) and the damage consistency condition (3.12) then yield

$$\dot{\boldsymbol{\sigma}} = (1-d)\, \frac{\partial^2 \Psi^o(\boldsymbol{\varepsilon}^e\,, \mathbf{q})}{\partial \boldsymbol{\varepsilon}^{e\,2}} : \dot{\boldsymbol{\varepsilon}} - H\, \dot{\xi}\, \bar{\boldsymbol{\sigma}}\,, \tag{3.14}$$

where $\bar{\boldsymbol{\sigma}} \equiv \dfrac{\partial \Psi^o}{\partial \boldsymbol{\varepsilon}^e}$ (the effective stress) and, for notational simplicity, the subscript t has been dropped. By taking the time derivative of Eq. (3.8), we obtain $\dot{\xi} = \bar{\boldsymbol{\sigma}} : \dot{\boldsymbol{\varepsilon}}$.

Substitution into (3.14) then yields $\dot{\boldsymbol{\sigma}} = \mathbf{C}(\boldsymbol{\varepsilon}^e , \mathbf{q} , d) : \dot{\boldsymbol{\varepsilon}}$, where $\mathbf{C}(\boldsymbol{\varepsilon}^e , \mathbf{q} , d)$ is the *elastic-damage tangent modulus* given by

$$\mathbf{C}(\boldsymbol{\varepsilon}^e , \mathbf{q} , d) \equiv [\, (1-d)\, \frac{\partial^2 \Psi^o(\boldsymbol{\varepsilon}^e , \mathbf{q})}{\partial \boldsymbol{\varepsilon}^{e\,2}} - H\, \bar{\boldsymbol{\sigma}} \otimes \bar{\boldsymbol{\sigma}} \,] \tag{3.15}$$

Note that $\mathbf{C}(\boldsymbol{\varepsilon}^e , \mathbf{q} , d)$ is a *symmetric* rank four tensor. It is often assumed that the undamaged tangent modulus $\mathbf{C}^o \equiv \partial^2 \Psi^o / \partial \boldsymbol{\varepsilon}^{e\,2}$ is constant.

I.3.3. Coupled elastoplastic damage response

Once microcracks occur, local stresses are redistributed to undamaged material micro-bonds over the effective area. Thus, true stresses of undamaged material points are *higher* than nominal stresses. Accordingly, it appears reasonable to state that the plastic flows occur only in the undamaged material micro-bonds by means of *effective* quantities. In fact, this is simply the underlying notion of the effective stress concept. Therefore, the characterization of the plastic response should be formulated in the *effective stress space* in terms of effective quantities $\bar{\boldsymbol{\sigma}}$ and $\mathbf{q}$. The homogenized stress tensor $\boldsymbol{\sigma}$ is replaced by the *effective* stress tensor $\bar{\boldsymbol{\sigma}}$ in the stress space yield criterion; i.e., the "elastic-damage" domain is defined by $f(\bar{\boldsymbol{\sigma}} , \mathbf{q}) \leq 0$. It is recognized that due to the existence of microcracks the plastic flow stresses and plastic material properties *degrade*. Use of effective quantities in the yield condition essentially has the net effect of *lowering* the plastic strength and flow stresses of materials. By assuming an associative flow rule, the rate-independent damaged plastic response is characterized as follows:

$$\dot{\boldsymbol{\varepsilon}}^p = \dot{\lambda}\, \frac{\partial f}{\partial \bar{\boldsymbol{\sigma}}} (\bar{\boldsymbol{\sigma}} , \mathbf{q}) \quad \textit{(flow rule)} \tag{3.16a}$$

$$\dot{\mathbf{q}} = \dot{\lambda}\, \mathbf{h}(\bar{\boldsymbol{\sigma}} , \mathbf{q}) \quad \textit{(plastic hardening law)} \tag{3.16b}$$

$$f(\bar{\boldsymbol{\sigma}} , \mathbf{q}) \leq 0 \quad \textit{(yield condition)} \tag{3.16c}$$

where $\dot{\lambda}$ denotes the plastic consistency parameter and $\mathbf{h}$ signifies the vectorial hardening function. It is interesting to notice that in spite of the normality rule assumption (3.16a)

in the *effective* stress space $\bar{\boldsymbol{\sigma}}$, the flow rule direction **departs** from normality in the *homogenized* stress space $\boldsymbol{\sigma}$. Hence, the damage-perturbed yield criterion and damage-induced non-associative flow rule (despite the associative flow rule in terms of $\bar{\boldsymbol{\sigma}}$) are accounted for in Eq. (3.16). Further, the loading/unloading conditions can be expressed in a compact form by requiring that

$$f(\bar{\boldsymbol{\sigma}}, \mathbf{q}) \leq 0, \quad \dot{\lambda} \geq 0, \quad \dot{\lambda} f(\bar{\boldsymbol{\sigma}}, \mathbf{q}) = 0 \tag{3.17}$$

$\dot{\lambda}$ is determined by requiring that $\dot{f} = 0$, the so-called *plastic consistency condition*. Hence, during plastic loading one has

$$\frac{\partial f}{\partial \bar{\boldsymbol{\sigma}}} : \dot{\bar{\boldsymbol{\sigma}}} + \frac{\partial f}{\partial \mathbf{q}} \bullet \dot{\mathbf{q}} = 0 \tag{3.18}$$

For simplicity, we shall assume *uncoupled* elastic and plastic potential energy functions; namely, $\Psi^o(\boldsymbol{\varepsilon}^e, \mathbf{q}) \equiv \Psi_e^o(\boldsymbol{\varepsilon}^e) + \Psi_p^o(\mathbf{q})$. Therefore, from Eq. (3.4) we obtain

$$\dot{\bar{\boldsymbol{\sigma}}} = \frac{\partial^2 \Psi^o}{\partial \boldsymbol{\varepsilon}^{e\,2}} : \dot{\boldsymbol{\varepsilon}}^e = \frac{\partial^2 \Psi^o}{\partial \boldsymbol{\varepsilon}^{e\,2}} : (\dot{\boldsymbol{\varepsilon}} - \dot{\lambda} \frac{\partial f}{\partial \bar{\boldsymbol{\sigma}}}) \tag{3.19}$$

where use has been made of the flow rule (3.16a). Thus, $\dot{\lambda}$ is determined as

$$\dot{\lambda} = \frac{\frac{\partial f}{\partial \bar{\boldsymbol{\sigma}}} : \frac{\partial^2 \Psi^o}{\partial \boldsymbol{\varepsilon}^{e\,2}} : \dot{\boldsymbol{\varepsilon}}}{\frac{\partial f}{\partial \bar{\boldsymbol{\sigma}}} : \frac{\partial^2 \Psi^o}{\partial \boldsymbol{\varepsilon}^{e\,2}} : \frac{\partial f}{\partial \bar{\boldsymbol{\sigma}}} - \frac{\partial f}{\partial \mathbf{q}} \bullet \mathbf{h}} \tag{3.20}$$

Substitution of (3.20) into (3.19) then yields $\dot{\bar{\boldsymbol{\sigma}}} = \bar{\mathbf{C}}^{ep} : \dot{\boldsymbol{\varepsilon}}$, where $\bar{\mathbf{C}}^{ep}$ is the *effective* elastoplastic tangent modulus (a *symmetric* fourth-order tensor) given by

$$\bar{\mathbf{C}}^{ep} \equiv \frac{\partial^2 \Psi^o}{\partial \boldsymbol{\varepsilon}^{e\,2}} - \frac{[\frac{\partial^2 \Psi^o}{\partial \boldsymbol{\varepsilon}^{e\,2}} : \frac{\partial f}{\partial \bar{\boldsymbol{\sigma}}}] \otimes [\frac{\partial^2 \Psi^o}{\partial \boldsymbol{\varepsilon}^{e\,2}} : \frac{\partial f}{\partial \bar{\boldsymbol{\sigma}}}]}{\frac{\partial f}{\partial \bar{\boldsymbol{\sigma}}} : \frac{\partial^2 \Psi^o}{\partial \boldsymbol{\varepsilon}^{e\,2}} : \frac{\partial f}{\partial \bar{\boldsymbol{\sigma}}} - \frac{\partial f}{\partial \mathbf{q}} \bullet \mathbf{h}} \tag{3.21}$$

To derive the elastoplastic-damage tangent moduli, we recall that $\boldsymbol{\sigma} = (1-d)\,\bar{\boldsymbol{\sigma}}$. Time differentiation then leads to

$$\dot{\boldsymbol{\sigma}} = (1-d)\,\dot{\bar{\boldsymbol{\sigma}}} - \dot{d}\,\bar{\boldsymbol{\sigma}} = (1-d)\,\bar{\mathbf{C}}^{ep} : \dot{\boldsymbol{\varepsilon}} - \dot{\xi} H\,\bar{\boldsymbol{\sigma}} \tag{3.22}$$

where use has been made of Eq. (3.10) and (3.12). In addition, time derivative of Eq. (3.8) along with Eq. (3.16) yield

$$\dot{\xi} = \bar{\boldsymbol{\sigma}} : (\dot{\boldsymbol{\varepsilon}} - \dot{\boldsymbol{\varepsilon}}^p) + \frac{\partial \Psi^o}{\partial \mathbf{q}} \bullet \dot{\mathbf{q}} = \bar{\boldsymbol{\sigma}} : \dot{\boldsymbol{\varepsilon}} - \dot{\lambda} \left[\bar{\boldsymbol{\sigma}} : \frac{\partial f}{\partial \bar{\boldsymbol{\sigma}}} - \frac{\partial \Psi^o}{\partial \mathbf{q}} \bullet \mathbf{h} \right] \tag{3.23}$$

Substitution of Eq. (3.20) and (3.23) into (3.22) then renders $\dot{\boldsymbol{\sigma}} = \mathbf{C}^{ep} : \dot{\boldsymbol{\varepsilon}}$. Here $\mathbf{C}^{ep}$ is the elastoplastic-damage tangent modulus given by

$$\mathbf{C}^{ep} = (1-d)\,\bar{\mathbf{C}}^{ep} - H\,[\bar{\boldsymbol{\sigma}} \otimes \bar{\boldsymbol{\sigma}}] + \frac{H\,(\bar{\boldsymbol{\sigma}} : \frac{\partial f}{\partial \bar{\boldsymbol{\sigma}}} - \frac{\partial \Psi^o}{\partial \mathbf{q}} \bullet \mathbf{h})}{\frac{\partial f}{\partial \bar{\boldsymbol{\sigma}}} : \frac{\partial^2 \Psi^o}{\partial \boldsymbol{\varepsilon}^{e\,2}} : \frac{\partial f}{\partial \bar{\boldsymbol{\sigma}}} - \frac{\partial f}{\partial \mathbf{q}} \bullet \mathbf{h}} [\bar{\boldsymbol{\sigma}} \otimes (\frac{\partial^2 \Psi^o}{\partial \boldsymbol{\varepsilon}^{e\,2}} : \frac{\partial f}{\partial \bar{\boldsymbol{\sigma}}})] \tag{3.24}$$

It is observed from Eq. (3.24) that $\mathbf{C}^{ep}$ is in general a non-symmetric rank four tensor. Nevertheless, in the particular event in which we have constant (linear) $\mathbf{C}^o \equiv \partial^2 \Psi^o / \partial \boldsymbol{\varepsilon}^{e\,2}$ and von Mises J_2-plasticity, $\mathbf{C}^{ep}$ in Eq. (3.24) is *symmetric*. The above coupled elastoplastic-damage formulation can be readily extended to accommodate non-associative flow rules (in the effective stress space $\bar{\boldsymbol{\sigma}}$) by simply replacing f in Eq. (3.16a) by a suitable plastic potential $Q\,(\bar{\boldsymbol{\sigma}}\,,\,\mathbf{q})$.

Remark 3.3. A damage-perturbed yield criterion and damage-induced non-associative flow rule in the *homogenized* stress space $\boldsymbol{\sigma}$ was proposed by Dragon [1985]. It is noted, however, that two different yield functions are used in Dragon [1985] to define the "genuine" yield potential and another damage-perturbed pseudo-potential, respectively. The tangent moduli are always non-symmetric. Moreover, the corresponding elastoplastic-damage return mapping algorithms are rather cumbersome due to two simultaneous consistency conditions. □

Remark 3.4. For the derivation of $\dot{\lambda}$ in Eq. (3.20) we have assumed that $\Psi^o(\boldsymbol{\varepsilon}^e\,,\,\mathbf{q}) \equiv \Psi^o_e(\boldsymbol{\varepsilon}^e) + \Psi^o_p(\mathbf{q})$. If this is not the case, the denominator in Eq. (3.20),(3.21) should be replaced by the following expression:

$$\left[\frac{\partial f}{\partial \bar{\boldsymbol{\sigma}}} : \frac{\partial^2 \Psi^o}{\partial \boldsymbol{\varepsilon}^{e\,2}} : \frac{\partial f}{\partial \bar{\boldsymbol{\sigma}}} - \frac{\partial f}{\partial \bar{\boldsymbol{\sigma}}} : \frac{\partial^2 \Psi^o}{\partial \boldsymbol{\varepsilon}^e\,\partial \mathbf{q}} \bullet \mathbf{h} - \frac{\partial f}{\partial \mathbf{q}} \bullet \mathbf{h} \right] \qquad \square \tag{3.25}$$

Remark 3.5. In the previous work by Simo and Ju [1987a][1987b], the formulation hinges on an additive split of the *stress* tensor. As a result, their elastoplastic-damage tangent moduli $\mathbf{C}^{ep}$ are *always* non-symmetric even with $\mathbf{C}^o$ constant. In addition, in the case of *nonlinear* elasticity (either physically or geometrically) coupled with damage-plasticity, the elastic and elastoplastic-damage tangent moduli ($\frac{\partial^2 \Psi^o(\boldsymbol{\varepsilon})}{\partial \boldsymbol{\varepsilon}^2}$ and $\mathbf{C}^{ep}$) are too "soft" due to the fact that the argument of differentiation is the *total* strain tensor $\boldsymbol{\varepsilon}$ (see Eq. (24) in Simo and Ju [1987a]; see also Simo and Ju [1987c] for the finite deformation case). These "soft" tangent moduli could lead to numerical difficulties when large strains are encountered. By contrast, present formulation employs more robust (stiffer) elastic tangent moduli $\frac{\partial^2 \Psi^o(\boldsymbol{\varepsilon}^e, \mathbf{q})}{\partial \boldsymbol{\varepsilon}^{e\,2}}$ and elastoplastic-damage tangent moduli $\mathbf{C}^{ep}$, with the *elastic* strain tensor $\boldsymbol{\varepsilon}^e$ as the argument of differentiation. This advantage together with our J-integral-like damage energy release rate ($\Psi^o(\boldsymbol{\varepsilon}^e, \mathbf{q})$) make the present formulation computationally and physically more attractive. □

Remark 3.6. (*Selection of* $\Psi^o(\boldsymbol{\varepsilon}^e, \mathbf{q})$). The specific forms of the undamaged free energy function Ψ^o depend on the mechanical behavior and thermodynamic processes of materials. From Eq. (3.5), it is observed that the thermodynamic forces conjugate to $\dot{\boldsymbol{\varepsilon}}^p$ and $\dot{\mathbf{q}}$ are $\frac{\partial \Psi^o}{\partial \boldsymbol{\varepsilon}^e}$ (or simply $\bar{\boldsymbol{\sigma}}$) and $-\frac{\partial \Psi^o}{\partial \mathbf{q}}$, respectively. In fact, in Eq. (3.16a), the partial derivative is taken with respect to $\bar{\boldsymbol{\sigma}}$. Therefore, it appears rational to postulate that

$$\dot{\mathbf{q}} \equiv \dot{\lambda} \frac{\partial f}{\partial (-\frac{\partial \Psi^o}{\partial \mathbf{q}})} \tag{3.26}$$

By comparing Eq. (3.26) with (3.16b), we obtain the relation

$$\mathbf{h}(\bar{\boldsymbol{\sigma}}, \mathbf{q}) = -\frac{\partial f}{\partial (\frac{\partial \Psi^o}{\partial \mathbf{q}})} \tag{3.27}$$

For demonstration purpose, let us assume that $\Psi^o(\boldsymbol{\varepsilon}^e, \mathbf{q}) = \Psi_e^o(\boldsymbol{\varepsilon}^e) + \Psi_p^o(\mathbf{q})$ and consider the von Mises plasticity with linear isotropic hardening. Thus, we have $\frac{d\Psi_p^o}{d\bar{e}^p} = R(\bar{e}^p)$,

with $\bar{e}^p$ and $R(\bar{e}^p)$ signifying the equivalent plastic strain and yield radius, respectively. Hence, we arrive at $\Psi_p^o = \int_0^{\bar{e}^p} R(\bar{e}^p)\, d\bar{e}^p$. For linear hardening, $R(\bar{e}^p) = R_o + \theta\, \bar{e}^p$, with R_o and θ denoting the initial yield radius and slope, respectively. Accordingly, $\Psi_p^o(\bar{e}^p) = R_o\, \bar{e}^p + \frac{1}{2}\, \theta\, \bar{e}^{p\,2}$. For other plasticity models, one could assume that $\Psi^o = \int_0^{\varepsilon} \bar{\sigma} : d\varepsilon$ and compute Ψ^o incrementally. On the other hand, the form of Ψ_e^o hinges on the particular hyperelasticity model employed; e.g., for linear elasticity case, one has $\Psi_e^o(\varepsilon^e) = \frac{1}{2}\, \varepsilon^e : C^o : \varepsilon^e$. □

I.3.4. Rate-dependent damage mechanism

Some experimental results (on rocks and concrete) show that the amount of micro-cracking at a particular strain level exhibits *rate sensitivity* to the applied rate of loading in a dynamic environment. Further, strain-softening and loss of strong ellipticity phenomena associated with damage mechanisms impose numerical difficulties in finite element computations. To account for rate dependency and to regularize the localization problems, a *viscous* damage mechanism is presented in this section. It is noted that the structure of this regularization is analogous to the viscoplastic regularization of the Perzyna type (Perzyna [1966]). In particular, rate equations governing visco-damage behavior are obtained from their rate-independent counterpart Eq. (3.10) by replacing the damage consistency parameter $\dot{\mu}$ by $\mu\, \bar{\phi}(g)$. Here μ is the damage viscosity coefficient, $\bar{\phi}(g)$ denotes the viscous damage flow function and g is defined in Eq. (3.9). With this at hand, we write

$$\begin{aligned} \dot{d}_t &= \mu < \bar{\phi}(g) > H(\xi_t, d_t, s, a, c, \rho) \\ \dot{r}_t &= \mu < \bar{\phi}(g) > \end{aligned} \tag{3.28}$$

where $< \bullet >$ denotes the McAuley bracket. In the event of *linear* viscous damage mechanism (i.e., $\bar{\phi}(g) \equiv g$), Eq. (3.28) then takes the form

$$\dot{d}_i = \mu < g > H(\xi_i, d_i, s, a, c, \rho)$$
$$\dot{r}_i = \mu < g > \equiv \mu < \xi_i - r_i > \tag{3.29}$$

The above viscous mechanism is capable of predicting retardation in microcrack growth at higher strain rates. In addition, the inviscid damage characterization can be recovered by letting μ go to infinity. On the other hand, as μ approaches zero we obtain the instantaneous elastic response (in the absence of plastic flow).

I.3.5. Microcrack opening and closing

Although the damage models presented in Sections 3.3 and 3.4 are isotropic, they can be easily extended to account for the "mode I" microcrack opening and closing effects. Let us start by considering the spectral decomposition of the strain tensor (see also Ortiz [1985])

$$\boldsymbol{\varepsilon} = \sum_{i=1}^{3} \varepsilon_i \, \mathbf{p}_i \otimes \mathbf{p}_i \quad , \quad \| \mathbf{p}_i \| = 1 \quad , \tag{3.30}$$

where ε_i is the i^{th} principal strain and $\mathbf{p}_i$ the i^{th} corresponding unit principal direction. Let $\mathbf{Q}$ and $\mathbf{Q}^+$, separately, be the regular and *positive* (tensile) spectral projection tensors defined as

$$\mathbf{Q} \equiv \sum_{i=1}^{3} \mathbf{p}_i \otimes \mathbf{p}_i \quad ; \quad \mathbf{Q}^+ \equiv \sum_{i=1}^{3} \hat{H}(\varepsilon_i) \, \mathbf{p}_i \otimes \mathbf{p}_i \tag{3.31}$$

where $\hat{H}(\bullet)$ is the Heaviside ramp function. We now introduce the fourth-order *positive* projection tensor $\mathbf{I\!P}^+$ with components

$$\mathbf{I\!P}^+_{ijkl} = Q^+_{ia} \, Q^+_{jb} \, Q_{ka} \, Q_{lb} \quad , \tag{3.32}$$

so that $\boldsymbol{\varepsilon}^+$ can be expressed as (see also Ortiz [1985])

$$\boldsymbol{\varepsilon}^+ = \mathbf{I\!P}^+ : \boldsymbol{\varepsilon} \quad , \quad i.e., \quad \varepsilon^+_{ij} = \mathbf{I\!P}^+_{ijkl} \, \varepsilon_{kl} \tag{3.33}$$

It is observed that $\mathbb{P}^+$ depends on the *total* strain $\boldsymbol{\varepsilon}$.

With these notations at hand, Eq. (3.4) is then rephrased to take into account the active (open) microcracks under tensile extensions. Specifically, we write

$$\boldsymbol{\sigma} = (\mathbf{I} - \mathbf{D}^{act}) : \frac{\partial \Psi^o}{\partial \boldsymbol{\varepsilon}^e} \tag{3.34}$$

where $\mathbf{D}^{act} \equiv d\, \mathbb{P}^+ \mathbf{I}\, \mathbb{P}^+ = d\, \mathbb{P}^+ \mathbb{P}^+$ is the fourth-order *active* anisotropic damage tensor. If all three principal strains ε_i are *tensile*, then we have $\mathbb{P}^+ = \mathbf{I}$ and $\mathbf{D}^{act} = d\, \mathbf{I}$; i.e., the local microcrack is open (active) in all three principal directions and we recover isotropic damage under current state. If all ε_i are *compressive*, then $\mathbb{P}^+ = \mathbf{0}$ and $\mathbf{D}^{act} = \mathbf{0}$; i.e., the local microcrack is entirely closed (passive) under current state. Clearly, other combinations of tensile and compressive states will give rise to various microcrack opening and closing situations.

The damage energy release rate $\xi \equiv \Psi^o$ in Eq. (3.8) can also be modified as follows to accommodate ductile and brittle (tensile) material damage:

$$\xi \equiv \begin{cases} \Psi^o(\boldsymbol{\varepsilon}^e, \mathbf{q}) & \textit{(ductile)} \\ \Psi^o(\boldsymbol{\varepsilon}^{e+}, \mathbf{q}) & \textit{(brittle)} \end{cases} \tag{3.35}$$

where $\boldsymbol{\varepsilon}^{e+} \equiv \mathbb{P}^+ : \boldsymbol{\varepsilon}^e$.

Remark 3.7. The above discussion on microcrack closure, Eq. (3.30)-(3.34), is quite similar to the proposal of Ortiz [1985]. However, there are some subtle differences between the two formulations. First, the *explicit form* of the positive orthogonal projection tensor $\mathbb{P}^+$ in Eq. (3.32) is more precise than that given in Ortiz [1985] (see Eq. (3.60) therein). Second, the present discussion employs the description of *stiffness degradation* through the active damage tensor $\mathbf{D}^{act}$ while Ortiz [1985] used the "added compliance" characterization $\mathbf{C}^c$ (see Eq. (3.11)-(3.14) in Ortiz [1985]). Third, $\mathbb{P}^+$ in Eq. (3.32) is a nonlinear, non-constant operator associated with the current total *strain* tensor $\boldsymbol{\varepsilon}$. In Ortiz [1985], by contrast, there are really *two* distinct orthogonal projections involved; see Eq. (3.9) and (3.60) therein. Specifically, the first one is $\mathbb{P}^+_{\boldsymbol{\varepsilon}}$ associated with

the current *strain* tensor $\boldsymbol{\varepsilon}$; i.e., $\boldsymbol{\varepsilon}^+ \equiv \mathbb{P}_{\boldsymbol{\varepsilon}}^+ : \boldsymbol{\varepsilon}$. The other one is $\mathbb{P}_{\boldsymbol{\sigma}}^+$ associated with the current *stress* tensor $\boldsymbol{\sigma}$; i.e., $\boldsymbol{\sigma}^+ \equiv \mathbb{P}_{\boldsymbol{\sigma}}^+ : \boldsymbol{\sigma}$ (see also Eq. (3.18) in Ortiz [1987b]). In general, $\mathbb{P}_{\boldsymbol{\varepsilon}}^+$ is **not** equal to $\mathbb{P}_{\boldsymbol{\sigma}}^+$. It appears that this distinction was not made clear in Ortiz [1985]. In addition, in a strain-driven algorithm, $\boldsymbol{\sigma}$ is yet *unknown* before local constitutive iteration. Hence, use of $\mathbb{P}_{\boldsymbol{\sigma}}^+$ introduces more computational efforts. Fourth, due to the existence of two distinct orthogonal projections in Ortiz [1985], Eq. (3.11)-(3.14) therein seem unclear. In particular, Eq. (3.13) in Ortiz [1985] could be interpreted as

$$\mathbf{C}^c = \mathbb{P}_{\boldsymbol{\varepsilon}}^+ : \overline{\mathbf{C}}^c : \mathbb{P}_{\boldsymbol{\sigma}}^+ \tag{3.36}$$

Accordingly, the active "added compliance" $\mathbf{C}^c$ becomes a non-symmetric tensor and Eq. (3.14) in Ortiz [1985] might be questionable because $\boldsymbol{\sigma}^+$ is not equal to $\mathbb{P}_{\boldsymbol{\varepsilon}}^+ : \boldsymbol{\sigma}$. In the present proposal, on the other hand, only one orthogonal projection $\mathbb{P}^+$ (see Eq. (3.32)) is needed and no confusion ever arises. □

I.4. Energy-based anisotropic elastoplastic damage models

The *energy*-based damage models developed in Section 3 are extended in this section to account for *anisotropic brittle* microcracking effects. In view of the significance of tensile extensions in brittle damage processes, proper damage characterization via tensile spectral decomposition is employed.

To illustrate the physical motivation of the proposed energy-based anisotropic brittle damage model, consider the idealized situation of a cylinder subject to *unconfined* increasing uniaxial compression. The objective is to simulate the "splitting mode". By properly including the tensile radial and hoop strains contribution to damage and screening out the compressive axial strain contribution, the proposed mechanism would predict progressive microcracking parallel to the the axis of loading (normal to the plane of tensile lateral strains) and ultimate failure of the specimen. This is a typical failure mode in many rock-like materials such as concrete. Note that a damage model based on tensile *stresses* could not possibly predict such a failure mode.

I.4.1. Thermodynamic basis

The proposed damage characterization is based on the concept of effective stress and features a simple and effective construction of the fourth-order transformation tensor $\mathbf{M}$ in Eq. (2.5). In fact, one could define $\mathbf{M} \equiv \mathbf{I} - \mathbf{D}$ (see also Cordebois and Sidoroff [1982]). The *damaged* secant (unloading) stiffness tensor then takes the form $\mathbf{C} = (\mathbf{I} - \mathbf{D})\, \mathbf{C}^o$, where $\mathbf{C}^o$ is the undamaged linear elasticity tensor. It is observed that the damaged stiffness $\mathbf{C}$ possesses a one-to-one correspondence with the fourth-order damage tensor $\mathbf{D}$. Hence, one could equivalently define $\mathbf{C}$ as the anisotropic damage variable. In addition, it is realized that $\mathbf{M} \equiv \mathbf{C}\, \mathbf{C}^{o\,-1}$.

As a point of departure, we postulate the following locally averaged free energy:

$$\Psi(\boldsymbol{\varepsilon}^e\,,\, \mathbf{q}\,,\, \mathbf{C}) \equiv \Psi_{ed}(\boldsymbol{\varepsilon}^e\,,\, \mathbf{C}) + \Psi_{pd}(\mathbf{q}\,,\, \mathbf{C}) = \tfrac{1}{2}\, \boldsymbol{\varepsilon}^e : \mathbf{C} : \boldsymbol{\varepsilon}^e + \Psi_{pd}(\mathbf{q}\,,\, \mathbf{C}) \qquad (4.1)$$

The Clausius-Duhem inequality then leads to

$$\dot{\boldsymbol{\varepsilon}} : [\boldsymbol{\sigma} - \mathbf{C} : \boldsymbol{\varepsilon}^e] - [\tfrac{1}{2}\,\boldsymbol{\varepsilon}^e : \dot{\mathbf{C}} : \boldsymbol{\varepsilon}^e + \frac{\partial \Psi_{pd}}{\partial \mathbf{C}} : \dot{\mathbf{C}}] + [\boldsymbol{\varepsilon}^e : \mathbf{C} : \dot{\boldsymbol{\varepsilon}}^p - \frac{\partial \Psi_{pd}}{\partial \mathbf{q}} \bullet \dot{\mathbf{q}}] \geq 0 \qquad (4.2)$$

Therefore, we obtain the following stress-strain relation

$$\boldsymbol{\sigma} = \frac{\partial \Psi}{\partial \boldsymbol{\varepsilon}} = \mathbf{C} : \boldsymbol{\varepsilon}^e \qquad (4.3)$$

along with the following damage and plastic dissipation inequalities

$$\mathbb{D}^d \equiv -\tfrac{1}{2}\,\boldsymbol{\varepsilon}^e : \dot{\mathbf{C}} : \boldsymbol{\varepsilon}^e - \frac{\partial \Psi_{pd}}{\partial \mathbf{C}} : \dot{\mathbf{C}} \geq 0 \qquad (4.4)$$

$$\mathbb{D}^p \equiv \boldsymbol{\sigma} : \dot{\boldsymbol{\varepsilon}}^p - \frac{\partial \Psi_{pd}}{\partial \mathbf{q}} \bullet \dot{\mathbf{q}} \geq 0 \qquad (4.5)$$

In addition, from Eq. (4.4) and the fact that

$$-\mathbf{Y} \equiv \frac{\partial \Psi}{\partial \mathbf{C}} = \frac{1}{2}\,\boldsymbol{\varepsilon}^e \otimes \boldsymbol{\varepsilon}^e + \frac{\partial \Psi_{pd}}{\partial \mathbf{C}} \qquad (4.6)$$

we conclude that $[\frac{1}{2}\,\boldsymbol{\varepsilon}^e \otimes \boldsymbol{\varepsilon}^e + \frac{\partial \Psi_{pd}}{\partial \mathbf{C}}]$ is the thermodynamic force conjugate to the damaged secant (unloading) stiffness $\mathbf{C}$. This thermodynamic force physically defines the "anisotropic damage energy release rate" and will be used to characterize damage evolution.

In particular, we shall assume that Ψ_{pd} is linear in $\mathbf{D}$ (or $\mathbf{C}$); e.g.,

$$\Psi_{pd}(\mathbf{q}, \mathbf{C}) \equiv [\,(\mathbf{I} - \mathbf{D}) : \mathbf{I}\,]\,\tilde{\Psi}_p^o(\mathbf{q}) \qquad (4.7)$$

where $\tilde{\Psi}_p^o(\mathbf{q}) \equiv \frac{1}{9}\,\Psi_p^o(\mathbf{q})$, the undamaged plastic free energy potential. Accordingly, we have $\frac{\partial \Psi_{pd}}{\partial \mathbf{C}} = \tilde{\Psi}_p^o(\mathbf{q})\,\mathbf{C}^{o\,-1}$. Eq. (4.6) can then be rephrased as

$$-\mathbf{Y} \equiv \frac{\partial \Psi}{\partial \mathbf{C}} = \frac{1}{2}\,\boldsymbol{\varepsilon}^e \otimes \boldsymbol{\varepsilon}^e + \tilde{\Psi}_p^o(\mathbf{q})\;\mathbf{C}^{o\,-1} \qquad (4.8)$$

I.4.2. Characterization of brittle damage

To account for the nature of *irreversibility* during microcracking processes, a damage criterion in terms of the anisotropic damage debonding-energy release rate ($-\mathbf{Y}$) is proposed as follows

$$g \equiv \hat{G}(-\mathbf{Y}, s, a, c, \rho) - r_t \leq 0 \tag{4.9}$$

where $\hat{G}$ is a function of the arguments. The damage process is then characterized in terms of the following irreversible, dissipative equations of evolution

$$\begin{gathered} \dot{\mathbf{C}} = -\dot{\mu}\,\frac{\partial g}{\partial(-\mathbf{Y})} \\ \dot{\mu} \geq 0, \quad g \leq 0, \quad \dot{\mu}\, g \equiv 0 \end{gathered} \tag{4.10}$$

Eq. (4.10) can be regarded as the Kuhn-Tucker conditions of the following "principle of maximum damage energy dissipation": "For a given local strain history, the actual damaged modulus $\mathbf{C}$ is the modulus that renders *maximum* damage energy dissipation". This principle is analogous to the principle of maximum plastic dissipation.

To properly include the anisotropic damage energy release rate $-\mathbf{Y}$ in the damage criterion (4.9) and the damage evolution equations (4.10), it is essential to define the *characteristic damage measure* ξ such that

$$\frac{\partial \xi}{\partial(-\mathbf{Y})} \equiv \mathbb{P}^{+}\, \mathbf{C}^{o}\, \mathbb{P}^{+} \tag{4.11}$$

where $\mathbb{P}^{+}$ is defined in Eq. (3.32). For an isotropic linear elasticity tensor $\mathbf{C}^{o}$, this warrants the following definition of ξ

$$\xi \equiv \tfrac{1}{2}\boldsymbol{\varepsilon}^{e+} : \mathbf{C}^{o} : \boldsymbol{\varepsilon}^{e+} + \tilde{\Psi}_{p}^{o} \left\{ \frac{(\frac{2}{3}G - K)}{6KG}\, \mathbf{1} : [\mathbb{P}^{+}\, \mathbf{C}^{o}\, \mathbb{P}^{+}] : \mathbf{1} + \frac{1}{2G} \sum_{i=1}^{9} \mathbf{e}_i : [\mathbb{P}^{+}\, \mathbf{C}^{o}\, \mathbb{P}^{+}] : \mathbf{e}_i \right\} \tag{4.12}$$

in which $\mathbf{e}_i$ is the i^{th} unit base tensor of the identity tensor $\mathbf{I}$, and K and G are the bulk and shear moduli, respectively. With this notation at hand, Eq. (4.9) is recast as follows

$$g \equiv \tilde{G}(\xi, s, a, c, \rho) - r_t \leq 0 \tag{4.13}$$

In addition, we define $H \equiv \frac{\partial \bar{G}}{\partial \xi}$ and $\dot{r}_t \equiv \dot{\mu} H$. From Eq. (4.13), it is observed that $\dot{r}_t \equiv \dot{\xi} H$ in the event of damage loading. Hence, we obtain $\dot{\mu} = \dot{\xi}$. The anisotropic damage (microcrack) evolution equation (4.10) then becomes

$$\dot{\mathbf{C}} = -\dot{\xi} H \, \mathbb{P}^+ \mathbf{C}^o \, \mathbb{P}^+ \tag{4.14}$$

It is emphasized that only tensile extensions in the principal directions contribute to microcrack growth according to Eq. (4.14). Physically, this treatment corresponds to anisotropic (*oriented*) brittle microcrack propagation. Clearly, the crucial quantities are ξ and $\mathbb{P}^+$. Note that $\frac{d}{dt}(\mathbb{P}^+ : \boldsymbol{\varepsilon}) \neq \mathbb{P}^+ : \dot{\boldsymbol{\varepsilon}}$ owing to the *nonlinear* nature of $\mathbb{P}^+$.

Remark 4.1. The anisotropic damage evolution rule (4.10) can be viewed as an extension of an earlier proposal in Ortiz [1985] (for mortar). There exist, nevertheless, several significant differences between the two formulations, which are as follows. (i) Ortiz [1985] assumed that the rate of irreversible (plastic) deformation is *coaxial* with the total rate of inelastic deformation (consisting of contributions of increasing damage and increasing permanent deformations). This assumption is not utilized in the present formulation. (ii) Ortiz's formulation [1985] focused on the rate of "added compliance" tensor while the present proposal focuses on the rate of "damaged secant (unloading) stiffness" tensor. It is emphasized that the two procedures are not equivalent. (iii) The "perfectly brittle" and "plastic microcracking" damage models in Ortiz [1985] are really *stress-based*. That is, the damage criterion and damage flow rule are based on the current *stress* tensor ($\boldsymbol{\sigma}$ or $\boldsymbol{\sigma}^+$); see Eq. (3.30),(3.34),(3.41),(3.47) in Ortiz [1985]. In particular, plastic (permanent) strains do *not* contribute to the damage criterion $\Phi(\boldsymbol{\sigma}, \mu)$ in Ortiz's models. As previously discussed in Sec. 3.2, stress-based damage criterion is inherently inadequate for coupled damage-elastoplasticity when plastic deformation is significant. □

Remark 4.2. Within the present context, plastic response can be characterized independently from the damage evolution in terms of *effective* stress quantities exactly as

in Section 3.3. □

Remark 4.3. A rate-dependent anisotropic damage mechanism can be constructed analogous to the formulation proposed in Section 3.4. In essence, we have the following evolution equations (see Eq. (3.28)):

$$\dot{\mathbf{C}} = -\mu < \bar{\phi}(g) > H \; \mathbb{P}^{+} \mathbf{C}^{o} \; \mathbb{P}^{+} \tag{4.15}$$

$$\dot{r}_t = \mu < \bar{\phi}(g) > H \qquad \square \tag{4.16}$$

Remark 4.4. The "mode I" microcrack opening and closing mechanisms can be easily accommodated within the proposed anisotropic damage framework. First, we define the "total stiffness loss tensor" as

$$\mathbf{C}^{d} \equiv \int_0^t (-\dot{\mathbf{C}})\, dt \tag{4.17}$$

Then we define the "active stiffness loss tensor" $\mathbf{C}^{d}_{act}$ (due to open microcracks) and the "active damaged secant stiffness tensor" $\mathbf{C}^{act}$ as follows:

$$\mathbf{C}^{d}_{act} \equiv \mathbb{P}^{+} \mathbf{C}^{d} \; \mathbb{P}^{+} \tag{4.18}$$

$$\mathbf{C}^{act} \equiv \mathbf{C}^{o} - \mathbf{C}^{d}_{act} \tag{4.19}$$

The stress/elastic-strain relationship then takes the form

$$\boldsymbol{\sigma} = \mathbf{C}^{act} : \boldsymbol{\varepsilon}^{e} \tag{4.20}$$

If all three principal strains ε_i are *tensile*, then we have $\mathbf{C}^{act} = \mathbf{C}$. On the other hand, if all ε_i are *compressive*, then $\mathbf{C}^{act} = \mathbf{C}^{o}$; i.e, the local microcrack is entirely *closed* under current state. It is noted that Ortiz [1985] proposed similar treatment to accommodate the active "added compliance" tensor. The results of the two treatments, however, are not equivalent since the inversion procedure destroys the equivalency. □

Remark 4.5. The anisotropic damage model presented in this section is based on *tensile* brittle failure mode. For some brittle materials such as concrete, however, both tensile and compressive failure modes can occur. To accommodate this phenomenon, Eq.

(4.14) can be modified, following an approach in Ortiz [1985] (see Eq. (3.18) therein), as follows to account for both tensile and compressive strain contributions:

$$\dot{\mathbf{C}} = -\dot{\xi}^{+} H^{+} \mathbb{P}^{+} \mathbf{C}^{o} \mathbb{P}^{+} - \dot{\xi}^{-} H^{-} \mathbb{P}^{-} \mathbf{C}^{o} \mathbb{P}^{-} \tag{4.21}$$

where the superscripts "+" and "-" signify the tensile and compressive damage evolution quantities, respectively. In addition, $\mathbb{P}^{-} \equiv \mathbf{I} - \mathbb{P}^{+}$. Therefore, tensile and compressive microcrack initiation and growth can develop simultaneously and separately (at different rates). □

Remark 4.6. Due to anisotropic damage evolution, an originally isotropic material becomes fully anisotropic, and the associated Poisson's ratio becomes a second-order anisotropic tensor. □

I.5. Computational algorithms for damage models

Numerical integration algorithms for the proposed elastoplastic-damage evolution equations are systematically explored in this section within the context of the finite element method. Use of the "operator split method" leads to a class of simple and efficient constitutive algorithms. In particular, new *three-step* operator split algorithms are presented for the proposed damage models. Strain softening and localization issues concerning damage models are also addressed.

I.5.1. Inviscid isotropic damage algorithm

We first summarize the locally averaged elastoplastic-damage rate constitutive equations:

$$\dot{\boldsymbol{\varepsilon}} = \nabla^s \dot{\mathbf{u}}(t)$$

$$\begin{cases} \dot{d}_t = \dot{\mu}\, H \\ \dot{r}_t = \dot{\mu} \\ \dot{\mu} \geq 0\,, \quad g(\xi_t\,, r_t) \leq 0\,, \quad \dot{\mu}\, g(\xi_t\,, r_t) = 0 \end{cases}$$

$$\dot{\boldsymbol{\sigma}} = \frac{\mathrm{d}}{\mathrm{d}t} \left[(1-d)\, \frac{\partial \Psi^o(\boldsymbol{\varepsilon}^e\,, \mathbf{q})}{\partial \boldsymbol{\varepsilon}^e} \right] \tag{5.1}$$

$$\begin{cases} \dot{\boldsymbol{\varepsilon}}^p = \dot{\lambda}\, \dfrac{\partial f}{\partial \bar{\boldsymbol{\sigma}}}\,(\bar{\boldsymbol{\sigma}}\,, \mathbf{q}) \\ \dot{\mathbf{q}} = \dot{\lambda}\, \mathbf{h}(\bar{\boldsymbol{\sigma}}\,, \mathbf{q}) \\ \dot{\lambda} \geq 0\,, \quad f(\bar{\boldsymbol{\sigma}}\,, \mathbf{q}) \leq 0\,, \quad \dot{\lambda}\, f(\bar{\boldsymbol{\sigma}}\,, \mathbf{q}) = 0 \end{cases}$$

where ξ is the damage energy release rate.

From an algorithmic point of view, the problem of integrating the evolution equations (5.1) amounts to updating the basic variables $\{ \boldsymbol{\sigma}, d, \boldsymbol{\varepsilon}^p, \mathbf{q} \}$ in a fashion consistent with the constitutive model. It is important to realize that during this updating process the history of strains $t \rightarrow \boldsymbol{\varepsilon} \equiv \nabla^s \mathbf{u}(t)$ is assumed to be given.

Equations of evolution (5.1) are to be solved incrementally over a sequence of given time steps $[t_n, t_{n+1}] \subset \mathbb{R}_+$, $n = 0, 1, 2, \cdots$. Thus, the initial conditions for Eq. (5.1) are

$$\{ \boldsymbol{\sigma}, d, \boldsymbol{\varepsilon}^p, \mathbf{q} \}\Big|_{t=t_n} = \{ \boldsymbol{\sigma}_n, d_n, \boldsymbol{\varepsilon}^p_n, \mathbf{q}_n \} \tag{5.2}$$

In accordance with the notion of *operator split*, we consider an *additive decomposition* of Eq. (5.1) into the following *elastic*, *plastic*, and *damage* parts.

Elastic part (5.3a)	*Plastic part* (5.3b)	*Damage part* (5.3c)
$\dot{\boldsymbol{\varepsilon}} = \nabla^S \dot{\mathbf{u}}(t)$	$\dot{\boldsymbol{\varepsilon}} = \mathbf{0}$	$\dot{\boldsymbol{\varepsilon}} = \mathbf{0}$
$\dot{d} = 0$	$\dot{d} = 0$	$\dot{d} = \begin{cases} \dot{\xi} H & \text{iff } g_t = \dot{g}_t = 0 \\ 0 & \text{otherwise} \end{cases}$
$\dot{r} = 0$	$\dot{r} = 0$	$\dot{r} = \begin{cases} \dot{\xi} & \text{iff } g_t = \dot{g}_t = 0 \\ 0 & \text{otherwise} \end{cases}$
$\dot{\boldsymbol{\sigma}} = (1-d)\, \frac{\partial^2 \Psi_o}{\partial \boldsymbol{\varepsilon}^{e\,2}} : \dot{\boldsymbol{\varepsilon}}$	$\dot{\boldsymbol{\sigma}} = -(1-d)\, \frac{\partial^2 \Psi_o}{\partial \boldsymbol{\varepsilon}^{e\,2}} : \dot{\boldsymbol{\varepsilon}}^p$	$\dot{\boldsymbol{\sigma}} = -\dot{d}\, \frac{\partial \Psi_o}{\partial \boldsymbol{\varepsilon}^e}$
$\dot{\boldsymbol{\varepsilon}}^p = \mathbf{0}$	$\dot{\boldsymbol{\varepsilon}}^p = \dot{\lambda}\, \frac{\partial f}{\partial \bar{\boldsymbol{\sigma}}} (\bar{\boldsymbol{\sigma}}, \mathbf{q})$	$\dot{\boldsymbol{\varepsilon}}^p = \mathbf{0}$
$\dot{\mathbf{q}} = \mathbf{0}$	$\dot{\mathbf{q}} = \dot{\lambda}\, \mathbf{h}(\bar{\boldsymbol{\sigma}}, \mathbf{q})$	$\dot{\mathbf{q}} = \mathbf{0}$

It is noted that the three columns of (5.3) do indeed add up to Eq. (5.1), in agreement with the notion of operator split (see Chorin et al. [1978]). Further, the first two columns of Eq. (5.3) define the classical elastoplastic problem (with damage variable d fixed) and the corresponding computational algorithm reduces to the elastic predictor/ plastic

corrector scheme. In what follows we give a step-by-step efficient integration procedure.

5.1.1. Elastic predictor. An algorithm consistent with problem (5.3a), referred to as the "elastic predictor" in the sequel, is given by the following process.

(i) *Strain update*: Given the incremental displacement field $\mathbf{u}_{n+1}$, the strain tensor is updated at Gauss points as

$$\boldsymbol{\varepsilon}_{n+1} = \boldsymbol{\varepsilon}_n + \nabla^S \mathbf{u}_{n+1} \tag{5.4}$$

(ii) *Elastic trial stress*: By merely performing function evaluation (**no** iteration), we obtain

$$\boldsymbol{\varepsilon}^{p\,trial}_{n+1} = \boldsymbol{\varepsilon}^p_n \quad ; \quad \mathbf{q}^{trial}_{n+1} = \mathbf{q}_n \quad ; \quad d^{trial}_{n+1} = d_n \tag{5.5}$$

$$\boldsymbol{\sigma}^{trial}_{n+1} = (1 - d_n)\, \frac{\partial \Psi^o (\boldsymbol{\varepsilon}_{n+1} - \boldsymbol{\varepsilon}^p_n\,,\, \mathbf{q})}{\partial \boldsymbol{\varepsilon}^e} \quad ; \quad \bar{\boldsymbol{\sigma}}^{trial}_{n+1} = \frac{\boldsymbol{\sigma}^{trial}_{n+1}}{(1 - d_n)} \tag{5.6}$$

5.1.2. Plastic corrector. To develop an algorithm consistent with the plastic part (5.3b), the plastic yield condition is checked first.

(iii) *Check for yielding*:

$$f\,(\bar{\boldsymbol{\sigma}}^{trial}_{n+1},\, \mathbf{q}^{trial}_{n+1}) \begin{cases} \leq 0 \ \textbf{elastic} \ \Rightarrow \ \text{go to step (v)} \\ > 0 \ \textbf{plastic} \ \Rightarrow \ \text{return mapping} \end{cases} \tag{5.7}$$

(iv) *Plastic return mapping corrector*: In the case of plastic loading, predictor stresses and internal variables are "returned back" to the yield surface along the algorithmic counterpart of the flow generated by (5.3b). One typically employs either the closest-point-projection or cutting plane algorithms (see, e.g., Simo and Ju [1987a,b]). Once the plastic consistency condition (in effective stress space) is enforced, state variables at the end of plastic corrector phase become

$$\{\, \bar{\boldsymbol{\sigma}}_{n+1}\,,\, d_n\,,\, \boldsymbol{\varepsilon}^p_{n+1}\,,\, \mathbf{q}_{n+1} \,\} \tag{5.8}$$

It should be noted that all existing return mapping algorithms for elastoplasticity become directly applicable (with **no** modification) in our elastoplastic-damage formulation.

5.1.3. Damage corrector. To complete the product formula algorithm, it remains to develop an algorithm consistent with the damage part (5.3c) which operates on *initial conditions* (5.8) to produce the final state $\{ \boldsymbol{\sigma}_{n+1}, d_{n+1}, \boldsymbol{\varepsilon}^p_{n+1}, \mathbf{q}_{n+1} \}$.

(v) *Damage evolution*: Compute "damage energy release rate" ξ_{n+1} according to

$$\xi_{n+1} \equiv \Psi^o(\boldsymbol{\varepsilon}^e_{n+1}, \mathbf{q}_{n+1}) \tag{5.9}$$

where $\boldsymbol{\varepsilon}^e_{n+1} \equiv \boldsymbol{\varepsilon}_{n+1} - \boldsymbol{\varepsilon}^p_{n+1}$. The damage variable d_{n+1} and damage threshold r_{n+1} are then given by

$$d_{n+1} = \begin{cases} d_n & \text{if } \xi_{n+1} - r_n \le 0 \\ d_n + (\xi_{n+1} - \xi_n)\, H_{n+1} & \textit{otherwise} \end{cases} \tag{5.10}$$

$$r_{n+1} \equiv max\, \{ r_n, \xi_{n+1} \} \tag{5.11}$$

$$\boldsymbol{\sigma}_{n+1} = (1 - d_{n+1})\, \bar{\boldsymbol{\sigma}}_{n+1} \tag{5.12}$$

It is emphasized that **no** iteration is required in the damage correction phase. Although plasticity and damage are *coupled* in rate equations (5.1), the algorithmic treatment renders *uncoupled* plasticity and damage algorithms. The simplicity and efficiency of the overall procedure are noteworthy.

I.5.2. Rate-dependent isotropic damage algorithm

The rate-dependent damage mechanism described in Section 3.4 can be efficiently implemented to obtain consistent and accurate incremental solutions. In this section, a *one-parameter* family of *unconditionally stable* integration algorithm is presented. Let us assume that damage loading is taking place; i.e., $g \equiv \xi_{n+1} - r_n > 0$. By applying the generalized mid-point rule to Eq. (3.29) we have

$$\begin{aligned} &\boldsymbol{\varepsilon}^e_{n+\alpha} \equiv \alpha\, \boldsymbol{\varepsilon}^e_{n+1} + (1-\alpha)\, \boldsymbol{\varepsilon}^e_n \quad ; \quad \xi_{n+\alpha} \equiv \Psi^0(\boldsymbol{\varepsilon}^e_{n+\alpha}, \mathbf{q}_{n+\alpha}) \\ &r_{n+\alpha} \equiv \alpha\, r_{n+1} + (1-\alpha)\, r_n \quad ; \quad d_{n+\alpha} = d_n + \Delta\mu_{n+\alpha}\, g_{n+\alpha}\, H_{n+\alpha} \\ &r_{n+\alpha} = r_n + \Delta\mu_{n+\alpha}\, g_{n+\alpha} \equiv r_n + \Delta\mu_{n+\alpha}\, (\xi_{n+\alpha} - r_{n+\alpha}) \end{aligned} \tag{5.13}$$

where $\alpha \in [0\,,\,1]$ and $\Delta\mu_{n+\alpha} \equiv \mu\,(t_{n+\alpha} - t_n)$. The amount of expansion experienced by the damage surface during the time step is computed from (5.13) by solving for r_{n+1} :

$$r_{n+\alpha} = \frac{[1 - (1-\alpha)\,\Delta\mu_{n+\alpha}]\,r_n + \Delta\mu_{n+\alpha}\,\xi_{n+1}}{1 + \alpha\,\Delta\mu_{n+\alpha}} \quad , \quad (\alpha \geq \tfrac{1}{2}) \tag{5.14}$$

From elementary numerical analysis, we note that algorithm (5.13),(5.14) is unconditionally stable for $\alpha \geq ½$ and second order accurate for $\alpha = ½$. Typically, the value $\alpha = 1$ corresponding to a backward-Euler finite difference scheme is employed. We will restrict our attention to this case in the ensuing development. The elastic predictor and plastic corrector are identical to the previous derivation shown in Section 5.1 . Only the damage corrector phase needs modification to account for rate dependency. The numerical integration scheme for rate-dependent damage corrector is summarized for convenience in Box **1** for the fully implicit case ($\alpha = 1$).

It is interesting to examine two limiting values $\mu \to 0$ and $\mu \to \infty$ of the damage viscosity coefficient, and their effect on the evolution of r_{n+1} and g_{n+1} .

(a) For $\mu \to 0$ (so that $\Delta\mu_{n+1} \to 0$), we obtain $r_{n+1} \to r_n$ and $g_{n+1} \to (\xi_{n+1} - r_n)$. Hence, *no* further damage takes place during the time increment and (in the absence of plastic flow) one has instantaneous elastic response.

(b) For $\mu \to \infty$ (so that $\Delta\mu_{n+1} \to \infty$), we have $r_{n+1} \to \xi_{n+1}$, $g_{n+1} \to 0$, and $\Delta d_{n+1} = \Delta\xi_{n+1}\,H_{n+1}$. This situation corresponds to the rate-independent damage characterization. Hence, as $\mu \to \infty$ we recover the inviscid damage model characterized in Section 3.2. Note that since $0 \leq \mu \leq \infty$ we must have $r_n \leq r_{n+1} \leq \xi_{n+1}$; namely, the expansion of the damage surface is properly bounded between the instantaneous elasticity and the inviscid damage limit.

BOX 1. *Rate-dependent damage corrector algorithm*

(1) Compute current "damage energy release rate" ξ_{n+1} according to

$$\xi_{n+1} \equiv \Psi^o(\boldsymbol{\varepsilon}^e_{n+1}, \mathbf{q}_{n+1}) .$$

(2) Check the damage loading criterion: $g(\xi_{n+1}, r_n) \equiv \xi_{n+1} - r_n > 0$?

YES : rate-dependent damage loading. Proceed to (3).

No : no further damage within this time step. Exit.

(3) Compute r_{n+1} and $\Delta\mu_{n+1}\, g_{n+1}$:

$$\Delta\mu_{n+1} = \mu\, \Delta t_{n+1}$$

$$r_{n+1} = \frac{[\, r_n + \Delta\mu_{n+1}\, \xi_{n+1}\,]}{[\, 1 + \Delta\mu_{n+1}\,]}$$

$$\Delta\mu_{n+1}\;\; g_{n+1} \equiv \Delta r_{n+1} = \frac{\Delta\mu_{n+1}}{1 + \Delta\mu_{n+1}} (\xi_{n+1} - r_n)$$

(4) Update damage parameter and stress:

$$\Delta d_{n+1} = \Delta\mu_{n+1}\;\; g_{n+1}\;\; H_{n+1}$$

$$d_{n+1} = d_n + \Delta d_{n+1}$$

$$\boldsymbol{\sigma}_{n+1} = (1 - d_{n+1})\, \bar{\boldsymbol{\sigma}}_{n+1}$$

I.5.3. Anisotropic damage algorithm

The operator splitting methodology developed in Section 5.1 can be immediately extended to accommodate anisotropic brittle damage mechanism outlined in Section 4.2. The three-step operator split is as follows.

Elastic part (5.15a)	*Plastic part* (5.15b)	*Damage part* (5.15c)
$\dot{\boldsymbol{\varepsilon}} = \nabla^S \dot{\mathbf{u}}(t)$	$\dot{\boldsymbol{\varepsilon}} = \mathbf{0}$	$\dot{\boldsymbol{\varepsilon}} = \mathbf{0}$
$\dot{\mathbf{C}} = \mathbf{0}$	$\dot{\mathbf{C}} = \mathbf{0}$	$\dot{\mathbf{C}} = \begin{cases} -\dot{\xi} H \, \mathbb{P}^+ \mathbf{C}^\circ \, \mathbb{P}^+ & \text{iff } g_t = \dot{g}_t = 0 \\ 0 & \text{otherwise} \end{cases}$
$\dot{r} = 0$	$\dot{r} = 0$	$\dot{r} = \begin{cases} \dot{\xi} & \text{iff } g_t = \dot{g}_t = 0 \\ 0 & \text{otherwise} \end{cases}$
$\dot{\boldsymbol{\sigma}} = \mathbf{C} : \dot{\boldsymbol{\varepsilon}}$	$\dot{\boldsymbol{\sigma}} = -\mathbf{C} : \dot{\boldsymbol{\varepsilon}}^p$	$\dot{\boldsymbol{\sigma}} = \dot{\mathbf{C}} : \boldsymbol{\varepsilon}^e$
$\dot{\boldsymbol{\varepsilon}}^p = \mathbf{0}$	$\dot{\boldsymbol{\varepsilon}}^p = \dot{\lambda} \frac{\partial f}{\partial \bar{\boldsymbol{\sigma}}} (\bar{\boldsymbol{\sigma}}, \mathbf{q})$	$\dot{\boldsymbol{\varepsilon}}^p = \mathbf{0}$
$\dot{\mathbf{q}} = \mathbf{0}$	$\dot{\mathbf{q}} = \dot{\lambda} \, \mathbf{h}(\bar{\boldsymbol{\sigma}}, \mathbf{q})$	$\dot{\mathbf{q}} = \mathbf{0}$

Computationally, the only modification needed concerns the anisotropic *damage corrector*, now involving an eigen-calculation to compute the positive (tensile) projection of the strain tensor.

5.3.1. Anisotropic damage corrector. Step (v) outlined in Section 5.1 is modified as follows.

(v) *Damage evolution:*

(a) Perform the spectral decomposition:

$$\boldsymbol{\varepsilon}_{n+1} = \sum_{i=1}^{3} \varepsilon_i \, \mathbf{p}_i \otimes \mathbf{p}_i \tag{5.16}$$

(b) Compute $\mathbf{Q}_{n+1}$ and $\mathbf{Q}^+_{n+1}$:

$$\mathbf{Q}_{n+1} = \sum_{i=1}^{3} \mathbf{p}_i \otimes \mathbf{p}_i \quad ; \quad \mathbf{Q}^+_{n+1} = \sum_{i=1}^{3} \hat{H}(\varepsilon_i) \, \mathbf{p}_i \otimes \mathbf{p}_i \tag{5.17}$$

Recall that $\hat{H}(\bullet)$ denotes the Heaviside step function.

(c) Compute the projection tensor $\mathbb{P}^{+}_{n+1}$ and the elastic tensile strain tensor $\boldsymbol{\varepsilon}^{e+}_{n+1}$:

$$\mathbb{P}^{+}_{ijkl} = Q^{+}_{ia}\, Q^{+}_{jb}\, Q_{ka}\, Q_{lb} \quad ; \quad \boldsymbol{\varepsilon}^{e+}_{n+1} = \mathbb{P}^{+}_{n+1} : \boldsymbol{\varepsilon}^{e}_{n+1} \tag{5.18}$$

(d) Compute the damage energy release rate ξ_{n+1} according to Eq. (4.12).

(e) Update anisotropic secant (unloading) stiffness modulus according to Eq. (4.13),(4.14):

$$\mathbf{C}_{n+1} = \begin{cases} \mathbf{C}_n & \text{if } \bar{G}(\xi_{n+1}, s, a, c, \rho) - r_n \le 0 \\ \mathbf{C}_n - (\xi_{n+1} - \xi_n)\, H_{n+1}\, \mathbb{P}^{+}_{n+1}\, \mathbf{C}^0\, \mathbb{P}^{+}_{n+1} & \textit{otherwise} \end{cases} \tag{5.19}$$

(f) Update the damage threshold r_{n+1} and Cauchy stress $\boldsymbol{\sigma}_{n+1}$:

$$r_{n+1} \equiv max\ \{\, r_n, \bar{G}_{n+1} \,\} \tag{5.20}$$

$$\boldsymbol{\sigma}_{n+1} = \mathbf{C}_{n+1} : \boldsymbol{\varepsilon}^{e}_{n+1} \tag{5.21}$$

Remark 5.1. A rate-dependent anisotropic damage algorithm can be constructed parallel to the rate-dependent isotropic damage algorithm given in Box 1 of Section 5.2. □

I.5.4. Strain softening and localization

It is now well known that there are uniqueness, well-posedness and numerical convergence problems associated with apparent "strain-softening" computations due to the loss of material *strong ellipticity*. As a result, finite element computations exhibit spurious mesh sensitivity when the mesh size goes to infinitesimal. These numerical difficulties may be overcome by means of the nonlocal damage theory (see, e.g, Eringen and Edelen [1972], Bazant et al. [1987], Xia et al. [1987]), or the viscous damage model presented in Section 3.4. The nonlocal damage characterization is physically very appealing at the microscale. However, experimental determination of the characteristic length l and the weighting function ω may be major problems. Recently, nevertheless, Bazant and Pijaudier-Cabot [1988] proposed an interesting method to determine the

characteristic length from experimental data. Further, nonlocal computation is to some extent incompatible with local finite element calculation and further enhancement in consistency and accuracy is needed. On the other hand, the proposed viscous damage mechanism is not only suitable for accommodating dynamic rate effect but also offers a possibility for controlling loss of ellipticity.

In particular, following a line of argument due to Valanis [1985], it can be shown that a viscous damage model of the type (3.29) satisfies the *positiveness* condition in Valanis [1985] and therefore leads to well-posed initial-value problems. To this end, we take differentiation of the relation $\boldsymbol{\sigma} = (1-d)\,\bar{\boldsymbol{\sigma}}$ and use Eq. (3.29) to obtain

$$\begin{aligned}\dot{\boldsymbol{\sigma}} &= (1-d)\,\dot{\bar{\boldsymbol{\sigma}}} - \dot{d}\,\bar{\boldsymbol{\sigma}} \\ &= (1-d)\,\bar{\mathbf{C}}^{ep} : \dot{\boldsymbol{\varepsilon}} - \mu < g > H\,\bar{\boldsymbol{\sigma}}\end{aligned} \tag{5.22}$$

We recall that $\bar{\boldsymbol{\sigma}} = \dfrac{\partial \Psi^o(\boldsymbol{\varepsilon}^e, \mathbf{q})}{\partial \boldsymbol{\varepsilon}^e}$ and $\bar{\mathbf{C}}^{ep}$ is the effective elastoplastic tangent stiffness given in Eq. (3.21). At a state defined by $\{\boldsymbol{\varepsilon}, d, r\}$, for two different stress rates $\dot{\boldsymbol{\sigma}}_1$, $\dot{\boldsymbol{\sigma}}_2$, and two different strain rates $\dot{\boldsymbol{\varepsilon}}_1$ and $\dot{\boldsymbol{\varepsilon}}_2$, it follows from (5.22) that

$$(\dot{\boldsymbol{\sigma}}_1 - \dot{\boldsymbol{\sigma}}_2) : (\dot{\boldsymbol{\varepsilon}}_1 - \dot{\boldsymbol{\varepsilon}}_2) = (1-d)\,(\dot{\boldsymbol{\varepsilon}}_1 - \dot{\boldsymbol{\varepsilon}}_2) : \bar{\mathbf{C}}^{ep} : (\dot{\boldsymbol{\varepsilon}}_1 - \dot{\boldsymbol{\varepsilon}}_2) > 0 \quad , \tag{5.23}$$

provided that the *undamaged* elastoplastic tangent modulus $\bar{\mathbf{C}}^{ep}$ is positive definite and $d < 1$. Thus, the material is *positive* in the sense of Valanis [1985].

In recent years, the applicability and limitations of distributed damage models to brittle materials such as concrete have been questioned by some researchers (see, e.g., Read and Hegemier [1984]). The fundamental question is to what extent the softening that is observed experimentally (for a boundary-value-type sufficiently large specimen) is a manifestation of local material behavior or, on the contrary, a global structural (boundary-value) effect brought about by fracture (macrocracks) and strain localization (such as shear band formation). To answer this question, we really should separate the issue into two parts. The first part concerns the boundary-value-type experimental testing

of specimens. The second part focuses on the local constitutive behavior (not boundary-value problem) within the framework of the unit cell based "*meso-mechanics*", the concept of characteristic length, together with the self-consistent method or homogenization technique. It is noted that, in the case of concrete, the characteristic length is approximately three times the aggregate size according to Bazant and Pijaudier-Cabot [1988], and a unit cell contains approximately 30-100 aggregates according to Krajcinovic and Fanella [1986].

For a sufficiently large (bigger than the unit cell) experimental specimen, the observed force-displacement curve indeed represents the *global* boundary-value-type response, rather than the *local* stress-strain behavior of a material element. In fact, in this boundary-value problem, there are three factors contributing to the *apparent* softening which is observed experimentally. These factors include: (a) The nucleation and growth of many distributed microcracks in the specimen, leading to local material softening in the sense of unit cell based meso-mechanics; (b) The strain localization phenomenon, resulting from the loss of ellipticity and stability of materials (see, e.g., Ortiz [1987b]); (c) The formation and propagation of global boundary-value-type macrocracks which are the direct products of *microcrack coalescence* in the specimen. It should be realized that the so-called "critical stress intensity factor" and "fracture toughness" in fracture mechanics literature are in fact also boundary-value-type *global* specimen properties, not local material properties. Based on the above statements, this writer agrees with those researchers who concluded that true material softening is less than the apparent global softening observed in experiments. Therefore, strictly speaking, the global force-displacement curve should not be directly interpreted as the local stress-strain curve of a material element.

On the other hand, within a statistically representative unit cell (meso-mechanics), distributed microcracks and strain softening (at the meso-scale) do make sense since distributed microcracks (within the unit cell) do induce stiffness degradation and strain

softening. One can factually apply the self-consistent method or the homogenization technique to compute the degradation of elastic and plastic material properties of a unit cell. These computations are, of course, related to the scale of the characteristic length of a material. Further, the so-called "size effects" (see, e.g., Sabnis and Mirza [1979], Bazant [1984], Fanella and Krajcinovic [1988]) are also closely related to the scale of characteristic length.

In summary, distributed damage models are suitable for modeling distributed (many) microcracks and material responses (*not* necessarily softening) in structural members before macrocracks become globally dominant. After the microcracks coalesce to form macrocracks, one can switch to fracture mechanics approaches provided that he takes into account: (i) the damage process zones in front of macrocracks (i.e., the macrocrack-microcrack interactions), and (ii) the damage-induced stiffness degradation and anisotropy in many (distributed) unit cells. Without these accounts, the resulting fracture calculations are not realistic nor meaningful. Conversely, direct application of a distributed damage model to solve a problem involving a single dominant macrocrack (in a boundary-value setting) is not likely to yield accurate results regarding macrocrack geometry and macrocrack opening displacement. Finally, distributed damage models are not suitable for predicting localization instability in materials.

I.6. Application to concrete and mortar. Experimental validation

Concrete is a three-phase cementitious composite material composed of aggregate, mortar and interface zone (see, e.g., Mehta [1986]). Each of the three phases is itself multi-phase in nature. For example, each aggregate particle may contain several minerals, and mortar is actually a mixture of cement paste and sand particles. Further, concrete has microcracks in the interface zone even before a structure is first loaded due to bleeding, shrinkage, cement hydration heat, etc.. The interface zone between the aggregate particle and mortar is typically 10 to 50 μm thick around large aggregate and is in general *weaker* than either aggregate or mortar. Due to this strength-limiting phase, the strength of concrete is considerably *lower* than that of mortar or aggregate.

Under compressive loading, microcracks initiate and propagate in the interface zone at low stress level, signifying a low energy barrier Ψ^o in the interface. These microcracks become unstable and propagate until they are arrested by cement paste matrix which has a higher value of debonding (damage) energy barrier Ψ^o . When the stress level is above 50% of the ultimate strength, matrix (mortar) microcracks initiate and gradually spread until they join the microcracks originating from the interface zone. The coalesced crack system then becomes continuous. The crack system may be arrested by aggregate, but may also leads to rupture of local materials. Most stable microcracks are of the size of aggregate facets. Hence, aggregate size is closely related to the characteristic length of concrete. Considerable damage energy is needed for the formation and extension of matrix microcracks under a compressive load. By contrast, under tensile loading much less damage energy is required to initiate and propagate microcracks in matrix and interface zone. Therefore, concrete fails in brittle fashion in tension mode and is much tougher (more ductile) in compression failure mode. It is also recognized that plasticity (permanent deformation) in concrete is primarily due to the extended microcrack surfaces which are not completely closed even under unloading.

Without resorting to multi-phase mixture theories and models, we employ either isotropic or anisotropic damage models in the following sections to simulate microcrack initiation and growth in the interface zone and mortar matrix of concrete. Experimental validation involves both rate-independent and rate-dependent concrete testing data. In addition, microstructural factors such as the average aggregate size/spacing ratio is considered in the microcrack kinetic equations.

I.6.1. Experimental validation of isotropic damage model

The isotropic energy-based damage mechanism developed in Section 3 is specialized in this section to capture basic features of the behavior of concrete and mortar within bounds of experimental error. A two-invariant cap plasticity model originally proposed by DiMaggio and Sandler [1971] (see also Sandler, DiMaggio and Baladi [1976]; Sandler and Rubin [1979]; Simo, Ju, Pister and Taylor [1988]) is employed to account for the plastic behavior of concrete. In view of the present shortcomings of experimental techniques and the wide scattering in available experimental data for concrete and mortar, a precise quantitative evaluation of the predicting capabilities of a given constitutive model does not seem to be warranted. Instead, it is felt that an *overall qualitative* reproduction of the main features of material behavior should play a dominant role in material modeling.

In particular, the kinetic law of microcrack growth Eq. (3.10) reduces to the following form:

$$\dot{d} = (k + \tfrac{1}{2})\, \dot{\xi}\, \tilde{H}(\xi\,, c\,, \rho) \tag{6.1}$$

where $k \equiv a/s$ is the average aggregate size/spacing ratio. Note that if aggregates are infinitely far away from one another, then k is 0. On the other hand, if aggregates are in contact, then k is 1 . The bigger k is, the higher the aggregate/cement interface area density is and hence the faster the microcrack density grows. Certainly, Eq. (6.1) is not a micromechanical kinetic equation. For exponentially growing progressive damage, the

evolution function $\bar{H}$ is assumed to be

$$\bar{H}(\xi, c, \rho) \equiv \frac{\xi_0 (1 - A)}{\xi^2} + A\, B\, \exp\left[B(\xi_0 - \xi)\right] \tag{6.2}$$

Here A and B are characteristic material parameters (implicit functions of c and ρ), and ξ_0 denotes the characteristic initial damage threshold. These parameters can be estimated in a systematic manner from suitable experimental data. The average aggregate size/spacing factor k is taken as 0.7 for the following concrete specimens.

6.1.1. Colorado concrete data. The data for the following examples are taken from the well-documented experimental program conducted at the University of Colorado (see Scavuzzo et al. [1983]) on a systematic three dimensional testing of concrete ($f'_c \approx 4$ ksi). The program consists of six major series of non-conventional multiaxial cyclic stress-strain curves. It is noted that replicate tests were run for some experiments, which enable us to assess the relative consistency of experimental data. The numerical results reported below not only include fitting of the model to complicated 3-D stress paths but, in addition, *predictions* of material behavior obtained by exercising the model against experimental results.

Circular stress path tests. Tests 3-3 and 3-4 are replicates concerning the following loading paths. The specimens are first subjected to hydrostatic monotonic loading to a specified deviatoric plane, followed by deviatoric loading along the triaxial compression path until completion of the specified circular path. The model parameters are obtained by optimal fitting with respect to test 3-3. These model parameters are then employed in the subsequent simulation intended to predict the behavior observed in the replicate test 3-4 under significant experimental data perturbations. In spite of considerable data corruption, good overall predictive capability of the model is observed, as illustrated in Figures 3 and 4. To demonstrate the effect of the aggregate size/spacing factor k on damage growth, three hypothetical k values (k = 0.1, 0.5, 0.9) are further employed to simulate test 3-3; see Figure 5. It is clear that as k increases, microcrack density increases and

therefore stress response degrades.

Cyclic simple shear tests. Tests 2-3 and 2-4 are intended to explore concrete response to deviatoric simple shear cycles with stress reversal about the hydrostatic state. Material parameter estimation is performed with respect to test 2-4, and prediction is exercised for test 2-3 (replicate). The results are shown in Figures 6 and 7. The overall qualitative agreement between simulations and experiments is satisfactory.

6.1.2. Uniaxial compression tests. In this example, we perform two replicate uniaxial unconfined compression tests of mortar (with $f'_c \approx 12$ ksi). The composition of mortar is as follows: cement 649 g, water 195 g, sand 150 g, plasticizer 9.1 ml. Ottawa sand with a fineness modulus of 2.11 is employed. The gradation is as follows: 33.33% retained on sieve #30, 77.77% retained on sieve #50 and 100% retained on sieve #100. Material parameters are obtained by optimal fitting with respect to test 'M1' and prediction is carried out for test 'M2'; see Figures 8 and 9. The effect of the inclusion size/spacing factor k (sand concentration) on damage growth can be seen again from Figure 10 in which three hypothetical k values (k = 0.1, 0.5, 0.9) are employed to simulate test 'M1'.

I.6.2. Experimental validation of rate-dependent isotropic damage model

Two dynamic uniaxial compression concrete tests (Suaris and Shah [1983][1984]) are considered in this section based on the rate-dependent isotropic damage algorithm given in BOX 1. Two different constant strain rates are employed: fast loading ($\dot{\varepsilon} = 0.088\ \text{sec}^{-1}$) and slow loading ($\dot{\varepsilon} = 1.0e{-}6\ \text{sec}^{-1}$). The static uniaxial compressive strength is estimated to be 6.8 ksi.

Figure 11 shows experimental and simulated results at two strain rates. Good *qualitative* and *quantitative* agreement between the model and the experimental data is obtained. The rate enhancement of stress response due to the viscous damage mechanism is clearly demonstrated. That is, growth of microcracks is *retarded* at higher strain rates.

I.6.3. Experimental validation of anisotropic damage model

The fourth order anisotropic damage mechanism presented in Section 4.2 is employed next to simulate anisotropic damage growth in mortar. We recall from Eq. (4.21) in Remark 4.4 that tensile and compressive strains can independently contribute to microcrack evolution. The uniaxial unconfined compression mortar tests previously considered in Sec. 6.1 are taken as examples again in this section. Under uniaxial compression, the fourth order anisotropic damage mechanism reduces to an orthotropic damage mechanism and the reproduction of the "splitting mode" of cylindrical specimens is sought.

Since the tensile strength f'_t is approximately one-tenth of the compressive strength f'_c , it appears reasonable to assume that the *compressive* microcrack growth rate (in the axial direction) is approximately 10% of the *tensile* (mode I) microcrack growth rate (in the lateral direction). As a consequence of the orthogonal eigenprojections ($\mathbb{P}^+$ and $\mathbb{P}^-$) and different growth rates, microcrack develop in the lateral and axial directions progressively and independently. In particular, microcracks form rapidly along axes parallel to the axis of loading, reduce the lateral stiffness gradually, and ultimately lead to the splitting failure mode. Experimental and numerical results for tests 'M1' and 'M2' are shown in Figures 12 and 13. In addition, the apparent Poisson's ratios for tests 'M1' and 'M2' are displayed in Figures 14 and 15. It is emphasized that microcrack growth and stiffness degradation in the lateral direction is much much faster than that in the axial direction due to our anisotropic damage mechanism.

I.6.4. Experimental validation of rate-dependent anisotropic damage model

We re-examine the rate-dependent concrete tests previously discussed in Section 6.2 by a rate-dependent anisotropic damage model (see Remark 5.1). Again, microcracks develop rapidly along axes parallel to the axis of loading, and the splitting failure mode is obtained. Experimental and numerical results for two different rates ($\dot{\varepsilon} = 0.088\ \text{sec}^{-1}$

and $\dot{\varepsilon} = 1.0e{-}6\ \mathrm{sec}^{-1}$) are shown in Figure 16. The capability of the proposed mechanism to simulate rate dependency and "splitting modes" of cylindrical concrete specimens is noteworthy.

I.7. Closure

A number of energy-based isotropic and anisotropic damage models have been proposed in this paper to characterize microcrack initiation and growth in ductile and brittle materials. Thermodynamics basis, general nonlinear response, strain rate dependency, damage threshold, damage kinetic law, microcrack opening and closing, coupling of damage and plasticity, and anisotropic (brittle) damage mechanism have been presented within the general framework of damage mechanics, unit cell and homogenization concept. Damage initiation and propagation are linked to the (locally averaged) "total undamaged strain energy" $\Psi^o(\boldsymbol{\varepsilon}^e, \mathbf{q})$, which is checked against the debonding energy (current damage threshold) required for unstable microcrack growth. It is noted that in the current literature damage models are either simply elastic-damageable or containing improper elastoplastic-damage thermodynamics and mechanisms.

Another essential purpose of the present work is to demonstrate that the proposed classes of elastoplastic-damage constitutive equations are well suited for large scale computation in spite of their sophistication. Use of the operator splitting methodology leads to three-step integration algorithms which, in addition to isotropic and anisotropic damage, are capable of accommodating general elastic-plastic response.

Experimental validation of the proposed models against concrete and mortar specimens are also given. We observe good qualitative and quantitative agreement between experimental data for concrete and mortar and the proposed models. In particular, softening behavior is well captured. Micromechanically based damage theories will be objectives of our future research.

I.8. References

Ashby, M.F. [1979], "Micromechanisms of fracture in static and cyclic failure," in *Fracture Mechanics: Current Status, Future Prospects,*" Proc. of a conference held at Cambridge Univ., March 1979, pp. 1-27.

Bakhtar, K., et. al. [1985], "Concrete material properties," TerraTek Research, *DNA Concrete Meeting*, April 1985, Utah.

Bazant, Z.P. [1984], "Size effect in blunt fracture: concrete, rock, and metal," *J. Eng. Mech.*, ASCE, Vol. 110, No. 4, pp. 518-535.

Bazant, Z.P., F.B. Lin and G. Pijaudier-Cabot [1987], "Yield limit degradation: Nonlocal continuum model with local strain," in Proc. of Int. Conf. on Comp. Plast., pp. 1757-1780, April 6-10, 1987, Barcelona, Spain.

Bazant, Z.P. and G. Pijaudier-Cabot [1988], "Nonlocal continuum damage and measurement of characteristic length," in *Mechanics of Composite Materials - 1988*, pp. 79-86, Proc. of Joint ASME/SES Conf., June 20-22, 1988, Berkeley, Calif..

Budiansky, B. and R.J. O'Connel [1976], "Elastic moduli of a cracked solid," *Int. J. Solids & Struct.*, Vol. 12, pp. 81-97.

Chaboche, J.L. [1974], "Une loi différentielle d'endommagement de fatigue avec cumulation non linéaire," *Rev. Francaise de Mécanique*, No. 50-51.

Chaboche, J.L. [1981], "Continuous damage mechanics - A tool to describe phenomena before crack initiation," *Nucl. Eng. Des.*, Vol. 64, pp. 233-247.

Chaboche, J.L. [1982], "Le Concept de contrainte effective appliqué à l'élasticité et à la viscoplasticité en présence d'un endommagement anisotrope," *Mechanical Behavior of Anisotropic Solids*, Proc. EUROMECH Colloque 115, June 1979, ed. by J.P. Boehler, Martinus Nijhoff Publishers, pp. 737-760.

Chorin, A., T.J.R. Hughes, M.F. McCracken and J.E. Marsden [1978], "Product formulas and numerical algorithms," *Commun. Pure Appl. Math.*, Vol. 31, pp. 205-256.

Chow, C.L. and J. Wang [1987a], "An anisotropic theory of continuum damage mechanics for ductile fracture," *Eng. Fract. Mech.*, Vol. 27, No. 5, pp. 547-558.

Chow, C.L. and J. Wang [1987b], "An anisotropic continuum damage theory and its application to ductile crack initiation," in Proc. of ASME Winter Annual Meeting, pp. 1-9, ed. by A.S.D. Wang and G.K. Haritos, Dec. 13-18, 1987, Boston, Mass..

Coleman, B.D. and M. Gurtin [1967], "Thermodynamics with internal variables," *J. Chem. Physics*, Vol. 47, pp. 597-613.

Cordebois, J.P. and F. Sidoroff [1979], "Damage induced elastic anisotropy," *Mechanical Behavior of Anisotropic Solids*, Proc. EUROMECH Colloque 115, June 1979, ed. by J.P. Boehler, Martinus Nijhoff Publishers, pp. 761-774.

Cordebois, J.P. and F. Sidoroff [1982], "Endommagement anisotrope en élasticité et plasticité," *J. de Mécanique Théorique et Appliquée* No. Spécial, pp. 45-59.

DiMaggio, F.L., and I.S. Sandler [1971], "Material models for granular soils," *J. Eng. Mech. Div.*, ASCE, Vol. 97, No. EM3, pp. 935-950.

Dragon, A. [1985], "Plasticity and ductile fracture damage: study of void growth in metals," *Engng. Fract. Mech.*, Vol. 21, No. 4, pp. 875-885.

Dragon, A. and A. Chihab [1985], "On finite damage: ductile fracture-damage evolution," *Mech. Mater.*, Vol. 4, pp. 95-106.

Eringen, A.C. [1968], "Mechanics of micromorphic continua," *Mechanics of Generalized Continua*, pp. 18-35, Ed. by E. Kroner, Springer-Verlag.

Eringen, A.C. [1983], "Interaction of a dislocation with a crack," *J. Appl. Phys.*, Vol. 54, No. 12, pp. 6811-6817.

Eringen, A.C. [1987], "Theory of nonlocal elasticity and some applications," *Res Mechanica*, Vol. 21, pp. 313-342.

Eringen, A.C. and D.G.B. Edelen [1972], "On nonlocal elasticity," *Int. J. Eng. Sci.*, Vol. 10, pp. 233-248.

Fanella, D. and D. Krajcinovic [1988], "Size effect in concrete," *J. of Eng. Mech.*, ASCE, Vol. 114, No. 4, pp. 704-715.

Francois, D. [1984], "Fracture and damage mechanics of concrete," *Application of Fracture Mechanics to Cementitious Composites*, NATO Advanced Research Workshop, Sep. 4-7, 1984, Northwestern University, ed. by S. P. Shah, pp. 97-110.

Grady, D.E. and M.E. Kipp [1980], "Continuum modelling of explosive fracture in Oil shale," *Int. J. Rock Mech. Min. Sci. & Geomech. Abstr.*, Vol. 17, pp. 147-157.

Hill, R. [1967], "The essential structure of constitutive laws for metal composites and polycrystals," *J. Mech. Phy. Solids*, Vol. 15, pp. 79-95.

Hill, R. [1972], "On constitutive macro-variables for heterogeneous solids at finite strain," *Proc. Royal Soc. London*, Ser. A, Vol. 326, pp. 131-147.

Horii, H. and S. Nemat-Nasser [1983], "Overall moduli of solids with microcracks: Load induced anisotropy," *J. Mech. Phys. Solids*, Vol. 31, No. 2, pp. 155-171.

Hult, J. [1974], "Creep in continua and structures," *Topics in Applied Continuum Mechanics*, Springer-Verlag, Vienna.

Ilankamban, R. and D. Krajcinovic [1987], "A constitutive theory for progressively deteriorating brittle solids," *Int. J. Solids & Struct.*, Vol. 23, No. 11, pp. 1521-1534.

Ju, J.W., P.J.M. Monteiro and A.I. Rashed [1989], "On continuum damage of cement paste and mortar as affected by porosity and sand concentration," *J. Eng. Mech.*, ASCE, Vol. 115, No. 1, pp. 105-130.

Ju, J.W., J.C. Simo, K.S. Pister and R.L. Taylor [1987], "A parameter estimation algorithm for inelastic material models," in Proc. of the Second Int. Conf. and Short Course on Constitutive Laws for Eng. Mater.: Theory and Appl., pp. 1233-1240, ed. by C.S. Desai et al., Jan. 5-10, 1987, Tucson, Arizona.

Kachanov, L.M. [1958], "Time of the rupture process under creep conditions," *IVZ Akad Nauk*, S.S.R., Otd Tech Nauk, No. 8, pp. 26-31.

Kachanov, M. [1980], "Continuum model of medium with cracks," *J. Eng. Mech. Div.*, ASCE, Vol. 106, No. EM5, pp. 1039-1051.

Kachanov, M. [1981], "Crack growth under conditions of creep and damage," in A. Ponter and D. Hayhurst (Eds.), *Creep in Structures*, Springer-Verlag, Berlin, pp. 520-524.

Kachanov, M. [1982], "A microcrack model of rock inelasticity. Part I" *Mech. Mater.*, Vol. 1, pp. 19-27. pp. 1039-1051.

Kachanov, M. [1984], "On brittle fracture of a thin plastic interlayer in creep conditions," in G. Dvorak and R. Shield (Eds.), *Mechanics of Material Behavior*, Elsevier Sc. Publ., Amsterdam, pp. 191-200.

Kachanov, M. [1987a], "Elastic solids with many cracks: A simple method of analysis," *Int. J. Solids & Struct.*, Vol. 23, No. 1, pp. 23-43.

Kachanov, M. [1987b], "On modelling of anisotropic damage in elastic-brittle materials - A brief review," in Proc. of ASME Winter Annual Meeting, pp. 99-105, ed. by A.S.D. Wang and G.K. Haritos, Dec. 13-18, 1987, Boston, Mass..

Krajcinovic, D. [1983a], "Creep of structures - A continuous damage mechanics approach," *ASME J. Struct. Mech.*, Vol. 11, No. 1, pp. 1-11.

Krajcinovic, D. [1983b], "Constitutive equations for damaging materials," *ASME J. Appl. Mech.*, Vol. 50, pp. 355-360.

Krajcinovic, D. [1985], "Constitutive theories for solids with defective microstructure," in *Damage Mechanics and Continuum Modeling*, ed. by N. Stubbs and D. Krajcinovic, ASCE, pp. 39-56.

Krajcinovic, D. [1987], "Micromechanical basis of phenomenological models," in *Continuum Damage Mechanics: Theory and Application*, Ed. by D. Krajcinovic and J. Lemaitre, Springer-Verlag, to appear.

Krajcinovic, D. and D. Fanella [1986] "A micromechanical damage model for concrete," *Eng. Fract. Mech.*, Vol. 25, No. 5/6, pp. 585-596.

Krajcinovic, D. and G.U. Fonseka [1981] "The continuous damage theory of brittle materials," Parts I & II, *ASME J. Appl. Mech.*, Vol. 48, pp. 809-824.

Leckie, F. and D. Hayhurst [1974], "Creep rupture of structures," *Proc. R. Soc. London,* A 240, pp. 323.

Lemaitre, J. [1971], "Evaluation of dissipation and damage in metals", Proc. I.C.M. (1), Kyoto, Japan.

Lemaitre, J. [1984], "How to use damage mechanics," *Nucl. Eng. Design,* Vol. 80, pp. 233-245.

Lemaitre, J. [1985], "A continuous damage mechanics model for ductile fracture," *J. of Eng. Mater. Tech.*, Vol. 107, pp. 83-89.

Lemaitre, J. [1986], "Plasticity and damage under random loading," in Proc. of the Tenth U.S. National Congress of Appl. Mech., ASME, pp. 125-134, ed. by J.P. Lamb, June 16-20, 1986, Austin, Texas.

Lemaitre, J. and J.L. Chaboche [1974], "A nonlinear model of creep-fatigue damage cumulation and interaction," Proc. IUTAM Symp. of Mech. of Visco-elastic Media and Bodies, Springer-Verlag, Gothenburg.

Lemaitre, J. and J.L. Chaboche [1978], "Aspects phénoménologiques de la rupture par endommagement," *J. de Méca. Appl.*, Vol. 2, No. 3, pp. 317-365.

Lemaitre, J. and J. Dufailly [1977], "Modélisation et identification de l'endommagement plastique des métaux," 3^{eme} Congrès Francais de Mécanique, Grenoble.

Lemaitre, J. and A. Plumtree [1979], "Application of damage concepts to predict creep-fatigue failures," *J. Eng. Mater. Tech.*, Trans. ASME, Vol. 101, pp. 284-292.

Loland, K.E. [1980], "Continuous damage model for load-response estimation of concrete", *Cem. and Conc. Res.*, Vol. 10, pp. 395-402.

Lorrain, M. and K.E. Loland [1983], "Damage theory applied to concrete," *Fracture Mechanics of Concrete*, ed. by F. H. Wittmann, pp. 341-369, Elsevier.

Marigo, J.J. [1985], "Modeling of brittle and fatigue damage for elastic material by growth of microvoids," *Engng. Fract. Mech.*, Vol. 21, No. 4, pp. 861-874.

Mazars, J. [1982], "Mechanical damage and fracture of concrete structures," *Advances in Fracture Research (Fracture 81)*, Vol. 4., pp. 1499-1506, Pergamon Press.

Mazars, J. [1986], "Description of the behavior of composite concretes under complex loadings through continuum damage mechanics," in Proc. of the Tenth U.S. National Congress of Appl. Mech., ASME, pp. 135-139, ed. by J.P. Lamb, June 16-20, 1986, Austin, Texas.

Mazars, J. and J. Lemaitre [1984], "Application of continuous damage mechanics to strain and fracture behavior of concrete," *Application of Fracture Mechanics to Cementitious Composites*, NATO Advanced Research Workshop, Sep. 4-7, 1984, Northwestern University, ed. by S. P. Shah, pp. 375-388.

Murakami, S. [1981], "Effects of cavity distribution in constitutive equations of creep and creep damage," EUROMECH Colloque on Damage Mechanics, Cachan, France.

Ortiz, M. [1985], "A constitutive theory for the inelastic behavior of concrete," *Mech. of Materials*, Vol. 4, pp. 67-93.

Ortiz, M. [1987a], "A method of homogenization of elastic media," *Int. J. Eng. Sci.*, Vol. 25, No. 7, pp. 923-934.

Ortiz, M. [1987b], "An analytical study of the localized failure modes of concrete," *Mech. of Materials*, Vol. 6, pp. 159-174.

Ortiz, M. and J.C. Simo [1986], "An analysis of a new class of integration algorithms for elastoplastic constitutive relations," *Int. J. Num. Meth. Engng.*, Vol. 23, pp. 353-366.

Perzyna, P. [1966], "Fundamental problems in viscoplasticity," *Advances in Applied Mechanics*, Vol. 9, pp. 244-368.

Pijaudier-Cabot, G. and Z.P. Bazant [1987], "Nonlocal damage theory," *J. Eng. Mech.*, ASCE, Vol. 113, No. 10, pp. 1512-1533.

Rabotnov, I.N. [1963], "On the equations of state for creep," *Progress in Applied Mechanics - the Prager Anniversary Volume*, pp. 307-315.

Read, H.E. and G.A. Hegemier [1984], "Strain softening of rock, soil and concrete - A review article," *Mech. of Materials*, Vol. 3, pp. 271-294.

Resende, L. and J.B. Martin [1984], "A progressive damage continuum model for granular materials," *Comp. Meth. in Appl. Mech. Engng.*, Vol. 42, pp. 1-18.

Sabnis, G.M. and S.M. Mirza [1979], "Size effects in model concretes," *J. Struct. Div.*, A.S.C.E., Vol. 105, No. ST6, pp. 1007-1020.

Sandler, I.S., F.L. DiMaggio, and G.Y. Baladi [1976], "Generalized cap model for geological materials," *J. Geotech. Eng. Div.*, A.S.C.E., Vol. 102, No. GT7, pp. 683-699.

Sandler, I.S. and D. Rubin [1979], "An algorithm and a modular subroutine for the cap model," *Int. J. Numer. Analy. Meth. Geomech.*, Vol. 3, pp. 173-186.

Scavuzzo, R., T. Stankowski, K.H. Gerstle and H.Y. Ko [1983], "Stress-strain curves for concrete under multiaxial load histories," NSF CME-80-01508, Department of Civil Engineering, University of Colorado, Boulder.

Simo, J.C. and J.W. Ju [1987a], "Stress and strain based continuum damage models. Part I: Formulation," *Int. J. Solids & Struct.*, Vol. 23, No. 7, pp. 821-840.

Simo, J.C. and J.W. Ju [1987b], "Stress and strain based continuum damage models. Part II: Computational aspects," *Int. J. Solids & Struct.*, Vol. 23, No. 7, pp. 841-869.

Simo, J.C. and J.W. Ju [1987c], "On continuum damage-elastoplasticity at finite strains: A computational framework," *Comput. Mech.*, in press.

Simo, J.C., J.W. Ju, K.S. Pister and R.L. Taylor [1988], "An assessment of the cap model: consistent return algorithms and rate-dependent extension," *J. Eng. Mech.*, ASCE, Vol. 114, No. 2, pp. 191-218.

Suaris, W. and S.P. Shah [1983], "Properties of concrete subjected to impact," *J. Struct. Eng.*, ASCE, Vol. 109, No. ST7, pp. 1727-1741.

Suaris, W. and S.P. Shah [1984], "Rate-sensitive damage theory for brittle solids," *J. Eng. Mech.*, ASCE, Vol. 110, No. 6, pp. 985-997.

Sumarac, D. and D. Krajcinovic [1987], "A self-consistent model for microcrack-weakened solids," *Mech. Mater.*, Vol. 6, pp. 39-52.

Takeda, J. and H. Tachikawa [1971], "Deformation and fracture of concrete subjected to dynamic load," in Proc. Int. Conf. on Mech. Behavior of Mater., Vol. 4, *Concrete and cement paste glass and ceramics*, pp. 267-277, Aug. 15-20, 1971, Kyoto, Japan.

Talreja, R. [1985], "A continuum mechanics characterization of damage in composite materials," *Proc. R. Soc. London*, Ser. A, Vol. 399, pp. 195-216.

Terrien, M. [1980], "Emission acoustique et comportement mécanique post-critique d'un béton sollicité en traction," *Bulletin de Liaison des laboratoires des Ponts et Chaussées*, No. 105, pp. 65-72.

Vakulenko, A.A. and M.L. Kachanov [1971], "Continuum theory of medium with cracks," *Mekh. Tverdogo Tela*, Vol. 4, pp. 159-166.

Valanis, K.C. [1985], "On the uniqueness of solution of the initial value problem in softening materials," *J. of Appl. Mech.*, Vol. 52, pp. 649-653.

Weitsman, Y. [1987], "Coupled damage and moisture-transport in fiber-reinforced, polymeric composites," *Int. J. Solids & Struct.*, Vol. 23, No. 7, pp. 1003-1025.

Wu, C.H. [1985], "Tension-compression test of a concrete specimen via a structure damage theory," in *Damage Mechanics and Continuum Modeling*, ed. by N. Stubbs and D. Krajcinovic, ASCE, pp. 1-12.

Xia, S., G. Li and H. Lee [1987], "A nonlocal damage theory," *Int. J. Fract.*, Vol. 34, pp. 239-250.

I.9. Figure captions and figures

Figure 1. Hypothesis of strain equivalence.

Figure 2. Illustration of added flexibility. $\hat{\varepsilon}^e$ and ε^d denote the truly elastic strain and added deformation due to microcracks, respectively.

Figure 3. Comparison of the experimental and isotropic simulated (*fitted*) data for Colorado concrete test 3-3.

Figure 4. Comparison of the experimental and isotropic simulated (*predicted*) data for Colorado concrete test 3-4.

Figure 5. Demonstration of the effect of the aggregate size/spacing factor k on the damage growth and stress response for test 3-3.

Figure 6. Comparison of the experimental and isotropic simulated (*fitted*) data for Colorado concrete test 2-4.

Figure 7. Comparison of the experimental and isotropic simulated (*predicted*) data for Colorado concrete test 2-3.

Figure 8. Comparison of the experimental and isotropic simulated (*fitted*) data for uniaxial compression mortar test 'M1'.

Figure 9. Comparison of the experimental and isotropic simulated (*predicted*) data for uniaxial compression mortar test 'M2'.

Figure 10. Demonstration of the effect of the aggregate size/spacing factor k on the damage growth and stress response for test 'M1'.

Figure 11. Comparison of the experimental and isotropic simulated dynamic stress-strain curves for uniaxial compression test of concrete specimens.

Figure 12. Comparison of the experimental and anisotropic simulated (*fitted*) data for uniaxial compression mortar test 'M1'.

Figure 13. Comparison of the experimental and anisotropic simulated (*predicted*) data for uniaxial compression mortar test 'M2'.

Figure 14. Apparent Poisson's ratio for the mortar test 'M1'.

Figure 15. Apparent Poisson's ratio for the mortar test 'M2'.

Figure 16. Comparison of the experimental and anisotropic simulated dynamic stress-strain curves for uniaxial compression test of concrete specimens.

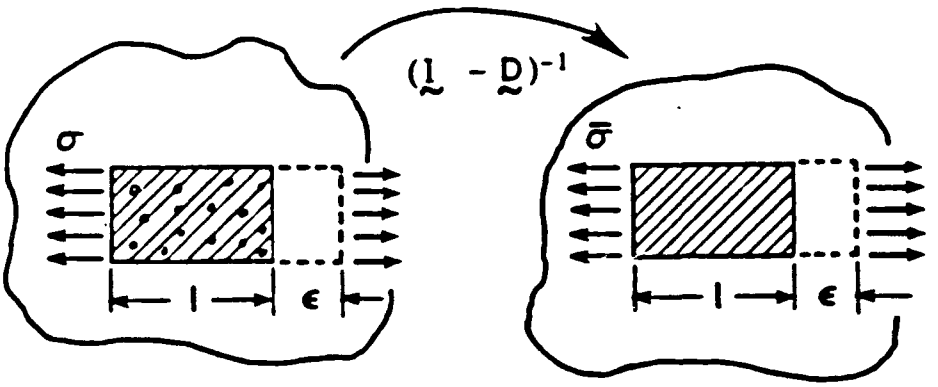

PHYSICAL SPACE

EFFECTIVE SPACE

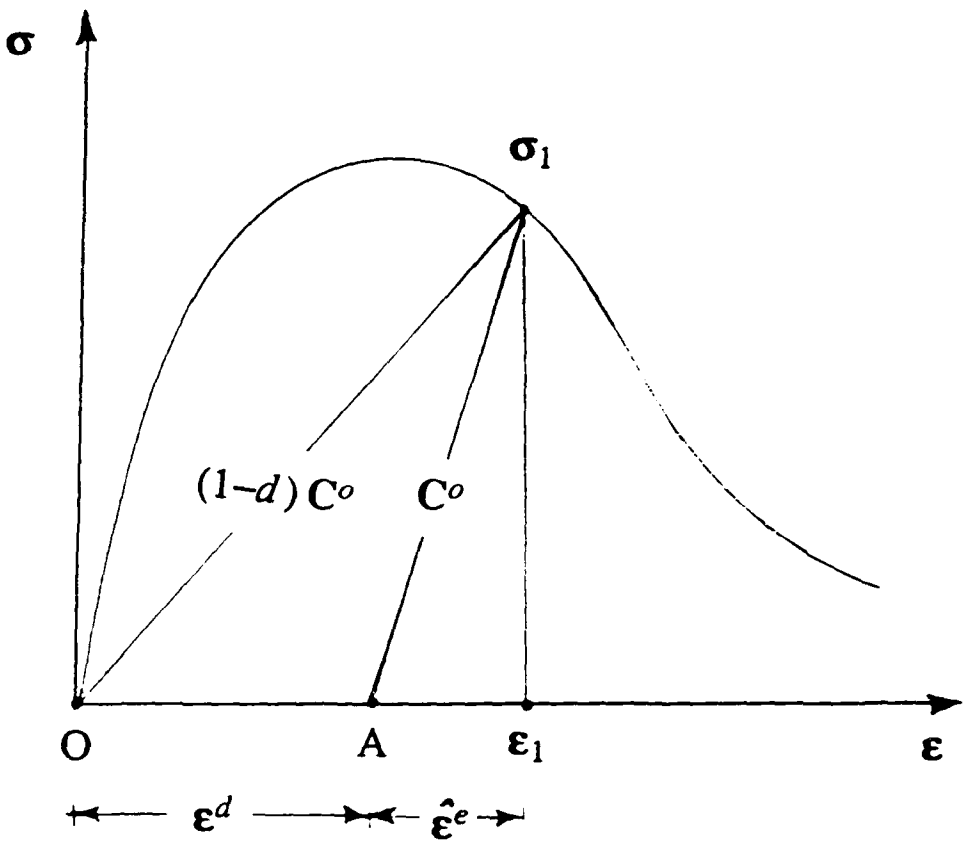
σ
σ1
(1–d) C^o
C^o
O
A
ε1
ε
ε^d
ε̂^e

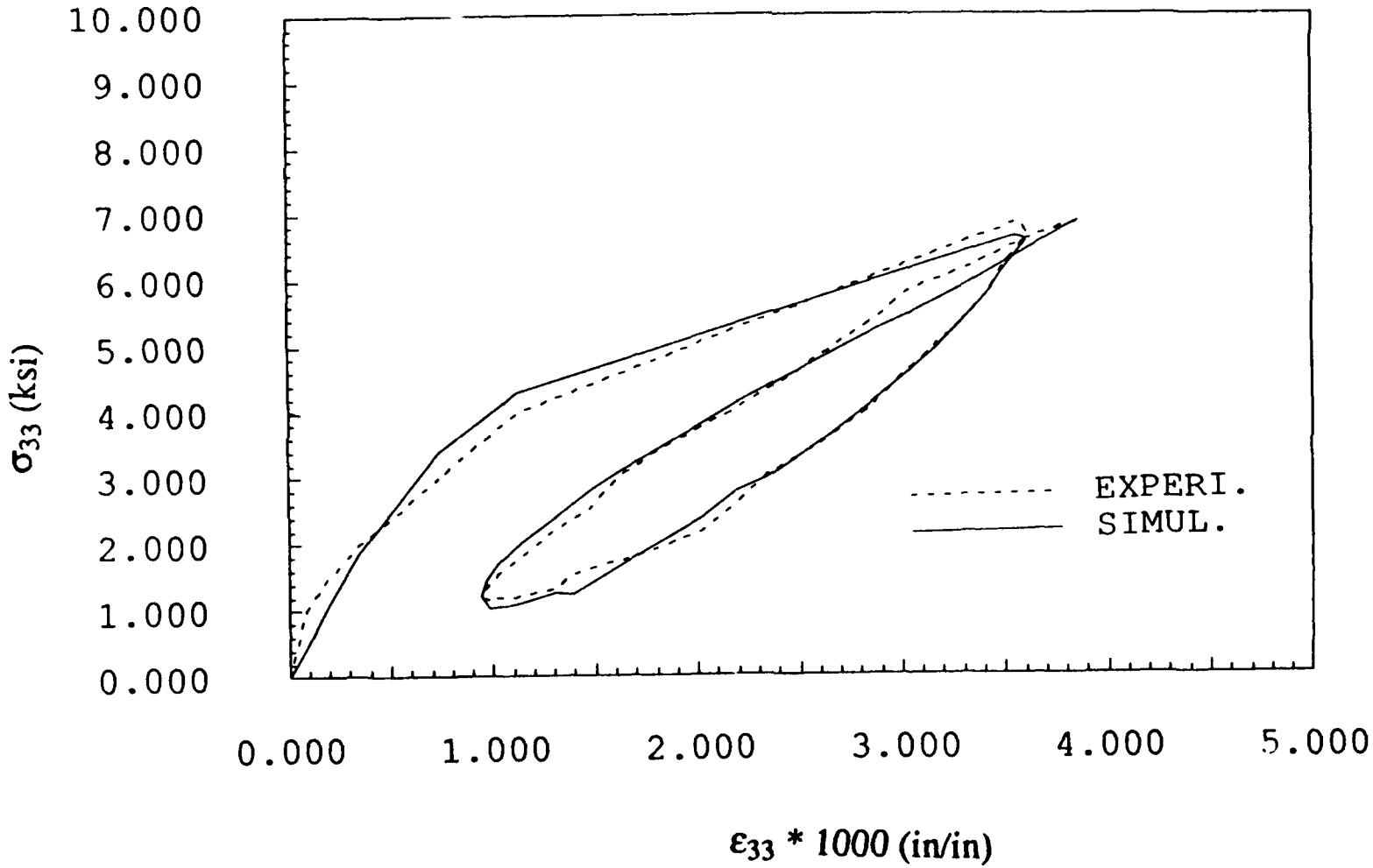
10.000
9.000
8.000
7.000
6.000
5.000
4.000
3.000
2.000
1.000
0.000
σ33 (ksi)
EXPERI.
SIMUL.
0.000
1.000
2.000
3.000
4.000
5.000
ε33 * 1000 (in/in)

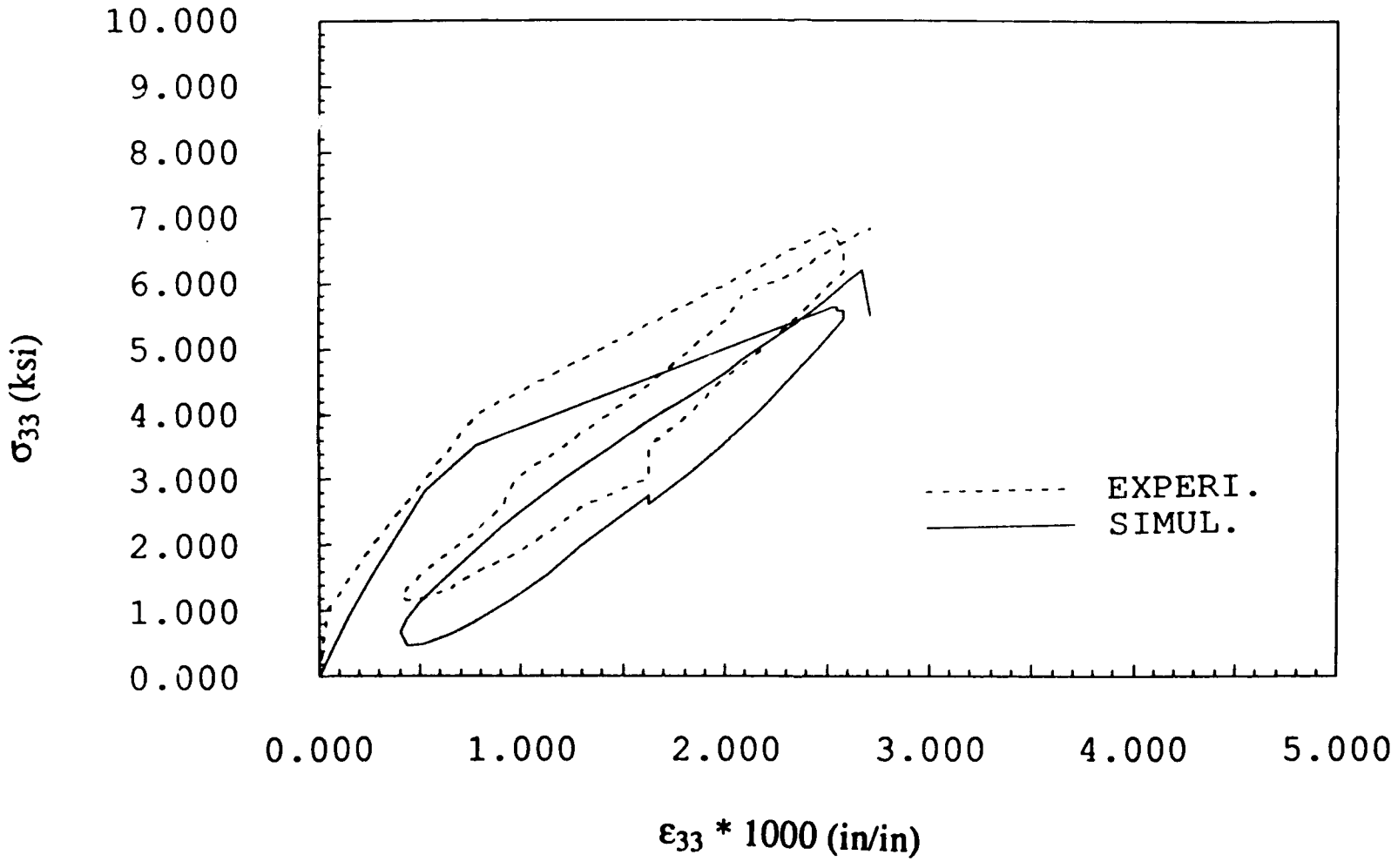
10.000
9.000
8.000
7.000
6.000
5.000
4.000
3.000
2.000
1.000
0.000
σ33 (ksi)
EXPERI.
SIMUL.
0.000
1.000
2.000
3.000
4.000
5.000
ε33 * 1000 (in/in)

10.000
9.000
8.000
7.000
6.000
5.000
4.000
3.000
2.000
1.000
0.000
σ33 (ksi)
0.000
1.000
2.000
3.000
4.000
5.000
ε33 * 1000 (in/in)
k=.1
k=.5
k=.9

13.000
11.696
10.392
9.088
7.784
6.480
5.176
3.873
2.569
1.265
-0.038
σ33 (ksi)
-3.740
-1.392
0.955
3.303
5.652
8.000
ε33 * 1000 (in/in)
EXPERI.
SIMUL.

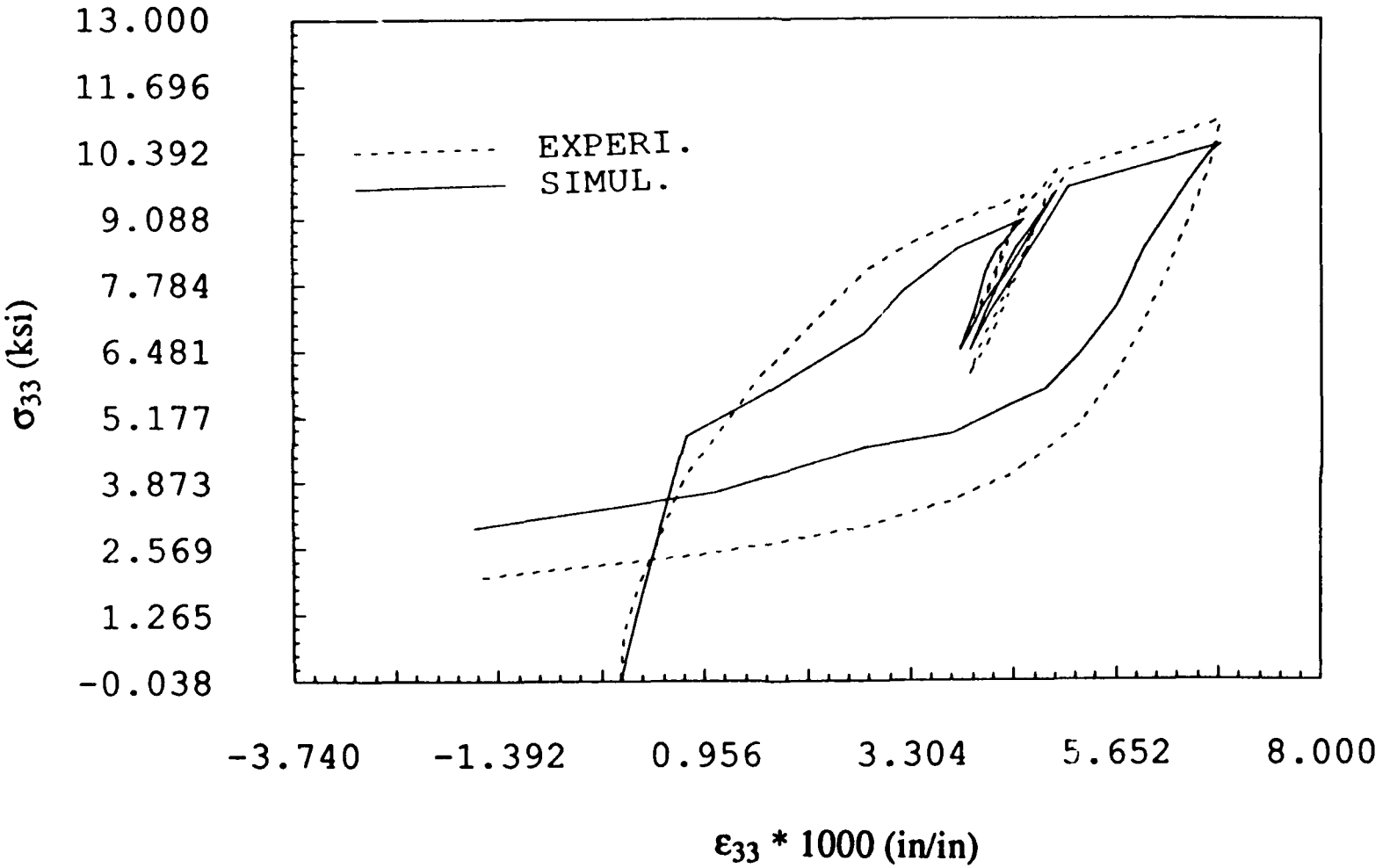
13.000
11.696
10.392
9.088
7.784
6.481
5.177
3.873
2.569
1.265
-0.038
EXPERI.
SIMUL.
σ33 (ksi)
-3.740
-1.392
0.956
3.304
5.652
8.000
ε33 * 1000 (in/in)

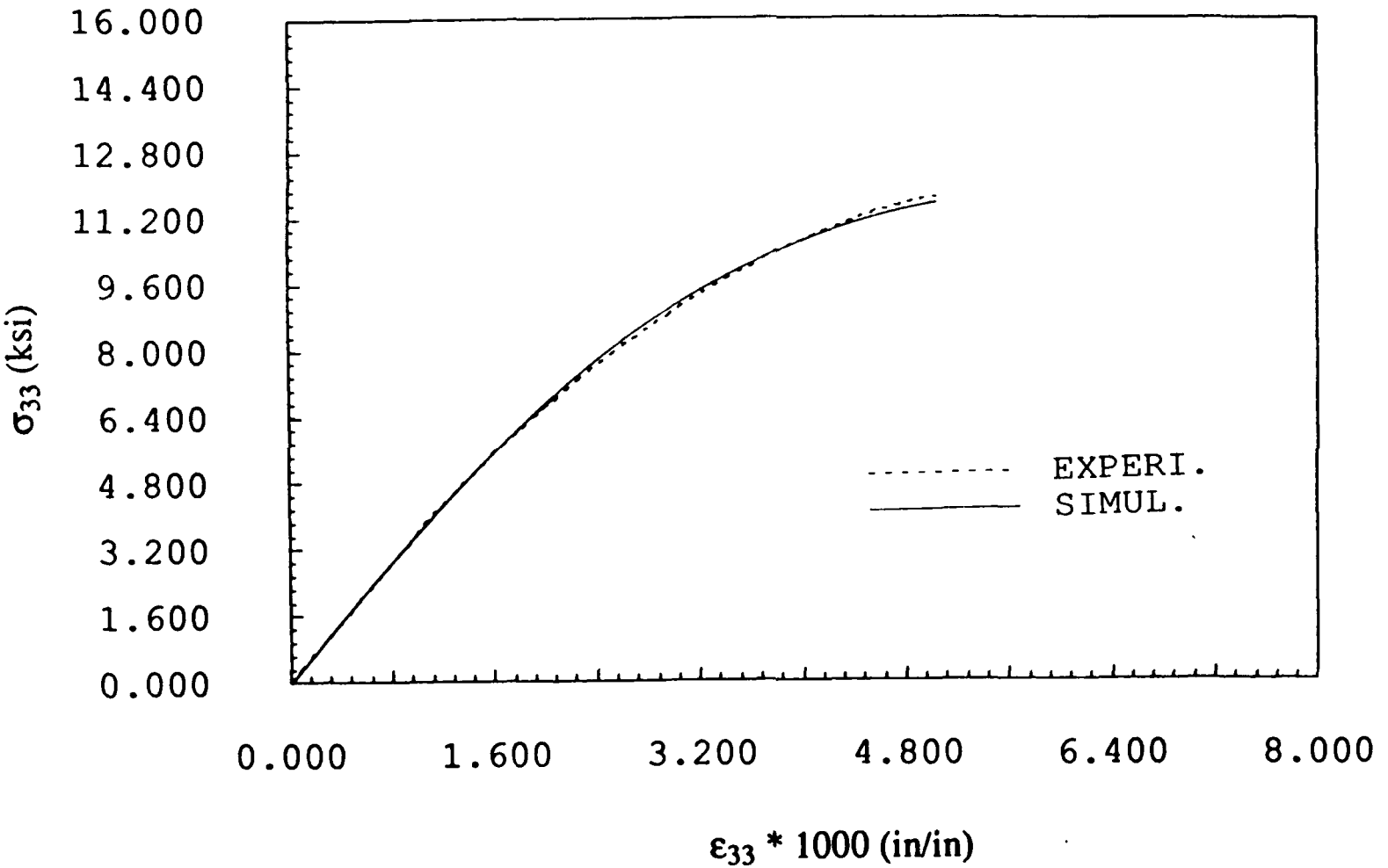
16.000
14.400
12.800
11.200
9.600
8.000
6.400
4.800
3.200
1.600
0.000
σ33 (ksi)
EXPERI.
SIMUL.
0.000
1.600
3.200
4.800
6.400
8.000
ε33 * 1000 (in/in)

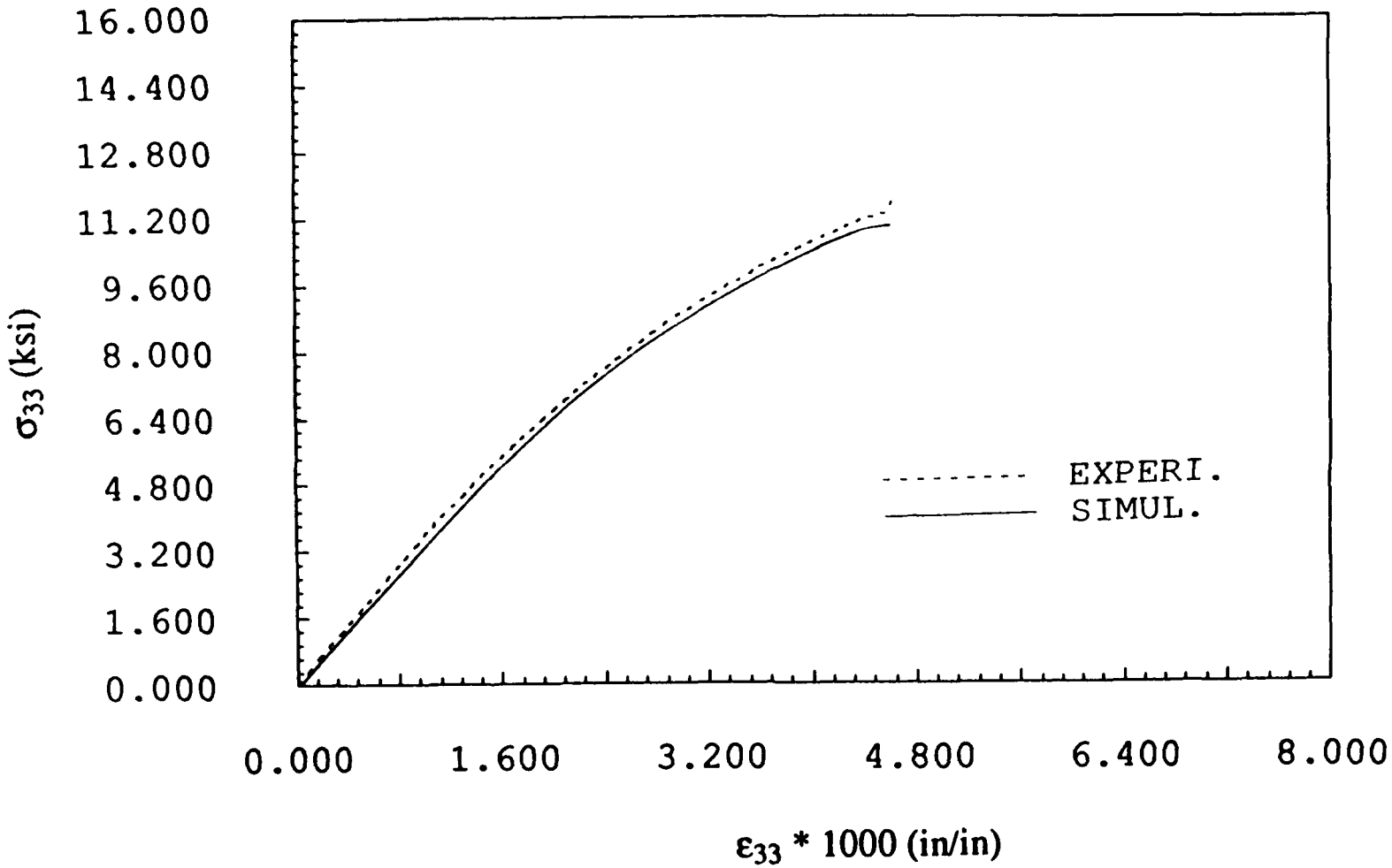
16.000
14.400
12.800
11.200
9.600
8.000
6.400
4.800
3.200
1.600
0.000
σ33 (ksi)
EXPERI.
SIMUL.
0.000
1.600
3.200
4.800
6.400
8.000
ε33 * 1000 (in/in)

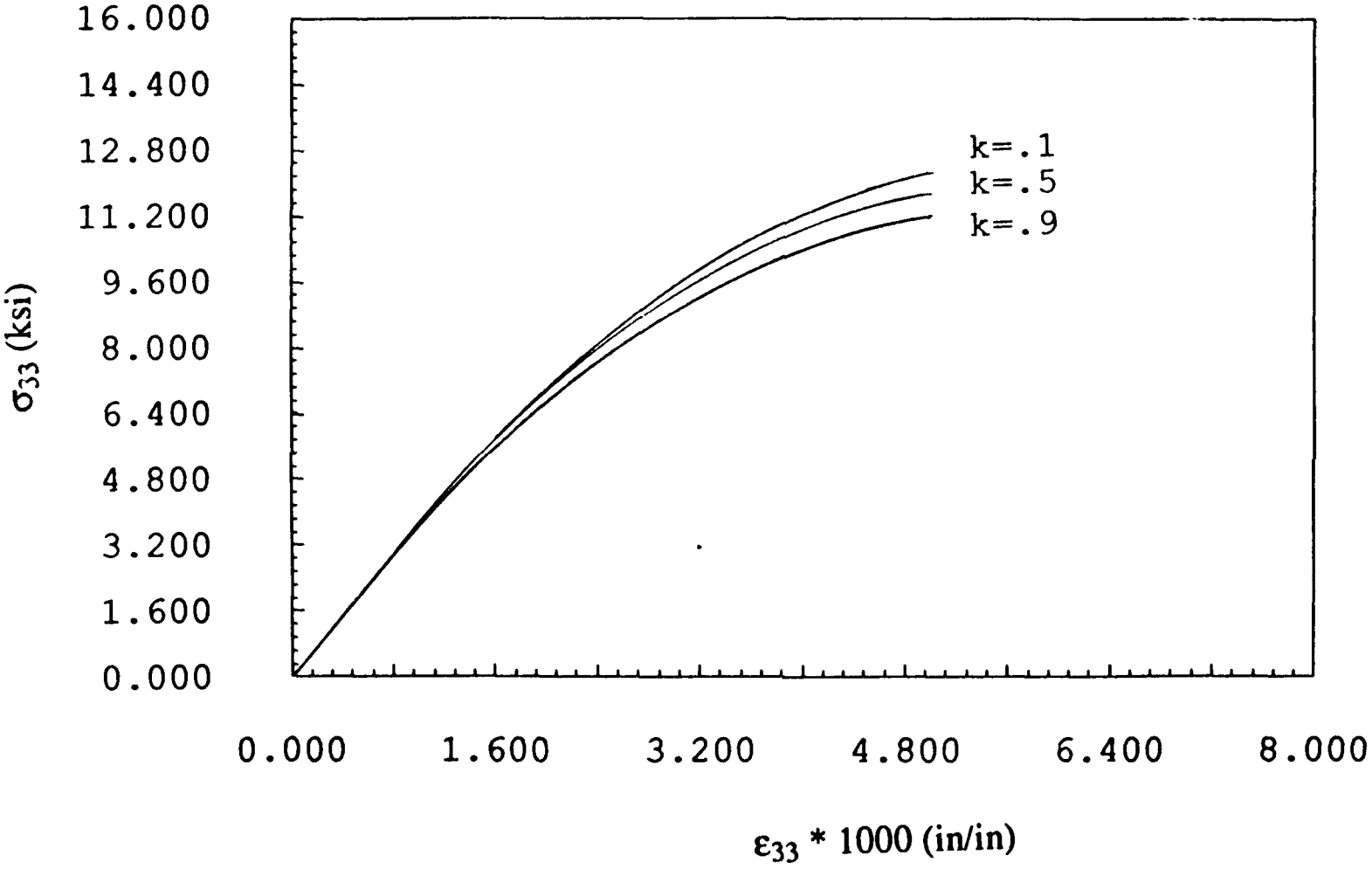
16.000
14.400
12.800
11.200
9.600
8.000
6.400
4.800
3.200
1.600
0.000
σ33 (ksi)
k=.1
k=.5
k=.9
0.000
1.600
3.200
4.800
6.400
8.000
ε33 * 1000 (in/in)

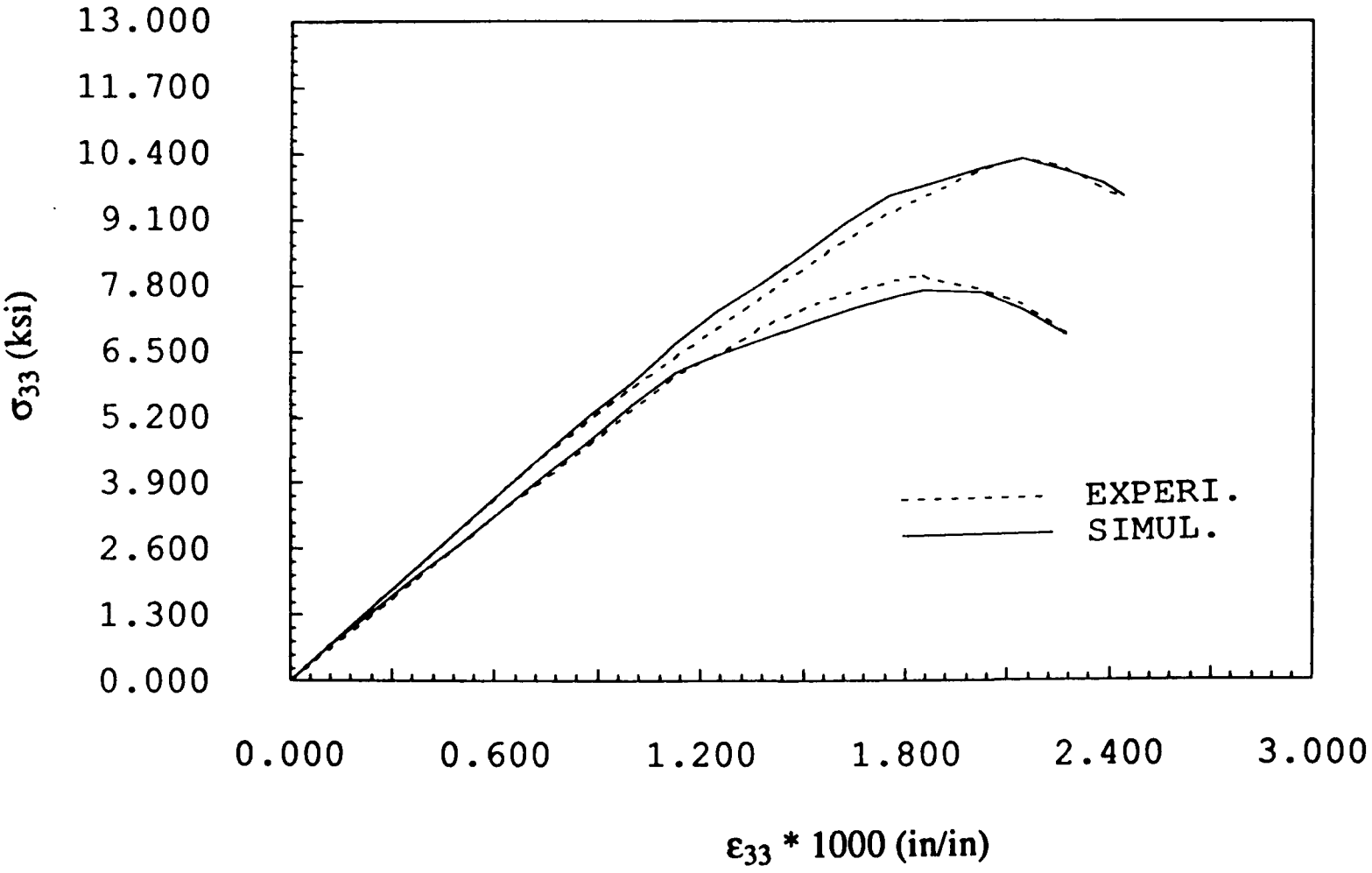
13.000
11.700
10.400
9.100
7.800
6.500
5.200
3.900
2.600
1.300
0.000
σ33 (ksi)
EXPERI.
SIMUL.
0.000
0.600
1.200
1.800
2.400
3.000
ε33 * 1000 (in/in)

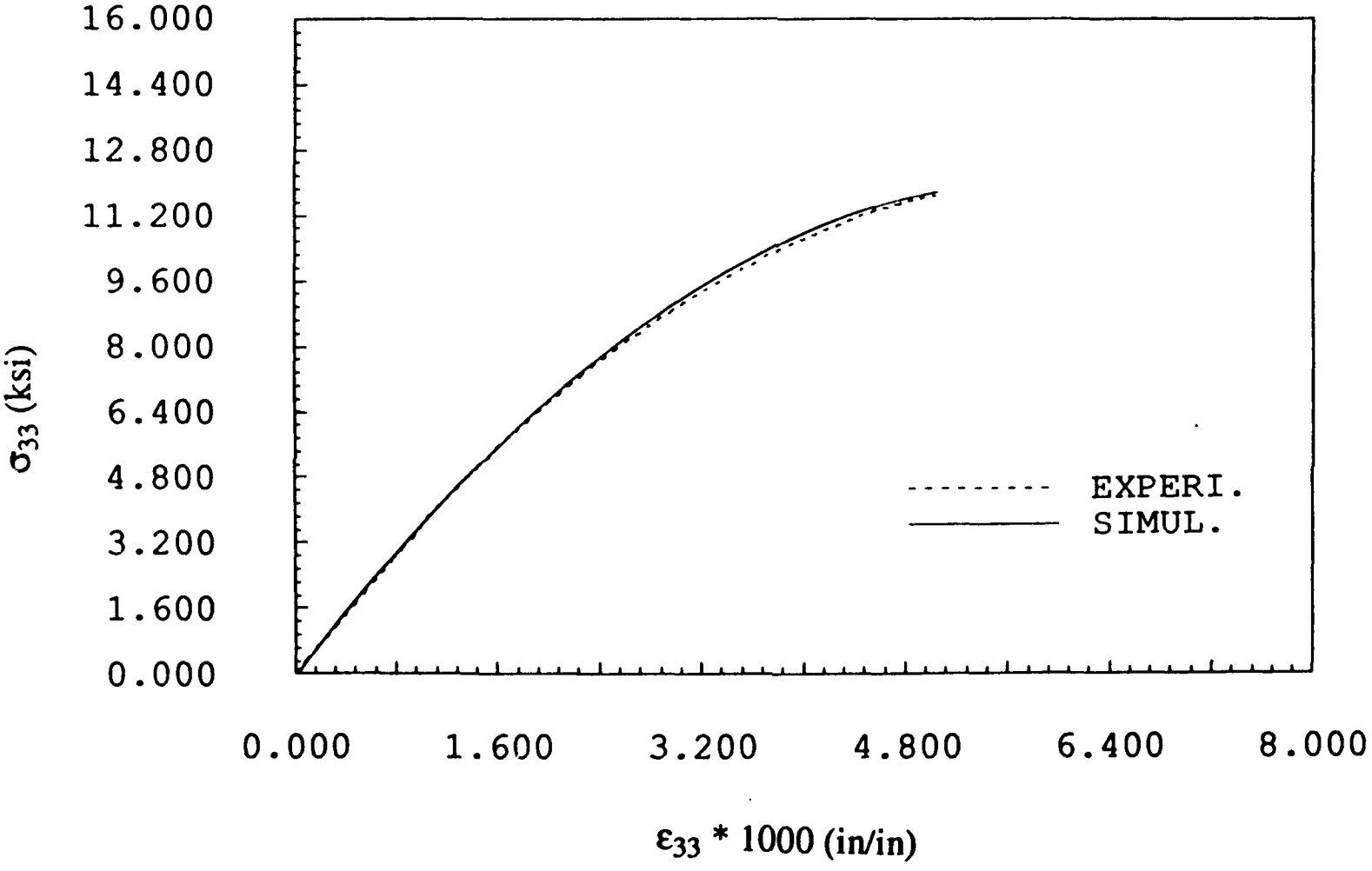
16.000
14.400
12.800
11.200
9.600
8.000
6.400
4.800
3.200
1.600
0.000
σ33 (ksi)
EXPERI.
SIMUL.
0.000
1.600
3.200
4.800
6.400
8.000
ε33 * 1000 (in/in)

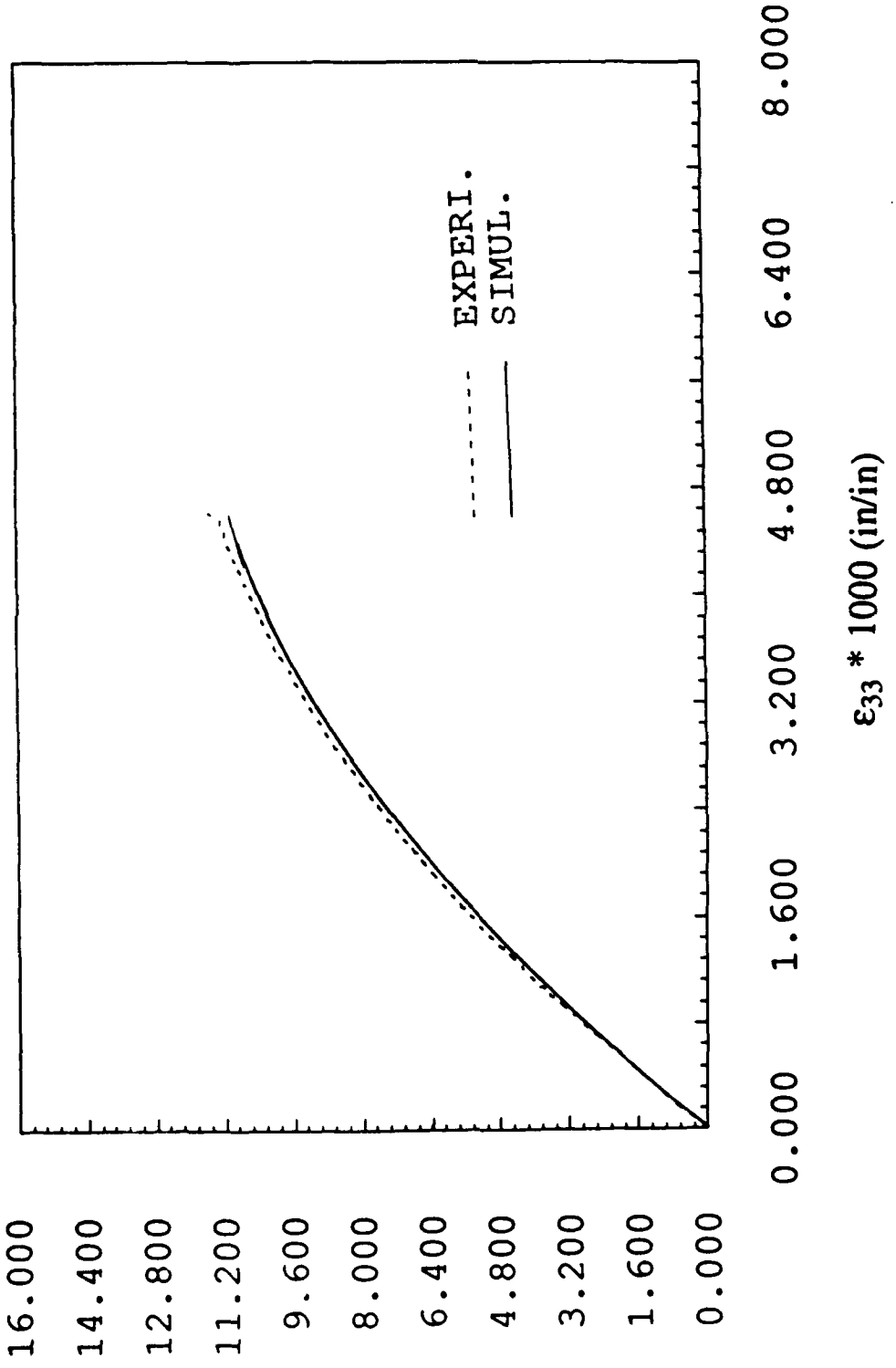
16.000
14.400
12.800
11.200
9.600
8.000
6.400
4.800
3.200
1.600
0.000
σ33 (ksi)
0.000
1.600
3.200
4.800
6.400
8.000
ε33 * 1000 (in/in)
EXPERI.
SIMUL.

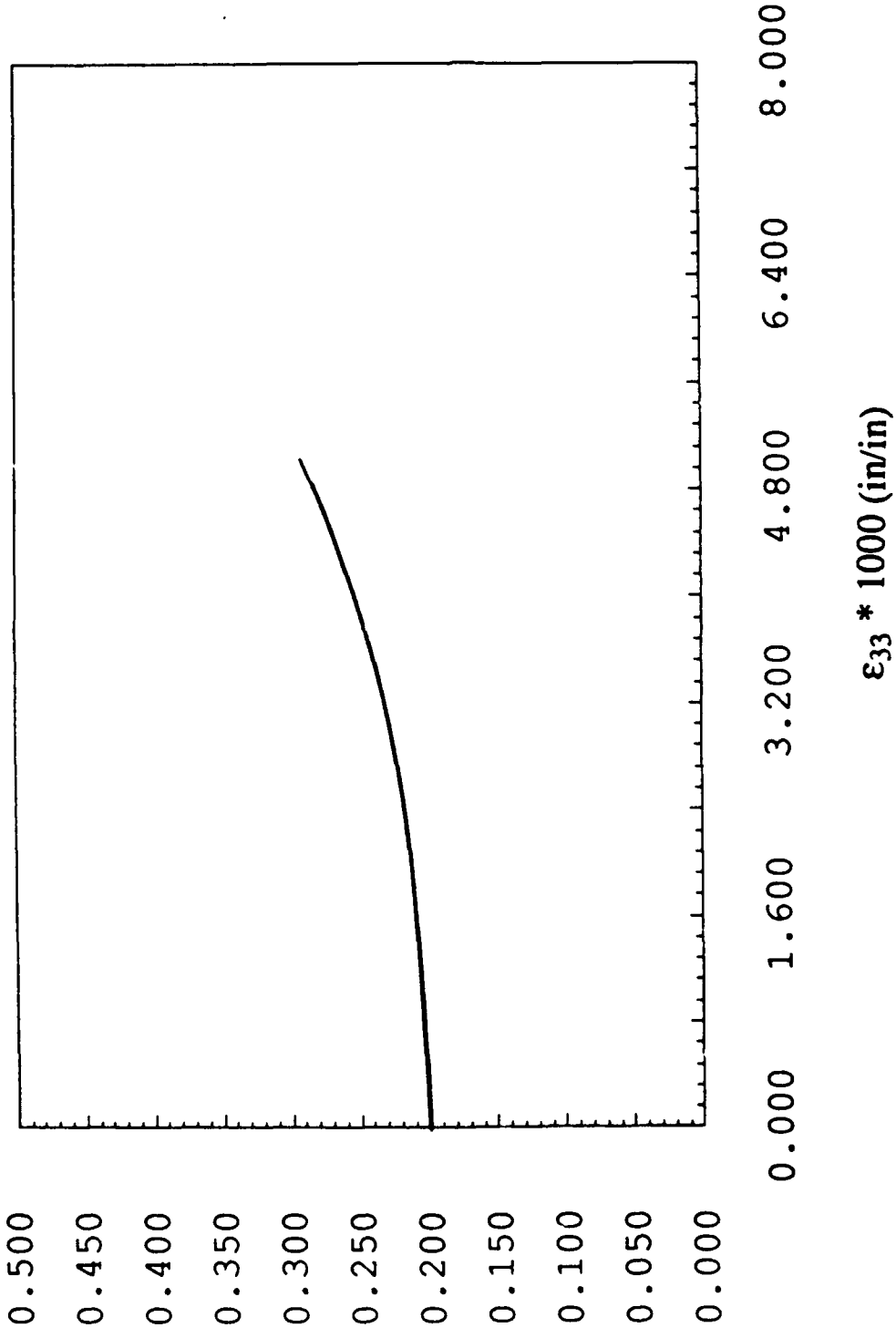
0.500
0.450
0.400
0.350
0.300
0.250
0.200
0.150
0.100
0.050
0.000
ν
0.000
1.600
3.200
4.800
6.400
8.000
ε33 * 1000 (in/in)

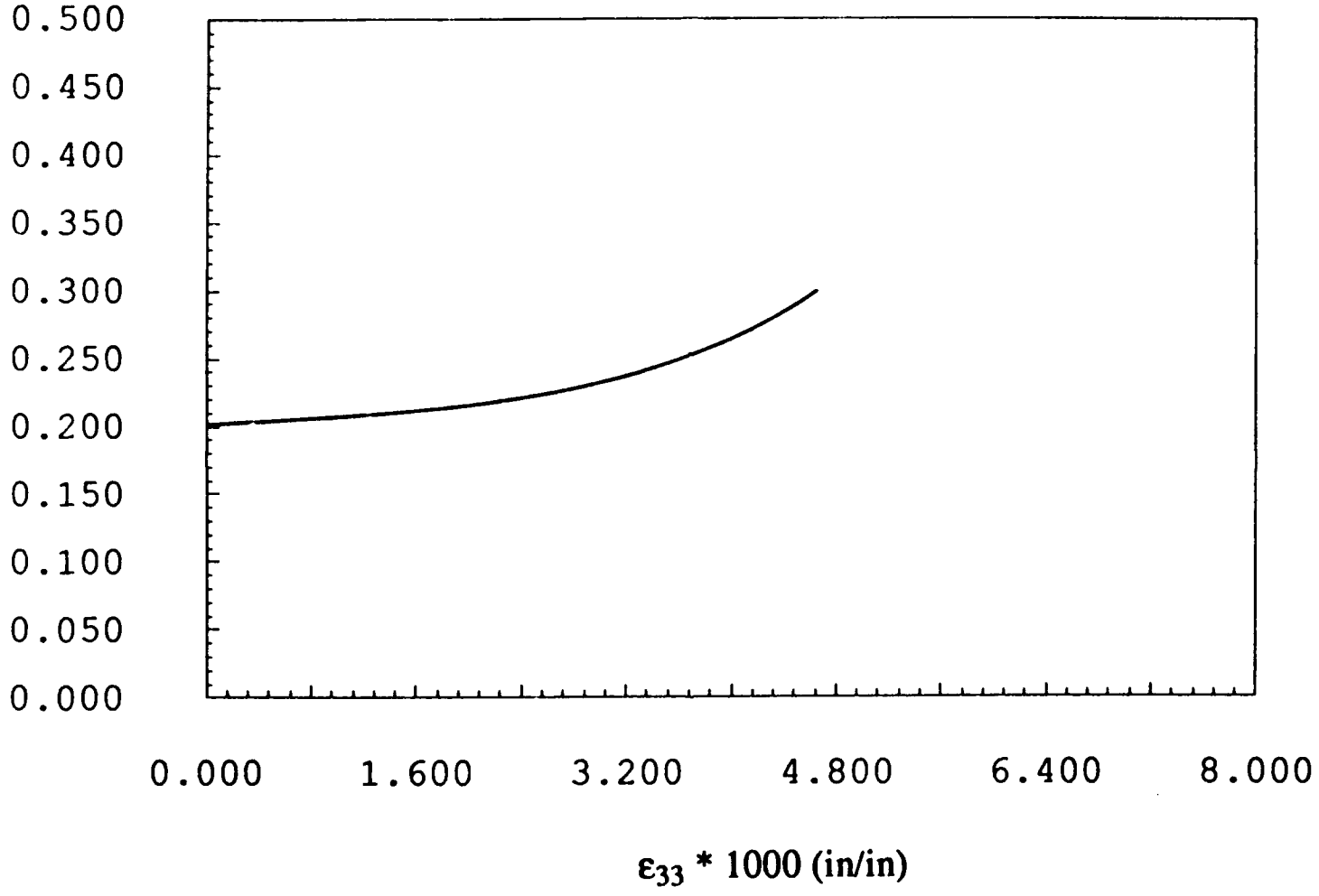
0.500
0.450
0.400
0.350
0.300
0.250
0.200
0.150
0.100
0.050
0.000
ν
0.000
1.600
3.200
4.800
6.400
8.000
ε33 * 1000 (in/in)

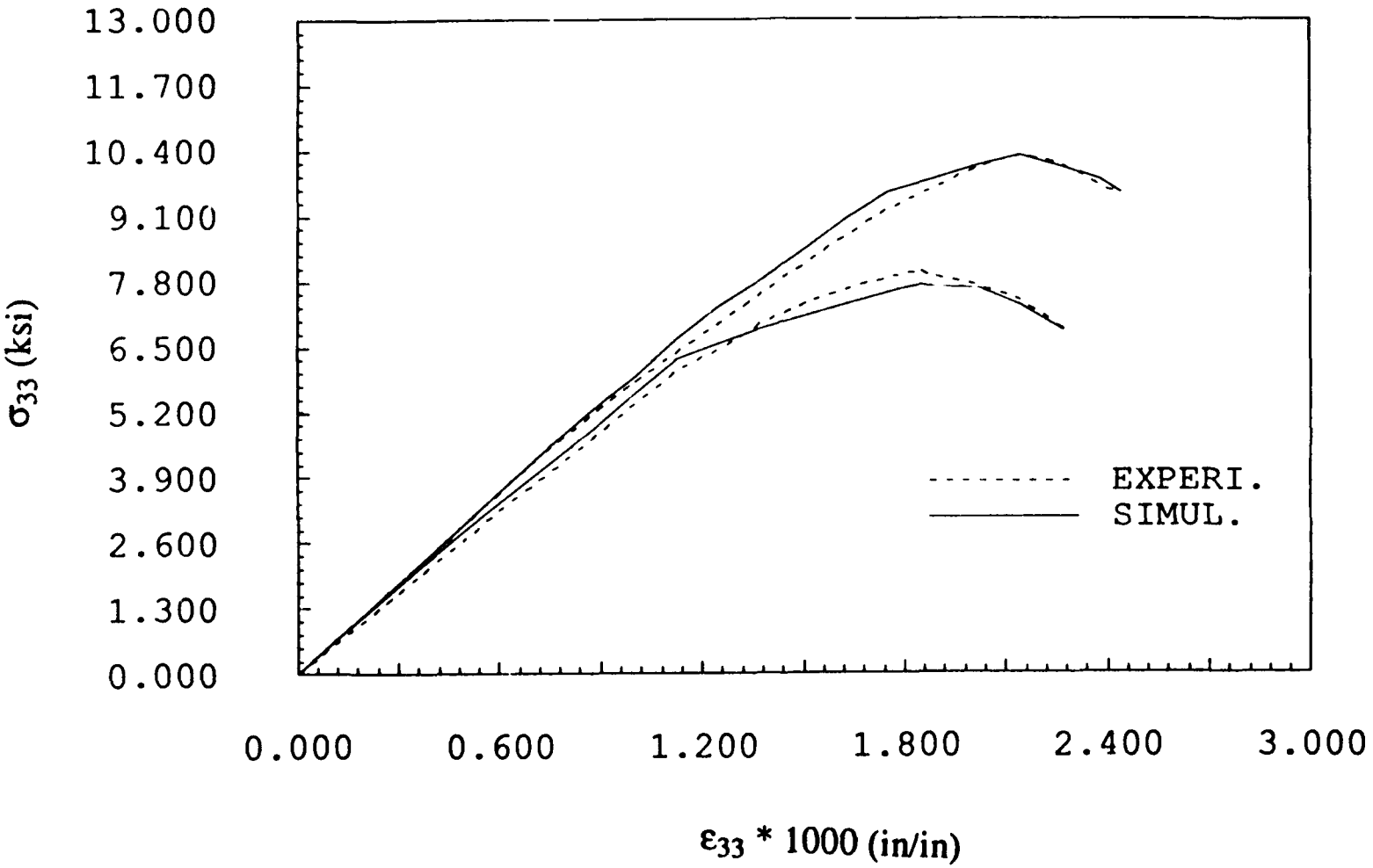
13.000
11.700
10.400
9.100
7.800
6.500
5.200
3.900
2.600
1.300
0.000
σ_{33} (ksi)
0.000
0.600
1.200
1.800
2.400
3.000
ε_{33} * 1000 (in/in)
EXPERI.
SIMUL.

PART II
On Energy-Based Coupled Elastoplastic Damage Models at Finite Strains

II.1. Introduction

Continuum energy-based damage models coupled with elastoplasticity at *finite strains* are proposed within the framework of *damage mechanics*. For a literature review on damage mechanics, see, e.g., Krajcinovic [1984][1986]. The proposed theories are natural extensions of the infinitesimal damage-elastoplasticity models previously developed by Ju [1988]. The thermodynamic elastoplastic-damage models are based on the *effective stress* concept, damage threshold loading/unloading conditions, and multiplicative split of finite kinematics. The models are linked to the history of "damage energy release rate" ($\rho_0 \psi^o$) within representative volumes (unit cells). Further, the energy-based characterization of damage is particularly well suited for large scale computations.

The proposed formulation falls into the category of phenomenological damage models as opposed to micromechanically inspired models (see, e.g., Krajcinovic and Fanella [1986], Sumarac and Krajcinovic [1987], Wu [1985]). In a forthcoming paper, however, feasible thermodynamic micromechanical damage theories will be proposed.

An outline of this paper is as follows. The energy-based elastoplastic-damage constitutive equations are derived in Sec. 2, including thermodynamic basis, characterization of damage, coupling of damage and plasticity, and anisotropic microcrack opening/closing mechanism. Both spatial (Eulerian) and material (Lagrangian) descriptions are discussed. In particular, a physically meaningful "damage energy release rate" is derived for finite strains. In contrast to previous work by Simo and Ju [1987c] (which features an additive split of the *stress* tensor), this paper assumes a multiplicative split of the deformation gradient from the outset (see Simo [1988]). It is shown that the present framework is physically more appealing and computationally more robust. Simple and

efficient computational integration algorithms for proposed models are given in Sec. 3. In particular, a *three-step* operator split algorithm is developed. As a result, the plastic and damage parts are *algorithmically uncoupled* in spite of the damage-plasticity coupling in its rate form. An interesting numerical experiment of a notched specimen involving damage coupled with plastic flow is presented in Sec. 4.

II.2. Energy-based elastoplastic damage models at finite strains

In this section, we describe the basic elements of damage mechanics, thermodynamic basis of damage mechanism, characterization of damage, coupled elastoplastic-damage response, and anisotropic microcrack opening/closing mechanism.

II.2.1. Background

"Damage" can be defined as a collection of *permanent* microstructural changes concerning material thermomechanical properties (e.g., stiffness, strength, anisotropy, etc.) brought about in a material by a set of *irreversible* physical microcrack/microvoid processes resulting from the application of thermomechanical loadings (Talreja [1985]). The selection of a "damage" variable should be based on prope. micromechanical considerations. Several definitions of damage have been proposed in the literature for consideration. For example, one can define the second-order "damage" (inelastic strain) tensor **D** as a spatial volume average:

$$\mathbf{D} \equiv \frac{1}{2V} \sum_{k} \int_{S^{(k)}} (\mathbf{b} \otimes \mathbf{n} + \mathbf{n} \otimes \mathbf{b})^{(k)} \, dS^{(k)} \tag{2.1}$$

in which **b** and **n** denote the displacement discontinuity vector and the unit normal vector across the k-th microcrack surface $S^{(k)}$, respectively (Vakulenko and Kachanov [1971], Kachanov [1980], Horii and Nemat-Nasser [1983]), and V is the volume of a representative *unit cell* in the mesostructure (with a characteristic length l). As pointed out by Krajcinovic [1985], the definition (2.1) is thermodynamically *incorrect* because it leads to energy dissipation during unloading. Eq. (2.1) is actually a good index for "added flexibility" (damage-induced inelastic strain) due to open microcracks or microvoids. In fact, a feasible thermodynamic micromechanical damage tensor can be the fourth-order "damaged secant moduli" as suggested in Simo and Ju [1987a,b], Ju [1988].

Alternatively, one could define the damage variable $d_{\mathbf{n}}$ (in the normal direction **n**) as

$$d_{\mathbf{n}} \equiv \frac{A_d}{A_T} \tag{2.2}$$

where A_d is the *damaged* surface area (taking into account the microcrack area, the micro-stress concentration and the interaction between microcracks) and A_T is the total cross-sectional area of a surface of a unit cell along a normal direction $\mathbf{n}$ (see, e.g., Lemaitre [1984][1985]). Or, one may define the damage measure d as (assuming only one single microvoid)

$$d \equiv \frac{a^3}{V} \tag{2.3}$$

where a is the *radius* of an assumed single spherical microvoid (see, e.g., Budiansky & O'Connell [1976], Krajcinovic [1987]).

Throughout this paper the *effective stress concept* and *hypothesis of strain equivalence* are employed (see Kachanov [1958], Lemaitre [1971], Lemaitre and Chaboche [1978]). The effective stress concept plays an essential role in the coupled damage-plasticity response presented in Sec. 2.4.

II.2.2. Thermodynamic basis. Multiplicative split

In this section, we describe the thermodynamic basis of an isotropic phenomenological finite deformation damage model. It is noted that if there are a large number of microcracks or microvoids so that their orientations are randomly distributed within a unit cell, then isotropic damage model is a reasonable representation. The extension to a simple yet effective anisotropic damage mechanism is given later in Sec. 2.5.

The multiplicative kinematic split of the deformation gradient tensor $\mathbf{F}$ into the elastic and plastic parts is assumed from the outset:

$$\mathbf{F} = \mathbf{F}^e \, \mathbf{F}^p \tag{2.4}$$

It is emphasized that "added flexibility" due to the existence of microcracks or microvoids is already embedded in $\mathbf{F}^e$ and $\mathbf{F}^p$ implicitly. By using the Lagrangian tensors (material description), we consider a locally homogenized general free energy potential $\Psi(\mathbf{E}, \mathbf{E}^p, \mathbf{Q}, d)$ of the following form:

$$\Psi(\mathbf{E}, \mathbf{E}^p, \mathbf{Q}, d) \equiv (1-d)\,\Psi^o(\mathbf{E}, \mathbf{E}^p, \mathbf{Q}) \equiv (1-d)\,[\,\Psi^o_e(\mathbf{E}, \mathbf{E}^p) + \Psi^o_p(\mathbf{Q})\,] \quad (2.5)$$

Here $\mathbf{E} \equiv \frac{1}{2}(\mathbf{C} - \mathbf{1})$ and $\mathbf{E}^p \equiv \frac{1}{2}(\mathbf{C}^p - \mathbf{1})$ denote the total and plastic Lagrangian strain tensors, respectively, with $\mathbf{C} \equiv \mathbf{F}^T\,\mathbf{F}$ and $\mathbf{C}^p \equiv \mathbf{F}^{pT}\,\mathbf{F}^p$. In addition, d designates the damage variable, $\mathbf{Q}$ is a suitable set of plastic variables, and Ψ^o signifies the total potential energy of an undamaged (virgin) material. In Eq. (2.5), Ψ^o is assumed to be uncoupled into the sum of Ψ^o_e and Ψ^o_p .

Within the context of the purely mechanical theory, the Clausius-Duhem inequality reduces to

$$-\rho_0\,\dot{\Psi} + \mathbf{S} : \dot{\mathbf{E}} \geq 0 \quad (2.6)$$

where ρ_0 is the mass density in the reference configuration and $\mathbf{S}$ is the symmetric Piola-Kirchhoff stress tensor. Standard procedures (Coleman and Gurtin [1967]) along with the additional assumption that damage and plastic unloading are *elastic* processes then lead to

$$\mathbf{S} = \rho_0\,(1-d)\,\frac{\partial \Psi^o_e(\mathbf{E}, \mathbf{E}^p)}{\partial \mathbf{E}} \quad (2.7)$$

together with the damage and plastic dissipative inequalities

$$\rho_0\,\Psi^o(\mathbf{E}, \mathbf{E}^p, \mathbf{Q})\,\dot{d} \geq 0 \quad (2.8)$$

$$-\frac{\partial \Psi^o_e}{\partial \mathbf{E}^p} : \dot{\mathbf{E}}^p - \frac{\partial \Psi^o_p}{\partial \mathbf{Q}} \bullet \dot{\mathbf{Q}} \geq 0 \quad (2.9)$$

It follows from (2.8) that the thermodynamic flux conjugate to the damage variable d is simply the total undamaged free energy function $\Psi^o(\mathbf{E}, \mathbf{E}^p, \mathbf{Q})$; i.e., the *"damage*

energy release rate". This is at variance with Lemaitre [1984][1985][1986], which considered only the *elastic* part of the undamaged free energy. Moreover, the "effective stress" $\bar{\mathbf{S}}$ (over the effective resisting area) is given by the expression

$$\bar{\mathbf{S}} = \frac{\mathbf{S}}{1-d} = \rho_0 \frac{\partial \Psi_e^o(\mathbf{E}, \mathbf{E}^p)}{\partial \mathbf{E}} \tag{2.10}$$

Remark 2.1. The spatial counterpart of the material description outlined above can be obtained by employing standard push-forward operations with the deformation gradients. For instance, the spatial counterpart of (2.7) reads

$$\boldsymbol{\tau} = \rho_0 (1-d) \frac{\partial \psi_e^o(\mathbf{e}, \mathbf{e}^p, \mathbf{F})}{\partial \mathbf{e}} \tag{2.11}$$

Here $\boldsymbol{\tau}$ is the Kirchhoff stress, $\mathbf{e}$ and $\mathbf{e}^p$ are the Eulerian strain tensors, and ψ_e^o denotes the stored energy function in terms of the Eulerian strains and deformation gradient. □

Remark 2.2. In the case of *anisotropic* damage due to microcrack opening and closing, (2.11) can be replaced by (as will be shown in Sec. 2.5)

$$\boldsymbol{\tau} = \rho_0 (\mathbf{I} - \mathbf{D}^{act}) : \frac{\partial \psi_e^o(\mathbf{e}, \mathbf{e}^p, \mathbf{F})}{\partial \mathbf{e}} \qquad \square \tag{2.12}$$

Remark 2.3. A different finite strain damage-plasticity formulation based on an additive split of the *stress* tensor was previously proposed by Simo and Ju [1987c]. □

II.2.3. Characterization of damage. Elastic-damage moduli

An energy-based characterization of isotropic damage mechanism at finite strains is discussed in this section. Motivated by Eq. (2.8), we employ the locally averaged free energy Ψ^o to characterize the damage loading/unloading conditions. For convenience, let us define the notation ξ as (in a material description)

$$\xi \equiv \rho_0 \Psi^o(\mathbf{E}, \mathbf{E}^p, \mathbf{Q}) \tag{2.13}$$

A *damage criterion* is then introduced by requiring that at any time t

$$g(\xi_t, r_t) \equiv \xi_t - r_t \leq 0 \ , \quad t \in \mathbf{R}_+ \tag{2.14}$$

where r_t signifies the *damage threshold* (energy barrier) at current time t . If r_0 denotes the initial damage threshold before any loading is applied, a property characteristic of the material, we must have $r_t \geq r_0$. Condition (2.14) then states that damage in the material is *initiated* when the damage energy release rate (ξ_t) exceeds the initial damage threshold r_0 . The above *energy*-based damage criterion is fundamentally linked to the history of *both* elastic and plastic variables. One should realize that a *stress*-based damage criterion in the presence of significant plastic flow is inherently *inadequate* for predicting realistic plastic damage growth.

To describe the growth of microcracks (microvoids) and the expansion of damage surfaces, equations of evolution for d and r are specified as follows

$$\begin{aligned} \dot{d}_t &= \dot{\lambda}\, \Xi(d_t, \xi_t, s, a) \\ \dot{r}_t &= \dot{\lambda} \end{aligned} \tag{2.15}$$

where s and a are the inclusion spacing and inclusion size, respectively. Furthermore, the irreversible nature of damage is captured by enforcing that the *damage consistency* parameter $\dot{\lambda}$ satisfy the (Kuhn-Tucker) unilateral restrictions

$$\dot{\lambda} \geq 0 \,, \quad g(\xi_t, r_t) \leq 0 \,, \quad \dot{\lambda} g(\xi_t, r_t) = 0 \tag{2.16}$$

One can show that these conditions are in fact optimality conditions for a *principle of maximum damage dissipation* (see Simo & Ju [1987a,b]). One can determine $\dot{\lambda}$ and r_t by requiring that during the damage loading

$$g(\xi_t, r_t) = \dot{g}(\xi_t, r_t) = 0 \quad \Rightarrow \quad \dot{\lambda} = < \dot{\xi}_t > \tag{2.17}$$

so that

$$r_t = \max \{ r_0 \,, \max_{s \in (-\infty, t]} \xi_s \} \tag{2.18}$$

where $< \bullet >$ is the McAuley bracket. A spatial version of the above characterization of damage can be carried out in exactly the same fashion.

2.3.1. Elastic-damage tangent moduli. In the absence of further plastic flow, the relation between strain rate and stress rate is obtained as follows. In a (damage) loading process, one has

$$\dot{\mathbf{S}} = \rho_0 (1-d) \frac{\partial^2 \Psi_e^o(\mathbf{E}, \mathbf{E}^p)}{\partial \mathbf{E}^2} : \dot{\mathbf{E}} - \dot{\xi} \Xi \rho_0 \frac{\partial \Psi_e^o(\mathbf{E}, \mathbf{E}^p)}{\partial \mathbf{E}} \tag{2.19}$$

From Eq. (2.10) and (2.13), we realize that $\dot{\xi} = \bar{\mathbf{S}} : \dot{\mathbf{E}}$. Hence, we obtain $\dot{\mathbf{S}} = \mathbf{A}(\mathbf{E}, \mathbf{E}^p, d) : \dot{\mathbf{E}}$, where $\mathbf{A}$ is a *symmetric* rank four tensor referred to as the *elastic-damage tangent modulus* at finite strain, and given by

$$\mathbf{A}(\mathbf{E}, \mathbf{E}^p, d) = \rho_0 (1-d) \frac{\partial^2 \Psi_e^o(\mathbf{E}, \mathbf{E}^p)}{\partial \mathbf{E}^2} - \Xi \bar{\mathbf{S}} \otimes \bar{\mathbf{S}} \tag{2.20}$$

The expression for the elastic-damage modulus in a spatial description follows at once from (2.20) by a push-forward operation, and is recorded in Box **1** along with a summary of the isotropic damage model. Note that $\mathbf{q} \equiv \boldsymbol{\phi}_* \mathbf{Q}$ is the push-forward of $\mathbf{Q}$.

Remark 2.4. *(Viscous damage model).* The damage model outlined above is *rate independent.* Typically, in the softening regime, lack of uniqueness will arise if such an approach is employed. To account for rate sensitivity of damage growth and to *regularize* the localization problems, one may consider a viscous damage mechanism. Essentially, one replaces the damage evolution equations (2.15) with the rate-dependent counterpart:

$$\begin{aligned} \dot{d}_t &= \mu < g(\xi_t, r_t) > \Xi(d_t, \xi_t, s, a) \\ \dot{r}_t &= \mu < g(\xi_t, r_t) > \end{aligned} \tag{2.21}$$

□

BOX 1. *Isotropic elastic-damage at finite strains*

Material (Convected)	*Spatial*

(i) Multiplicative split and stress response: $\mathbf{F} = \mathbf{F}^e\,\mathbf{F}^p$

$$\bar{\mathbf{S}} = \rho_0 \frac{\partial \Psi_e^o(\mathbf{E}, \mathbf{E}^p)}{\partial \mathbf{E}} \qquad \bar{\boldsymbol{\tau}} = \rho_0 \frac{\partial \psi_e^o(\mathbf{e}, \mathbf{e}^p, \mathbf{F})}{\partial \mathbf{e}}$$

$$\mathbf{S} = (1-d)\,\bar{\mathbf{S}} \qquad \boldsymbol{\tau} = (1-d)\,\bar{\boldsymbol{\tau}}$$

(ii) Damage evolution: $\xi \equiv \rho_0 \Psi^o(\mathbf{E}, \mathbf{E}^p, \mathbf{Q}) = \rho_0 \psi^o(\mathbf{e}, \mathbf{e}^p, \mathbf{F}, \mathbf{q})$

$$\dot{d} = \dot{\lambda}\,\Xi(d, \xi, s, a) \;\; ; \;\; \dot{\lambda} \geq 0$$

$$g \equiv \xi - r \leq 0 \;\; ; \;\; \dot{\lambda}\, g = 0$$

(iii) Elastic-damage modulus: (similar in a material description)

$$\mathbf{a} \equiv \rho_0 (1-d) \frac{\partial^2 \psi_e^o}{\partial \mathbf{e}^2} - \Xi\, \bar{\boldsymbol{\tau}} \otimes \bar{\boldsymbol{\tau}}$$

(iv) Plasticity: See Box **2**.

II.2.4. Coupled elastoplastic damage response. Tangent moduli

Within the proposed framework, plastic response is characterized in the so-called *effective stress space* in terms of the effective stresses. We refer to Ju [1986], Simo & Ju [1987a], Ju [1988] for discussions of these notions. It is emphasized that use of effective quantities in the yield condition has the net effect of *lowering* the plastic strength and flow stresses of materials.

2.4.1. Yield condition. In a spatial description, one assumes a yield condition that depends on the current *effective stress* $\bar{\boldsymbol{\tau}}$ and a suitable set of internal plastic variables $\mathbf{q}$. Since this function may depend on $\bar{\boldsymbol{\tau}}$ through its invariants or deviator, one needs to include *explicitly* the dependence on the spatial metric tensor, denoted by $\mathbf{g}$. Accordingly, one writes

$$\phi(\bar{\boldsymbol{\tau}}, \mathbf{g}, \mathbf{q}) \leq 0 \tag{2.22}$$

One could also define the yield condition entirely in the *strain space* by postulating at the outset the form $\phi(\mathbf{e}, \mathbf{e}^p, \mathbf{q}, \mathbf{F}) \leq 0$. Alternatively, one may think of this strain space form as emanating from (2.22) through the stress-strain relation (2.11).

In a material description, the yield condition consistent with material frame indifference takes the form

$$\Phi(\mathbf{E}, \mathbf{E}^p, \mathbf{Q}) \leq 0 \tag{2.23}$$

2.4.2. Flow rule and hardening law. Although more general formulations are possible, we shall restrict our attention to the case of an associative flow rule. In view of the (material) plastic dissipative inequality (2.9), the evolution equations for $\dot{\mathbf{E}}^p$ and $\dot{\mathbf{Q}}$ need to be defined. Specifically, let us assume an evolution equation for $\mathbf{E}^p$ of the form (see Simo and Ju [1987c], Simo [1988])

$$\dot{\mathbf{E}}^p = -\dot{\gamma}\, \mathbf{M}^{-1} : \frac{\partial \Phi(\mathbf{E}, \mathbf{E}^p, \mathbf{Q})}{\partial \mathbf{E}} \tag{2.24}$$

where

$$\mathbf{M}^{-1} \equiv \rho_0 \frac{\partial^2 \Psi_e^o(\mathbf{E}, \mathbf{E}^p)}{\partial \mathbf{E}\, \partial \mathbf{E}^p} = \frac{\partial \bar{\mathbf{S}}}{\partial \mathbf{E}^p} \tag{2.25}$$

Furthermore, $\dot{\gamma}$ is a plastic consistency parameter that determines the *irreversible* nature of the plastic flow according to the Kuhn-Tucker conditions

$$\dot{\gamma} \geq 0, \quad \Phi(\mathbf{E}, \mathbf{E}^p, \mathbf{Q}) \leq 0, \quad \dot{\gamma}\, \Phi(\mathbf{E}, \mathbf{E}^p, \mathbf{Q}) \equiv 0 \tag{2.26}$$

Equivalently, one can rephrase the above flow rule as follows

$$\overset{\star}{\mathbf{S}}^{p} \equiv -\mathbf{M} : \dot{\mathbf{E}}^{p} = \dot{\gamma}\,\frac{\partial \Phi(\mathbf{E}\,,\,\mathbf{E}^{p}\,,\,\mathbf{Q})}{\partial \mathbf{E}} \tag{2.27}$$

Eq. (2.24),(2.25),(2.27) in fact correspond to the case of "maximum effective plastic dissipation" in the strain space. The characterization of the effective elastoplastic response is completed by prescribing the evolution of the internal (plastic) state variable $\mathbf{Q}$ according to a rate equation of the form

$$\dot{\mathbf{Q}} = \dot{\gamma}\,\mathbf{H}(\mathbf{E}\,,\,\mathbf{E}^{p}\,,\,\mathbf{Q}) \tag{2.28}$$

One refers to the function $\mathbf{H}$ as the generalized hardening modulus. The spatial formulation can be obtained by the standard push-forward procedures.

2.4.3. Elastoplastic-damage tangent moduli The plastic consistency parameter $\dot{\gamma}$ is determined by enforcing the so-called plastic consistency condition. Explicitly, upon loading ($\dot{\gamma} > 0$) one must have $\Phi(\mathbf{E}\,,\,\mathbf{E}^{p}\,,\,\mathbf{Q}) = 0$ and $\dot{\Phi}(\mathbf{E}\,,\,\mathbf{E}^{p}\,,\,\mathbf{Q}) = 0$. Direct application of the chain rule and use of the flow rule yield the following expression for $\dot{\gamma}$

$$\dot{\gamma} = \frac{\dfrac{\partial \Phi}{\partial \mathbf{E}} : \dot{\mathbf{E}}}{\dfrac{\partial \Phi}{\partial \mathbf{E}^{p}} : \mathbf{M}^{-1} : \dfrac{\partial \Phi}{\partial \mathbf{E}} - \dfrac{\partial \Phi}{\partial \mathbf{Q}} \bullet \mathbf{H}} \tag{2.29}$$

By inserting (2.29) into the flow rule (2.27) and using the rate form of (2.10), we obtain $\overset{\star}{\mathbf{S}} = \overline{\mathbf{A}}^{ep} : \dot{\mathbf{E}}$, where $\overline{\mathbf{A}}^{ep}$ is the *effective* elastoplastic tangent modulus given by (see Simo [1988])

$$\overline{\mathbf{A}}^{ep} \equiv \mathbf{A}^{o} - \frac{\dfrac{\partial \Phi}{\partial \mathbf{E}} \otimes \dfrac{\partial \Phi}{\partial \mathbf{E}}}{\dfrac{\partial \Phi}{\partial \mathbf{E}^{p}} : \mathbf{M}^{-1} : \dfrac{\partial \Phi}{\partial \mathbf{E}} - \dfrac{\partial \Phi}{\partial \mathbf{Q}} \bullet \mathbf{H}} \tag{2.30}$$

with $\mathbf{A}^{o} \equiv \rho_0\, \partial^2 \Psi_e^{o} / \partial \mathbf{E}^2$. To derive the elastoplastic-damage tangent moduli, we first recall that $\mathbf{S} = (1-d)\,\overline{\mathbf{S}}$. Time differentiation then leads to

$$\dot{\mathbf{S}} = (1-d)\,\overset{\star}{\overline{\mathbf{S}}} - \dot{d}\,\overline{\mathbf{S}} = (1-d)\,\overline{\mathbf{A}}^{ep} : \dot{\mathbf{E}} - \dot{\xi}\,\Xi\,\overline{\mathbf{S}} \tag{2.31}$$

where use has been made of Eq. (2.15) and (2.17). In addition, time derivative of Eq. (2.13) along with Eq. (2.24),(2.28) yield

$$\dot{\xi} = \bar{\mathbf{S}} : \dot{\mathbf{E}} - \dot{\gamma}\,[\,\rho_0 \frac{\partial \Psi_e^o}{\partial \mathbf{E}^p} : \mathbf{M}^{-1} : \frac{\partial \Phi}{\partial \mathbf{E}} - \rho_0 \frac{\partial \Psi_p^o}{\partial \mathbf{Q}} \bullet \mathbf{H}\,] \tag{2.32}$$

Substitution of Eq. (2.29) and (2.32) into (2.31) then renders $\dot{\mathbf{S}} = \mathbf{A}^{ep} : \dot{\mathbf{E}}$. Here $\mathbf{A}^{ep}$ is the elastoplastic-damage tangent modulus given by

$$\mathbf{A}^{ep} = (1-d)\,\bar{\mathbf{A}}^{ep} - \Xi\,[\bar{\mathbf{S}} \otimes \bar{\mathbf{S}}] + \frac{\Xi(\rho_0 \frac{\partial \Psi_e^o}{\partial \mathbf{E}^p} : \mathbf{M}^{-1} : \frac{\partial \Phi}{\partial \mathbf{E}} - \rho_0 \frac{\partial \Psi_p^o}{\partial \mathbf{Q}} \bullet \mathbf{H})}{\frac{\partial \Phi}{\partial \mathbf{E}^p} : \mathbf{M}^{-1} : \frac{\partial \Phi}{\partial \mathbf{E}} - \frac{\partial \Phi}{\partial \mathbf{Q}} \bullet \mathbf{H}} [\bar{\mathbf{S}} \otimes \frac{\partial \Phi}{\partial \mathbf{E}}] \tag{2.33}$$

It is observed from Eq. (2.33) that $\mathbf{A}^{ep}$ is in general a non-symmetric rank four tensor unless $\bar{\mathbf{S}} = \frac{\partial \Phi}{\partial \mathbf{E}}$. For easy reference, basic equations derived in this section have been summarized in Boxes **1** and **2**. Note that $L_v\,\bar{\boldsymbol{\tau}}^p$ denotes the *Lie derivative* of the effective spatial contravariant tensor $\bar{\boldsymbol{\tau}}^p$; i.e.,

$$L_v\,\bar{\boldsymbol{\tau}}^p \equiv \mathbf{F}\,\dot{\bar{\mathbf{S}}}^p\,\mathbf{F}^T \tag{2.34}$$

Remark 2.5. A damage-perturbed yield criterion and damage-induced non-associative flow rule in the *homogenized* stress space $\boldsymbol{\sigma}$ was proposed by Dragon [1985], Dragon and Chihab [1985]. It is noted, however, that *two* different yield functions are used in Dragon [1985] to define the "genuine" yield potential and another damage-perturbed pseudo-potential, respectively. The corresponding elastoplastic-damage return mapping algorithms are rather cumbersome due to two simultaneous consistency conditions. □

Remark 2.6. In the previous work by Simo and Ju [1987c], the formulation relies on an *additive* split of the *stress* tensor. The elastoplastic and elastoplastic-damage tangent moduli are too "soft" due to the fact that the differentiation involves the store energy function $\Psi^o(\mathbf{E})$ with $\mathbf{E}$ as its argument (see Eq. (2.22) in Simo and Ju [1987c]). These "soft" tangent moduli could lead to numerical difficulties when large strains are

encountered. By contrast, present formulation employs more robust (stiffer) tangent moduli with $\mathbf{E}$ and $\mathbf{E}^p$ as arguments of the store energy function $\Psi_e^o(\mathbf{E}, \mathbf{E}^p)$ in every differentiation. This advantage together with our J-integral-like damage energy release rate ($\rho_0 \Psi^o(\mathbf{E}, \mathbf{E}^p, \mathbf{Q})$) make the present formulation physically and computationally more attractive. □

II.2.5. Anisotropic microcrack opening/closing mechanism

Although the damage model presented in Sec. 2.3 and 2.4 are isotropic, they can be easily extended to account for anisotropic "mode I" microcrack opening and closing effects and the damage-induced anisotropy. The treatment here is similar to the previous proposal of Ortiz [1985] for (infinitesimal deformation) microcracks. A spatial description is employed in this section. Let us begin by considering the spectral decomposition of the strain tensor

$$\mathbf{e} = \sum_{i=1}^{3} e_i \, \mathbf{p}_i \otimes \mathbf{p}_i \quad , \quad |\mathbf{p}_i| = 1 \tag{2.35}$$

where e_i is the i^{th} principal spatial strain and $\mathbf{p}_i$ the i^{th} corresponding unit principal direction. Let $\hat{\mathbf{Q}}$ and $\hat{\mathbf{Q}}^+$, separately, be the regular and *positive* (tensile) spectral projection tensors defined as follows

$$\hat{\mathbf{Q}} \equiv \sum_{i=1}^{3} \mathbf{p}_i \otimes \mathbf{p}_i \quad ; \quad \hat{\mathbf{Q}}^+ \equiv \sum_{i=1}^{3} \hat{H}(e_i) \, \mathbf{p}_i \otimes \mathbf{p}_i \tag{2.36}$$

where $\hat{H}(\bullet)$ is the Heaviside ramp function. In addition, we define the fourth-order *positive* projection tensor $\mathbb{P}^+$ with components

$$\mathbb{P}^{\dagger}_{ijkl} \equiv \hat{Q}^{+}_{ia} \, \hat{Q}^{\dagger}_{jb} \, \hat{Q}_{ka} \, \hat{Q}_{lb} \tag{2.37}$$

With these notations at hand, Eq. (2.11) is then rephrased to take into account the anisotropic active (open) microcracks under tensile extensions. Specifically, we write

$$\boldsymbol{\tau} = \rho_0 \, (\mathbf{I} - \mathbf{D}^{act}) : \frac{\partial \psi_e^o(\mathbf{e}, \boldsymbol{\varepsilon}^p, \mathbf{F})}{\partial \mathbf{e}} \tag{2.38}$$

BOX 2. *Elastoplastic-damage constitutive model*

Material (Convected)	*Spatial*
(i) Multiplicative split and stress response: see (i) in Box **1**	
(ii) Damage evolution: see (ii) in Box **1**	
(iii) Tangent tensors:	
$\mathbf{A}^o \equiv \rho_0 \dfrac{\partial^2 \Psi_e^o}{\partial \mathbf{E}^2}$	$\mathbf{a}^o \equiv \rho_0 \dfrac{\partial^2 \psi_e^o}{\partial \mathbf{e}^2}$
$\mathbf{M} \equiv \rho_0 \dfrac{\partial^2 \Psi_e^o}{\partial \mathbf{E}\, \partial \mathbf{E}^p}$	$\mathbf{m} \equiv \rho_0 \dfrac{\partial^2 \psi_e^o}{\partial \mathbf{e}\, \partial \mathbf{e}^p}$
(iv) Plastic flow rule:	
$\dot{\mathbf{E}}^p = -\dot{\gamma}\, \mathbf{M}^{-1} : \dfrac{\partial \Phi(\mathbf{E}, \mathbf{E}^p, Q)}{\partial \mathbf{E}}$	$L_v \mathbf{e}^p = -\dot{\gamma}\, \mathbf{m}^{-1} : \dfrac{\partial \phi(\mathbf{e}, \mathbf{e}^p, \mathbf{q}, \mathbf{F})}{\partial \mathbf{e}}$
$\overset{\bullet}{\mathbf{S}}{}^p \equiv -\mathbf{M} : \dot{\mathbf{E}}^p$	$L_v \bar{\boldsymbol{\tau}}^p \equiv -\mathbf{m} : L_v \mathbf{e}^p$
(v) Hardening law:	
$\dot{Q} = \dot{\gamma}\, H(\mathbf{E}, \mathbf{E}^p, Q)$	$L_v \mathbf{q} = \dot{\gamma}\, \mathbf{h}(\mathbf{e}, \mathbf{e}^p, \mathbf{q}, \mathbf{F})$
(vi) Loading/unloading conditions:	
$\dot{\gamma} \geq 0\,,\ \Phi \leq 0$	$\dot{\gamma} \geq 0\,,\ \phi \leq 0$
$\dot{\gamma}\, \Phi = 0$	$\dot{\gamma}\, \phi = 0$
(vii) Elastoplastic and elastoplastic-damage tangent moduli: see Eq. (2.30),(2.33)	

where $\mathbf{D}^{act} \equiv d\, \mathbb{P}^+ \mathbf{I}\, \mathbb{P}^+ = d\, \mathbb{P}^+ \mathbb{P}^+$ is the fourth-order *active* anisotropic damage tensor.

If all three principal strains e_i are *tensile*, then we have $\mathbb{P}^+ = \mathbf{I}$ and $\mathbf{D}^{act} = d\, \mathbf{I}$; i.e., the

local microcrack is open (active) in all three principal directions and isotropic damage is recovered. On the other hand, if all e_i are *compressive*, then $\mathbf{P}^{+} = \mathbf{0}$ and $\mathbf{D}^{act} = \mathbf{0}$; i.e., the local microcrack is entirely closed (passive) under current state. Clearly, other combinations of tensile and compressive states will give rise to various microcrack opening and closing situations.

II.3. Computational integration algorithm

We now focus on the algorithmic treatment for the proposed elastoplastic-damage mechanisms. A spatial setting is adopted here and a general isotropic/anisotropic *three-step* elastic-plastic-damage return mapping algorithm is presented.

In accordance with the notion of operator split, the elastic-plastic-damage rate equations can be consistently and efficiently integrated by a three-step return mapping algorithm. The three-step operator split results in an "elastic predictor/ plastic corrector / damage corrector" algorithm. In particular, the "plastic corrector" utilizes the cutting plane algorithm (see, e.g., Ortiz and Simo [1986]) with damage value *fixed*. By contrast, in the "damage corrector" phase, plastic internal variables are fixed. The details are given in the following step-by-step integration procedures.

3.1. Elastic predictor. The initial conditions at Gauss points for the elastic predictor are $\{ \boldsymbol{\tau}_n , d_n , \mathbf{b}_n^e , \mathbf{q}_n \}$, with $\mathbf{b}_n^e \equiv \mathbf{F}_n^e \, \mathbf{F}_n^{eT}$.

(i) *Geometric update*: given the incremental displacement field $\mathbf{u}$

$$\boldsymbol{\phi}_{n+1} = \boldsymbol{\phi}_n + \mathbf{u} \quad ; \quad \mathbf{F}_{\mathbf{u}} = \mathbf{1} + \nabla_{\mathbf{x}_n} \mathbf{u} \tag{3.1}$$

$$\mathbf{F}_{n+1} = \mathbf{F}_{\mathbf{u}} \, \mathbf{F}_n \tag{3.2}$$

(ii) *Elastic predictor*: by using hyperelastic potential and multiplicative split. Set initial iteration count $k = 0$.

$$\mathbf{b}_{n+1}^{e\,(0)} = \mathbf{F}_{\mathbf{u}} \, \mathbf{b}_n^e \, \mathbf{F}_{\mathbf{u}}^T \quad ; \quad \mathbf{q}_{n+1}^{(0)} = \mathbf{F}_{\mathbf{u}} . \, \mathbf{q}_n \quad ; \quad d_{n+1}^{(0)} = d_n \tag{3.3}$$

$$\bar{\boldsymbol{\tau}}_{n+1}^{(0)} = 2 \, \rho_0 \, \frac{\partial \psi_e^o(\mathbf{g}_{n+1} , \mathbf{b}_{n+1}^{e\,-1\,(0)} , \mathbf{F}_{n+1})}{\partial \mathbf{g}} = \rho_0 \, \frac{\partial \psi_e^o(\mathbf{e}_{n+1} , \mathbf{e}_{n+1}^{p\,(0)} , \mathbf{F}_{n+1})}{\partial \mathbf{e}} \tag{3.4}$$

where $\mathbf{e}_{n+1}^{p\,(0)} \equiv \frac{1}{2} \, (\mathbf{b}_{n+1}^{e\,-1\,(0)} - \mathbf{b}_{n+1}^{-1})$ with $\mathbf{b}_{n+1} \equiv \mathbf{F}_{n+1} \, \mathbf{F}_{n+1}^T$.

3.2. Plastic corrector: damage is *fixed* in this phase and computations are performed in the effective space.

(iii) *Check for yielding*:

$$\phi(\mathbf{g}_{n+1}\,,\,\mathbf{b}_{n+1}^{e-1\,(k)}\,,\,\mathbf{q}_{n+1}^{(k)}\,,\,\mathbf{F}_{n+1}) \leq TOL\ ? \tag{3.5}$$

YES: Set $(\bullet)_{n+1} = (\bullet)_{n+1}^{(k)}$. GO TO (v)
NO: Continue (3.6)

(iv) *Plastic return mapping corrector*:

(a) Compute plastic consistency parameter:

$$\Delta\gamma_{n+1}^{(k+1)} = \phi_{n+1}^{(k)} \Big/ \left[4\,\frac{\partial\phi}{\partial \mathbf{b}^{e-1}} : \mathbf{m}^{-1} : \frac{\partial\phi}{\partial \mathbf{g}} - \frac{\partial\phi}{\partial \mathbf{q}} \bullet \mathbf{h} \right]_{n+1}^{(k)} \tag{3.7}$$

(b) Update state variables:

$$\bar{\boldsymbol{\tau}}_{n+1}^{(k+1)} = \bar{\boldsymbol{\tau}}_{n+1}^{(k)} - 2\,\Delta\gamma_{n+1}^{(k+1)}\,\frac{\partial\phi}{\partial \mathbf{g}}\Bigg]_{n+1}^{(k)} \tag{3.8}$$

$$\mathbf{b}_{n+1}^{e-1\,(k+1)} = \mathbf{b}_{n+1}^{e-1\,(k)} - 2\,\Delta\gamma_{n+1}^{(k+1)}\,\mathbf{m}^{-1} : \frac{\partial\phi}{\partial \mathbf{g}}\Bigg]_{n+1}^{(k)} \tag{3.9}$$

$$\mathbf{q}_{n+1}^{(k+1)} = \mathbf{q}_{n+1}^{(k)} + \Delta\gamma_{n+1}^{(k+1)}\ \mathbf{h}_{n+1}^{(k)} \tag{3.10}$$

$$\text{Set } k \leftarrow k+1 \ \ ;\ \ \text{GO TO (iii)} \tag{3.11}$$

At the end of this step, the state variables become $\{\ \bar{\boldsymbol{\tau}}_{n+1}\,,\,d_n\,,\,\mathbf{b}_{n+1}^{e}\,,\,\mathbf{q}_{n+1}\ \}$. It should be noted that all existing return mapping algorithms for elastoplasticity become directly applicable (with no modification) in our elastoplastic-damage formulation.

3.3. Damage corrector: to produce the final state $\{\ \boldsymbol{\tau}_{n+1}\,,\,d_{n+1}\,,\,\mathbf{b}_{n+1}^{e}\,,\,\mathbf{q}_{n+1}\ \}$. Plastic variables are *fixed* in this phase.

(v) *Damage evolution*:

(a) Compute "damage energy release rate" ξ_{n+1} according to

$$\xi_{n+1} \equiv \rho_0\,\psi^o(\mathbf{g}_{n+1}\,,\,\mathbf{b}_{n+1}^{e-1}\,,\,\mathbf{F}_{n+1}\,,\,\mathbf{q}_{n+1}) \tag{3.12}$$

(b) Update the isotropic damage variable and damage threshold r_{n+1} :

$$d_{n+1} = \begin{cases} d_n & \text{if } \xi_{n+1} - r_n \leq 0 \\ d_n + (\xi_{n+1} - \xi_n)\,\Xi_{n+1} & \text{otherwise} \end{cases} \tag{3.13}$$

$$r_{n+1} \equiv max \{ r_n , \xi_{n+1} \} \tag{3.14}$$

(c) Update Kirchhoff stress:

$$\boldsymbol{\tau}_{n+1} = \begin{cases} (1 - d_{n+1})\, \bar{\boldsymbol{\tau}}_{n+1} & \text{if isotropic} \\ (\mathbf{I} - \mathbf{D}^{acl}_{n+1}) : \bar{\boldsymbol{\tau}}_{n+1} & \text{if anisotropic} \end{cases} \tag{3.15}$$

For details pertaining to the computation of $\mathbf{D}^{acl}_{n+1}$, we refer to Eq. (2.35)-(2.37) in Sec. 2.5. It is emphasized that **no** iteration is required in the damage correction phase. Although plasticity and damage are *coupled* in rate equations, the algorithmic treatment renders *uncoupled* plasticity and damage algorithms. The simplicity and efficiency of the overall procedures are noteworthy.

Remark 3.1. It is well known that there exist uniqueness, well-posedness and numerical convergence problems associated with apparent "strain-softening" computations due to the loss of local *strong ellipticity*. As a result, finite element computations exhibit spurious mesh sensitivity when the mesh size goes to infinitesimal. In view of the concepts of homogenization (unit cell) and characteristic length, a nonlocal damage theory may be considered to overcome these numerical difficulties; see, e.g, Bazant et al. [1987][1988], Pijaudier-Cabot and Bazant [1987]. Nevertheless, nonlocal computation is to some extent incompatible with local finite element calculation and further enhancement in consistency and accuracy is needed. On the other hand, the viscous damage mechanism outlined in Remark 2.4 may be considered to accommodate dynamic (rate) damage effects and to control loss of ellipticity. □

II.4. Numerical experiment

The performance of proposed elastoplastic-damage constitutive models is illustrated through a numerical experiment in this section. Our finite element treatment relies on a mixed variational formulation of the Hu-Washizu type. The four-node element with bilinear isoparametric displacement field and constant (current) volume is employed. A combination of BFGS updates and line search with periodic re-factorizations are used for the proposed models.

II.4.1. Selection of ψ^o

In order to carry out evolution of damage, selection of the spatial "damage energy release rate" (the undamaged total potential energy function) $\rho_0 \psi^o(\mathbf{g}, \mathbf{b}^{e-1}, \mathbf{F}, \mathbf{q})$ has to be addressed. In general, the specific form of ψ^o depends on the mechanical behavior and thermodynamic processes of materials. In particular, from Eq. (2.9), it is seen that the spatial thermodynamic force conjugate to $\dot{\mathbf{q}}$ is actually $-\frac{\partial \psi_p^o}{\partial \mathbf{q}}$. Therefore, it is rational to postulate that

$$\dot{\mathbf{q}} \equiv \dot{\gamma} \frac{\partial \phi(\mathbf{g}, \mathbf{b}^{e-1}, \mathbf{q}, \mathbf{F})}{\partial (-\frac{\partial \psi_p^o}{\partial \mathbf{q}})} \tag{4.1}$$

By comparing Eq. (4.1) with (2.28), we realize that

$$\mathbf{h}(\mathbf{g}, \mathbf{b}^{e-1}, \mathbf{q}, \mathbf{F}) \equiv -\frac{\partial \phi(\mathbf{g}, \mathbf{b}^{e-1}, \mathbf{q}, \mathbf{F})}{\partial (\frac{\partial \psi_p^o}{\partial \mathbf{q}})} \tag{4.2}$$

The von Mises J_2-flow theory with isotropic linear hardening is considered for the effective plastic response in what follows. This leads to $\frac{d\psi_p^o}{d\bar{e}^p} = R(\bar{e}^p)$, with $\bar{e}^p$ and $R(\bar{e}^p)$ signifying the equivalent plastic strain and yield radius, respectively. We then arrive at $\psi_p^o = \int_0^{\bar{e}^p} R(\bar{e}^p)\, d\bar{e}^p$. For linear isotropic hardening, one writes

$$R(\bar{e}^p) = \sqrt{\tfrac{2}{3}}\,\kappa(\bar{e}^p) = \sqrt{\tfrac{2}{3}}\,(Y_0 + \eta\,\bar{e}^p) \tag{4.3}$$

with Y_o and η denoting the initial effective yield stress and linear hardening slope, respectively. As a result, we obtain

$$\psi_p^o(\bar{e}^p) = \sqrt{\tfrac{2}{3}}\,(Y_o\,\bar{e}^p + \tfrac{1}{2}\,\eta\,\bar{e}^{p\,2}) \tag{4.4}$$

On the other hand, the form of ψ_e^o hinges on the particular hyperelasticity model employed. We shall consider the following hyperelastic store energy function with uncoupled volumetric and deviatoric parts

$$\psi_e^o(\mathbf{g}\,,\,\mathbf{b}^{e-1}\,,\,\mathbf{F}) = K\,(J\,\ln\Theta - J + 1) + \tfrac{1}{2}\,\mu^o\,(\tilde{I}_{\mathbf{b}^e} - 3) \tag{4.5}$$

where $\Theta = J \equiv \det\mathbf{F}$, μ^o = initial shear modulus, K = initial bulk modulus, and $\tilde{I}_{\mathbf{b}^e} \equiv J^{-2/3}\,\mathbf{b}^e : \mathbf{g}$.

II.4.2. Quasi-static damage propagation of a notched specimen

Consider the quasi-static damage propagation (including *micro*crack and *macro*-crack growth) in a notched specimen under tension and plane strain condition for the proposed elastoplastic-damage models. Of particular interest is the coupling between the plasticity and damage mechanisms. Due to the *energy*-based characterization of damage, the model predicts *higher* (faster) damage accumulation in the presence of *plastic flow*. This is in agreement with experimental observations and the so-called "plastic correction" procedure typically employed in fracture mechanics.

A finite element mesh consisting of 288 elements is shown in Figure 1. For exponentially growing progressive damage, the evolution function Ξ is assumed to be

$$\Xi = \frac{\xi_0(1-A)}{\xi^2} + A\,B\,\exp[B\,(\xi_0 - \xi)] \tag{4.6}$$

Here A and B are characteristic material properties and ξ_0 denotes the initial damage threshold. These material properties can be estimated in a systematic manner from

suitable experimental data. The numerical values of the (metallic) material properties used in computation are taken as $E = 206.916$ GPa, $\nu = 0.29$, $A = 0.85$, $B = 14$ GPa^{-1}, $\xi_0 = 0.0004$ GPa, $Y_0 = .45$ GPa, and $\eta = 100$ GPa.

The specimen is under displacement boundary control. As the magnitude of the control displacement is increased, one observes a corresponding increase in value of the damage variable d in those elements ahead of the notch tip. Eventually, complete damage (corresponding to $d = .995$) is obtained. Thus, *crack propagation* is characterized as the *locus of points* for which the damage variable $d = 0.995$. Figure 2 shows the global load-deflection curve of the loading histories. It is observed that the number of fully damaged elements increases as the crack mouth opening displacement (CMOD) increases.

The relationship among the number of fully damaged elements (ahead of the notch tip), the number of plastically yielded elements (ahead of the notch tip), and the time-step count is summarized in Table 1. Note that the number of yielded elements is always *higher* than that of fully damaged elements; and that the latter number increases with the former number. This illustrates the strong coupling between plasticity and damage mechanisms, and demonstrates the fundamental role played by plastic flow in damage growth. Such a mode of response is in qualitative agreement with available physical evidence. The damage contours of the specimen at the 15th and 20th load steps are shown in Figures 3 and 4, respectively. In addition, the yielded zone at the 20th load step is displayed in Fig. 5. Finally, at the end of the experiment, an interesting *macrocrack* path and yielded zone are recorded in Figures 6 and 7, respectively. The capability of the proposed models to simulate damage initiation and growth as well as crack propagation is demonstrated.

Table 1. *Number of fully damaged elmts vs. load steps*

Step	No. "cracked"	No. yielded
3	0	1
5	0	2
6	1	3
9	2	5
11	3	7
12	4	7
14	5	8
19	6	10
21	7	11

II.5. Closure

Energy-based isotropic and anisotropic elastoplastic damage models at finite strains have been presented in this paper to characterize progressive damage and crack growth. The proposed framework is capable of accommodating general nonlinear elastoplastic response, anisotropic microcrack opening and closing, and the coupling of damage and plasticity. Damage initiation and propagation are linked to the homogenized "damage energy release rate" $\rho_0 \psi^o$. The loading/unloading criterion compares $\rho_0 \psi^o$ with the current damage threshold (debonding energy level) to determine whether unstable microcrack growth will occur. It is noted that the proposed damage models are compatible with general finite strain elastoplasticity formulation previously proposed by Simo [1988].

An essential purpose of the present work is to demonstrate that the proposed classes of elastoplastic-damage constitutive equations are suitable for large scale computation. In particular, use of the operator splitting methodology leads to a three-step integration algorithm which algorithmically uncouples the coupled plastic and damage responses. This is possible because of the effective stress concept. A numerical experiment is also given to illustrate the potential applicability of the proposed models.

II.6. References

Bazant, Z.P., F.B. Lin and G. Pijaudier-Cabot [1987], "Yield limit degradation: Nonlocal continuum model with local strain," in Proc. of Int. Conf. on Comp. Plast., pp. 1757-1780, April 6-10, 1987, Barcelona, Spain.

Bazant, Z.P. and G. Pijaudier-Cabot [1988], "Nonlocal continuum damage and measurement of characteristic length," in *Mechanics of Composite Materials - 1988*, pp. 79-86, Proc. of Joint ASME/SES Conf., June 20-22, 1988, Berkeley, Calif..

Budiansky, B. and R.J. O'Connel [1976], "Elastic moduli of a cracked solid," *Int. J. Solids & Struct.*, Vol. 12, pp. 81-97.

Coleman, B.D. and M. Gurtin [1967], "Thermodynamics with internal variables," *J. Chem. Physics*, Vol. 47, pp. 597-613.

Dragon, A. [1985], "Plasticity and ductile fracture damage: study of void growth in metals," *Engng. Fract. Mech.*, Vol. 21, No. 4, pp. 875-885.

Dragon, A. and A. Chihab [1985], "On finite damage: ductile fracture-damage evolution," *Mech. Mater.*, Vol. 4, pp. 95-106.

Horii, H. and S. Nemat-Nasser [1983], "Overall moduli of solids with microcracks: Load induced anisotropy," *J. Mech. Phys. Solids*, Vol. 31, No. 2, pp. 155-171.

Ju, J.W., [1986], "Constitutive modeling for inelastic materials including damage and finite strain effects," Ph.D. Dissertation, Department of Civil Engineering, University of California, Berkeley.

Ju, J.W., [1988], "On energy-based coupled elastoplastic damage theories: constitutive modeling and computational aspects," *Int. J. Solids & Struct.*, accepted for publication.

Kachanov, L.M. [1958], "Time of the rupture process under creep conditions," *IVZ Akad Nauk*, S.S.R., Otd Tech Nauk, No. 8, pp. 26-31.

Kachanov, M.L. [1980], "Continuum model of medium with cracks," *J. Eng. Mech. Div.*, A.S.C.E., Vol. 106, pp. 1039-1051.

Krajcinovic, D. [1984], "Continuum damage mechanics," *Appl. Mech. Rev.*, Vol. 37: 1-6, pp. 397-402.

Krajcinovic, D. [1985], "Constitutive theories for solids with defective microstructure," in *Damage Mechanics and Continuum Modeling*, ed. by N. Stubbs and D. Krajcinovic, ASCE, pp. 39-56.

Krajcinovic, D. [1986], "Update to continuum damage mechanics," *Appl. Mech. Update*, pp. 403-406.

Krajcinovic, D. [1987], "Micromechanical basis of phenomenological models," in *Continuum Damage Mechanics: Theory and Application*, Ed. by D. Krajcinovic and J. Lemaitre, Springer-Verlag, to appear.

Krajcinovic, D. and D. Fanella [1986] "A micromechanical damage model for concrete," *Eng. Fract. Mech.*, Vol. 25, No. 5/6, pp. 585-596.

Lemaitre, J. [1971], "Evaluation of dissipation and damage in metals", Proc. I.C.M. (1), Kyoto, Japan.

Lemaitre, J. [1984], "How to use damage mechanics," *Nucl. Eng. Design*, Vol. 80, pp. 233-245.

Lemaitre, J. [1985], "A continuous damage mechanics model for ductile fracture," *J. of Eng. Mater. Tech.*, Vol. 107, pp. 83-89.

Lemaitre, J. [1986], "Plasticity and damage under random loading," in Proc. of the Tenth U.S. National Congress of Appl. Mech., ASME, pp. 125-134, ed. by J.P. Lamb, June 16-20, 1986, Austin, Texas.

Lemaitre, J. and J.L. Chaboche [1978], "Aspects phénoménologiques de la rupture par endommagement," *J. de Méca. Appl.*, Vol. 2, No. 3, pp. 317-365.

Ortiz, M. [1985], "A constitutive theory for the inelastic behavior of concrete," *Mech. of Materials,* Vol. 4, pp. 67-93.

Ortiz, M. and J.C. Simo [1986], "An analysis of a new class of integration algorithms for elastoplastic constitutive relations," *Int. J. Num. Meth. Engng.*, Vol. 23, pp. 353-366.

Pijaudier-Cabot, G. and Z.P. Bazant [1987], "Nonlocal damage theory," *J. Eng. Mech.*, ASCE, Vol. 113, No. 10, pp. 1512-1533.

Simo, J.C. [1988], "A framework for finite strain elastoplasticity based on maximum plastic dissipation and the multiplicative decomposition. Part I: Continuum formulation," *Comp. Meth. Appl. Mech. Eng.*, Vol. 66, No. 2, pp. 199-219.

Simo, J.C. and J.W. Ju [1987a], "Stress and strain based continuum damage models. Part I: Formulation," *Int. J. Solids & Struct.*, Vol. 23, No. 7, pp. 821-840.

Simo, J.C. and J.W. Ju [1987b], "Stress and strain based continuum damage models. Part II: Computational aspects," *Int. J. Solids & Struct.*, Vol. 23, No. 7, pp. 841-869.

Simo, J.C. and J.W. Ju [1987c], "On continuum damage-elastoplasticity at finite strains: A computational framework," *Comput. Mech.*, accepted for publication.

Sumarac, D. and D. Krajcinovic [1987], "A self-consistent model for microcrack-weakened solids," *Mech. Mater.*, Vol. 6, pp. 39-52.

Talreja, R. [1985], "A continuum mechanics characterization of damage in composite materials," *Proc. R. Soc. London,* Ser. A, Vol. 399, pp. 195-216.

Vakulenko, A.A. and M.L. Kachanov [1971], "Continuum theory of medium with cracks," *Mekh. Tverdogo Tela,* Vol. 4, pp. 159-166.

Wu, C.H. [1985], "Tension-compression test of a concrete specimen via a structure damage theory," in *Damage Mechanics and Continuum Modeling*, ed. by N. Stubbs and D. Krajcinovic, ASCE, pp. 1-12.

II.7. Figure captions and figures

Figure 1. Finite element mesh (288 elements) of a notched specimen. Due to symmetry, only 1/4 configuration is shown. Dimensions are in terms of *cm*.

Figure 2. The global load-deflection (CMOD) curve.

Figure 3. The damage contours at the 15th load step. Lines a , b , c , d , e denote damage values = 0.2, 0.4, 0.6, 0.8, 0.95, respectively.

Figure 4. The damage contours at the 20th load step. Lines a , b , c , d , e denote damage values = 0.2, 0.4, 0.6, 0.8, 0.95, respectively.

Figure 5. The yielded zone at the 20th load step.

Figure 6. The macrocrack path (d = 0.95) at the end of simulation.

Figure 7. The yielded zone at the end of simulation.

Fig. 1

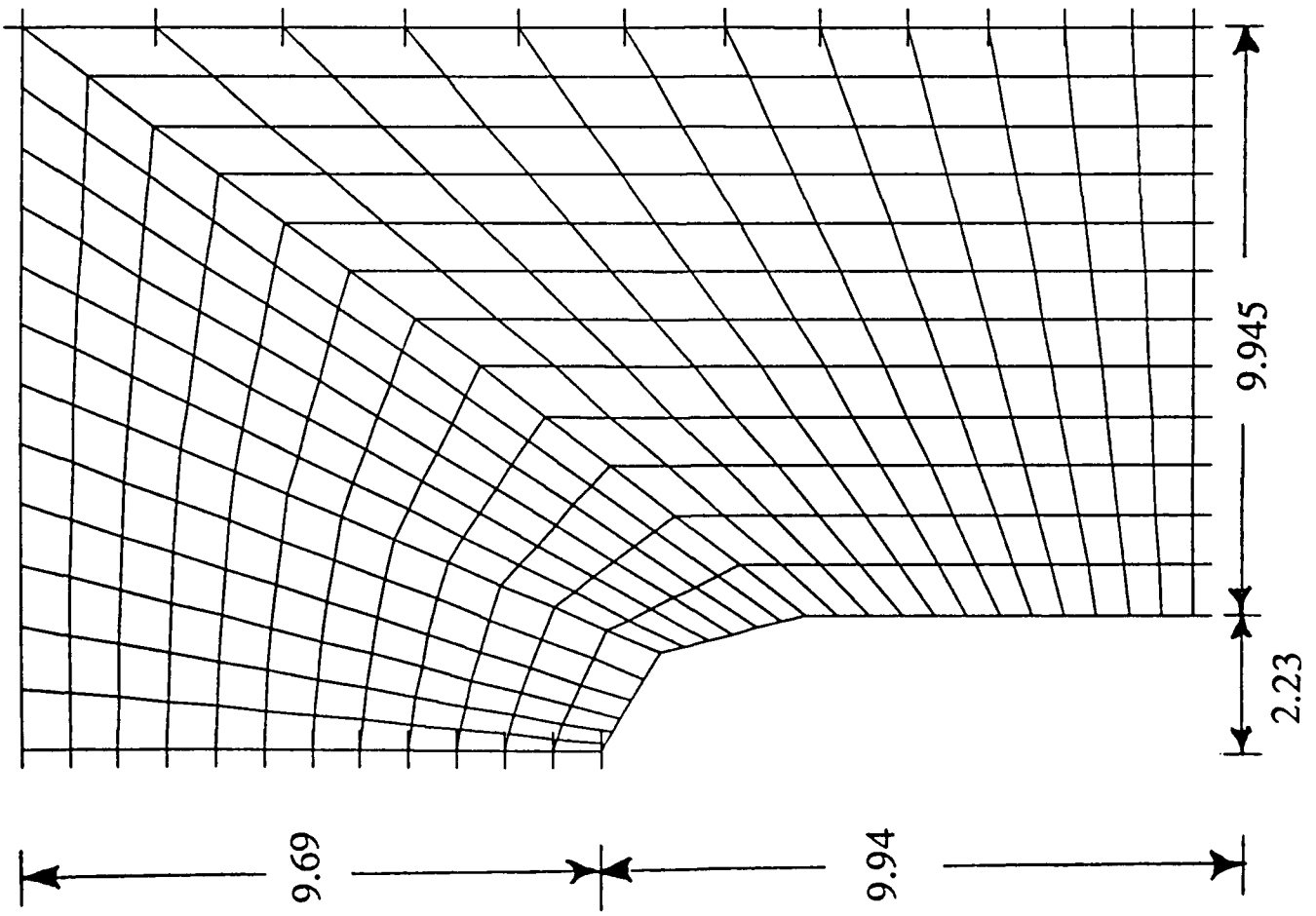

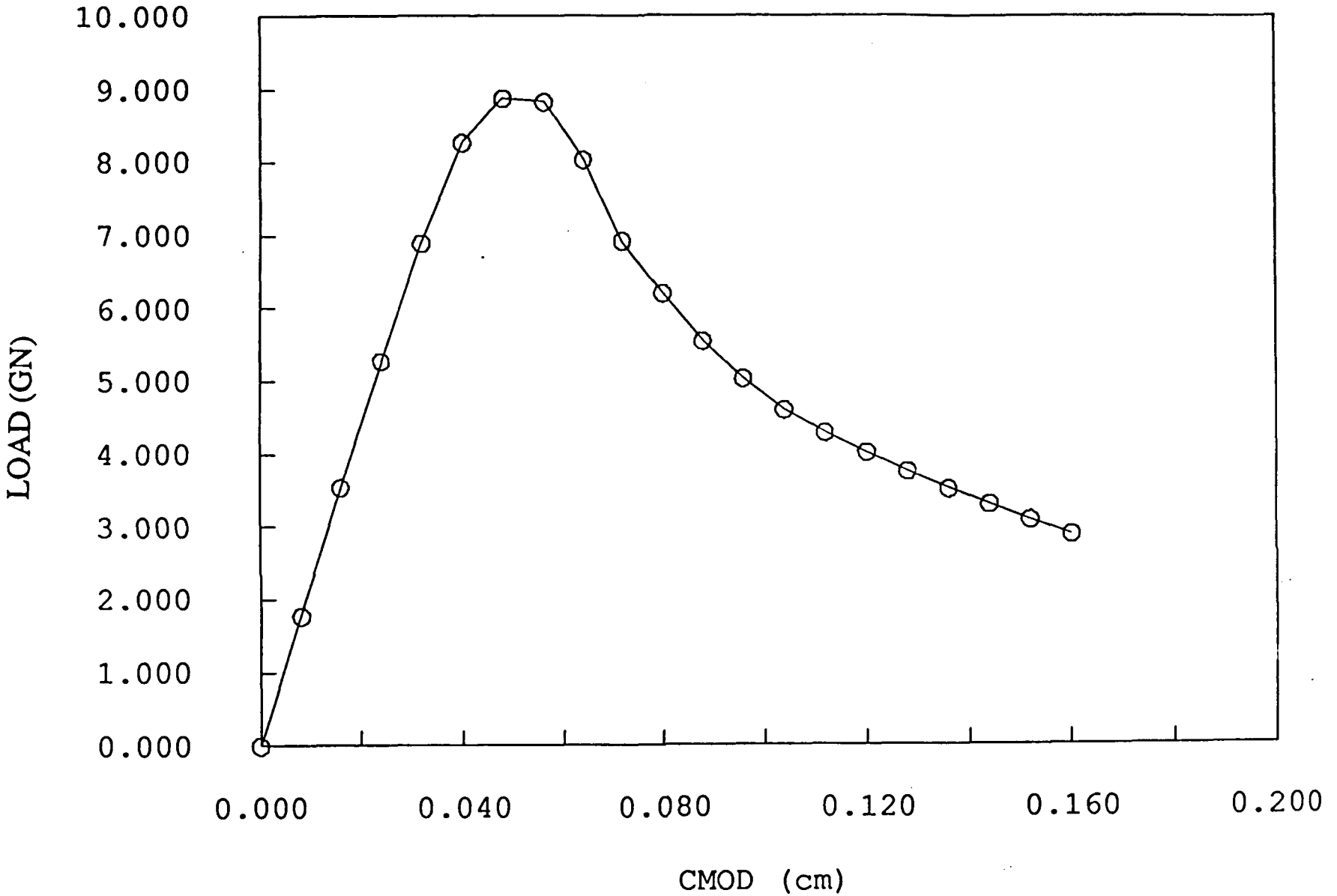
10.000
9.000
8.000
7.000
6.000
5.000
4.000
3.000
2.000
1.000
0.000
LOAD (GN)
0.000
0.040
0.080
0.120
0.160
0.200
CMOD (cm)

Fig. 2

Fig. 3

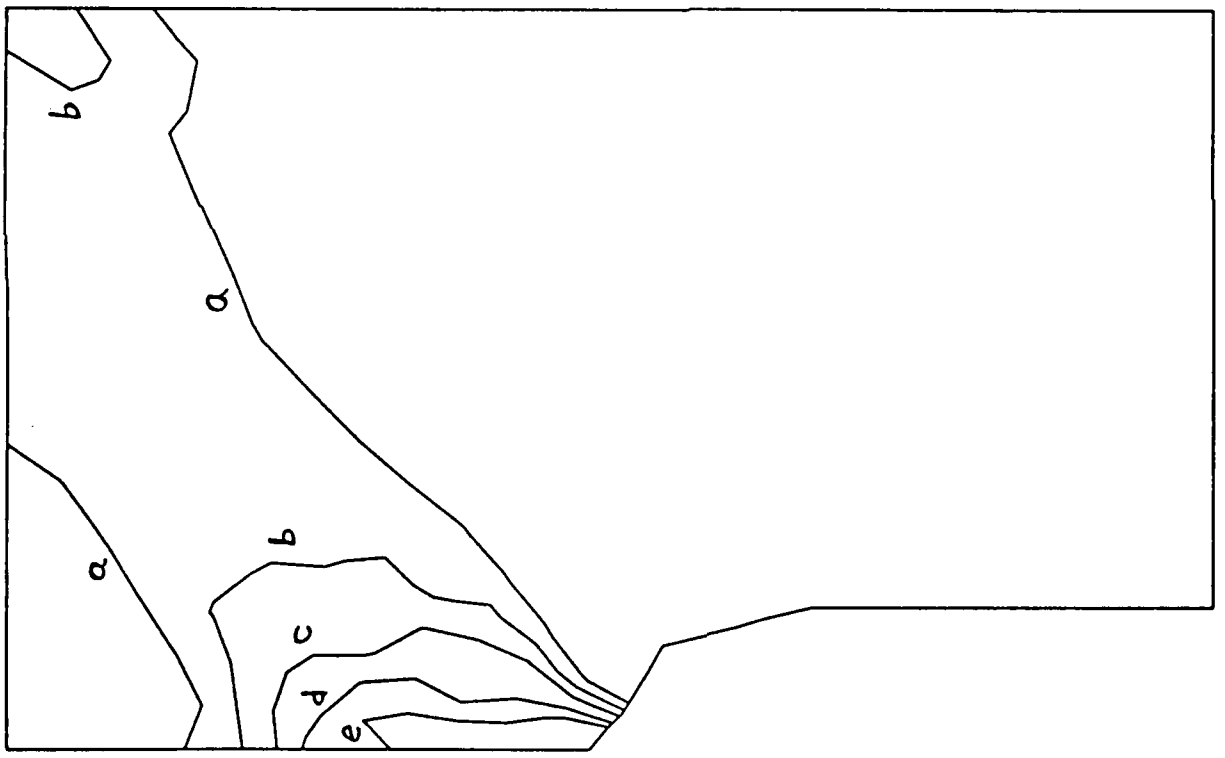

Fig. 4

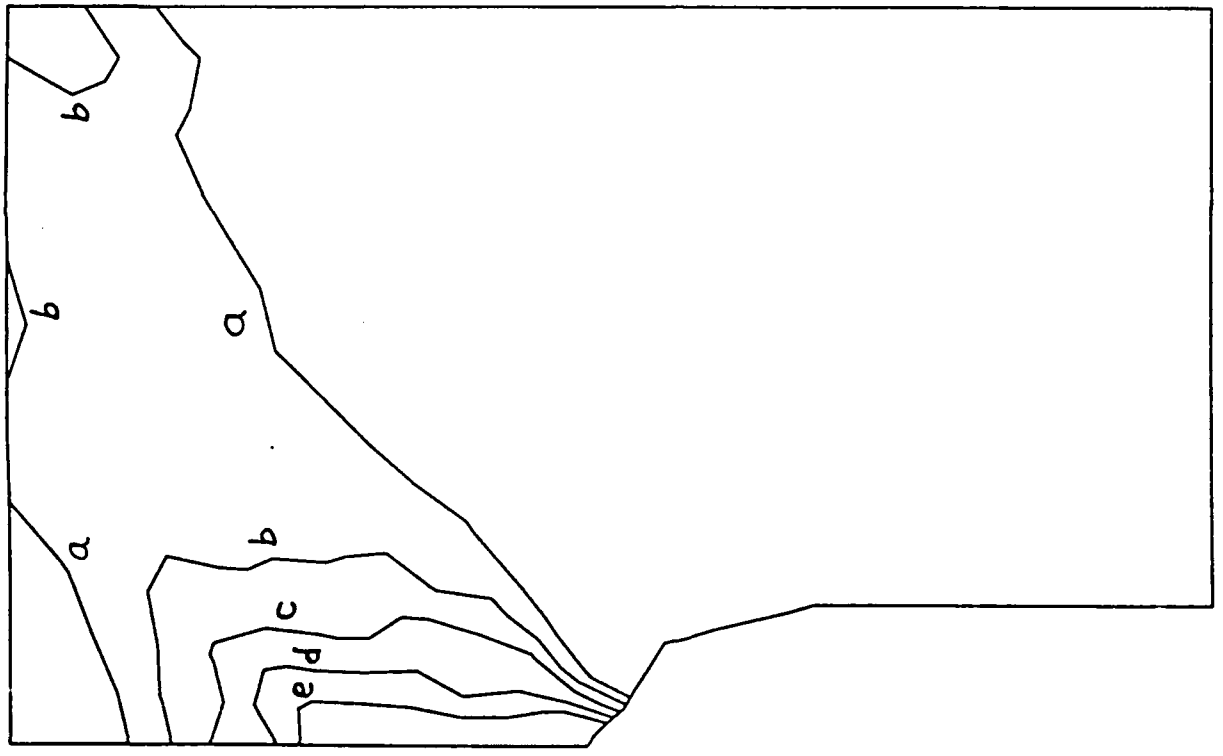

Fig. 5

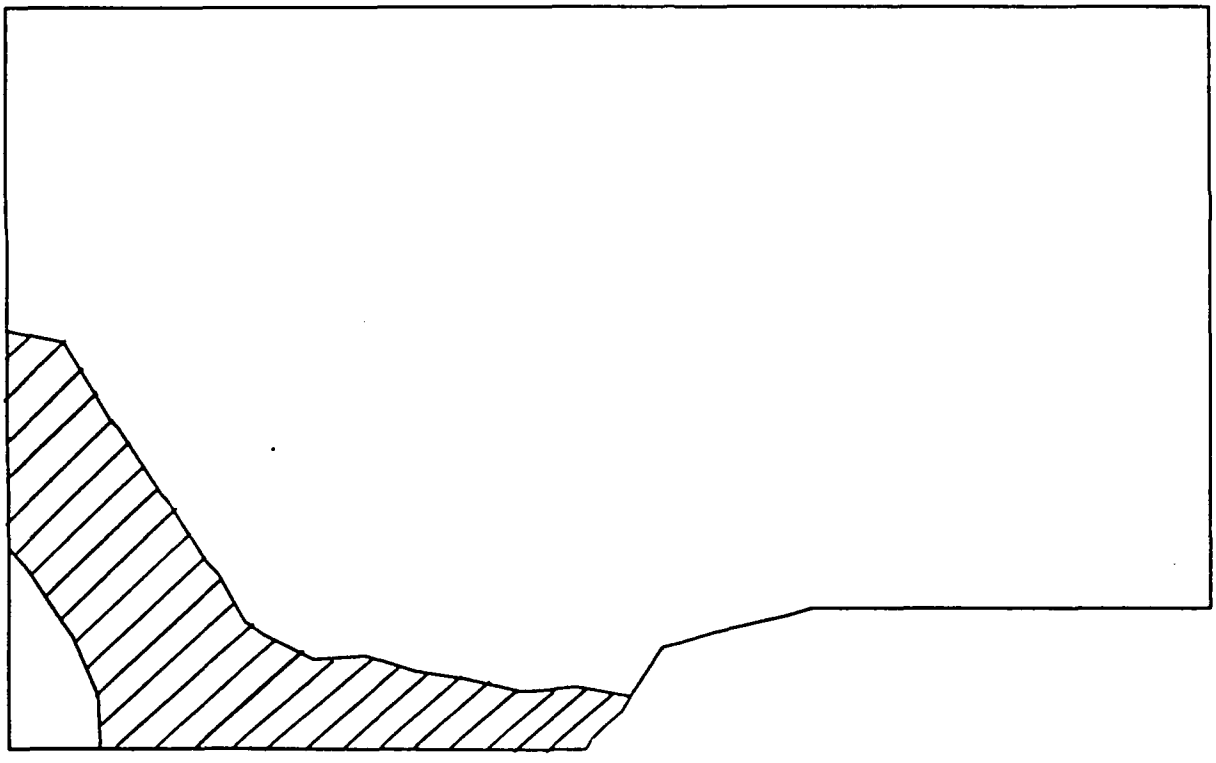

Fig. 6

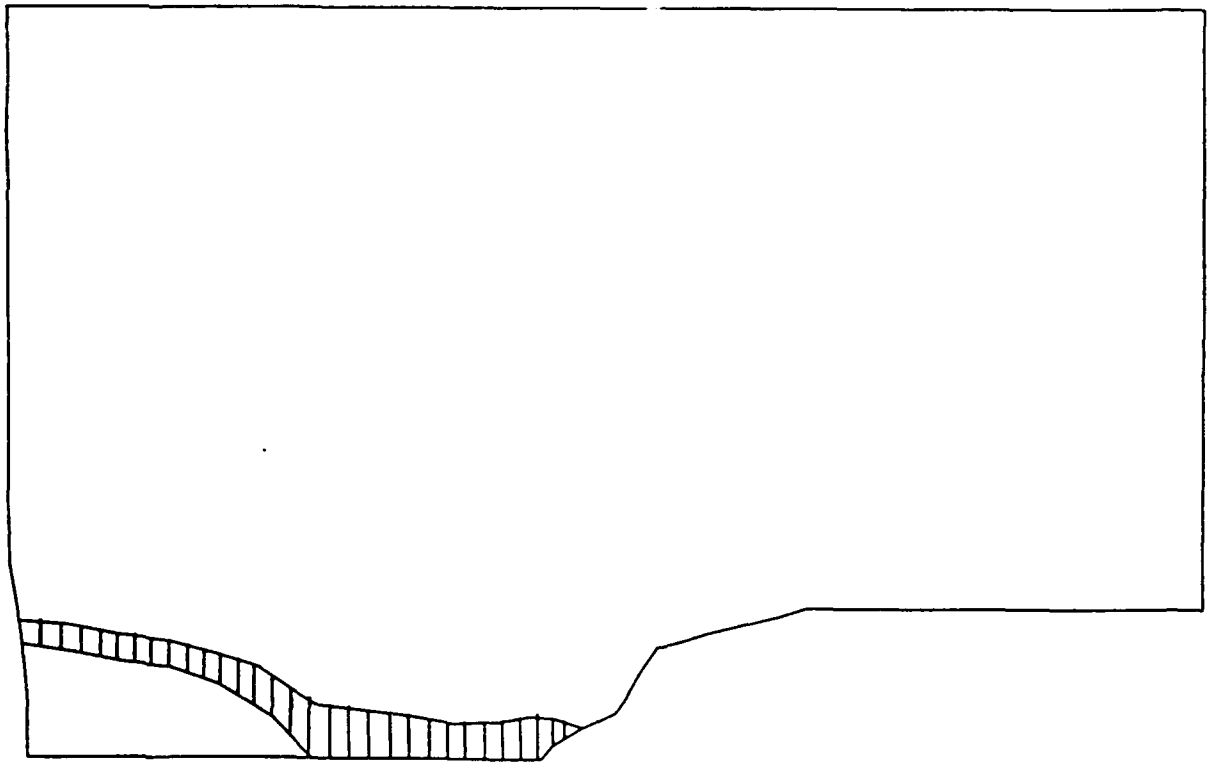

Fig. 7

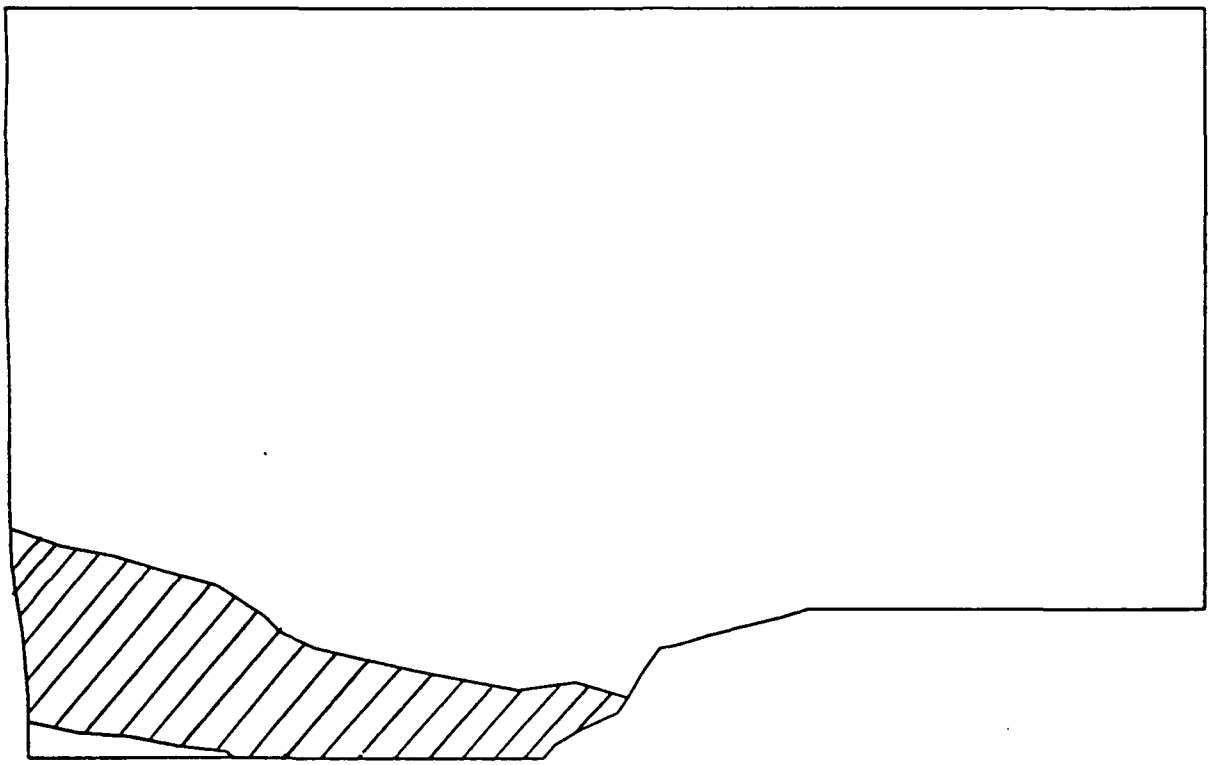

PART III
On Two-Dimensional Self-Consistent Micromechanical Damage Models for Brittle Solids

III.1. Introduction

Micromechanical (or mesomechanical) damage models for microcrack-weakened brittle solids are presented within the context of the self-consistent method and damage mechanics. For simplicity, only two-dimensional problems are considered. Though phenomenological continuum damage models provide a viable constitutive framework for efficient modeling of brittle solids (e.g., concrete, mortar and brittle composite materials), they typically do not offer insightful descriptions of mesostructural microcrack kinetics. Further, use of several fitted "material parameters" in damage evolution equations only renders vague and averaged information on underlying microcracking processes at the mesoscale (Krajcinovic and Fanella [1986]). Therefore, micromechanical damage theories, which incorporate mesostructural and micromechanical *information* into the damage mechanics framework, are warranted.

For a literature review on continuum damage mechanics, see, e.g., Krajcinovic [1984][1986], Ortiz [1985], Ju [1989]. On the other hand, micromechanical damage theories ("process models") are limited in the current literature. Some valuable examples are Wu [1985], Krajcinovic and Fanella [1986], Sumarac and Krajcinovic [1987,1989], Fanella and Krajcinovic [1988], and Krajcinovic and Sumarac [1989]. In addition, micromechanical "*non-process*" damage models (i.e., no microcrack growth) were proposed, for instance, by Budiansky and O'Connel [1976], Hoenig [1979], Horii and Nemat-Nasser [1983], and Kachanov [1987] for *static stable* microcracks. Some single crack stress and crack opening displacement analyses (boundary-value problems) were proposed by, for instance, Willis [1968], Sneddon and Lowengrub [1969], Hoenig [1978][1982], and Mura [1982]. Moreover, certain valuable *non-process*, strong microcrack interaction analyses (not quite damage constitutive theories) were proposed , e.g.,

by Horii and Nemat-Nasser [1985a], Chudnovsky, Dolgopolsky, and Kachanov [1987a,b], and Kachanov [1987].

An outline of this paper is as follows. Two-dimensional microcrack opening displacements, effective overall (secant) compliance moduli and thermodynamic basis are given in Sec. 2 for initially linear elastic (isotropic or anisotropic) brittle solids within the context of the unit-cell based self-consistent method. It is assumed that distributed microcrack concentration justifies the use of effective continuum medium theory. The microdefects are considered as line microcracks, and microcrack interaction is assumed to be weak or at most moderate. Thus, effects of strong microcrack interaction and exact locations of microcrack centers are not accounted for in this paper (see Kachanov [1987]). Localization failure modes are not considered, either. In Sec. 3, mode I, mode II and mixed mode discrete microcrack kinetic equations are examined based on mesostructural microcrack geometry and fracture mechanics stability criteria for brittle "cleavage 1" deformation processes (Ashby [1979], Sumarac and Krajcinovic [1987]). No phenomenological (fitted) "material parameters" are used in kinetic equations of microcrack growth. Further, loading/unloading stress paths are permitted, and microcrack status changes from opening to closing (or vice versa) are trivially accommodated. In Sec. 4, we present efficient computational algorithms for the proposed micromechanical damage models. Mode I uniaxial tension, mode II uniaxial compression, and mixed mode tension/compression numerical simulations are also presented in Sec. 4.

III.2. Basic framework of self-consistent elastic-damage models

In this section, we present thermodynamic basis of damage mechanics, derive and summarize *symmetric* or *non-symmetric* "displacement transformation matrices" $\mathbf{B}'$ and anisotropic overall (secant) elastic-damage compliance moduli $\bar{\mathbf{S}}$ for brittle materials. The matrix material is assumed to be perfectly linear elastic.

III.2.1. Thermodynamic basis

It has been shown (see, e.g., Simo and Ju [1987], Ju [1989]) that there exists a *one-to-one* correspondence between the fourth-order elastic-damage secant compliance tensor $\bar{\mathbf{S}}$ and the fourth-order anisotropic damage tensor $\bar{\mathbf{D}}$ (signifying volume average micro-crack density, sizes, orientations and opening/closing status). Therefore, it is rational to treat the secant compliance $\bar{\mathbf{S}}(\bar{\mathbf{D}})$ itself as the anisotropic damage variable. Within the framework of the unit-cell based homogenization concept for inhomogeneous effective continuum medium, let us define the homogenized (volume-average) complementary free energy function as (see also Krajcinovic and Sumarac [1989])

$$\chi = \tfrac{1}{2}\,\bar{\boldsymbol{\sigma}} : \bar{\mathbf{S}}(\bar{\mathbf{D}}) : \bar{\boldsymbol{\sigma}} \tag{2.1}$$

where $\bar{\boldsymbol{\sigma}}$ is the *volume-average* stress tensor (Hill [1965]). By the Clausius-Duhem inequality for isothermal process, we have (with $\bar{\boldsymbol{\varepsilon}}$ denoting the volume-average strain)

$$\dot{\chi} - \dot{\bar{\boldsymbol{\sigma}}} : \bar{\boldsymbol{\varepsilon}} \geq 0 \tag{2.2}$$

where (according to (2.1))

$$\dot{\chi} = \dot{\bar{\boldsymbol{\sigma}}} : \bar{\mathbf{S}} : \bar{\boldsymbol{\sigma}} + \tfrac{1}{2}\,\bar{\boldsymbol{\sigma}} : \overset{\bullet}{\bar{\mathbf{S}}} : \bar{\boldsymbol{\sigma}} \tag{2.3}$$

The standard Coleman's method then lead to the following macroscopic stress-strain law and the damage dissipative inequality:

$$\bar{\boldsymbol{\varepsilon}} = \bar{\mathbf{S}} : \bar{\boldsymbol{\sigma}} \tag{2.4a}$$

$$\tfrac{1}{2}\,\bar{\boldsymbol{\sigma}} : \overset{\bullet}{\bar{\mathbf{S}}} : \bar{\boldsymbol{\sigma}} \geq 0 \tag{2.4b}$$

From Eq. (2.4b), it is observed that the evolution $\dot{\bar{\mathbf{S}}}$ plays an essential role in microcrack energy dissipation and evolutions (i.e., "process models"). During a damage *loading* process (in which some microcracks increase their lengths), the total strain tensor $\bar{\boldsymbol{\varepsilon}}$ is amenable to an additive decomposition: $\bar{\boldsymbol{\varepsilon}} = \bar{\boldsymbol{\varepsilon}}^e + \bar{\boldsymbol{\varepsilon}}^d$, with $\bar{\boldsymbol{\varepsilon}}^e$ and $\bar{\boldsymbol{\varepsilon}}^d$ denoting the elastic and inelastic (damage-induced) strains, respectively. It is assumed that $\bar{\boldsymbol{\varepsilon}}^d \simeq \mathbf{0}$ upon complete unloading; that is, the residual strain at zero stress is negligible for brittle materials. The elastic-damage secant compliance tensor is also suitable for an additive decomposition: $\bar{\mathbf{S}} = \mathbf{S}^o + \mathbf{S}^d$, with $\mathbf{S}^o$ and $\mathbf{S}^d$ denoting the virgin undamaged elastic compliance and the damage-induced additional compliance, respectively (see, e.g., Mura [1982], Horii and Nemat-Nasser [1983]).

It is emphasized that once a material contains distributed microcracks, the material becomes *inelastic* due to its load-path dependency. There are different stress-strain curves corresponding to different load paths leading to same final stress state. Under some loading/unloading paths within the context of "non-process models", a damaged material may exhibit linear and reversible response within a limited range. However, one should not regard the damaged material as a perfectly elastic one. For example, when damage state $\bar{\mathbf{D}}$ is *fixed* (i.e., no microcracks increase their sizes or opening/closing status) and no frictional slip occurs, the overall response remains linear and reversible and therefore we have $\bar{\boldsymbol{\varepsilon}} = \partial\chi/\partial\bar{\boldsymbol{\sigma}}$ and $\bar{\mathbf{S}} = \partial^2\chi/\partial\bar{\boldsymbol{\sigma}}^2$ (*symmetric*). Nevertheless, this is not true when damage state is not fixed or when frictional slip is taking place. In addition, the differentiation of (2.4a) renders elastic-damage *tangent* compliance tensor $\bar{\mathbf{S}}^{tang}$ under damage loading condition:

$$\bar{\mathbf{S}}^{tang} \equiv \frac{\partial\bar{\boldsymbol{\varepsilon}}}{\partial\bar{\boldsymbol{\sigma}}} = \bar{\mathbf{S}} + \frac{\partial\bar{\mathbf{S}}}{\partial\bar{\boldsymbol{\sigma}}} : \bar{\boldsymbol{\sigma}} \tag{2.5}$$

From (2.5), it is clear that $\bar{\mathbf{S}}^{tang} \neq \bar{\mathbf{S}}$ in general.

Assuming moderate microcrack concentration and microcracks being away from unit-cell boundaries, we have $\bar{\boldsymbol{\sigma}} \simeq \boldsymbol{\sigma}^{\infty}$, where $\boldsymbol{\sigma}^{\infty}$ signifies the remotely applied stress

field around unit-cell boundaries (Hill [1965]). Therefore, the microcrack-induced inelastic strain may be approximately expressed as (Vakulenko and Kachanov [1971], Kachanov [1980], Horii and Nemat-Nasser [1983])

$$\bar{\boldsymbol{\varepsilon}}^d = \frac{1}{2V} \sum_k \left[\int_S (\mathbf{b} \otimes \mathbf{n} + \mathbf{n} \otimes \mathbf{b})\, dS \right]^{(k)} \tag{2.6}$$

where V is the representative volume of a unit-cell, $\sum$ is a summation operator over all active (open or sliding) microcracks, $\mathbf{b}$ denotes the crack opening displacement vector, and $\mathbf{n}$ signifies the normal vector associated with $\mathbf{b}$. For two-dimensional line microcracks, Eq. (2.6) can be rephrased as (with A denoting the area of unit-cell surface):

$$\bar{\boldsymbol{\varepsilon}}^d = \frac{1}{2A} \sum_k \left[\int_l (\mathbf{b} \otimes \mathbf{n} + \mathbf{n} \otimes \mathbf{b})\, dl \right]^{(k)} \tag{2.7}$$

As was pointed out by Krajcinovic [1985], the alternative definition of the damage variable in terms of $\bar{\boldsymbol{\varepsilon}}^d$ in (2.6) or (2.7) is thermodynamically incorrect. The reason is obvious as follows. During "mode I" elastic unloading, $\mathbf{b}$ decreases and the damage variable (defined by Eq. (2.6) or (2.7)) changes its state, thus leading to energy dissipation even under "mode I" elastic unloading. Therefore, though Eq. (2.6) is an acceptable measure of the damage-induced inelastic deformation, it is not a good choice for anisotropic damage variable. The derivation of appropriate "thermodynamic force" conjugate to the "rate of change of the microcrack density" will be given in the next section.

III.2.2. Elastic-damage secant compliance

In a two-dimensional setting (e.g., plane strain), Eq. (2.4a) can be rewritten using Voigt's notation (see Eq. (22) in Horii and Nemat-Nasser [1983])

$$\bar{e}_i = \bar{S}_{ij}\, \bar{\tau}_j \quad ; \quad i\,, j = 1\,, 2\,, 3 \tag{2.8}$$

where $\bar{e}_1 = \bar{\varepsilon}_{11}$, $\bar{e}_2 = \bar{\varepsilon}_{22}$, $\bar{e}_3 = 2\,\bar{\varepsilon}_{12}$, $\bar{\tau}_1 = \bar{\sigma}_{11}$, $\bar{\tau}_2 = \bar{\sigma}_{22}$, $\bar{\tau}_3 = \bar{\sigma}_{12}$, and $\bar{\mathbf{S}}$ is a three by three elastic-damage secant compliance matrix. For *open* microcracks, the secant compliance

is in fact the *unloading* compliance. Therefore, the secant compliance $\bar{\mathbf{S}}$ is *symmetric* (though anisotropic) according to Sec. **2.1**. In the case of mode II frictional sliding on *closed* microcrack faces, by contrast, the elastic-damage secant compliance $\bar{\mathbf{S}}$ is *non-symmetric* ($\bar{S}_{ij} \neq \bar{S}_{ji}$) during either loading or unloading processes. In addition, coordinate transformation matrices $\mathbf{g}$ and $\mathbf{g}'$ relating the secant compliance matrices $\bar{\mathbf{S}}$ and $\bar{\mathbf{S}}'$ (in global and local Cartesian coordinate systems, respectively) are available from Eq. (24) in Horii and Nemat-Nasser [1983]:

$$\bar{S}'_{ij} = g'_{im}\, g'_{jn}\, \bar{S}_{mn} \quad ; \quad \bar{S}_{ij} = g_{mi}\, g_{nj}\, \bar{S}'_{mn} \tag{2.9a}$$

$$[\mathbf{g}'] \equiv \begin{bmatrix} \cos^2\theta & \sin^2\theta & \tfrac{1}{2}\sin 2\theta \\ \sin^2\theta & \cos^2\theta & -\tfrac{1}{2}\sin 2\theta \\ -\sin 2\theta & \sin 2\theta & \cos 2\theta \end{bmatrix} \quad ; \quad [\mathbf{g}] \equiv \begin{bmatrix} \cos^2\theta & \sin^2\theta & \sin 2\theta \\ \sin^2\theta & \cos^2\theta & -\sin 2\theta \\ -\tfrac{1}{2}\sin 2\theta & \tfrac{1}{2}\sin 2\theta & \cos 2\theta \end{bmatrix} \tag{2.9b}$$

It is remarked that the "local" (primed) coordinate system is the intrinsic coordinate system associated with a particular microcrack such that the y'-axis is parallel to the microcrack unit normal vector $\mathbf{n}$, see Fig. 1. Within the context of the self-consistent method, it remains to determine the crack opening displacement $\mathbf{b}'$ across an isolated line-microcrack embedded into an "equivalent" two-dimensional anisotropic homogeneous elastic solid. First, from the geometric compatibility condition, we obtain

$$\frac{\partial^2 \bar{e}_1}{\partial y'^2} + \frac{\partial^2 \bar{e}_2}{\partial x'^2} - \frac{\partial^2 \bar{e}_3}{\partial x' \partial y'} = 0 \tag{2.10}$$

For an *open* microcrack, substitution of (2.8) into (2.10) then yields (Lekhnitskii [1950])

$$\bar{S}'_{11} \frac{\partial^4 U}{\partial y'^4} - 2\bar{S}'_{13} \frac{\partial^4 U}{\partial x' \partial y'^3} + (2\bar{S}'_{12} + \bar{S}'_{33}) \frac{\partial^4 U}{\partial x'^2 \partial y'^2}$$

$$- 2\bar{S}'_{23} \frac{\partial^4 U}{\partial x'^3 \partial y'} + \bar{S}'_{22} \frac{\partial^4 U}{\partial x'^4} = 0 \tag{2.11}$$

where U is a proper stress function. The characteristic equation of (2.11) takes the form:

$$\bar{S}'_{11}\lambda'^4 - 2\bar{S}'_{13}\lambda'^3 + (2\bar{S}'_{12} + \bar{S}'_{33})\lambda'^2 - 2\bar{S}'_{23}\lambda' + \bar{S}'_{22} = 0 \tag{2.12}$$

Of course, the elastic-damage secant compliance moduli $\bar{S}'_{ij}$ are yet *unknown* in accordance with the self-consistent method. According to Lekhnitskii [1950] and Sih et al. [1965], the displacement jump across an (k-th) *open* microcrack (under mode I or mixed I/II mode loading) in an anisotropic homogeneous elastic solid can be expressed as:

$$b_1^{(k)'} = 2\sqrt{a^{(k)2} - x'^2}\,\bar{S}'_{11}\left[(r'_1 s'_2 + r'_2 s'_1)\bar{\tau}'_2 + (s'_1 + s'_2)\bar{\tau}'_3\right]^{(k)} \tag{2.13a}$$

$$b_2^{(k)'} = 2\sqrt{a^{(k)2} - x'^2}\,\bar{S}'_{22}\left[\left(\frac{s'_1}{r'^2_1 + s'^2_1} + \frac{s'_2}{r'^2_2 + s'^2_2}\right)\bar{\tau}'_2 + \frac{r'_1 s'_2 + r'_2 s'_1}{[r'^2_1 + s'^2_1][r'^2_2 + s'^2_2]}\bar{\tau}'_3\right]^{(k)} \tag{2.13b}$$

where $\lambda'_j = r'_j + i\,s'_j$ ($j = 1, 2$), with $s'_1, s'_2 > 0$, are the roots of the characteristic equation (2.12). Eq. (2.12) is a fourth order equation and can be solved analytically. Further, let us define the 2 by 2 "displacement transformation matrix" $\mathbf{B}^{(k)'}$ as:

$$[\mathbf{B}^{(k)'}] \equiv \begin{bmatrix} \bar{S}'_{11}(s'_1 + s'_2) & \bar{S}'_{11}(r'_1 s'_2 + r'_2 s'_1) \\ \bar{S}'_{22}\dfrac{r'_1 s'_2 + r'_2 s'_1}{[r'^2_1 + s'^2_1][r'^2_2 + s'^2_2]} & \bar{S}'_{22}\left[\dfrac{s'_1}{r'^2_1 + s'^2_1} + \dfrac{s'_2}{r'^2_2 + s'^2_2}\right] \end{bmatrix}^{(k)} \tag{2.14}$$

so that (2.13a,b) may be recast as

$$b_i^{(k)'} = 2\sqrt{a^{(k)2} - x'^2}\,B_{ij}^{(k)'}\,\bar{\sigma}'_{2j} \tag{2.15}$$

From Eq. (2.14), it appears that $\mathbf{B}^{(k)'}$ is a *non-symmetric* matrix since the off-diagonal components $B_{12}^{(k)'}$ and $B_{21}^{(k)'}$ may not always be equal; see also Eq. (14)-(15) in Sumarac and Krajcinovic [1989]. This observation, however, is incorrect since it can be proved that $B_{12}^{(k)'} = B_{21}^{(k)'}$ is guaranteed for an open microcrack. To see this, we note that

$$r'^2_1 + s'^2_1 = (r'_1 + i\,s'_1)(r'_1 - i\,s'_1) = \lambda'_1 \lambda'_3 \tag{2.16a}$$

$$r'^2_2 + s'^2_2 = (r'_2 + i\,s'_2)(r'_2 - i\,s'_2) = \lambda'_2 \lambda'_4 \tag{2.16b}$$

where λ'_3 and λ'_4 are two complex roots of (2.12) conjugate to the roots λ'_1 and λ'_2, respectively. Since $\lambda'_1, \lambda'_2, \lambda'_3$ and λ'_4 are the roots of (2.12), they must satisfy

$$\lambda'_1 \lambda'_2 \lambda'_3 \lambda'_4 = \bar{S}'_{22} / \bar{S}'_{11} \tag{2.17}$$

Therefore, we arrive at

$$(r'^2_1+s'^2_1)\,(r'^2_2+s'^2_2)=\bar{S}'_{22}/\bar{S}'_{11} \tag{2.18}$$

$$\bar{S}'_{22}\,\frac{r'_1 s'_2+r'_2 s'_1}{[r'^2_1+s'^2_1]\,[r'^2_2+s'^2_2]}=\bar{S}'_{11}\,(r'_1 s'_2+r'_2 s'_1) \tag{2.19}$$

Hence, $B^{(k)'}_{12}=B^{(k)'}_{21}$ and $\mathbf{B}^{(k)'}$ is always *symmetric* for an open microcrack. For a *closed* microcrack under mode II *frictional* sliding, Eq. (2.13a,b) and (2.14) must be appropriately modified; see Horii and Nemat-Nasser [1983] (p. 162 therein) for an approximate treatment. Essentially, one may set $B^{(k)'}_{21}=B^{(k)'}_{22}=b^{(k)'}_{2}=0$, and replace $\bar{\sigma}'_{22}$ and $\bar{\sigma}'_{21}$ by $\bar{\sigma}'_{22}-\bar{\sigma}^{c'}_{22}$ and $\bar{\sigma}'_{21}+\mu\,sgn\,(\bar{\sigma}'_{21})\,\bar{\sigma}^{c'}_{22}$, respectively. Here, μ is the coefficient of friction, and $\bar{\sigma}^{c'}_{22}$ is the compressive normal stress transmitted across the closed crack (see Eq. (28) in Horii and Nemat-Nasser [1983]). Further, the matrix $\mathbf{B}^{(k)'}$ is *non-symmetric* as a direct consequence of frictional slip.

Using the fact that $n'_1=0$ and Eq. (2.7),(2.8),(2.13a,b), we arrive at

$$S^{d(k)'}_{11}=S^{d(k)'}_{12}=S^{d(k)'}_{21}=S^{d(k)'}_{13}=S^{d(k)'}_{31}=0 \tag{2.20a}$$

$$S^{d(k)'}_{22}=\frac{\pi\,a^{(k)2}}{A}\left[\frac{s'_1}{r'^2_1+s'^2_1}+\frac{s'_2}{r'^2_2+s'^2_2}\right]\bar{S}'_{22}=\frac{\pi\,a^{(k)2}}{A}\,B^{(k)'}_{22} \tag{2.20b}$$

$$S^{d(k)'}_{33}=\frac{\pi\,a^{(k)2}}{A}\,(s'_1+s'_2)\,\bar{S}'_{11}=\frac{\pi\,a^{(k)2}}{A}\,B^{(k)'}_{11} \tag{2.20c}$$

$$S^{d(k)'}_{23}=\frac{\pi\,a^{(k)2}}{A}\,\frac{r'_1 s'_2+r'_2 s'_1}{[r'^2_1+s'^2_1]\,[r'^2_2+s'^2_2]}\,\bar{S}'_{22}=\frac{\pi\,a^{(k)2}}{A}\,B^{(k)'}_{21} \tag{2.20d}$$

$$S^{d(k)'}_{32}=\frac{\pi\,a^{(k)2}}{A}\,(r'_1 s'_2+r'_2 s'_1)\,\bar{S}'_{11}=\frac{\pi\,a^{(k)2}}{A}\,B^{(k)'}_{12} \tag{2.20e}$$

where $S^{d(k)'}_{ij}$ denotes the k-th microcrack-induced "additional inelastic compliance". From Eq. (2.20d) and (2.20e), it is realized that $S^{d(k)'}_{23}=S^{d(k)'}_{32}$ for an open microcrack. By contrast, $S^{d(k)'}_{22}=S^{d(k)'}_{23}=0$ and $S^{d(k)'}_{23}\neq S^{d(k)'}_{32}$ for a closed sliding microcrack (see Eq. (32) in Horii and Nemat-Nasser [1983]). Thus, $\mathbf{S}^{d(k)'}$ is *symmetric* and *non-symmetric*, respectively, for an *open* and a *closed* microcrack. In addition, the inelastic

compliance $\mathbf{S}^d$ due to an ensemble of microcracks within a unit-cell can be expresses as

$$S_{ij}^d = \sum_k g_{mi}^{(k)} g_{nj}^{(k)} S_{mn}^{d(k)'} = \sum_k S_{ij}^{d(k)} = N < S_{ij}^{d(k)} > \tag{2.21a}$$

in which N signifies the total number of active (open or sliding) microcracks per unit-cell surface, and $< \bullet >$ represents the expected value. In the limit (a large number of microcracks per unit-cell), the summation operator can be replaced by the integral operator over all active microcracks:

$$S_{ij}^d = N \int_\Omega S_{ij}^{d(k)} p(\theta, a) \, d\Omega \tag{2.21b}$$

where $p(\theta, a)$ is a joint probability density function of orientation and crack size, and Ω is the domain of all active microcracks. It is emphasized that $\mathbf{S}^d$ depends on the yet *unknown* elastic-damage secant compliance $\bar{\mathbf{S}}$. Consequently, the self-consistent method demands iterative schemes to solve strains and compliances. Since $\bar{\boldsymbol{\varepsilon}} = \bar{\boldsymbol{\varepsilon}}^e + \bar{\boldsymbol{\varepsilon}}^d$, the elastic-damage secant compliance takes the form: $\bar{\mathbf{S}} = \mathbf{S}^o + \mathbf{S}^d(\bar{\mathbf{S}})$.

Remark 2.1. For mode II frictional sliding, secant compliance moduli are non-symmetric and hence Eq. (2.11)-(2.12) should not be used. Instead, according to (2.8) and (2.10), one should use the following equation to solve complex roots:

$$\bar{S}'_{11} \lambda'^4 - (\bar{S}'_{13} + \bar{S}'_{31}) \lambda'^3 + (\bar{S}'_{12} + \bar{S}'_{21} + \bar{S}'_{33}) \lambda'^2 - (\bar{S}'_{23} + \bar{S}'_{32}) \lambda' + \bar{S}'_{22} = 0 \tag{2.22}$$

That is, Eq. (2.22) should be utilized in conjunction with Eq. (2.20a-e) for open microcracks, and together with Eq. (32) in Horii and Nemat-Nasser [1983] for closed microcracks, respectively. To carry out the self-consistent scheme, a general non-symmetric anisotropic matrix iteration algorithm is warranted. In addition, numerical integration scheme for (2.21b) is needed. These issues will be addressed in Sec. **4**. □

Moreover, the "thermodynamic force" conjugate to the "rate of change of the microcrack density" can be derived straightforwards. Let us define

$$S_{ij}^{*(k)} \equiv \frac{A}{\pi a^{(k)2}} S_{ij}^{d(k)} \quad or \quad S_{ij}^{d(k)} \equiv \frac{\pi a^{(k)2}}{A} S_{ij}^{*(k)} \tag{2.23}$$

where i , j = 1, 2, 3. In the spirit of thermodynamics, we may consider statistical area-average damage by treating $a^{(k)}$ and $\mathbf{n}^{(k)}$ as random variables (not necessarily perfectly random); see also Wu [1985]. Therefore, the area-average values may be replaced by their appropriate *expected* values. Hence, we have

$$< \mathbf{S} > = \mathbf{S}^o + < \mathbf{S}^d > = \mathbf{S}^o + N < \frac{\pi a^{(k)2}}{A} \mathbf{S}^{*(k)} > = \mathbf{S}^o + < \omega^{(k)} \mathbf{S}^{*(k)} > \qquad (2.24)$$

in which $\omega^{(k)} \equiv \frac{N \pi a^{(k)2}}{A}$; i.e, the non-dimensional microcrack area-concentration parameter per unit surface (see Budiansky and O'Connel [1976]). The time derivative of (2.24) then yields (see also Wu [1985])

$$< \dot{\mathbf{S}} > = < \dot{\omega}^{(k)} \mathbf{S}^{*(k)} > + < \omega^{(k)} > < \frac{\partial \mathbf{S}^{*(k)}}{\partial \mathbf{S}} > : < \dot{\mathbf{S}} > \qquad (2.25)$$

Note that $<\dot{\omega}^{(k)}>$ in general includes both effects of *initiation* of new microcracks ($\dot{N}$) and *growth* of existing microcracks ($\dot{a}$). From (2.25), we obtain

$$< \dot{\mathbf{S}} > = \left[\mathbf{I} - < \omega^{(k)} > < \frac{\partial \mathbf{S}^{*(k)}}{\partial \mathbf{S}} > \right]^{-1} : < \dot{\omega}^{(k)} > < \mathbf{S}^{*(k)} > \qquad (2.26)$$

where $\mathbf{I}$ is the fourth-order identity tensor. Substitution of (2.26) into the damage dissipation inequality (2.4b) then leads to

$$\tfrac{1}{2} \bar{\boldsymbol{\sigma}} : \left(\left[\mathbf{I} - < \omega^{(k)} > < \frac{\partial \mathbf{S}^{*(k)}}{\partial \mathbf{S}} > \right]^{-1} : < \dot{\omega}^{(k)} > < \mathbf{S}^{*(k)} > \right) : \bar{\boldsymbol{\sigma}} \geq 0 \qquad (2.27)$$

where $\bar{\boldsymbol{\sigma}}$ is now a vector of three components $(\bar{\tau}_1, \bar{\tau}_2, \bar{\tau}_3)$ for two-dimensional case. From (2.27), it is observed that the "thermodynamic driving force" ξ conjugate to the rate of change of the microcrack area-concentration parameter $< \dot{\omega}^{(k)} >$ is simply

$$\xi \equiv \tfrac{1}{2} \bar{\boldsymbol{\sigma}} : \left(\left[\mathbf{I} - < \omega^{(k)} > < \frac{\partial \mathbf{S}^{*(k)}}{\partial \mathbf{S}} > \right]^{-1} : < \mathbf{S}^{*(k)} > \right) : \bar{\boldsymbol{\sigma}} \qquad (2.28)$$

The above result is at variance with that given in Wu [1985] (Eq. (38) therein, i.e., $\xi \equiv \tfrac{1}{2} \bar{\boldsymbol{\sigma}} : < \mathbf{S}^{*(k)} > : \bar{\boldsymbol{\sigma}}$). The latter work, although interesting and valuable, indeed

misses some terms in (2.28) and hence results in some anomalies regarding thermodynamic "strain energy release rate density" ξ. For example, ξ given in Wu [1985] may *decrease* while $\bar{\boldsymbol{\varepsilon}}$ increases, thus predicting no further damage in the post-peak (softening) branch of the macroscopic (unit-cell) stress-strain curve.

Remark 2.2. In the case of three-dimensional *isotropic* damage, the damage tensor $\bar{\mathbf{D}}$ reduces to a scalar variable d. By definition, the scalar damage variable d is the microcrack volume-concentration parameter $<\omega^{(k)}> \equiv <Na^{(k)3}/V>$. Therefore, we have (for three-dimensional elastic-damage):

$$\bar{\mathbf{S}} = \frac{1}{(1-d)}\,\mathbf{S}^o \quad ; \quad \mathbf{S}^d = \frac{d}{(1-d)}\,\mathbf{S}^o \tag{2.29}$$

Analogous to (2.24), we can identify that

$$< \mathbf{S}^{*(k)} > = \frac{1}{(1-d)}\,\mathbf{S}^o = < \mathbf{S} > \tag{2.30}$$

Therefore, ξ defined in Wu [1985] renders

$$\xi = \tfrac{1}{2}\,\bar{\boldsymbol{\sigma}} : < \mathbf{S} > : \bar{\boldsymbol{\sigma}} = \tfrac{1}{2}\,\bar{\boldsymbol{\sigma}} : \bar{\boldsymbol{\varepsilon}} \tag{2.31}$$

while ξ given by (2.28) leads to

$$\xi = \tfrac{1}{2}\,\bar{\boldsymbol{\sigma}} : \frac{1}{(1-d)} < \mathbf{S} > : \bar{\boldsymbol{\sigma}} = \tfrac{1}{2}\,\frac{\bar{\boldsymbol{\sigma}} : \bar{\boldsymbol{\varepsilon}}}{(1-d)} \tag{2.32}$$

However, $\bar{\boldsymbol{\sigma}}/(1-d)$ is precisely the so-called "effective stress" $\tilde{\boldsymbol{\sigma}}$ (Kachanov [1958]). Denoting the undamaged virgin elastic stiffness by $\mathbf{C}^o$, we then arrive at

$$\xi = \tfrac{1}{2}\,\tilde{\boldsymbol{\sigma}} : \bar{\boldsymbol{\varepsilon}} = \tfrac{1}{2}\,(\mathbf{C}^o : \bar{\boldsymbol{\varepsilon}}) : \bar{\boldsymbol{\varepsilon}} \equiv \Psi^o(\bar{\boldsymbol{\varepsilon}}) \tag{2.33}$$

where $\Psi^o(\bar{\boldsymbol{\varepsilon}})$ is the undamaged strain energy density defined in Ju [1989]. □

III.3. Microcrack evolution equations

It is likely that brittle materials (such as concrete, crystals, polycrystalline ceramics, etc.) have initial microcracks along some weak planes (e.g., the aggregate-cement interface in concrete) even before specimens are first loaded. Before the initial (existing) microcracks are arrested by some higher energy barriers (such as the cement paste in normal strength concrete), they propagate approximately along the same weak planes in a self-similar manner. The problem can be significantly simplified by assuming that activated initial microcracks grow to certain characteristic *final* lengths along weak planes (Zaitsev [1983], Krajcinovic and Fanella [1986]). For example, initial microcracks on aggregate-cement interface planes of concrete may grow from $2a_0$ (initial crack length) to $2a_f$ (the aggregate facet size) in an unstable manner. Inevitably, there are randomness in initial and final microcrack lengths, orientations and center locations in brittle materials. As a consequence of the two-stage approximation of weak-plane microcrack lengths (either $2a_0$ or $2a_f$), the problem of keeping track of weak-plane microcrack growth in a representative unit-cell reduces to a series of microcrack *stability* checks. Thus, classical fracture mechanics stability criteria can be used as tools to determine whether an initial microcrack will be *activated*. This procedure, nonetheless, can *not* accommodate nucleation of new microcracks along different weak planes.

A microcrack kinetic algorithm based on fracture criteria (see, e.g., Krajcinovic and Fanella [1987]) is intrinsicly *stress-controlled*. This type of mechanism, however, can only depict the ascending portion of a macroscopic stress-strain curve, not the descending ("softening") portion. Before a "point" on a stress-strain curve reaches the peak, a stress-controlled loading criterion is qualitatively equivalent to a strain-controlled one. In the "softening" branch, however, a stress-controlled loading criterion will not suffice since the stress level is *decreasing*. In fact, in the descending branch of a stress-strain curve, there must be significant number of microcrack *nucleations*, and hence the "cleavage 1" process assumption is no longer valid. These and related issues should be

further investigated in the future.

Restricting our attention to the "cleavage 1" deformation processes in this work, we consider the following three types of damage modes under *biaxial* loadings: (1) mode I (open) microcrack growth only, (2) mode II (closed) microcrack growth only, and (3) mixed modes I and II (open/ closed) microcrack growth. In particular, excellent mode I tensile damage kinetic equations were presented by Krajcinovic and Fanella [1986] and Sumarac and Krajcinovic [1987], whereas valuable mode II compressive damage kinetic equations were proposed by Fanella and Krajcinovic [1988]. Their presentations were, nontheless, restricted to *monotonically increasing* loading cases. Therefore, no unloading/reloading stress paths or microcrack opening/closing effects were permitted in their presentations. The restriction on status change from opening to closing (or vice versa) can be removed by checking the *sign* of individual local *normal* stress. The corresponding symmetric or non-symmetric damage-induced inelastic compliance components can be obtained from Eq. (2.20a)-(2.20e) for *open* microcracks, and from Eq. (32) in Horii and Nemat-Nasser [1983] for *closed* microcracks. It is remarked that in general Eq. (2.22) should be used to solve complex roots. On the other hand, the restriction on "monotonically increasing loads" can be removed by computing and checking whether there are *undergoing* microcrack growth (excluding those previously propagating and currently arrested microcracks). If there is no "angle fan" domain in which *additional* microcrack growth is now taking place, then the current incremental load step is in an *unloading* state. Therefore, "active microcrack growth" is the valid current loading condition, regardless of prior existence (or non-existence) of certain "angle fans" where microcracks previously experienced growth.

Accordingly, the additional inelastic compliance S^d takes the form:

$$S^d = S_u^d + S_t^d + S_f^d \tag{3.1}$$

where $\mathbf{S}_u^d$ denotes the compliance contribution from undergoing microcrack growth, $\mathbf{S}_i^d$ signifies the contribution from arrested microcracks having *initial* sizes $2a_0^{(k)}$, and $\mathbf{S}_f^d$ represents the contribution from arrested microcracks having *final* sizes $2a_f^{(k)}$ due to *previous* microcrack growth. In particular, if $\mathbf{S}_u^d = \mathbf{0}$, then the current load level is not high enough to cause further damage and therefore all existing microcracks are arrested. Finally, $\mathbf{S}^d$ is added to $\mathbf{S}^o$ to obtain the secant compliance $\bar{\mathbf{S}}$. In what follows, for computational simplicity, it is assumed that all initial and final microcracks are of uniform sizes $2a_0$ and $2a_f$, respectively. For non-uniform initial microcrack sizes, we refer to Krajcinovic and Fanella [1986]. Microcrack kinking will be addressed in Sec. 3.3.

Remark 3.1. If all microcracks are open and arrested with non-uniform sizes, then overall loading and unloading responses are linear and reversible (but not perfectly elastic). By contrast, if some microcracks propagate, then the loading response is nonlinear. Moreover, in mode II or mixed mode I/II with friction, some microcracks may be open and some closed. Therefore, the resulting loading and unloading responses are *nonlinear* for either "process models" or "non-process models". □

Remark 3.2. In the case of mixed mode I/II loadings, the strain energy release rate G' for a microcrack along a weak plane should include both mode I contribution G'_1 and mode II contribution G'_2. In terms of secant compliance, G' may be expressed as (Sih et al. [1965], Rice [1975], Sumarac and Krajcinovic [1989]):

$$G' = G'_1 + G'_2 = C_{ij}^{(k)'} K'_i K'_j \quad ; \quad i, j = 1, 2 \tag{3.2a}$$

$$[\mathbf{C}^{(k)'}] = \frac{1}{2} \begin{bmatrix} B'_{22} & B'_{21} \\ B'_{12} & B'_{11} \end{bmatrix}^{(k)} \tag{3.2b}$$

Therefore, we have

$$G' = \tfrac{1}{2} [B_{22}^{(k)'} K_I'^2 + (B_{21}^{(k)'} + B_{12}^{(k)'}) K'_I K'_{II} + B_{11}^{(k)'} K_{II}'^2] \tag{3.2c}$$

It is noted that K'_I and K'_{II} represent the mode I and II stress intensity factors at a particular orientation, respectively. The expressions for $B_{ij}^{(k)'}$ are given in Eq. (2.14) for an open microcrack, and in Horii and Nemat-Nasser [1983] for a closed microcrack. The computed G' value is then compared against a given mixed mode critical strain energy release rate G_c to determine whether a microcrack will propagate. □

III.3.1. Mode I microcrack growth

Under uniaxial or biaxial tensile loads, microcracks primarily grow in "mode I" fashion. Let us define the (global, homogenized) axial tensile stress by $\bar{\tau}_2 = q$ and the lateral tensile stress by $\bar{\tau}_1 = q^*$, respectively. The normal stress $\bar{\tau}'_2$ on the face of a typical microcrack at θ-angle then reads

$$\bar{\tau}'_2 = q \cos^2\theta + q^* \sin^2\theta > 0 \tag{3.3}$$

According to Eq. (3.2c), one should compute K'_I, K'_{II} and G' even in the case of uniaxial or biaxial tension. However, since "mode I" is the primary concern (Sumarac and Krajcinovic [1987]), it is computationally simpler to use the mode I fracture criterion. In addition, strictly speaking, the "stress intensity factor" used in the microcrack growth stability criterion should take into account direct microcrack interaction effects:

$$f = K'^{eff} - K_{Ic} = 0 \tag{3.4a}$$

where K'^{eff} is the mode I *effective* stress intensity factor, and K_{Ic} is the mode I critical stress intensity factor for a weak plane. We refer to Horii and Nemat-Nasser [1985a] and Kachanov [1987] for the derivation of K'^{eff} and K'^{eff}_{II} for line microcracks under various geometric configurations. Alternatively, within the applicable range (moderate microcrack concentration) of the self-consistent method, one may employ the simple "single crack" stability criterion (Krajcinovic and Fanella [1986]):

$$f = K'_I - K_{Ic} = 0 \tag{3.4b}$$

where $K'_I = \bar{\tau}'_2 \sqrt{\pi a_0}$ is the mode I stress intensity factor for a typical microcrack. Naturally, exact microcrack interaction effects on K'^{eff} (or K'^{eff}_{II}) depend on exact microcrack geometries such as number of interacting cracks, relative center locations, relative spacing, relative orientations, inner-tip or outer-tip, etc. In practice, however, it is not feasible to keep track of microstructural configuration for each microcrack.

By using (3.4b), the mode I microcrack stability criterion can be recast as

$$f = \bar{\tau}'_2 \sqrt{\pi a_0} - K_{IC} = 0 \tag{3.5}$$

For computational simplicity, let us assume that the lateral tension q^* is constant and the axial tension q is bigger than q^*. The value of q does *not* have to be monotonically increasing as long as $q > q^*$; i.e., unloading paths are permitted. In particular, from Eq. (3.3) and (3.5), we have

$$q = \frac{K_{IC}}{\sqrt{\pi a_0 \cos^2\theta}} - q^* \tan^2\theta \tag{3.6a}$$

Clearly, the first cracks to become activated are those for which q is a minimum, and are oriented in the plane $\theta = 0$ given the assumption that $q^* < K_{IC}/\sqrt{\pi a_0}$. Therefore, the corresponding minimum value of q is

$$q(\theta=0) \equiv q_0 = \frac{K_{IC}}{\sqrt{\pi a_0}} \tag{3.6b}$$

The microcrack growth kinetic sequence proceeds as follows. Note that $q^* < q_0$.

(a) As $q < q_0$, all microcracks are stable and of initial size. Since all microcracks are open, perfectly randomly oriented and of equal size, the overall response is isotropic. Though the response is linear and reversible under the present stress level, the material state is really *elastic-damage*. In fact, the current elastic-damage compliance $\bar{S}$ is bigger than the virgin undamaged elastic compliance S^o .

(b) As $q = q_0 > q^*$, those microcracks in the plane $\theta = 0$ become unstable and increase their lengths from $2a_0$ to $2a_f$. It is assumed that there exists a higher energy

barrier in the matrix so that microcracks become arrested once they reach $2a_f$.

(c) As $q \equiv q_1 > q_0$, microcracks in the angle domain $(-\theta_1, \theta_1)$ become activated and increase in size from $2a_0$ to $2a_f$. The material behaves anisotropically and the elastic-damage compliance increases. θ_1 value depends on q_1, q_0 and q^*. Specifically, in view of Eq. (3.5)-(3.6b), θ_1 can be obtained by solving

$$q_1 \cos^2\theta_1 + q^* \sin^2\theta_1 = q_0 \tag{3.7}$$

Thus, we arrive at

$$\cos\theta_1 = \sqrt{(q_0 - q^*)/(q_1 - q^*)} \quad or \quad \pm\theta_1 = \cos^{-1}\left[\sqrt{(q_0 - q^*)/(q_1 - q^*)}\right] \tag{3.8}$$

The compliance contributions $\mathbf{S}_u^d$ and $\mathbf{S}_i^d$ in Eq. (3.1) can be computed (integrated) through Eq. (2.20a-e) and (2.21b):

$$\mathbf{S}_u^d = \frac{N}{\pi}\int_{-\theta_1}^{\theta_1} \mathbf{g}^{(k)T}\, \mathbf{S}^{d(k)'}(\theta, a_f)\, \mathbf{g}^{(k)}\, d\theta \tag{3.9}$$

$$\mathbf{S}_i^d = \frac{N}{\pi}\int_{\pm\theta_1}^{\pm\pi/2} \mathbf{g}^{(k)T}\, \mathbf{S}^{d(k)'}(\theta, a_0)\, \mathbf{g}^{(k)}\, d\theta \tag{3.10}$$

where $1/\pi$ is the assumed *uniform* probability density function of microcrack orientation. Certainly, other probability density functions may be used when appropriate. For notational compactness, the integration bounds $(-\pi/2, -\theta_1)$ and $(\theta_1, \pi/2)$ are written together in (3.10) and in what follows. Readers should interpret the notation $(\pm\theta_1, \pm\pi/2)$ as the sum of two integration domains: $(-\pi/2, -\theta_1)$ and $(\theta_1, \pi/2)$. Note that Eq. (3.9) and (3.10) are somewhat at variance with Eq. (42) in Sumarac and Krajcinovic [1987] and Eq. (55) in Sumarac and Krajcinovic [1989].

(d) As $q_0 < q < q_1$, the *unloading* case is taking place. There is no further microcrack growth because the apparent "active angle fan" shrinks. Therefore, $\mathbf{S}_u^d = \mathbf{0}$. It is emphasized that the *actual* "angle fan" (featuring $2a_f$ size) does *not* reduce owing to the *irreversible* nature of damage. Therefore, the elastic-damage compliance remains its previous value.

(e) As $q > q_1$, more microcracks are activated. The "angle fan" domain $(-\theta , \theta)$ can be computed from (3.8), with q_1 replaced by q. However, only the microcracks within domains $(-\theta, -\theta_1)$ and (θ_1, θ) are actually experiencing *unstable* growth. Hence, the compliance contribution $\mathbf{S}_u^d$ should be obtained from (2.20a-e) and (2.21b) with $(-\theta, -\theta_1)$ and (θ_1, θ) as integration bounds:

$$\mathbf{S}_u^d = \frac{N}{\pi} \int_{\pm\theta_1}^{\pm\theta} \mathbf{g}^{(k)T} \mathbf{S}^{d(k)'}(\tilde{\theta}, a_f)\, \mathbf{g}^{(k)}\, d\tilde{\theta} \tag{3.11}$$

In addition, $\mathbf{S}_i^d$ and $\mathbf{S}_f^d$ in (3.1) now take the form:

$$\mathbf{S}_i^d = \frac{N}{\pi} \int_{\pm\theta}^{\pm\pi/2} \mathbf{g}^{(k)T} \mathbf{S}^{d(k)'}(\tilde{\theta}, a_0)\, \mathbf{g}^{(k)}\, d\tilde{\theta} \tag{3.12}$$

$$\mathbf{S}_f^d = \frac{N}{\pi} \int_{-\theta_1}^{\theta_1} \mathbf{g}^{(k)T} \mathbf{S}^{d(k)'}(\tilde{\theta}, a_f)\, \mathbf{g}^{(k)}\, d\tilde{\theta} \tag{3.13}$$

(f) At some higher stress level $q = q_c$, K_I at $\theta = 0$ reaches the critical stress intensity factor K_{fC} of the matrix energy barrier. Therefore, microcracks having size $2a_f$ will resume to propagate through the matrix, and eventually lead to final failure:

$$q_c = \frac{K_{fC}}{\sqrt{\pi a_f}} \tag{3.14}$$

As was commented by Sumarac and Krajcinovic [1987], the above scheme implicitly assumes that ultimate failure prefers "runaway cracks" in comparison with "localization modes". Numerical simulations by using both the self-consistent method and the "Taylor's model" will be given in Sec. 4.2.

III.3.2. Mode II microcrack growth

Under uniaxial or biaxial *compressive* loads, microcracks are closed and primarily grow in "mode II" fashion. Fanella and Krajcinovic [1988] proposed excellent kinetic equations for flat penny-shaped interface microcracks in concrete under mode II loading by using the "Taylor's model"; i.e., microcrack interaction effects are completely

ignored. Our procedure here basically follows their treatment. However, the self-consistent method is employed here and weak microcrack interaction is taken into account through the damage-induced stiffness degradation and anisotropy. Mode II microcrack kinking into brittle matrix is considered in Sec. 3.3. Further, microcracks under consideration are line microcracks in stead of penny-shaped microcracks. It is also noted that unloading/reloading is permitted in our treatment.

In accordance with Eq. (3.2c), the mixed mode fracture criterion should be used. Nonetheless, since there is no mode I action under uniaxial or biaxial compressive loads, it is equivalent to employ the mode II fracture criterion only. Consequently, K'_{II} (or $K_I'^{eff}$) will be compared against K_{IIC} for a microcrack to determine whether it will propagate or not. Further, due to frictional sliding of closed microcracks, Eq. (2.22) should be utilized to solve complex roots of characteristic equations; see **Remark 2.1.**

Let us denote by q and q^* the axial and lateral compressive stresses, respectively. q^* is assumed to be constant and $q > q^*$. The normal stress σ_n and shear stress τ_n on the face of a typical microcrack at θ-angle are (Fanella and Krajcinovic [1988]):

$$\sigma_n = \bar{\tau}'_2 = q\cos^2\theta + q^*\sin^2\theta > 0 \tag{3.15}$$

$$\tau_s = \bar{\tau}'_3 - \mu\bar{\tau}'_2 = F(\theta)\left[q - \left[1 + \frac{\mu}{F(\theta)}\right]q^*\right] \tag{3.16}$$

where compression is taken as positive and $F(\theta) \equiv \pm\sin\theta\cos\theta - \mu\cos^2\theta$. According to Coulomb's law of friction, microcrack surfaces will slide relative to each other when $\tau_s \geq 0$ is met. Therefore, (3.16) can be solved for the upper and lower bounds ($\pm\theta_{s2}$ and $\pm\theta_{s1}$) of microcrack *orientations* for given values of q and q^*

$$\tan(\pm\theta_{s1,s2}) = \frac{1 \pm \sqrt{1 - 4C_1(C_1+\mu)}}{2C_1} \quad , \quad q \geq [2\mu(\sqrt{\mu^2+1}+\mu)+1]q^* \tag{3.17}$$

where $C_1 \equiv \mu q^*/(q - q^*)$. Only those microcracks within ($\pm\theta_{s1}$, $\pm\theta_{s2}$) will experience relative frictional slip on their faces. Note that if $q^* = 0$ (uniaxial compression) or if

$q \to \infty$, then $F(\theta)=0$ and $\theta_{s1}=\tan^{-1}\mu$, $\theta_{s2}=\pi/2$. That is, microcracks within the fan $(-\tan^{-1}\mu, \tan^{-1}\mu)$ will never slide and therefore will not contribute to S^d .

A microcrack with relative sliding faces will exhibit mode II microcrack growth once its crack tip stress intensity factor K'_{II} (or K_{II}^{eff}) reaches the critical value K_{IIC} along a weak plane. Accordingly, the mode II stability criterion can be expressed as

$$\tau_s = \frac{K_{IIC}}{\sqrt{\pi a_0}} \tag{3.18}$$

From (3.16) and (3.18), we can solve for the q value needed to activate unstable mode II microcrack growth from $2a_0$ to $2a_f$ at a specific orientation θ:

$$q = \frac{K_{IIC}}{\sqrt{\pi a_0} F(\theta)} + \left[1 + \frac{\mu}{F(\theta)}\right] q^* \tag{3.19}$$

As in the previous section, an unstable microcrack propagation will be arrested by the matrix having a higher critical stress intensity factor K_{IIC} . Again, the first microcracks to increase in size are those for which q is a minimum. Thus, critical angles $\pm\theta_0$ for the first microcrack growth are (Fanella and Krajcinovic [1988]):

$$\pm\theta_0 = \pm\tan^{-1}(\mu + \sqrt{\mu^2+1}) \tag{3.20}$$

The corresponding threshold value of q_0 is

$$q_0 = \frac{K_{IIC}}{\sqrt{\pi a_0} F(\theta_0)} + \left[1 + \frac{\mu}{F(\theta_0)}\right] q^* \tag{3.21}$$

Therefore, mode II microcrack kinetic sequence is as follows.

(a) As $q < q_0$, no microcracks will increase in size. Nevertheless, microcracks oriented within the "angle fans" $(\pm\theta_{s1}, \pm\theta_{s2})$ will *slide*.

(b) As $q = q_0$, those microcracks in the plane $\pm\theta_0$ become unstable and change their lengths from $2a_0$ to $2a_f$.

(c) As $q \equiv q_1 > q_0$, microcracks within the "angle fans" $(\pm\theta_{u1}, \pm\theta_{u2})$ become unstable and grow from $2a_0$ to $2a_f$. The sliding "angle fans" $(\pm\theta_{s1}, \pm\theta_{s2})$ also increase. The values of $(\pm\theta_{u1}, \pm\theta_{u2})$ can be obtained from Eq. (3.19):

$$\tan(\pm\theta_{u1,u2}) = \pm\left\{\frac{1 \pm \sqrt{1-4C_2(C_2+\mu)}}{2C_2}\right\}, \quad q \geq q_0 \tag{3.22}$$

where $C_2 \equiv \{[K_{fIC}/\sqrt{\pi a_0}] + \mu q^*\}/(q - q^*)$. Since all microcracks are *closed*, the "displacement transformation matrix" $\mathbf{B}^{(k)'}$ in Eq. (2.14) must be modified. Specifically, $B_{21}^{(k)'}$ and $B_{22}^{(k)'}$ are set to 0, while $B_{12}^{(k)'}$ and $B_{11}^{(k)'}$ are available from Eq. (32) in Horii and Nemat-Nasser [1983] together with Eq. (2.22) in **Remark 2.1.** The inelastic compliance $\mathbf{S}_i^d$ attributable to stable *sliding* microcracks having initial size $2a_0$ can be computed as follows:

$$\mathbf{S}_i^d = \frac{N}{\pi}\left[\int_{\pm\theta_{s1}}^{\pm\theta_{u1}} \mathbf{g}^{(k)T}\,\mathbf{S}^{d(k)'}(\theta, a_0)\,\mathbf{g}^{(k)}\,d\theta + \int_{\pm\theta_{u2}}^{\pm\theta_{s2}} \mathbf{g}^{(k)T}\,\mathbf{S}^{d(k)'}(\theta, a_0)\,\mathbf{g}^{(k)}\,d\theta\right] \tag{3.23}$$

Further, $\mathbf{S}_u^d$ in (3.1) reads

$$\mathbf{S}_u^d = \frac{N}{\pi}\int_{\pm\theta_{u1}}^{\pm\theta_{u2}} \mathbf{g}^{(k)T}\,\mathbf{S}^{d(k)'}(\theta, a_f)\,\mathbf{g}^{(k)}\,d\theta \tag{3.24}$$

(d) As $q_0 < q < q_1$, the *unloading* case occurs. Therefore, $\mathbf{S}_u^d = \mathbf{0}$ and

$$\mathbf{S}_f^d = \mathbf{S}_u^d\big|_{old} = \frac{N}{\pi}\int_{\pm\theta_{u1,old}}^{\pm\theta_{u2,old}} \mathbf{g}^{(k)T}\,\mathbf{S}^{d(k)'}(\theta, a_f)\,\mathbf{g}^{(k)}\,d\theta \tag{3.25}$$

where $(\pm\theta_{u1,old}, \pm\theta_{u2,old})$ is the *previous* range of unstable microcrack growth (assuming sliding). The domain of sliding microcracks also reduces and the *new* values of $\pm\theta_{s1}$ and $\pm\theta_{s2}$ may be obtained from (3.17). Hence, it follows that

$$\mathbf{S}_i^d = \frac{N}{\pi}\left[\int_{\pm\theta_{s1,new}}^{\pm\theta_{u1,old}} \mathbf{g}^{(k)T}\,\mathbf{S}^{d(k)'}(\theta, a_0)\,\mathbf{g}^{(k)}\,d\theta + \int_{\pm\theta_{u2,old}}^{\pm\theta_{s2,new}} \mathbf{g}^{(k)T}\,\mathbf{S}^{d(k)'}(\theta, a_0)\,\mathbf{g}^{(k)}\,d\theta\right] \tag{3.26}$$

It is noted that the new value of $\mathbf{S}_i^d$ is smaller than its previous value given by (3.23) because the sliding domain shrinks. As a consequence, the unloading compliance is *smaller* than its previous value.

(e) As $q > q_1$, more microcracks are activated. Both new sliding and unstable angle domains, $(\pm\theta_{s1}, \pm\theta_{s2})$ and $(\pm\theta_{u1}, \pm\theta_{u2})$, increase. The corresponding S_i^d and $S_u^d + S_f^d$ can be computed by using (3.23) and (3.24), respectively.

III.3.3. Mixed Mode I/II microcrack growth

Under combined tensile and compressive loads, some microcracks are closed while others are open. In addition, some open microcracks may become closed during loading/unloading processes. Open microcracks grow in mixed mode fashion whereas closed microcracks grow in "mode II" manner. The mixed mode fracture criterion given in Eq. (3.2c) is used to determine microcrack stability. To facilitate numerical analysis, however, it is further assumed that the cross term $(B_{21}^{(k)'} + B_{12}^{(k)'}) K'_I K'_{II}$ in (3.2c) can be neglected. Accordingly, (3.2c) can be recast as (Kanninen and Popelar [1985]):

$$\left[\frac{K'_I}{K_{IC}}\right]^2 + \left[\frac{K'_{II}}{K_{IIC}}\right]^2 = 1 \tag{3.27a}$$

where K_{IC} and K_{IIC} denote critical stress intensity factors of a homogenized unit-cell. Nonetheless, since all initial microcracks are assumed to be along weak planes, it is more rational to write

$$\left[\frac{K'_I}{K_{fc}}\right]^2 + \left[\frac{K'_{II}}{K_{fIC}}\right]^2 = 1 \tag{3.27b}$$

where K_{fc} and K_{fIC} are critical stress intensity factors of weak planes. Again, it is emphasized that Eq. (2.22) should be employed to solve complex roots.

Let us consider a typical combined loading case in which the axial *compressive* stress is denoted by q and the lateral *tensile* stress is denoted by q^*. Moreover, q^* is assumed to be constant (relatively small) while q is varying from 0 to a certain value. Due to obvious symmetry of the problem, we will derive formulas only for θ within the $(0,\pi/2)$ domain. During actual numerical intergration of compliance components, however, both positive and negative θ bounds should be included. The stresses σ_n $(= \bar{\tau}'_2)$

and $\bar{\tau}'_3$ ($= \bar{\sigma}'_{12}$) on the face of a typical microcrack at θ-angle are

$$\sigma_n = \bar{\tau}'_2 = -q\cos^2\theta + q^* \sin^2\theta \tag{3.28}$$

$$\bar{\tau}'_3 = (-q - q^*)\sin\theta\cos\theta \tag{3.29}$$

where tension is taken as positive. The "angle boundary" separating the domains of *open* and *closed* microcracks can be found by setting $\sigma_n = 0$. Hence, we obtain

$$\tan^2\theta_b = \frac{q}{q^*} \quad ; \quad \theta_b = \tan^{-1}(\sqrt{q/q^*}) \tag{3.30}$$

The upper and lower bounds for open microcracks are $\pi/2$ and θ_b, respectively.

For *closed* microcracks ($\sigma_n < 0$), the sliding shear stress reads

$$\tau_s = \bar{\tau}'_3 - \mu\bar{\tau}'_2 = -F(\theta)\left[q + \left[1 + \frac{\mu}{F(\theta)}\right]q^*\right] \tag{3.31}$$

where $F(\theta) \equiv \sin\theta\cos\theta - \mu\cos^2\theta$. The criterion for microcrack surface-sliding is

$$\tau_s = -(q + q^*)\sin\theta\cos\theta + \mu(q\cos^2\theta - q^*\sin^2\theta) \le 0 \tag{3.32}$$

The θ-bound can be obtained by setting $\tau_s = 0$:

$$\tan\theta_s = \frac{-1 \pm \sqrt{1 + 4H_1(\mu - H_1)}}{2H_1} \tag{3.33a}$$

where $H_1 \equiv \mu q^*/(q + q^*)$. Since we require that $\theta_s > 0$, there should exist only one θ_s:

$$\theta_s = \tan^{-1}\left[\frac{-1 + \sqrt{1 + 4H_1(\mu - H_1)}}{2H_1}\right] \tag{3.33b}$$

This θ_s value is, in fact, the *lower* angle bound for closed microcrack sliding. The *upper* bound is simply θ_b given in (3.30) since sliding shear stress τ_s is negative at the θ_b plane. Only those microcracks within $(\pm\theta_s, \pm\theta_b)$ will exhibit relative frictional slip on their faces. Again, it is noted that as $q^* = 0$ (uniaxial compression) or as $q \to \infty$, then $F(\theta) = 0$ and $\theta_s = \tan^{-1}\mu$, $\theta_b = \pi/2$. As q increases from 0, θ_s and θ_b also increase but never exceed $\tan^{-1}\mu$ and $\pi/2$, respectively.

For closed microcracks, the mixed mode fracture criterion (3.27b) reduces to the mode II fracture criterion. Therefore, as in the previous section, a sliding microcrack will experience mode II microcrack growth once its crack tip stress intensity factor K'_{II} reaches the critical value K_{fIC} along a weak plane. Accordingly, mode II stability criterion requires the following loading level q for a specified θ

$$q = \frac{K_{fIC}}{\sqrt{\pi a_0}F(\theta)} - \left[1 + \frac{\mu}{F(\theta)}\right] q^* \tag{3.34}$$

The first microcracks to propagate are those for which q is a minimum:

$$\theta_0^{II} = \tan^{-1}(\mu + \sqrt{\mu^2 + 1}) \tag{3.35}$$

where it has been assumed that $\mu q^* \neq K_{fIC}/\sqrt{\pi a_0}$. If $\theta_0^{II} > \theta_b$ (opening/closing boundary), then set $\theta_0^{II} = \theta_b$. The corresponding threshold value of q_0^{II} is

$$q_0^{II} = \frac{K_{fIC}}{\sqrt{\pi a_0}F(\theta_0^{II})} - \left[1 + \frac{\mu}{F(\theta_0^{II})}\right] q^* \tag{3.36}$$

The mode II angle bounds for unstable weak-plane microcrack growth, $(\theta_{u1}^{II}, \theta_{u2}^{II})$, can be obtained from Eq. (3.34):

$$\tan\theta_{u1,u2}^{II} = \frac{1 \pm \sqrt{1-4H_2(H_2+\mu)}}{2H_2} \quad , \quad (q+q^*)^2 \geq 4\left[\frac{K_{fIC}}{\sqrt{\pi a_0}} - \mu q^*\right]\left[\frac{K_{fIC}}{\sqrt{\pi a_0}} + \mu q\right] \tag{3.37a}$$

where $H_2 \equiv \{[K_{fIC}/\sqrt{\pi a_0}] - \mu q^*\}/(q + q^*)$. If $\mu q^* < K_{fIC}/\sqrt{\pi a_0}$ (typically), then there are two roots θ_{u1}^{II} and θ_{u2}^{II}. On the other hand, if $\mu q^* > K_{fIC}/\sqrt{\pi a_0}$ (unlikely), then there is only one root θ_u^{II}:

$$\tan\theta_u^{II} = \frac{1 - \sqrt{1 - 4H_2(H_2+\mu)}}{2H_2} \tag{3.37b}$$

Note that θ_{u1}^{II} and θ_{u2}^{II} (or simply θ_u^{II}) should fall within the sliding range (θ_s, θ_b); see Figure 2 for a schematic plot.

For *open* microcracks, a mixed mode fracture criterion such as (3.27b) may be used to check microcrack stability. For convenience, let us define $\alpha \equiv K_{IIC} / K_{IC}$. Hence, (3.27b) can be rephrased as

$$\alpha^2 (K'_I)^2 + (K'_{II})^2 = K_{IIC}^2 \tag{3.38}$$

Substitution of (3.28), (3.29) into (3.38) then renders the microcrack stability condition:

$$\alpha^2 (-q \cos^2\theta + q^* \sin^2\theta)^2 + (q + q^*)^2 \sin^2\theta \cos^2\theta = \frac{K_{IIC}^2}{\pi a_0} \tag{3.39}$$

or, equivalently,

$$(\alpha^2 q^{*2} - \frac{K_{IIC}^2}{\pi a_0}) \tan^4\theta + (q^2 + q^{*2} - 6 q\, q^* - 2 \frac{K_{IIC}^2}{\pi a_0}) \tan^2\theta + (\alpha^2 q^2 - \frac{K_{IIC}^2}{\pi a_0}) = 0 \tag{3.40}$$

From (3.40), we can express q in terms of $\tan\theta$, q^*, α, and $K_{IIC}^2/\pi a_0$ (analogous to (3.34)), and solve for threshold values θ_{II}^{tr} and q_{II}^{tr} corresponding to first microcracks to increase in size from $2a_0$ to $2a_f$ within $(\theta_b, \pi/2)$ domain.

In order to define the unstable "angle domain" for a given q value, we have to solve Eq. (3.40). Obviously, (3.40) is amenable to exact solutions. Due to the constraint that $\theta > 0$, there are at most *two* real solutions to (3.40): $\theta_u^{m_1}$ and $\theta_u^{m_2}$. We recall that the other two negative θ solutions will be accounted for during actual numerical integration of compliance components. These angle bounds should fall within the $(\theta_b, \pi/2)$ range. Otherwise, we should disregard $\theta_u^{m_1}$ and/or $\theta_u^{m_2}$. In the event that both roots are feasible, then unstable open microcrack growth domain is defined by $(\theta_u^{m_1}, \theta_u^{m_2})$ assuming that $q^* < K_{IC}/\sqrt{\pi a_0}$. If there is only *one* feasible root θ_u^m to (3.40), then the unstable growth domain is defined by (θ_b, θ_u^m) for open microcracks. See Figure 2 for a schematic representation. Typically, $q_{II}^{tr} < q_{II}^{tr}$ and there is only one feasible root to (3.40).

Therefore, the mixed mode kinetic evolution for open and closed microcracks proceeds as follows.

(a) As $q < q_0^{II}$ and $q < q_0^{m}$, all microcracks are arrested. At the very beginning, $q = 0$ and $q^* > 0$, thus all microcracks are open. As q increases, some previously open microcracks become *closed*. Microcracks oriented within the "angle fans" $(\pm\theta_s, \pm\theta_b)$ will *slide* and therefore the overall response is nonlinear. Further, the "stick" domain increases as q increases.

(b) As $q = q_0^{II}$ or $q = q_0^{m}$, those microcracks in the plane $\pm\theta_0^{II}$ (closed) or $\pm\theta_0^{m}$ (open) become unstable and change their lengths from $2a_0$ to $2a_f$. Note that the mode II and mixed mode microcrack growth generally do not initiate at the same time.

(c) As $q \equiv q_1 > q_0^{II}$ or $q \equiv q_1 > q_0^{m}$, microcracks within the "angle fans" $(\pm\theta_{u1}^{II}, \pm\theta_{u2}^{II})$ or $(\pm\theta_{u1}^{m}, \pm\theta_{u2}^{m})$ become activated. The sliding "angle fans" $(\pm\theta_s, \pm\theta_b)$ also increase. We refer to (3.33b), (3.37a,b) and (3.40) for these load-dependent angle values. For open microcracks, the "displacement transformation matrix" $\mathbf{B}^{(k)'}$ is given in Eq. (2.14). For closed microcracks, $\mathbf{B}^{(k)'}$ is given in Horii and Nemat-Nasser [1983]. It is important to recall that the resulting $\mathbf{S}^d$ and $\bar{\mathbf{S}}$ are non-symmetric in nature. The inelastic compliance $\mathbf{S}_i^{dII}$ attributable to stable mode II *sliding* microcracks having initial size $2a_0$ can be computed by

$$\mathbf{S}_i^{dII} = \frac{N}{\pi}\left[\int_{\pm\theta_s}^{\pm\theta_{u1}^{II}} \mathbf{g}^{(k)T}\,\mathbf{S}^{d(k)'}(\theta, a_0)\,\mathbf{g}^{(k)}\,d\theta + \int_{\pm\theta_{u2}^{II}}^{\pm\theta_b} \mathbf{g}^{(k)T}\,\mathbf{S}^{d(k)'}(\theta, a_0)\,\mathbf{g}^{(k)}\,d\theta\right] \quad (3.41)$$

while $\mathbf{S}_u^{dII}$ due to unstable closed microcracks can be obtained by

$$\mathbf{S}_u^{dII} = \frac{N}{\pi}\int_{\pm\theta_{u1}^{II}}^{\pm\theta_{u2}^{II}} \mathbf{g}^{(k)T}\,\mathbf{S}^{d(k)'}(\theta, a_f)\,\mathbf{g}^{(k)}\,d\theta \quad (3.42)$$

In addition, $\mathbf{S}_i^{dm}$ attributable to stable mixed mode open microcracks having initial size $2a_0$ takes the form

$$\mathbf{S}_i^{dm} = \frac{N}{\pi}\left[\int_{\pm\theta_b}^{\pm\theta_{u1}^{m}} \mathbf{g}^{(k)T}\,\mathbf{S}^{d(k)'}(\theta, a_0)\,\mathbf{g}^{(k)}\,d\theta + \int_{\pm\theta_{u2}^{m}}^{\pm\pi/2} \mathbf{g}^{(k)T}\,\mathbf{S}^{d(k)'}(\theta, a_0)\,\mathbf{g}^{(k)}\,d\theta\right] \quad (3.43)$$

while $\mathbf{S}_u^{dm}$ attributable to unstable open microcracks can be obtained by

$$S_u^{dm} = \frac{N}{\pi} \int_{\pm\theta_{u1}^{m}}^{\pm\theta_{u2}^{m}} g^{(k)T} S^{d(k)'}(\theta, a_f)\, g^{(k)}\, d\theta \tag{3.44}$$

If there is only one feasible root to (3.40), the integration limits in (3.43) and (3.44) should be replaced by $(\pm\theta_u^m, \pm\pi/2)$ and $(\pm\theta_b, \pm\theta_u^m)$, respectively.

(d) As $q_0 < q < q_1$, the *unloading* case occurs and $S_u^{dII} = S_u^{dm} = 0$. Further, for sliding closed microcracks, we have

$$S_f^{dII} = S_u^{dII}\Big|_{old} = \frac{N}{\pi} \int_{\pm\theta_{u1,old}^{II}}^{\pm\theta_{u2,old}^{II}} g^{(k)T} S^{d(k)'}(\theta, a_f)\, g^{(k)}\, d\theta \tag{3.45}$$

where $(\pm\theta_{u1,old}^{II}, \pm\theta_{u2,old}^{II})$ are the *old* ranges of mode II unstable microcrack growth at the *previous* load step. Note that if $\theta_{u2,old}^{II} > \theta_{b,new}$, then $\theta_{u2,old}^{II}$ in (3.45) should be replaced by $\theta_{b,new}$ since some microcracks now become open and the corresponding compliance contribution should belong to open (mixed mode) region. The domain of sliding closed microcracks also reduces and the *new* values of $\pm\theta_s$ may be obtained from (3.33b). Hence, it follows that

$$S_i^{dII} = \frac{N}{\pi}\left[\int_{\pm\theta_{s,new}}^{\pm\theta_{u1,old}^{II}} g^{(k)T} S^{d(k)'}(\theta, a_0)\, g^{(k)}\, d\theta + \int_{\pm\theta_{u2,old}^{II}}^{\pm\theta_{b,new}} g^{(k)T} S^{d(k)'}(\theta, a_0)\, g^{(k)}\, d\theta\right] \tag{3.46}$$

For open microcracks, we have

$$S_f^{dm} = S_u^{dm}\Big|_{old} = \frac{N}{\pi} \int_{\pm\theta_{u1,old}^{m}}^{\pm\theta_{u2,old}^{m}} g^{(k)T} S^{d(k)'}(\theta, a_f)\, g^{(k)}\, d\theta \tag{3.47}$$

where $(\pm\theta_{u1,old}^{m}, \pm\theta_{u2,old}^{II})$ is the *old* range of mixed mode unstable microcrack growth at the *previous* load step. We have assumed that $\theta_{u2,old}^{II} < \theta_{b,new}$. The domain of open microcracks increases and therefore S_i^{dm} should be updated:

$$S_i^{dm} = \frac{N}{\pi}\left[\int_{\pm\theta_{b,new}}^{\pm\theta_{u1,old}^{m}} g^{(k)T} S^{d(k)'}(\theta, a_0)\, g^{(k)}\, d\theta + \int_{\pm\theta_{u2,old}^{m}}^{\pm\pi/2} g^{(k)T} S^{d(k)'}(\theta, a_0)\, g^{(k)}\, d\theta\right] \tag{3.48}$$

(e) As $q > q_1$, more microcracks are activated. The mode II sliding and unstable angle domains, $(\pm\theta_s, \pm\theta_b)$ and $(\pm\theta_{u1}^{II}, \pm\theta_{u2}^{II})$, increase. Similarly, the mixed mode unstable angle domain, $(\pm\theta_{u1}^{m}, \pm\theta_{u2}^{m})$ or $(\pm\theta_b, \pm\theta_u^m)$ increases. The corresponding S_i^{dII},

$[S_u^{dII} + S_f^{dII}]$, S_i^{dm} and $[S_u^{dm} + S_f^{dm}]$ values can be computed by using (3.41)-(3.44), respectively.

Remark 3.3. Mode II weak-plane (interface) microcracks having the size $2a_f$ are arrested by higher energy barrier of matrix material. However, if axial compressive stress is increased to a certain level, these microcracks may kink into brittle matrix in a stable fashion and eventually align with the axial compressive load direction; see, e.g., Nemat-Nasser and Horii [1982], Horii and Nemat-Nasser [1985b,1986]. The kinking threshold stress q_{kink} can be obtained from (see, e.g., Zaitsev [1982,1983]):

$$q_{kink} = \frac{\sqrt{3}\,K_{fC}}{2\sqrt{\pi a_f}\,F(\theta_0^{II})} - \left[1 + \frac{\mu}{F(\theta_0^{II})}\right] q^* \tag{3.49}$$

The angle bounds for initiation of stable kinked microcracks, $(\theta_{k1}, \theta_{k2})$, can be expressed analogous to (3.37a):

$$\tan\theta_{k1,k2} = \frac{1 \pm \sqrt{1 - 4H_3(H_3+\mu)}}{2H_3}\ ,\ (q+q^*)^2 \geq 4\left[\frac{\sqrt{3}K_{fC}}{2\sqrt{\pi a_f}} - \mu q^*\right]\left[\frac{\sqrt{3}K_{fC}}{2\sqrt{\pi a_f}} + \mu q\right] \tag{3.50}$$

where $H_3 \equiv \{[\sqrt{3}K_{fC}/2\sqrt{\pi a_f}] - \mu q^*\}/(q+q^*)$. For $\mu q^* < \sqrt{3}K_{fC}/2\sqrt{\pi a_f}$, there are two real roots. Note that θ_{k1} and θ_{k2} should fall within $(\theta_{u1}^{II}, \theta_{u2}^{II})$; see Figure 2.

Assuming *stable* microcrack kinking, the "kink length" l can be related to the sliding shear stress τ_s; see, e.g., Zaitsev [1983], Horii and Nemat-Nasser [1986], Fanella and Krajcinovic [1988]. For cementitious composites below the brittle-ductile transition point, a simple formula may be used (Zaitsev [1983]):

$$l = \frac{4a_f^2\tau_s^2\cos^2\theta}{\pi K_{fC}^2} \tag{3.51}$$

where τ_s is available from Eq. (3.31). Finally, the additional compliance contribution S_{kink}^d due to kinked microcracks can be computed by

$$S_{kink}^d = \frac{N}{\pi}\int_{\pm\theta_{k1}}^{\pm\theta_{k2}} \mathbf{g}^{(k)T}\,\mathbf{S}^{d(k)'}(\theta, l)\,\mathbf{g}^{(k)}\,d\theta \qquad \square \tag{3.52}$$

III.4. Computational algorithms and numerical simulations

In this section, computational algorithms are given for the proposed self-consistent damage models. In addition, three detailed numerical simulations are presented. These include a mode I uniaxial tension test, a mode II uniaxial compression test, and a mixed mode tension/compression test of brittle materials. Due to lack of *plane strain* experimental data at this stage, however, actual experimental validation is not presented. Extensive experimental verification of the proposed models should be performed in the future. Nevertheless, the presented numerical simulations demonstrate the potential capability of the proposed micromechanical damage models to qualitatively explain and model physical behavior of brittle materials, without resorting to any fitted "material parameter" commonly utilized in phenomenological continuum damage models.

III.4.1. Computational algorithms

A self-consistent kinetic damage model naturally requires iterative schemes to obtain the yet *unknown* elastic-damage compliance $\bar{\mathbf{S}}$ corresponding to specified area-average stresses $\bar{\boldsymbol{\sigma}}$ or remote stresses $\boldsymbol{\sigma}^{\infty}$. As mentioned in Sec. 2.1, it is assumed that $\bar{\boldsymbol{\sigma}} \simeq \boldsymbol{\sigma}^{\infty}$ in our problems. For mode I, mode II and mixed mode damage models discussed in Sec. 3, fortunately, the "sliding angles" $\pm\theta_s$, "unstable angles" $\pm\theta_u$ and "kink angles" $\pm\theta_k$ are *independent* of the iterative processes in finding compliances $\bar{\mathbf{S}}$ for sequentially applied loads q. Therefore, the computational schemes involved in solving the proposed stress-controlled micromechanical damage models proceed as follows.

(1) For a given load q , compute "unstable angles" $\pm\theta_u$ according to (3.8) for mode I, (3.22) for mode II, as well as (3.37a,b) and (3.40) for mixed mode. "Sliding angles" $\pm\theta_s$ are computed according to (3.17) for mode II and (3.33b) for mixed mode. In addition, "kink angles" $\pm\theta_k$ are calculated according to (3.50). The "unstable" and "kink" angle domains should be stored as *history variables*. They depend on q only, independent of iterative steps in the following.

(2) Solve $\bar{\mathbf{S}}$ iteratively for a specified load q . The natural initial guess for the current $\bar{\mathbf{S}}$ is the *previous* secant compliance $\bar{\mathbf{S}}_{old}$. At the first loading step, we use the virgin elastic compliance $\mathbf{S}^o$ as an initial guess; see also Horii and Nemat-Nasser [1983, p. 168]. For each trial compliance $\bar{\mathbf{S}}^{(n)}$, we have to solve Eq. (2.22) so that displacement transformation matrix $\mathbf{B}^{(k)'}$, crack opening displacements, and inelastic compliance $\mathbf{S}^{d(k)'}$ can be evaluated. As noted before, the secant compliance $\bar{\mathbf{S}}$ is in general a *non-symmetric* matrix when frictional sliding of microcrack faces is present. Eq. (2.22) is simply a fourth order algebraic equation and is amenable to a closed-form exact solution. Further, we only need to solve (2.22) *once* (for each trial compliance $\bar{\mathbf{S}}^{(n)}$) at the orientation plane $\theta=0$. For other orientations, the local roots λ'_j can be expressed by the roots λ_j at $\theta=0$ (Lekhnitskii [1950, p. 51]):

$$\lambda'_j = \frac{\lambda_j \cos\theta - \sin\theta}{\cos\theta + \lambda_j \sin\theta} \quad ; \quad \bar{\lambda}'_j = \frac{\bar{\lambda}_j \cos\theta - \sin\theta}{\cos\theta + \bar{\lambda}_j \sin\theta} \tag{4.1}$$

where $\bar{\lambda}_j$ are the complex conjugate roots to λ_j . Once the roots of (2.22) in every desired orientation are obtained from closed-form solutions, $\mathbf{B}^{(k)'}$, $\mathbf{S}^{d(k)'}$ and $\mathbf{S}^{d(k)}$ for each microcrack contribution can be obtained from (2.9a), (2.14) and (2.20a-e) in Sec. 2.2, and from Eq. (32) in Horii and Nemat-Nasser [1983].

(3) Obtain the damage-induced compliance $\mathbf{S}^d$ in (2.21b) by numerical integration. Here, we use Simpson's rule with 201 integration points at various orientations between $(-\pi/2, \pi/2)$. The compliance contributions from $\mathbf{S}^d_u$, $\mathbf{S}^d_t$, $\mathbf{S}^d_f$ and $\mathbf{S}^d_{kink}$ can be computed by using (3.9)-(3.13) for mode I, (3.23)-(3.26) for mode II, (3.41)-(3.48) for mixed mode, and (3.49)-(3.52) for kinked microcracks.

(4) Obtain new trial compliance $\bar{\mathbf{S}}^{(n+1)}$ by adding $\mathbf{S}^d$ to $\mathbf{S}^o$. Compare this new trial compliance $\bar{\mathbf{S}}^{(n+1)}$ with the previous trial $\bar{\mathbf{S}}^{(n)}$. If the relative error is smaller than a preset tolerance, then the iterative process is said to be converged. On the other hand, if the relative error is unacceptable, then use $\bar{\mathbf{S}}^{(n+1)}$ as a new estimate, and go back to Step (2) to re-iterate until convergence is reached. This iterative procedure

leads to superlinear rate of convergence, and typically requires only 5 to 7 iterations. The convergence criteria we employ here are based on L_2 and L_∞ norms. In particular, we check the following ($TOL = 10^{-6}$):

$$\frac{\| \bar{S}^{(n)} - \bar{S}^{(n+1)} \|_2}{\| \bar{S}^{(n+1)} \|_\infty} \leq TOL \quad or \quad \frac{\| \bar{S}^{(n)} - \bar{S}^{(n+1)} \|_\infty}{\| \bar{S}^{(n+1)} \|_\infty} \leq TOL \tag{4.2}$$

If (4.2) is satisfied, then convergence is reached. Set $\bar{S} \equiv \bar{S}^{(n+1)}$ and go to Step (5).

(5) Apply the next load q_{new} . Set converged elastic-damage compliance $\bar{S}$ in Step (4) to $\bar{S}_{old}$ and go to Step (1).

III.4.2. A uniaxial tension test

A mode I uniaxial tension test is considered in this section (see also Sumarac and Krajcinovic [1987]). For comparison purpose, the results of the self-consistent method are compared with those of Taylor's model. The virgin material is assumed to be isotropic linear elastic with Young's modulus E^o = 4000 ksi (27600 MPa) and ν^o = 0.2. Moreover, K_{IC} is taken as 5 ksi-$in.^{1/2}$ (5.5 MN/$m^{3/2}$), and $a_0 = 0.6\, a_f$.

Two different initial microcrack area-concentration parameters are considered: ω_0 = 0.1131 and 0.2262. Recall that by definition $<\omega> = N \pi <a^2>/A$. Although the maximum allowable value of ω is 1 for the self-consistent model, actual brittle materials fail at ω less than 1. At the beginning ($q \leq q_0$) and the asymptotic end ($q = \infty$) of the loading sequence, damaged materials are *isotropic* because microcrack orientations are perfectly random and microcrack sizes are uniform. Thus, both the self-consistent model and Taylor's model can be computed analytically for $q \leq q_0$ and $q = \infty$; see Horii and Nemat-Nasser [1983], and Sumarac and Krajcinovic [1987]. The integration formulas for Taylor's model are analogous to the self-consistent model (3.9)-(3.13) with $S^{d(k)'}$ replace by (plane strain condition):

$$S_{ij}^{d(k)'} = \frac{2\pi a^2 (1-\nu^{o2})}{A\, E^o} (\delta_{2i}\, \delta_{2j} + \delta_{3i}\, \delta_{3j}) \quad ; \quad i, j = 1, 2, 3 \tag{4.3}$$

The relative difference in lateral compliances (dotted line) and axial compliances (solid lines) between the self-consistent model and Taylor's model for two values of initial damage ω_0 are shown in Fig. *3a*,*3b*. Notice that the responses of two models are not equivalent even at $q/q_o \leq 1$ due to initial (pre-existing) damage. It is also noted that as q approaches ∞ (not feasible), the final microcrack area-concentration parameters ω_f become 0.3142 and 0.6283, respectively. Further, the relative difference between the self-consistent model and Taylor's model depends on the degree of mean microcrack area-concentration $<\omega>$. See Fig. *4a*,*4b* where the relative difference in compliances between the two models are plotted vs. $<\omega>$. For low damage concentration ($<\omega>$ smaller than 27%), the relative difference in compliances is less than 10%; see Fig. *4a*. For moderate damage ($<\omega>$ between 27% to 45%), the relative difference ranges from 10% (at $q/q_0 \simeq 1.04$) to approximately 30% (at $q/q_0 \simeq 2.5$); see Fig. *4b*. Thus, it appears that use of Taylor's model is acceptable for low damage concentration, in agreement with the finding reported in Sumarac and Krajcinovic [1987].

Fig. *5a*,*5b* display normalized stresses versus normalized strains computed by the two models for the same two values of ω_0. Again, the relative difference is smaller than 10% for $<\omega>$ less than 27%. In addition, the averaged stress-strain behavior is qualitatively reasonable for the self-consistent damage model. The ratios of $\bar{S}_{22}/\bar{S}_{11}$ versus the normalized axial stresses q/q_0 are exhibited in Fig. *6a*,*6b*. In Fig. *7a*,*7b*, the ratios $\bar{S}_{22}/\bar{S}_{11}$ are plotted against the microcrack area-concentration parameter $<\omega>$.

III.4.3. Uniaxial compression and biaxial tension/compression tests

A mode II uniaxial compression test and a mixed mode biaxial tension/compression test are considered in this section. The virgin brittle composite material is assumed to be isotropic linear elastic with Young's modulus E^o = 6000 ksi (41400 MPa) and ν^o = 0.2. Fracture toughness properties of weak plane (interface) and matrix are taken to be K_{IIC} = 0.15 ksi-$in.^{1/2}$ (0.165 MN/$m^{3/2}$), K_{IIC} = 0.3 ksi-$in.^{1/2}$ (0.33 MN/$m^{3/2}$), and K_{IC} = 0.525

ksi-$in.^{1/2}$

(0.578 MN/$m^{3/2}$). The initial and final microcrack lengths on weak planes are taken as a_f = 0.375 in. (0.953 cm) and a_0 = 0.225 in. (0.572 cm). The coefficient of friction on microcrack faces is 0.6. In addition, q^* = 0 for the uniaxial compression test, q^* = 0.1 ksi (0.69 MPa, tensile) for the mixed mode test, and ω_0 = 0.2262.

The axial load q is gradually increased from 0 to a certain peak value. For the uniaxial compression test, all microcracks are *closed* throughout the loading sequence. By contrast, for the tension/compression test, a small lateral tension is applied at the very beginning and all microcracks are initially *open*. As q increases, more and more microcracks change states from open to *closed*. Therefore, for the mixed mode test, some microcracks are open and grow in mixed mode, while others are closed and grow in mode II fashion during the loading sequence. After mode II microcracks kink into matrix material, however, kinked microcracks are considered as "tension cracks" and aligned with the axial loading direction. In both tests, kinked microcracks are assumed to grow in a *stable* fashion.

The macroscopic axial stress vs. the axial (2-direction) and lateral (1-direction) strain curves are plotted in Fig. 8 for the plane strain *uniaxial compression* test. The mode II microcrack propagation and kinking threshold stresses are found to be q^{II} = 1.27 ksi (8.76 MPa) and q_{kink} = 1.48 ksi (10.21 MPa). Fig. 9 depicts the "*active* microcrack area-concentration" parameter $<\omega^a>$ (defined as $N\pi<a^2>/A$) vs. the axial load q. It is emphasized that "no-slip" microcracks are *excluded* from $<\omega^a>$ since they do not contribute to either strain or secant compliance. Moreover, no-slip and sliding angle fans are *fixed* throughout the loading process. That is, $\theta_{s1} = \tan^{-1}\mu$ and $\theta_{s2} = \pi/2$. As a consequence, $<\omega^a>$ is *fixed* before mode II microcrack propagation occurs. Fig. 10 displays $\bar{S}_{11}$ and $\bar{S}_{22}$ vs. $<\omega^a>$. It is observed that the lateral compliance component $\bar{S}_{11}$ is much larger than the axial compliance component $\bar{S}_{22}$ because of the formation of many

kinked microcracks. $\bar{S}_{12}$ and $\bar{S}_{21}$ vs. $<\omega^a>$ are given in Fig. 11. Notice that $\bar{S}_{21}$ is larger than $\bar{S}_{12}$ due to sliding microcrack displacements. Furthermore, Fig. 12 exhibits the shear compliance component $\bar{S}_{33}$ vs. $<\omega^a>$.

For the mixed mode tension/compression test, the response is initially *isotropic* at q = 0 and q^* = 0.1 ksi (0.69 MPa, a small lateral tension) because all microcracks are initially open and of uniform size. Later, as q increases, some microcracks become closed and even become stuck (no-slip). Thus, $\bar{\mathbf{S}}$ and $<\omega^a>$ slightly *decrease* before mode II microcrack propagation starts. From numerical computation, the mode II microcrack propagation threshold stress is found to be q^{II} = 0.95 ksi (6.56 MPa), the microcrack kinking threshold stress q_{kink} = 1.17 ksi (8.07 MPa), and the mixed mode threshold stress q^{*} = 1.28 ksi (8.83 MPa). This implies that mode II microcrack growth in *closed* domain occurs well before mixed mode microcrack growth takes place in *open* domain. Eventually, it is numerically observed that $\theta_2^{II} = \theta_b = \theta_1^{*}$. The macroscopic axial stress vs. the axial and lateral strain curves are plotted in Fig. 13. Fig. 14 shows $<\omega^a>$ vs. the axial load q. Fig. 15 displays $\bar{S}_{11}$ and $\bar{S}_{22}$ vs. $<\omega^a>$. Again, $\bar{S}_{11}$ is much larger than $\bar{S}_{22}$ because of kinked microcracks. $\bar{S}_{12}$ and $\bar{S}_{21}$ vs. $<\omega^a>$ are shown in Fig. 16. Fig. 17 gives the shear compliance component $\bar{S}_{33}$ vs. $<\omega^a>$. Note that $\bar{S}_{11}$, $\bar{S}_{22}$ and $\bar{S}_{33}$ slightly decrease at the beginning due to the increase of "no-slip" microcrack domain.

By comparing Fig. 8 with 13, it is seen that microcrack propagation and kinking threshold stresses q^{II} and q_{kink} as well as the peak stress significantly decrease in the presense of a small lateral tension q^*. In addition, the lateral strain of the biaxial tension/compression test is higher than that of the uniaxial compression test.

iII.5. Closure

Following the framework proposed by Krajcinovic and Fanella [1986], the proposed micromechanical brittle damage models do not require the use of additional fitted "material parameters" other than well-defined elastic constants and mesostructural fracture toughness of constituent phases. Thermodynamic basis, effective averaged field equations, microcrack opening displacements and damage-induced inelastic compliance are given within the context of two-dimensional self-consistent method. It is emphasized that secant compliances are generally non-symmetric.

Fracture mechanics stability criteria together with mesostructural geometry are employed to characterize microcrack evolutions under mode I, mode II and mixed mode loadings. Simple and efficient computational algorithms are presented. In addition, three detailed numerical simulations are given. Finally, it is emphasized that loading/unloading stress paths and microcrack opening/closing status changes are easily accommodated within the context of the proposed damage models.

III.6. References

Ashby, M. F. [1979], "Micromechanisms of fracture in static and cyclic failure," in: R. A. Smith, ed., *Fracture Mechanics, Current Status, Future Prospects,* Pergamon Press, Oxford, Vol. 1.

Budiansky, B. and R. J. O'Connel [1976], "Elastic moduli of a cracked solid," *Int. J. Solids & Struct.,* Vol. 12, pp. 81-97.

Chudnovsky, A., A. Dolgopolsky and M. Kachanov [1987a], "Elastic interaction of a crack with a microcrack array - I: Formulation of the problem and general form of the solution," *Int. J. Solids & Struct.,* Vol. 23, No. 1, pp. 1-10.

Chudnovsky, A., A. Dolgopolsky and M. Kachanov [1987b], "Elastic interaction of a crack with a microcrack array - II: Elastic solution for two crack configurations (piece-wise constant and linear approximations)," *Int. J. Solids & Struct.,* Vol. 23, No. 1, pp. 11-21.

Fanella, D. and D. Krajcinovic [1988], "A micromechanical model for concrete in compression," *Eng. Fract. Mech,* Vol. 29, No. 1, pp. 49-66.

Hill, R. [1965], "A self-consistent mechanics of composite materials," *J. Mech. Phy. Solids,* Vol. 13, pp. 213-222.

Hoenig, A. [1978], "The behavior of a flat elliptical crack in an anisotropic elastic body," *Int. J. Solids & Struct.,* Vol. 14, pp. 925-934.

Hoenig, A. [1979], "Elastic moduli of a non-randomly cracked body," *Int. J. Solids & Struct.;* Vol. 15, pp. 137-154.

Hoenig, A. [1982], "Near-tip behavior of a crack in a plane anisotropic elastic body," *Eng. Fract. Mech.,* Vol. 16, No. 3, pp. 393-403.

Horii, H. and S. Nemat-Nasser [1983], "Overall moduli of solids with microcracks: load induced anisotropy," *J. Mech. Phys. Solids,* Vol. 31, No. 2, pp. 155-171.

Horii, H. and S. Nemat-Nasser [1985a], "Elastic fields of interacting inhomogeneities," *Int. J. Solids & Struct.*, Vol. 21, No. 7, pp. 731-745.

Horii, H. and S. Nemat-Nasser [1985b], "Compression induced microcrack growth in brittle solids: axial splitting and shear failure," *J. Geophys. Res.*, Vol. 90, pp. 3105-3125.

Horii, H. and S. Nemat-Nasser [1986], "Brittle failure in compression: splitting, faulting and brittle-ductile transition," *Phil. Trans. R. Soc.*, Vol. 319, pp. 337-374.

Ju, J. W. [1989], "On energy-based coupled elastoplastic damage theories: Constitutive modeling and computational aspects," *Int. J. Solids & Struct.*, in press.

Kachanov, L. M. [1958], "Time of the rupture process under creep conditions," *IVZ Akad Nauk*, S.S.R., Otd Tech Nauk, No. 8, pp. 26-31.

Kachanov, M. [1980], "Continuum model of medium with cracks," *J. Eng. Mech. Div.*, ASCE, Vol. 106, No. EM5, pp. 1039-1051.

Kachanov, M. [1987], "Elastic solids with many cracks: A simple method of analysis," *Int. J. Solids & Struct.*, Vol. 23, No. 1, pp. 23-43.

Kanninen, M. F. and C. H. Popelar [1985], *Advanced Fracture Mechanics*, Oxford University Press, New York, and Clarendon Press, Oxford.

Krajcinovic, D. [1984], "Continuum damage mechanics," *Appl. Mech. Rev.*, Vol. 37: 1-6, pp. 397-402.

Krajcinovic, D. [1985], "Constitutive theories for solids with defective microstructure," in *Damage Mechanics and Continuum Modeling*, ed. by N. Stubbs and D. Krajcinovic, ASCE, pp. 39-56.

Krajcinovic, D. [1986], "Update to continuum damage mechanics," *Appl. Mech. Update*, pp. 403-406.

Krajcinovic, D. and D. Fanella [1986] "A micromechanical damage model for concrete," *Eng. Fract. Mech.*, Vol. 25, No. 5/6, pp. 585-596.

Krajcinovic, D. and D. Sumarac [1989] "A mesomechanical model for brittle deformation processes: Part I," *J. Appl. Mech.*, Vol. 56, No. 3, pp. 51-56.

Lekhnitskii, S. G. [1950], *Theory of Elasticity of an Anisotropic Elastic Body*, by the Government Publishing House for Technical-Theoretical Works, Moscow and Leningrad, 1950; and by Holden-Day, Inc., San Francisco, 1963.

Mura, T. [1982], *Micromechanics of Defects in Solids*, Nijhoff, The Hague.

Nemat-Nasser, S. and H. Horii [1982], "Compression-induced nonplanar crack extension with application to splitting, exfoliation, and rock burst," *J. Geophys. Res.*, Vol. 87, 6805-6821.

Ortiz, M. [1985], "A constitutive theory for the inelastic behavior of concrete," *Mech. of Materials*, Vol. 4, pp. 67-93.

Rice, J. R. [1975], "Continuum mechanics and thermodynamics of plasticity in relation to microscale deformation mechanisms," *Constitutive Equations in Plasticity*, A. Argon, ed., MIT Press, Cambridge Mass.

Sih, G. C., P. C. Paris and G. R. Irwin [1965], "On cracks in rectilinearly anisotropic bodies," *Int. J. Fract. Mech.*, Vol. 1, No. 3, pp. 189-203.

Simo, J. C. and J. W. Ju [1987], "Stress and strain based continuum damage models. Part I: Formulation," *Int. J. Solids & Struct.*, Vol. 23, No. 7, pp. 821-840.

Sneddon, I. N. and M. Lowengrub [1969], *Crack Problems in the Classical Theory of Elasticity*, Wiley, New York.

Sumarac D. and D. Krajcinovic [1987], "A self-consistent model for microcrack-weakened solids," *Mech. Mater.*, Vol. 6, pp. 39-52.

Sumarac D. and D. Krajcinovic [1989], "A mesomechanical model for brittle deformation processes: Part II," *J. Appl. Mech.*, Vol. 56, No. 3, pp. 57-62.

Vakulenko, A. A. and M. L. Kachanov [1971], "Continuum theory of medium with cracks," *Mekh. Tverdogo Tela*, Vol. 4, pp. 159-166.

Willis, J. R. [1968], "The stress field around an elliptical crack in an anisotropic elastic medium," *Int. J. Eng. Sci.*, Vol. 6, pp. 253-263.

Wu, C. H. [1985], "Tension-compression test of a concrete specimen via a structure damage theory," in *Damage Mechanics and Continuum Modeling*, ed. by N. Stubbs and D. Krajcinovic, ASCE, pp. 1-12.

Zaitsev, Y. [1982], *Deformation and Strength Models for Concrete Based on Fracture Mechanics*, Stroiizdat, Moscow.

Zaitsev, Y. [1983], "Crack propagation in a composite material," in *Fracture Mechanics of Concrete*, pp. 251-299, edited by F. H. Wittmann, Elsevier, Amsterdam.

III.7. Figure captions and figures

Figure 1. The local (primed) and global Cartesian coordinate systems.

Figure 2. An example of domains of mode II microcrack face sliding, unstable microcrack growth, and mixed mode unstable microcrack growth. θ_b separates the open region from the closed region.

Figure 3. The ratios of compliances computed by using the self-consistent and Taylor's models in axial (solid line) and lateral (dashed) directions vs. the normalized stress q/q_0. Part (a) is for $\omega_0 = 0.1131$, and (b) for $\omega_0 = 0.2262$.

Figure 4. The ratios of compliances computed by using the self-consistent and Taylor's models in axial and lateral directions vs. the evolving microcrack concentration parameter ω for $\omega_0 = 0.1131$ (a) and 0.2262 (b), respectively.

Figure 5. The normalized stress vs. the normalized strain computed by using the self-consistent and Taylor's models for $\omega_0 = 0.1131$ (a) and 0.2262 (b), respectively.

Figure 6. $\bar{S}_{22}/\bar{S}_{11}$ ratio vs. the normalized stress computed by using the self-consistent and Taylor's models for $\omega_0 = 0.1131$ (a) and 0.2262 (b), respectively.

Figure 7. $\bar{S}_{22}/\bar{S}_{11}$ ratio vs. the microcrack concentration parameter ω for $\omega_0 = 0.1131$ (a) and 0.2262 (b), respectively.

Figure 8. The axial stress q vs. the axial ($\bar{e}_2$) and lateral ($\bar{e}_1$) strains for the uniaxial compression test.

Figure 9. The "active microcrack area-concentration" parameter $<\omega^a>$ vs. the axial stress q for the uniaxial compression test.

Figure 10. $\bar{S}_{11}$ and $\bar{S}_{22}$ vs. $<\omega^a>$ for the uniaxial compression test.

Figure 11. $\bar{S}_{12}$ and $\bar{S}_{21}$ vs. $<\omega^a>$ for the uniaxial compression test.

Figure 12. $\bar{S}_{33}$ vs. $<\omega^a>$ for the uniaxial compression test.

Figure 13. The axial stress q vs. the axial ($\bar{e}_2$) and lateral ($\bar{e}_1$) strains for the biaxial tension/compression test.

Figure 14. The "active microcrack area-concentration" parameter $<\omega^a>$ vs. the axial stress q for the biaxial tension/compression test.

Figure 15. $\bar{S}_{11}$ and $\bar{S}_{22}$ vs. $<\omega^a>$ for the biaxial tension/compression test.

Figure 16. $\bar{S}_{12}$ and $\bar{S}_{21}$ vs. $<\omega^a>$ for the biaxial tension/compression test.

Figure 17. $\bar{S}_{33}$ vs. $<\omega^a>$ for the biaxial tension/compression test.

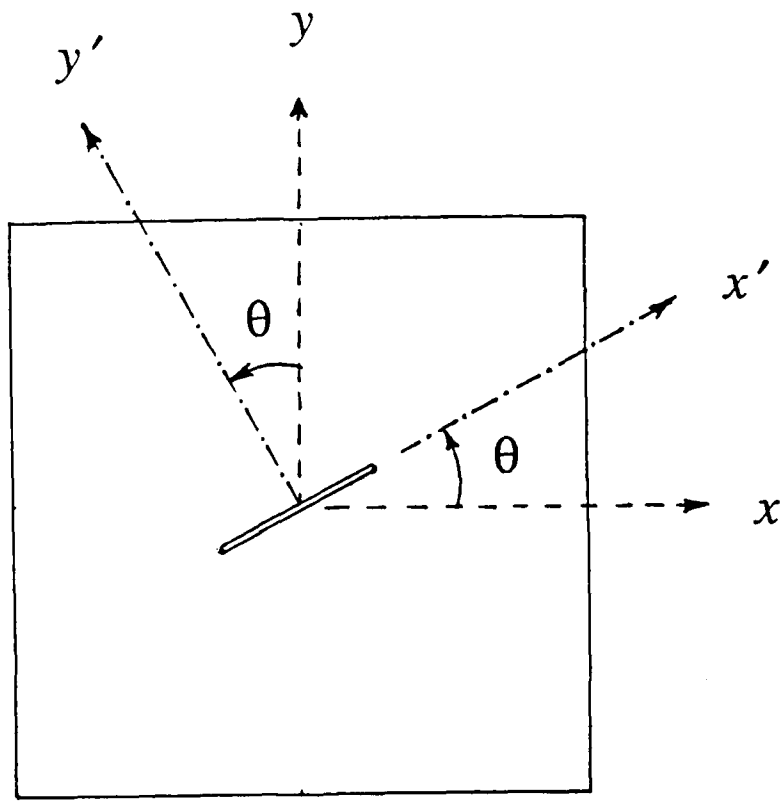

Figure 1. The local (primed) and global Cartesian coordinate systems.

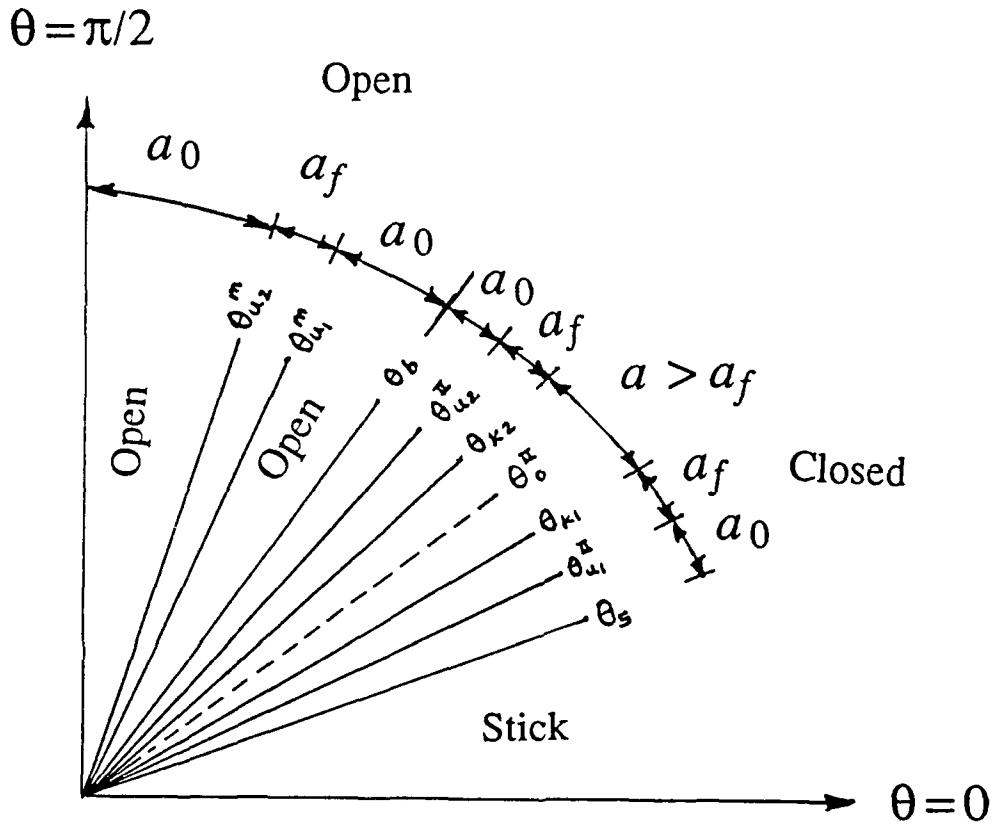

Figure 2. An example of domains of mode II microcrack face sliding, unstable microcrack growth, and mixed mode unstable microcrack growth. θ_b separates the open region from the closed region.

Figure 3. The ratios of compliances computed by using the self-consistent and Taylor's models in axial (solid line) and lateral (dashed) directions vs. the normalized stress q/q_0. Part (a) is for $\omega_0 = 0.1131$, and (b) for $\omega_0 = 0.2262$.

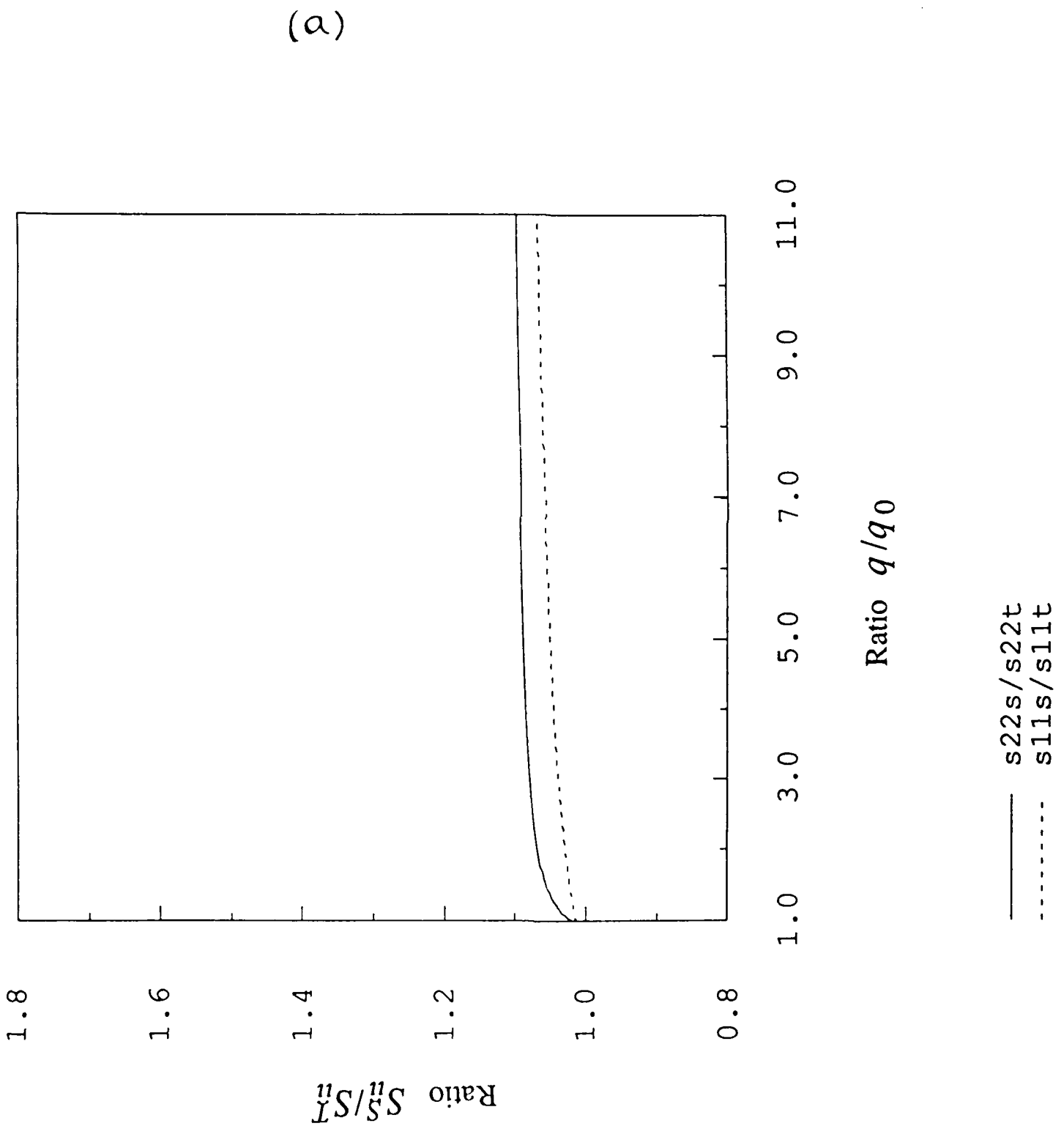

Fig. 36

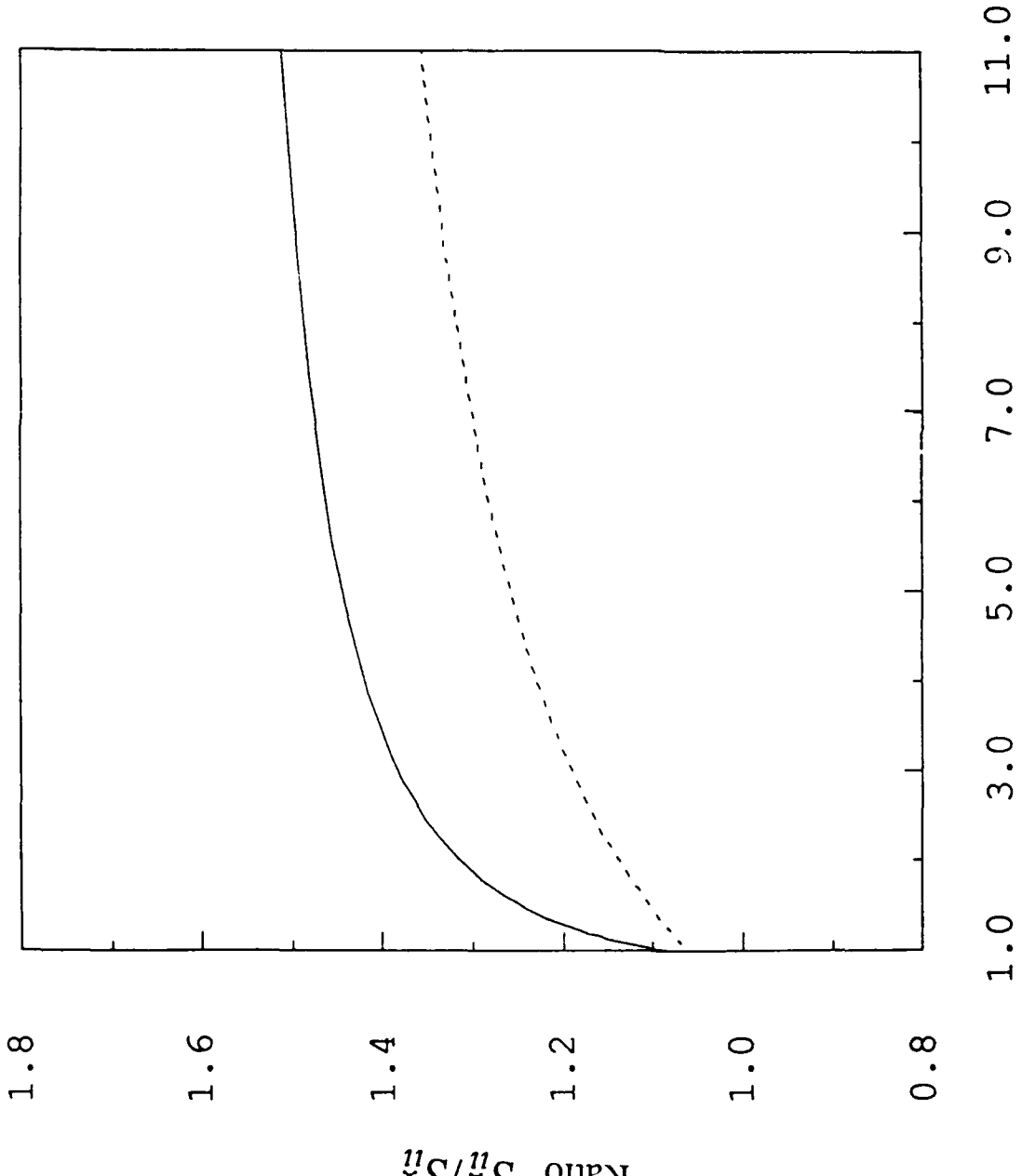
Ratio S_{ii}^S/S_{ii}^T
1.8
1.6
1.4
1.2
1.0
0.8
1.0
3.0
5.0
7.0
9.0
11.0
Ratio q/q_0
s22s/s22t
s11s/s11t

Figure 4. The ratios of compliances computed by using the self-consistent and Taylor's models in axial and lateral directions vs. the evolving microcrack concentration parameter ω for ω_0 = 0.1131 (a) and 0.2262 (b), respectively.

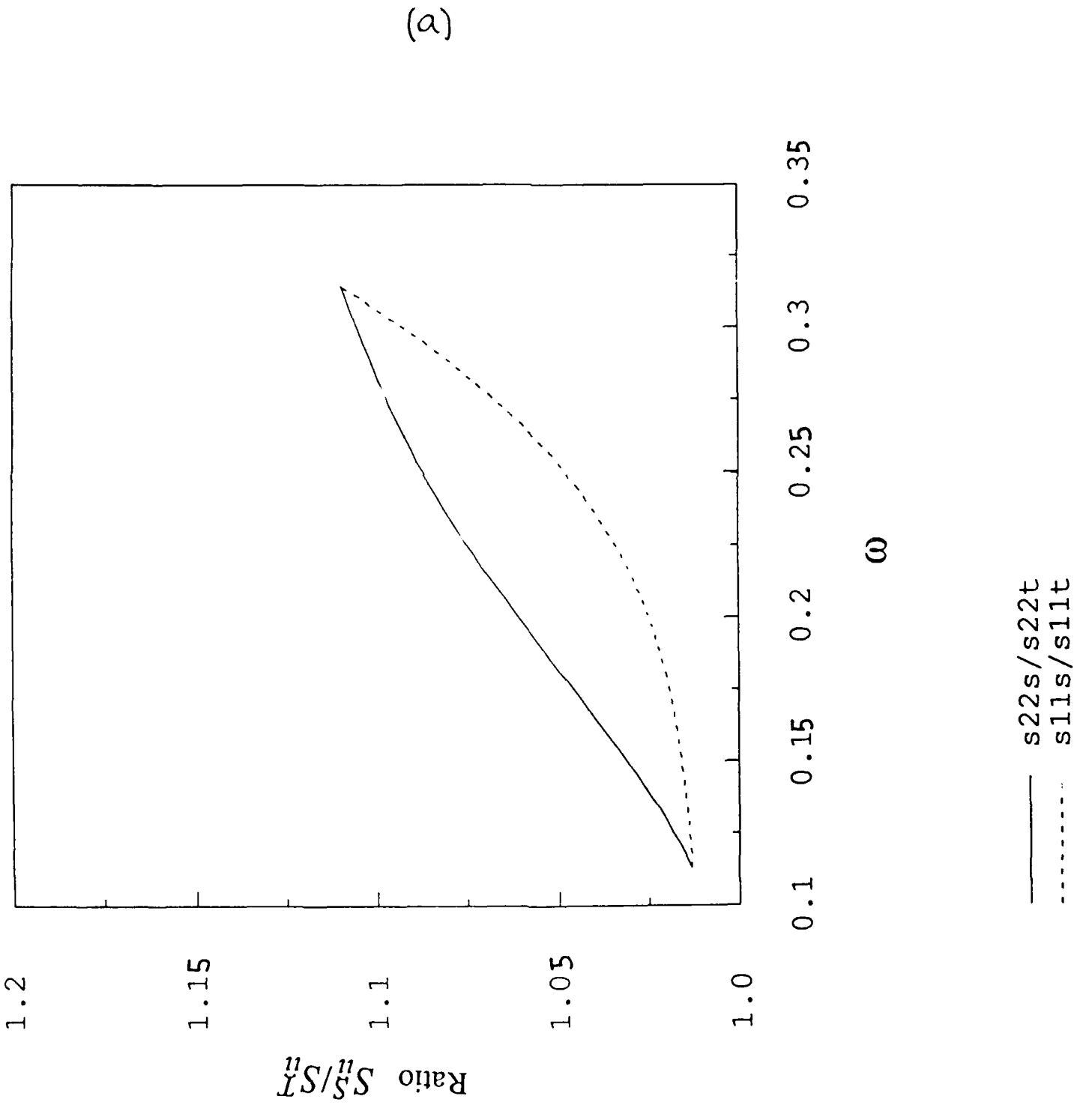

Fig. 4b

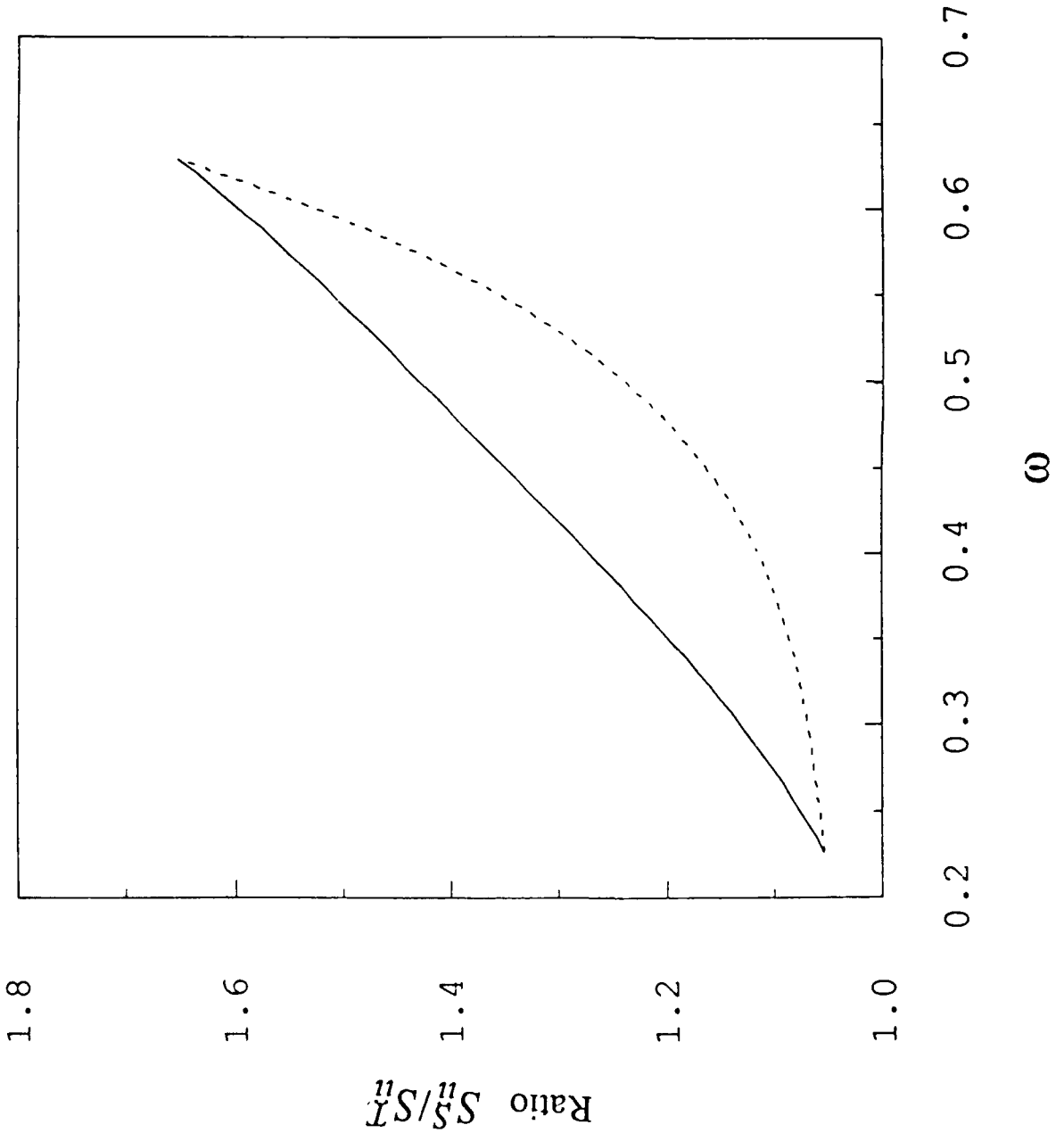
Ratio S_{ii}^{S}/S_{ii}^{T}
1.8
1.6
1.4
1.2
1.0
0.2
0.3
0.4
0.5
0.6
0.7
ω
s22s/s22t
s11s/s11t

Figure 5. The normalized stress vs. the normalized strain computed by using the self-consistent and Taylor's models for $\omega_0 = 0.1131$ (a) and 0.2262 (b), respectively.

(a)

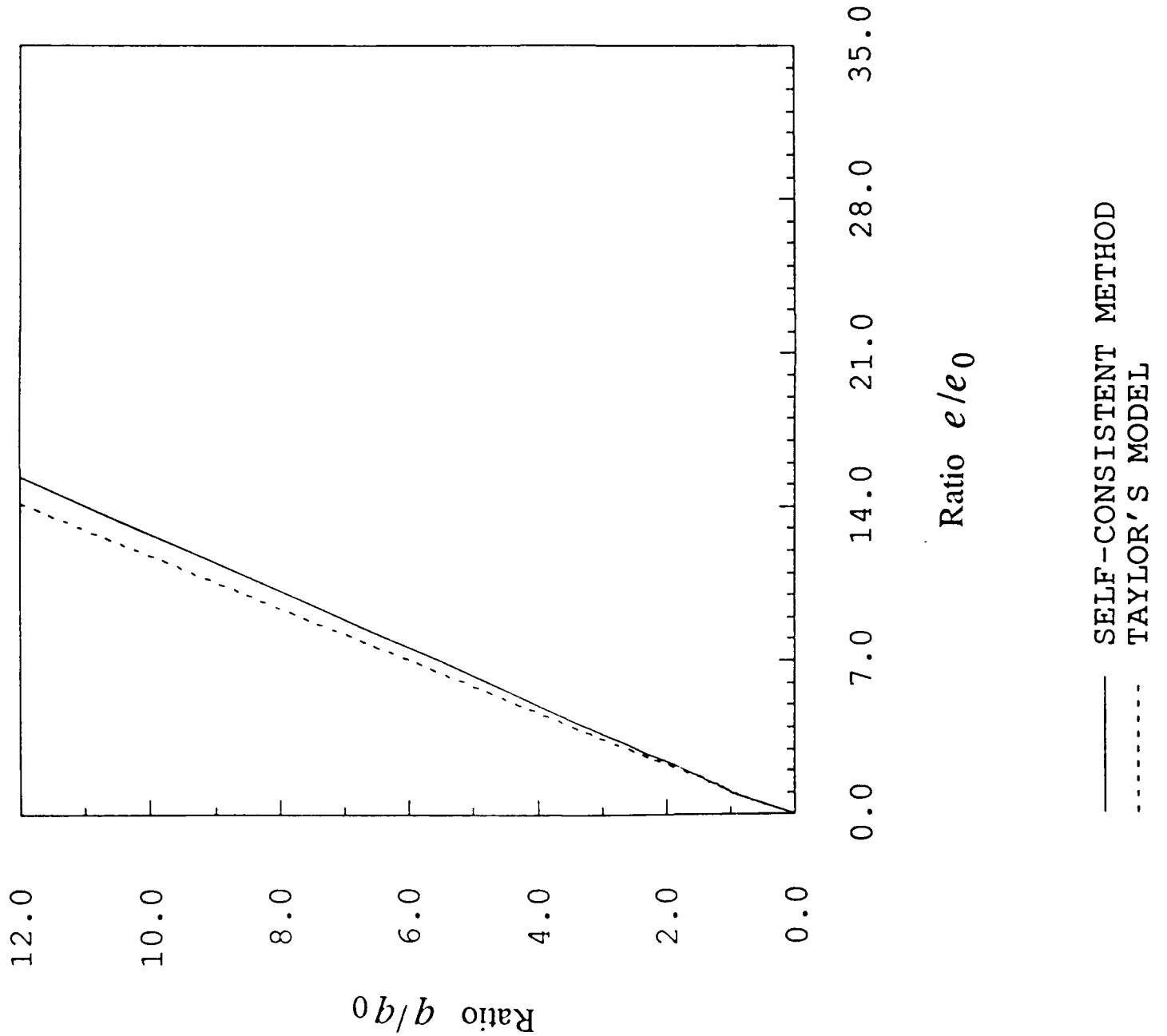

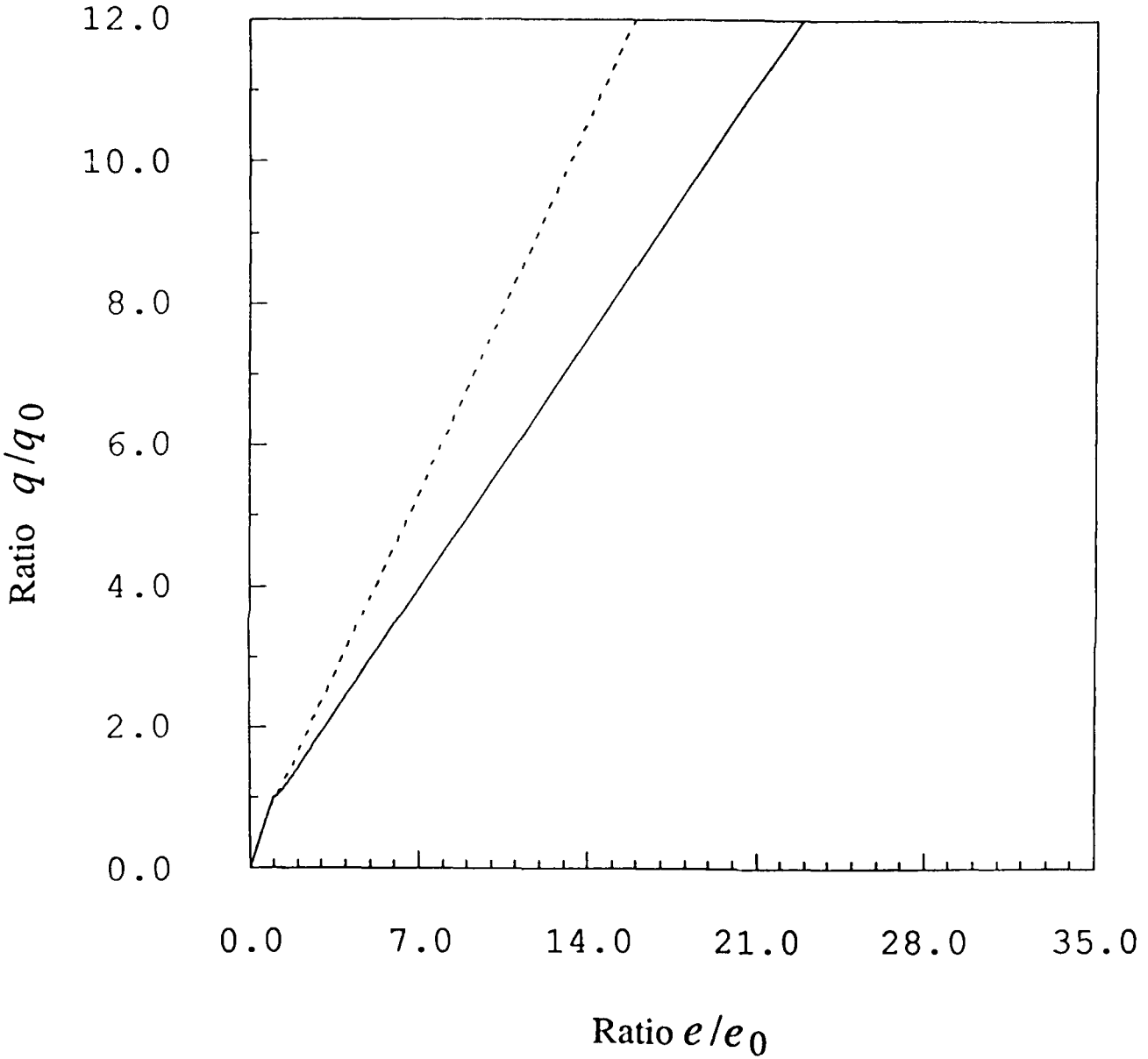
12.0
10.0
8.0
6.0
4.0
2.0
0.0
Ratio q/q_0
0.0
7.0
14.0
21.0
28.0
35.0
Ratio e/e_0
SELF-CONSISTENT METHOD
TAYLOR'S MODEL

Fig. 5b

Figure 6. $\bar{S}_{22}/\bar{S}_{11}$ ratio vs. the normalized stress computed by using the self-consistent and Taylor's models for ω_0 = 0.1131 (a) and 0.2262 (b), respectively.

(a)

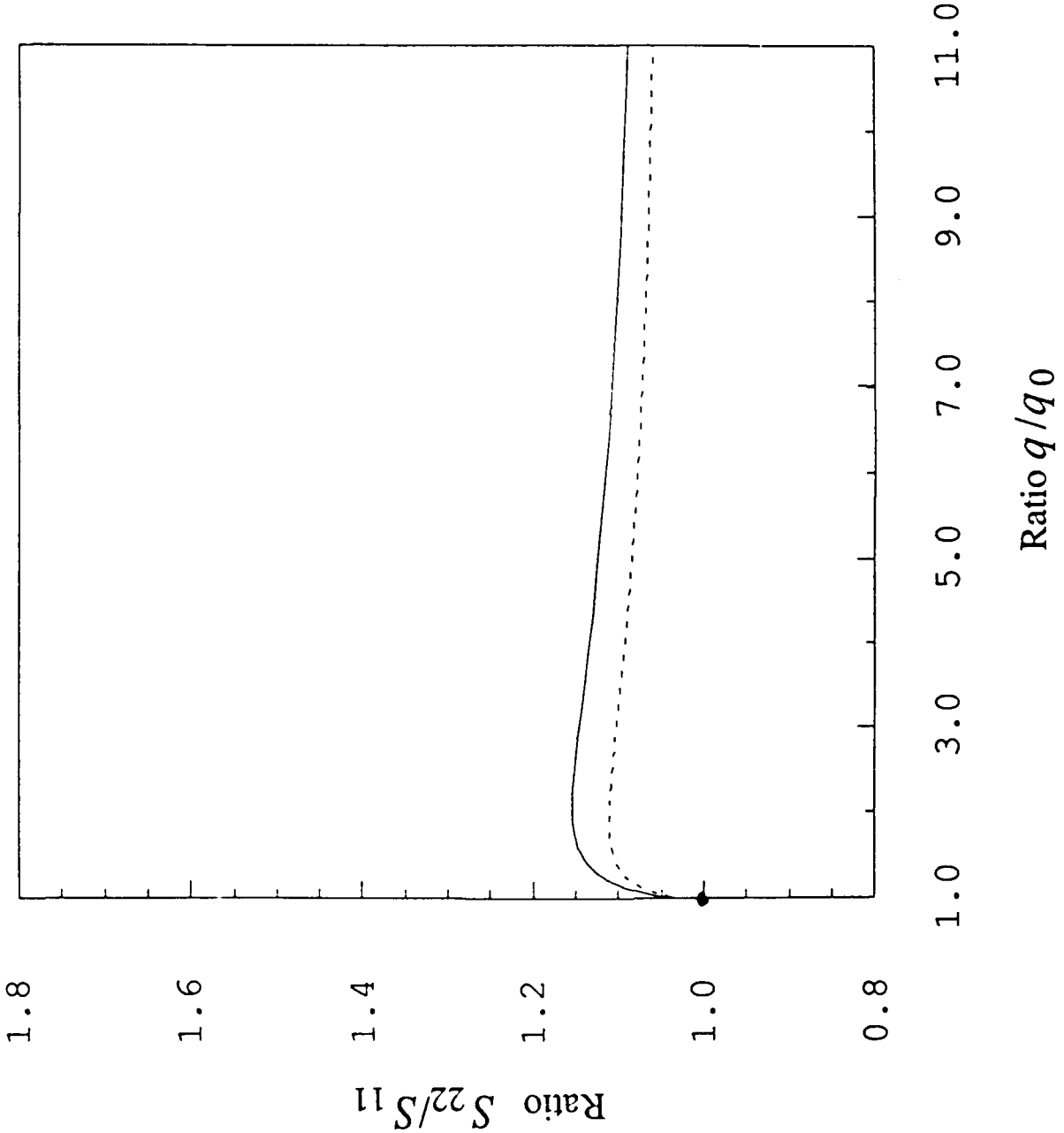

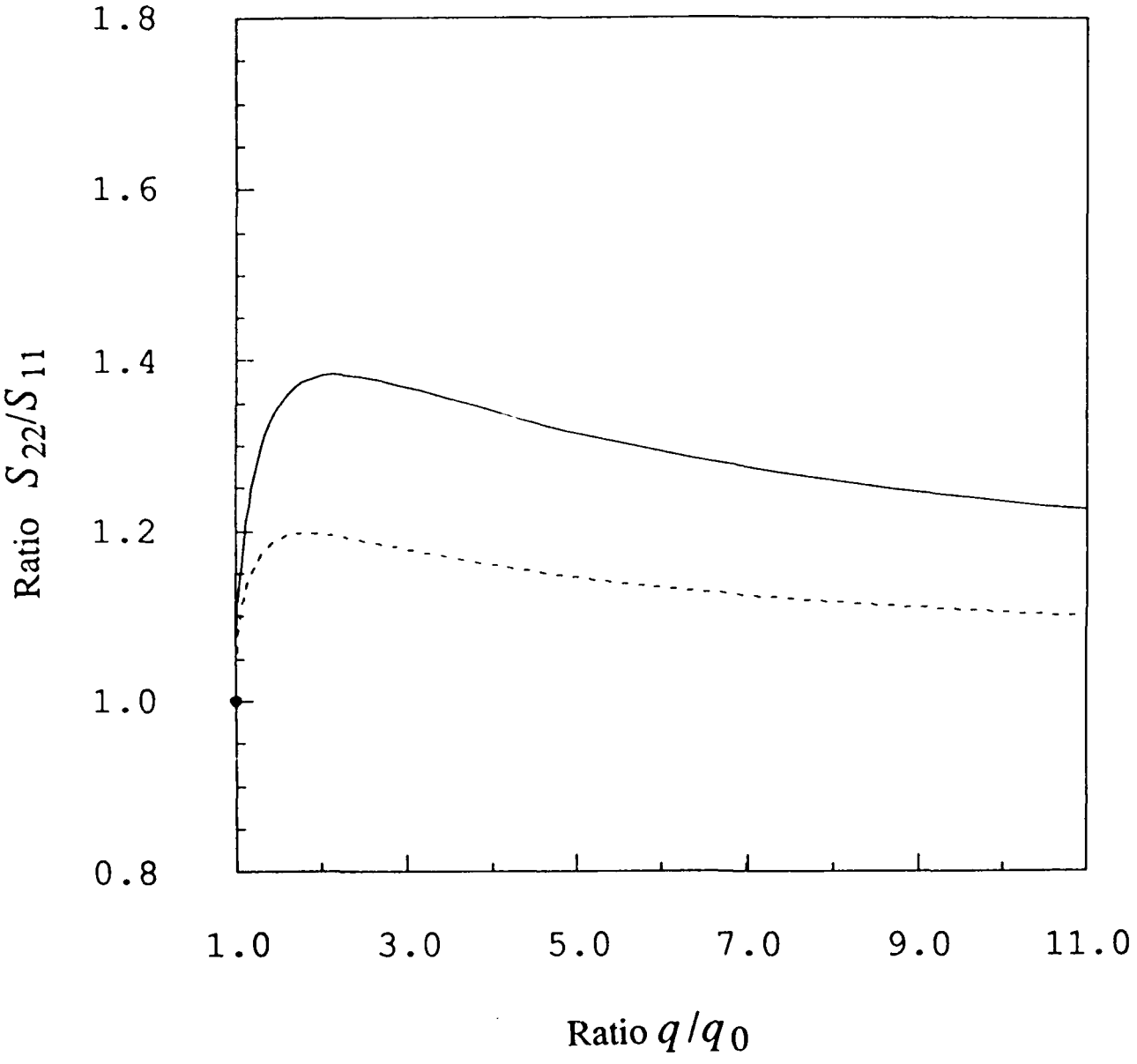
1.8
1.6
1.4
1.2
1.0
0.8
Ratio S_{22}/S_{11}
1.0
3.0
5.0
7.0
9.0
11.0
Ratio q/q_0
SELF-CONSISTENT METHOD
TAYLOR'S MODEL

Fig. 6b

Figure 7. $\bar{S}_{22}/\bar{S}_{11}$ ratio vs. the microcrack concentration parameter ω for $\omega_0 = 0.1131$ (a) and 0.2262 (b), respectively.

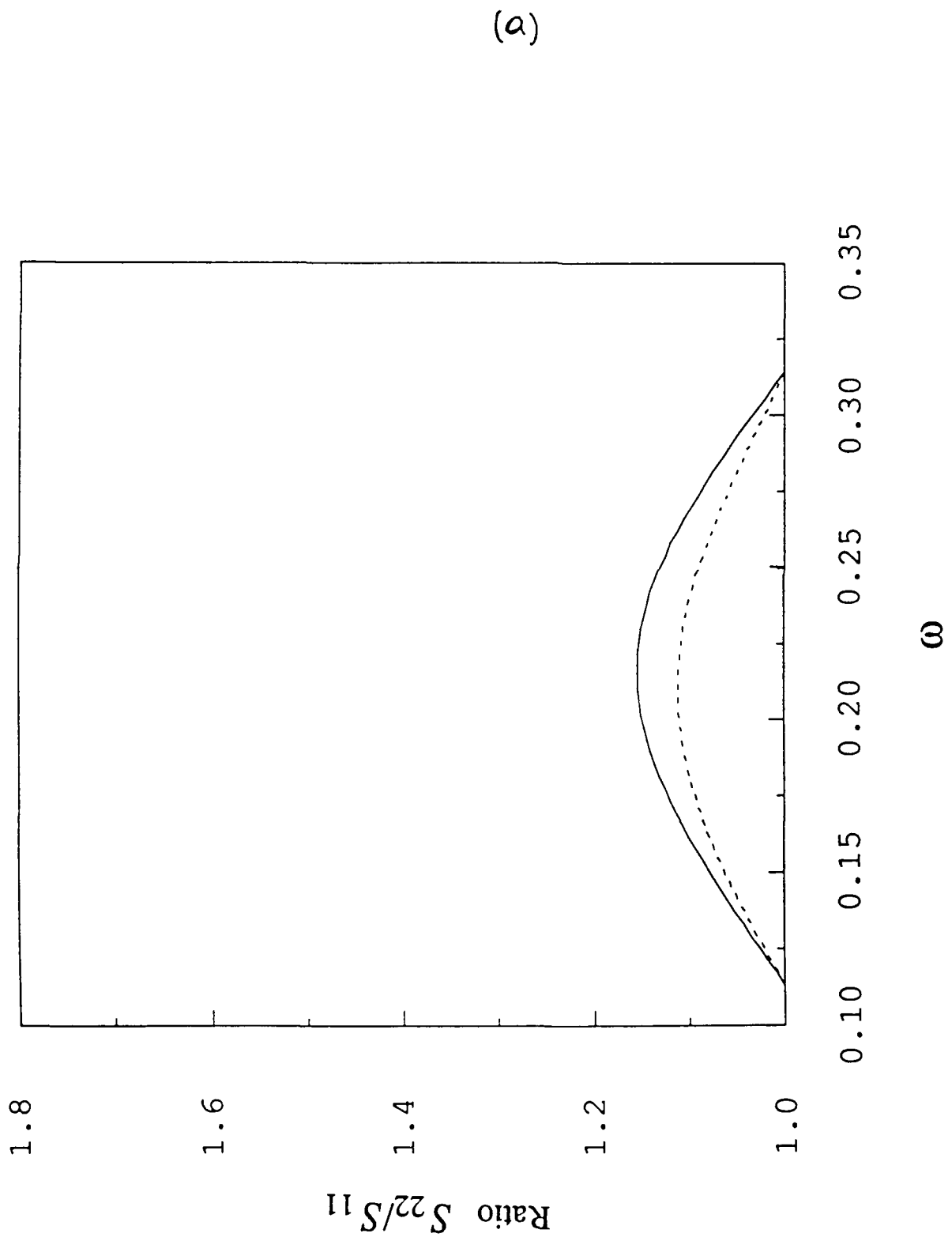

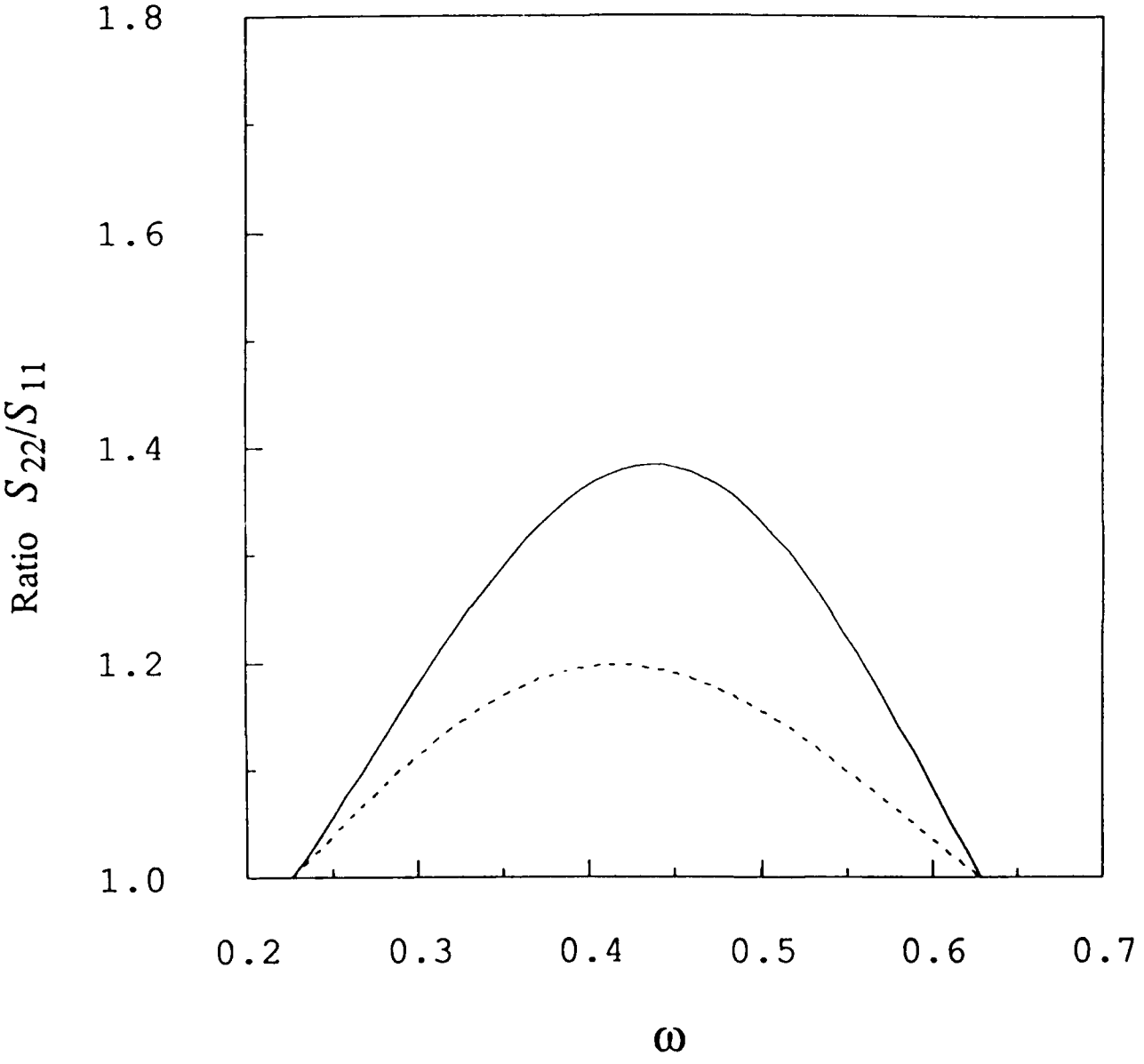
1.8
1.6
1.4
1.2
1.0
Ratio S_{22}/S_{11}
0.2
0.3
0.4
0.5
0.6
0.7
ω
SELF-CONSISTENT METHOD
TAYLOR'S MODEL

Fig. 7b

Figure 8. The axial stress q vs. the axial ($\bar{e}_2$) and lateral ($\bar{e}_1$) strains for the uniaxial compression test.

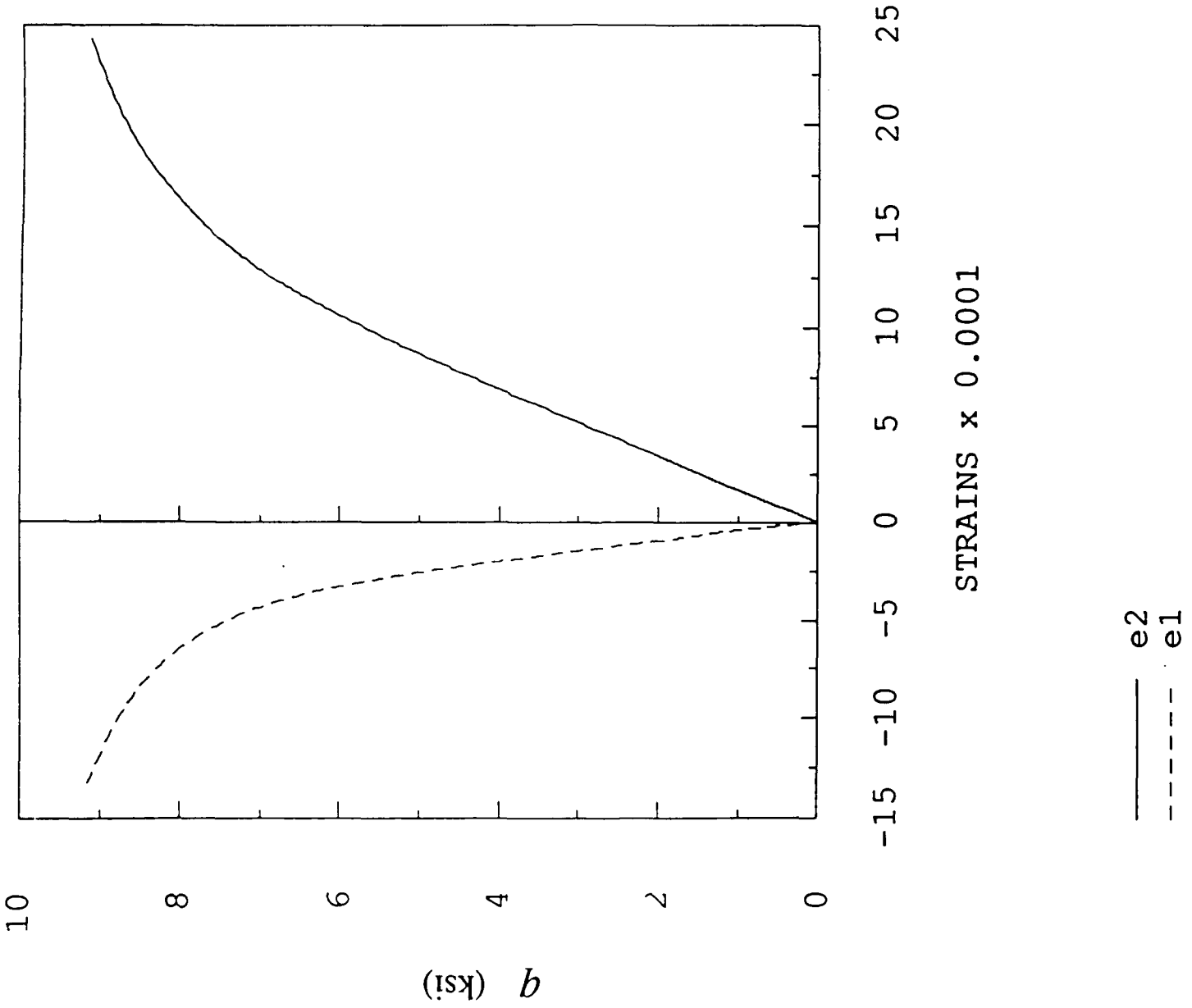

Figure 9. The "active microcrack area-concentration" parameter $<\omega^a>$ vs. the axial stress q for the uniaxial compression test.

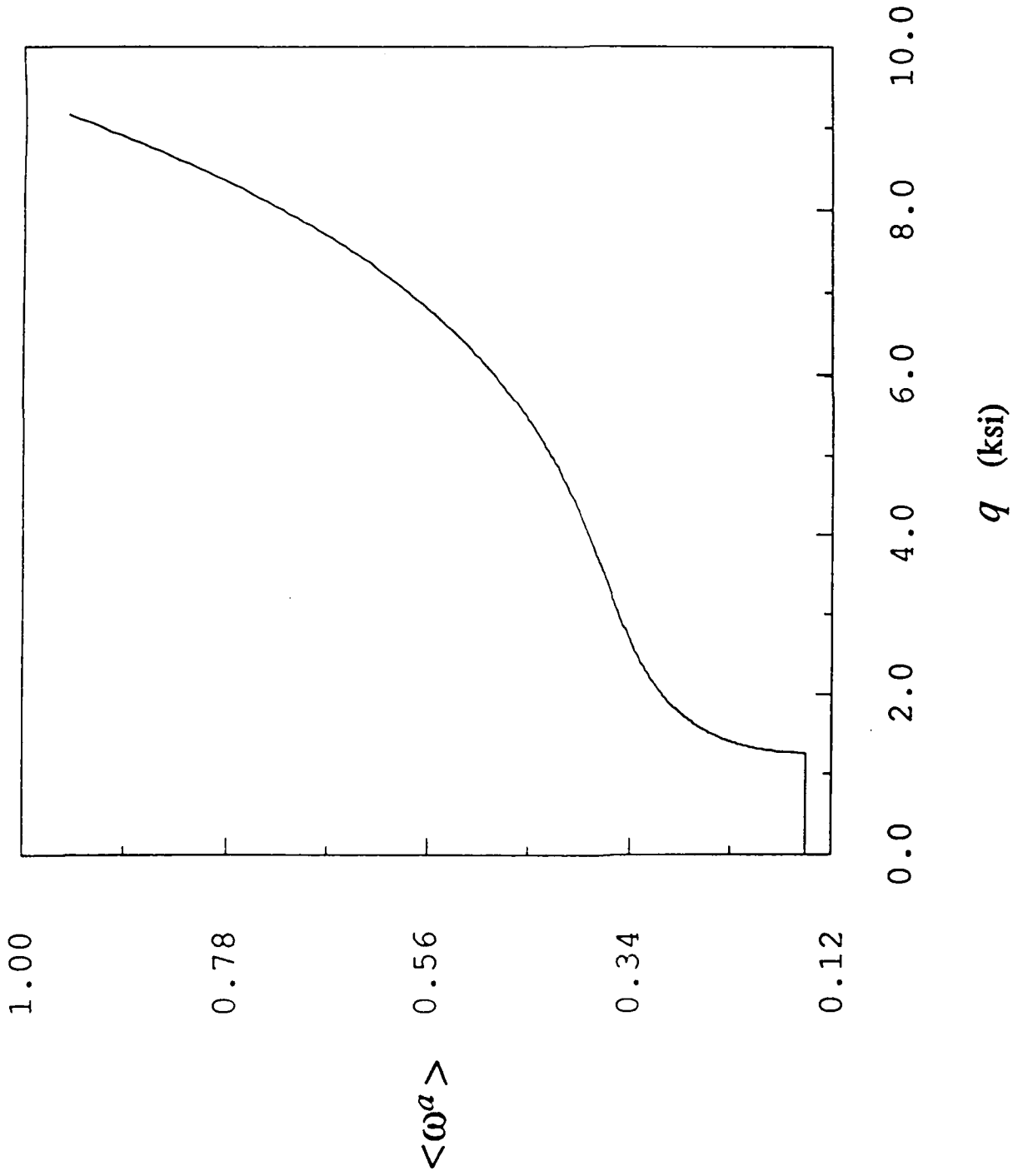

Figure 10. $\bar{S}_{11}$ and $\bar{S}_{22}$ vs. $<\omega^a>$ for the uniaxial compression test.

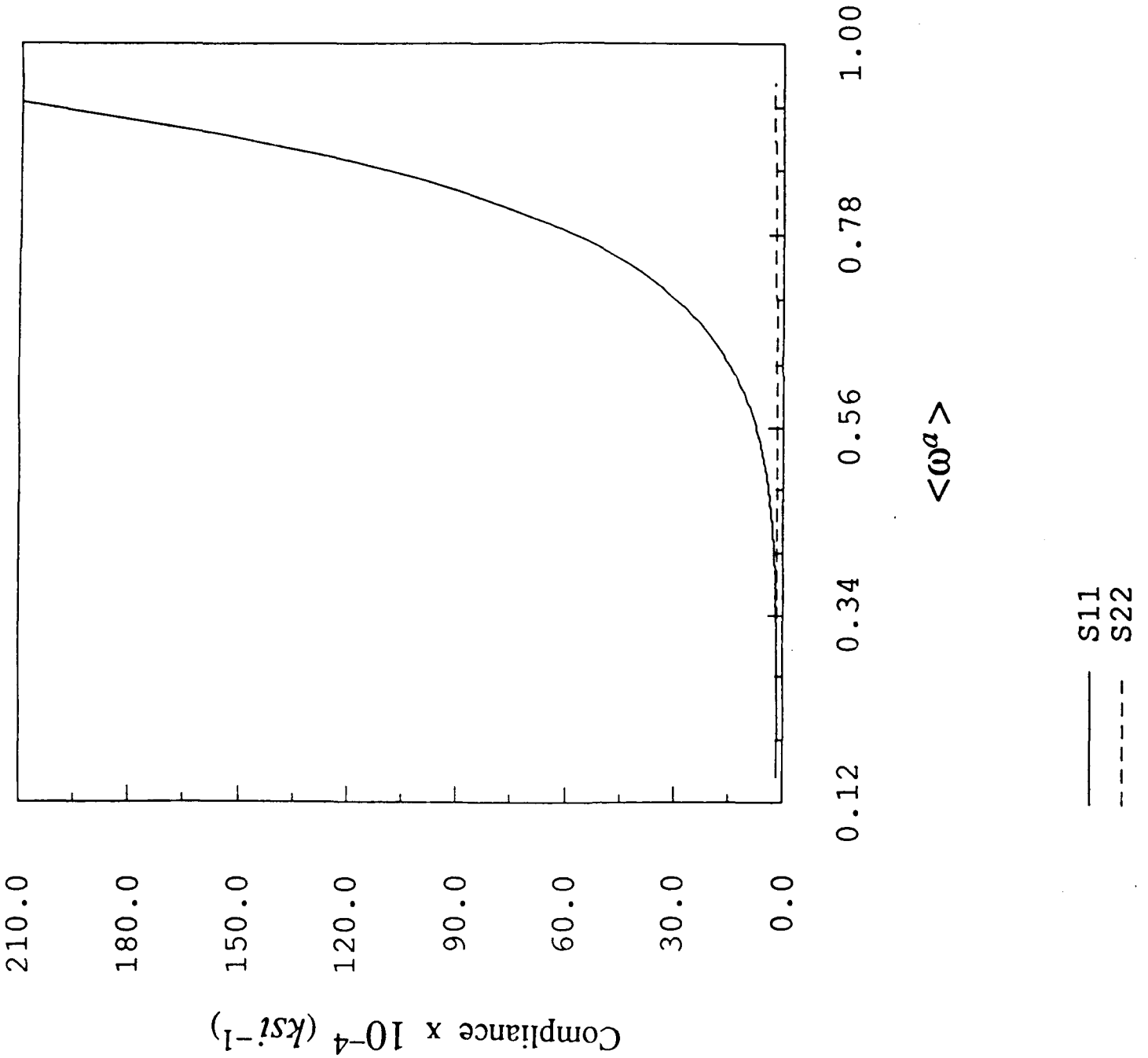

Figure 11. $\bar{S}_{12}$ and $\bar{S}_{21}$ vs. $<\omega^a>$ for the uniaxial compression test.

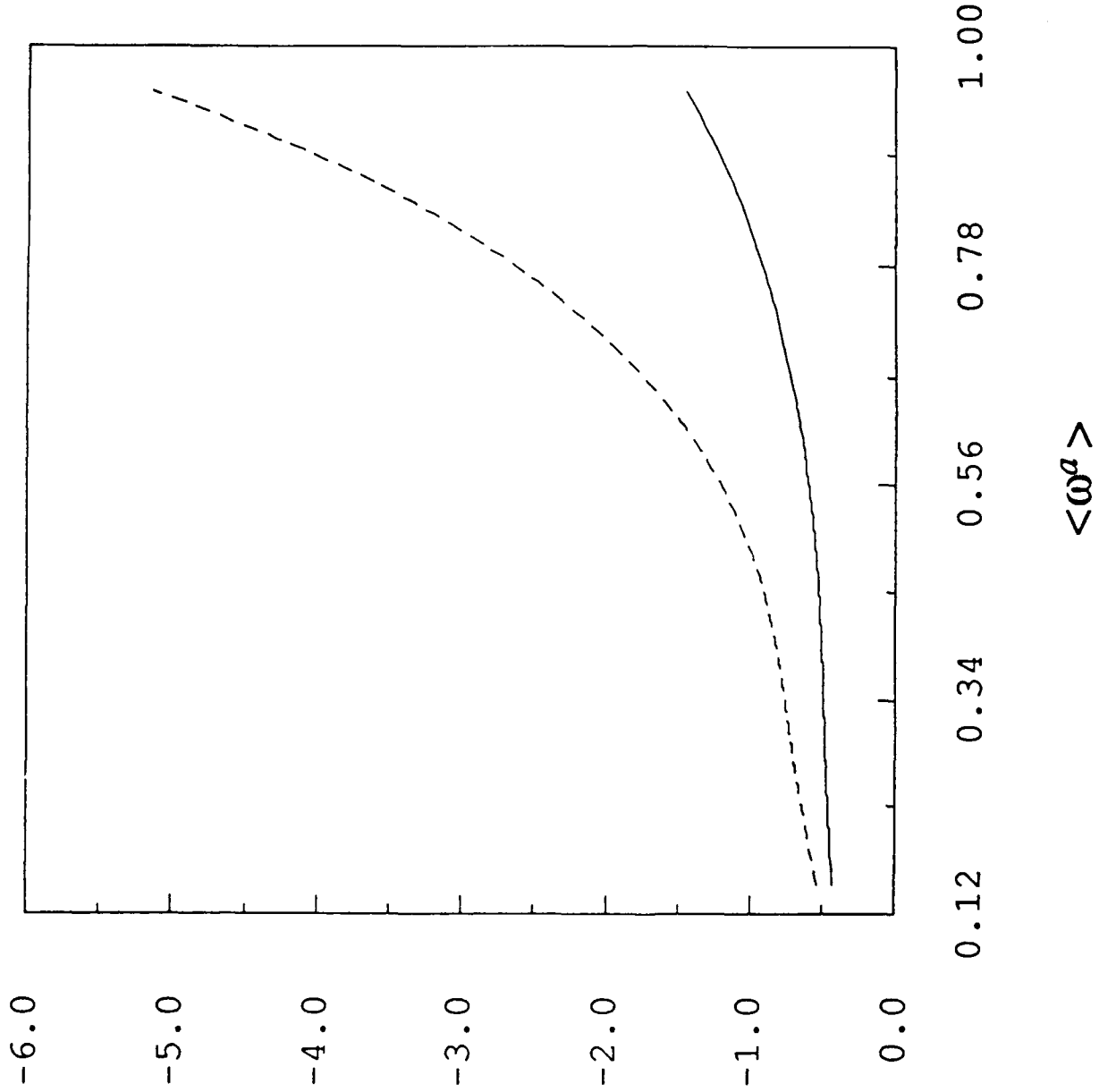

Figure 12. $\bar{S}_{33}$ vs. $<\omega^a>$ for the uniaxial compression test.

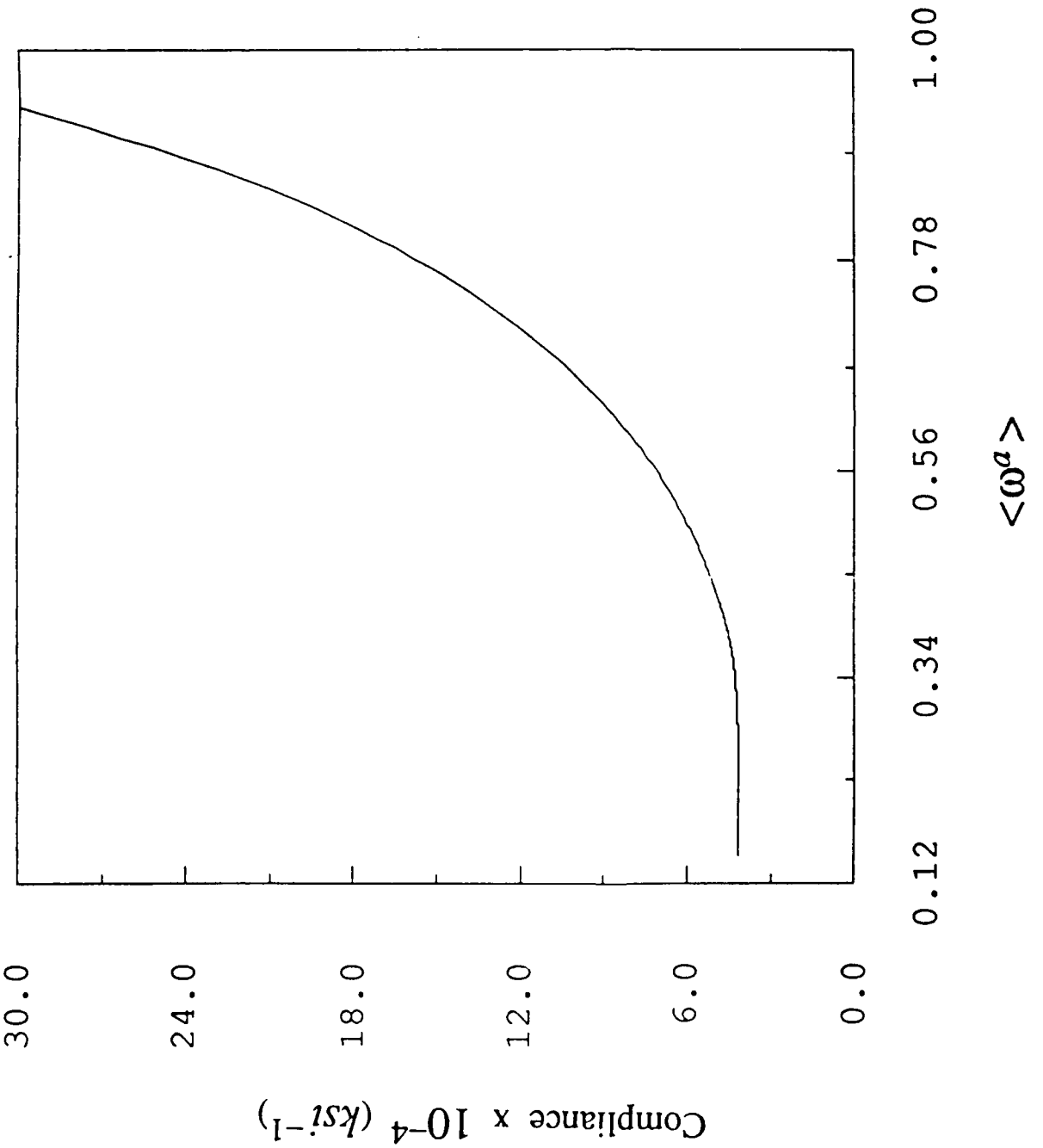

Figure 13. The axial stress q vs. the axial ($\bar{e}_2$) and lateral ($\bar{e}_1$) strains for the biaxial tension/compression test.

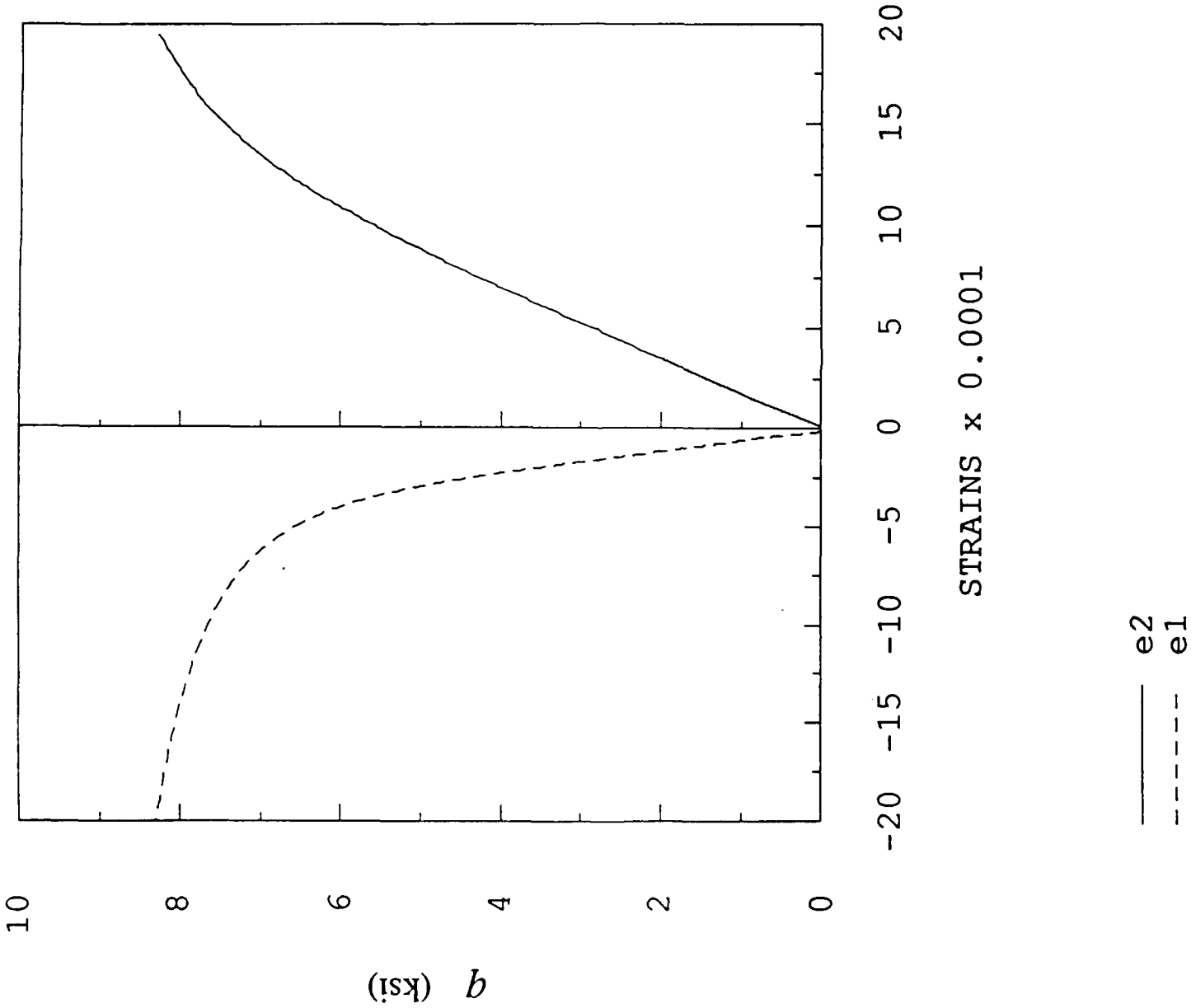

Figure 14. The "active microcrack area-concentration" parameter $<\omega^a>$ vs. the axial stress q for the biaxial tension/compression test.

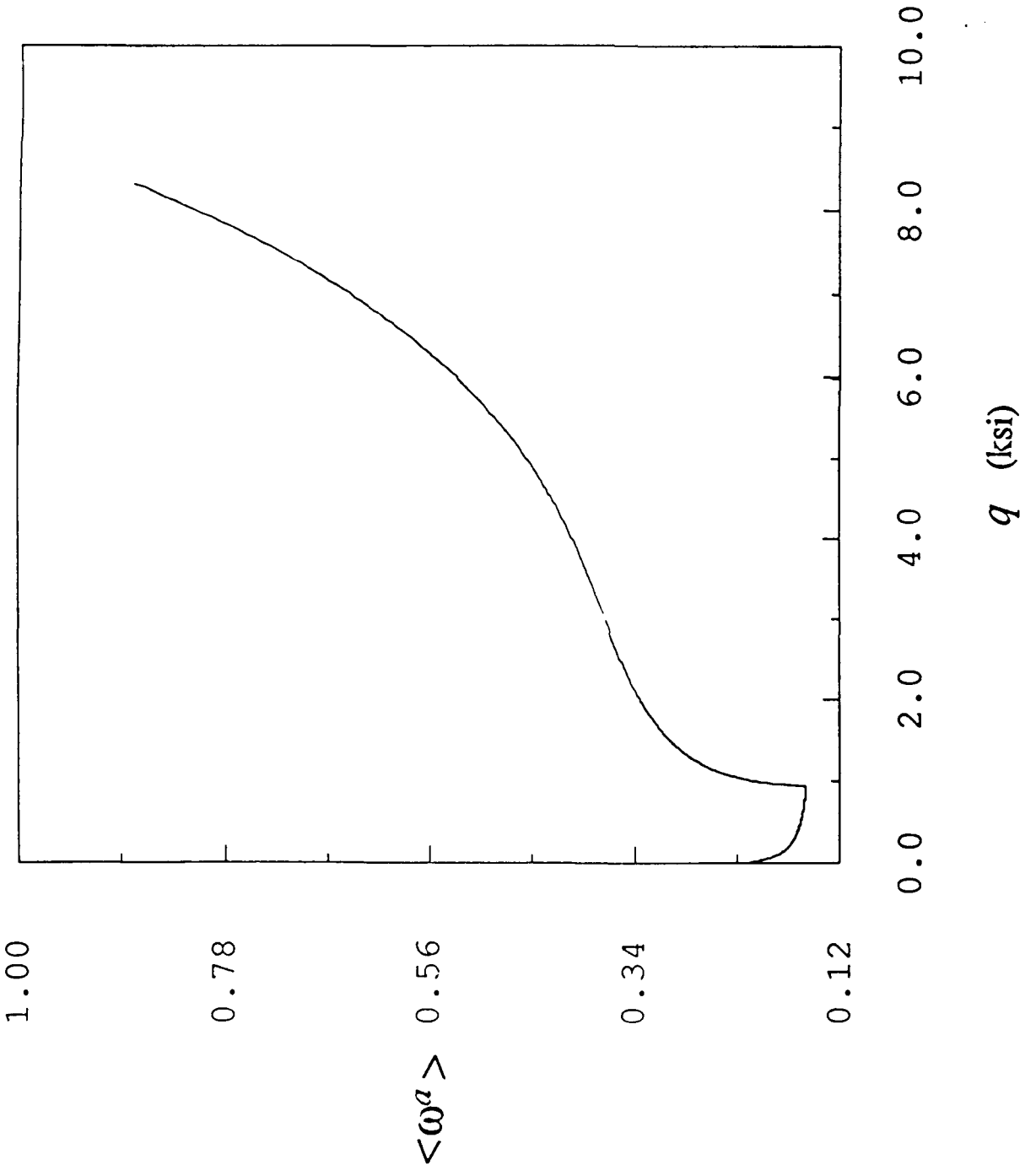

Figure 15. $\bar{S}_{11}$ and $\bar{S}_{22}$ vs. $<\omega^a>$ for the biaxial tension/compression test.

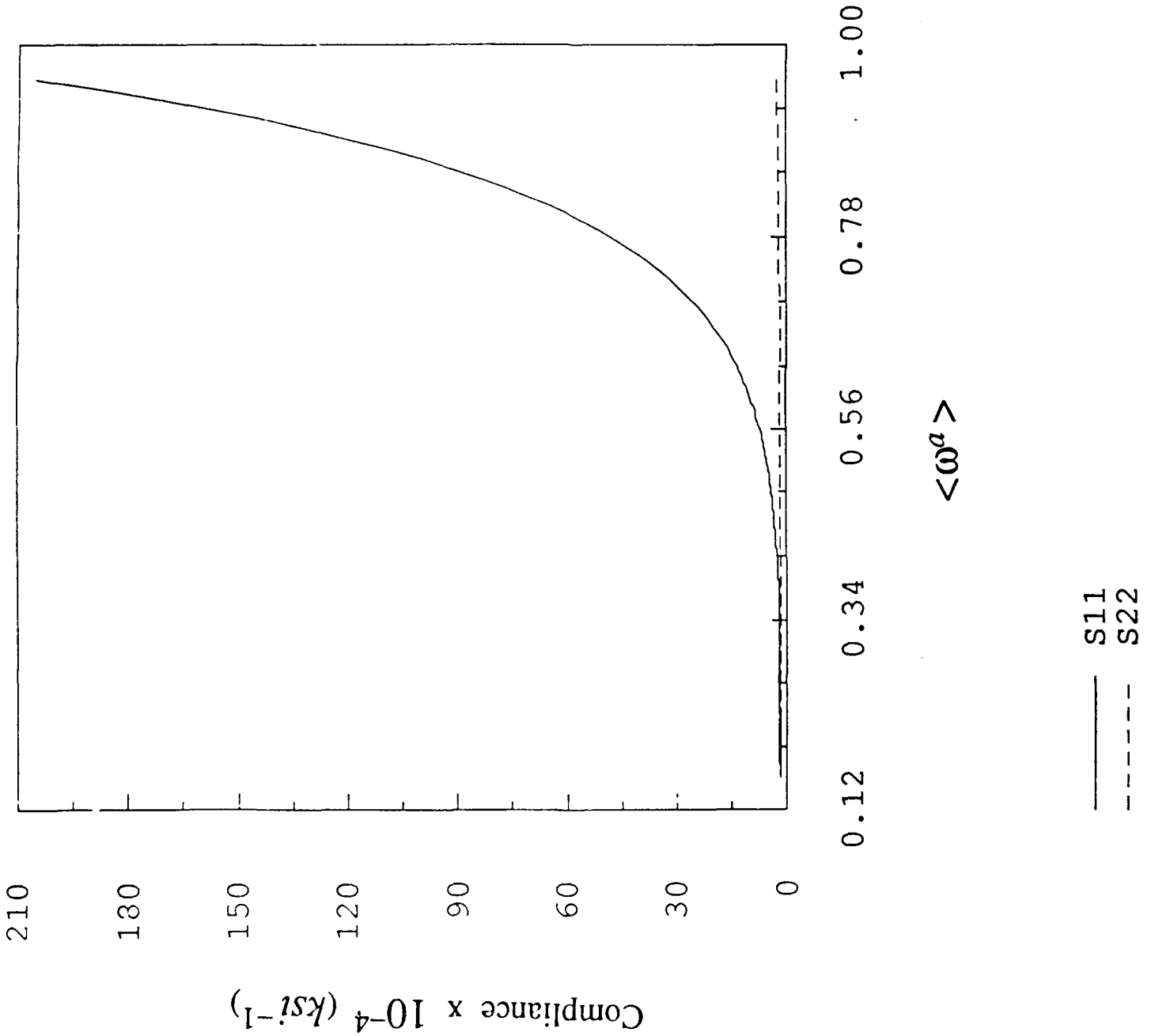

Figure 16. $\bar{S}_{12}$ and $\bar{S}_{21}$ vs. $<\omega^a>$ for the biaxial tension/compression test.

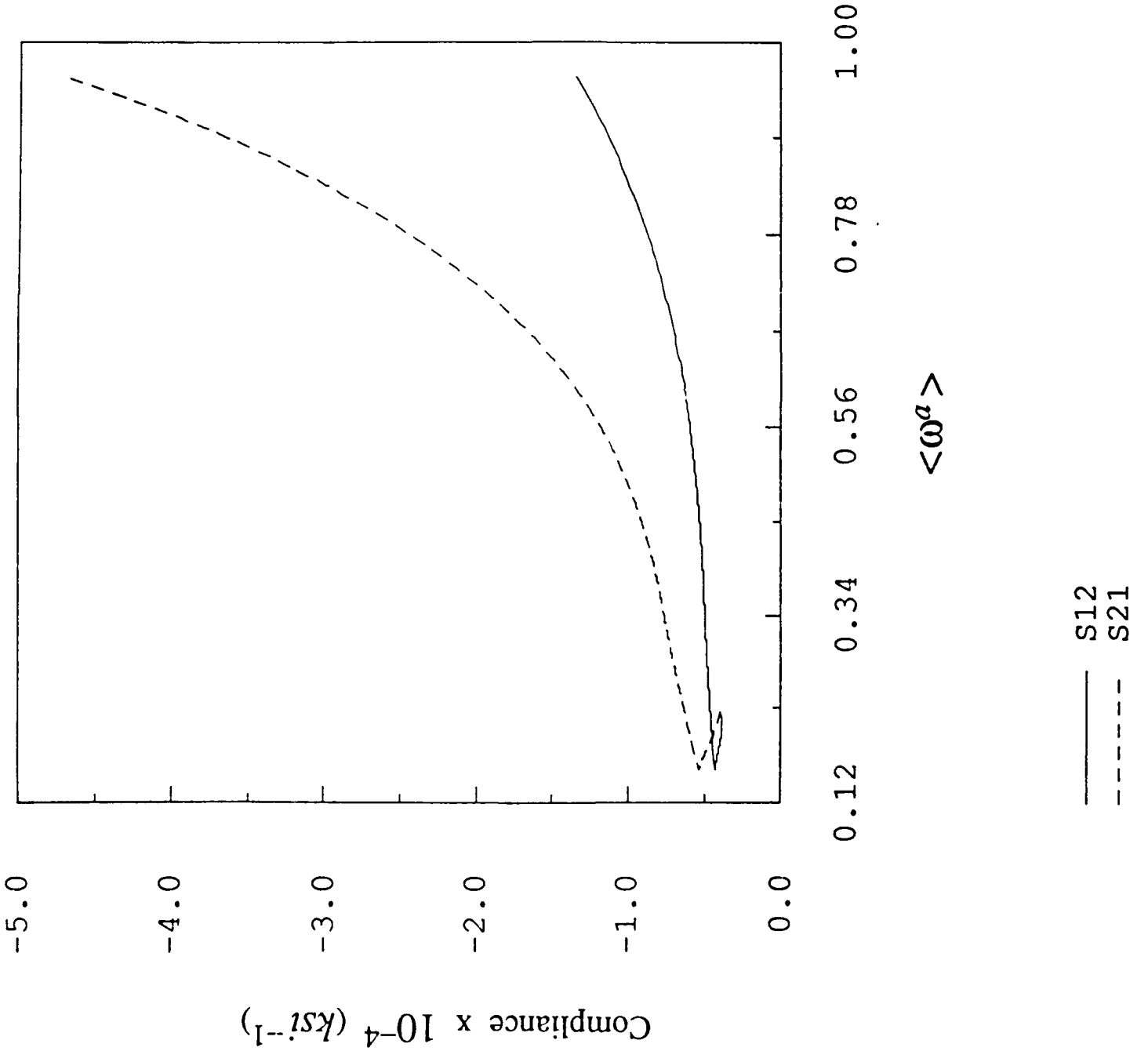

Figure 17. $\bar{S}_{33}$ vs. $<\omega^a>$ for the biaxial tension/compression test.

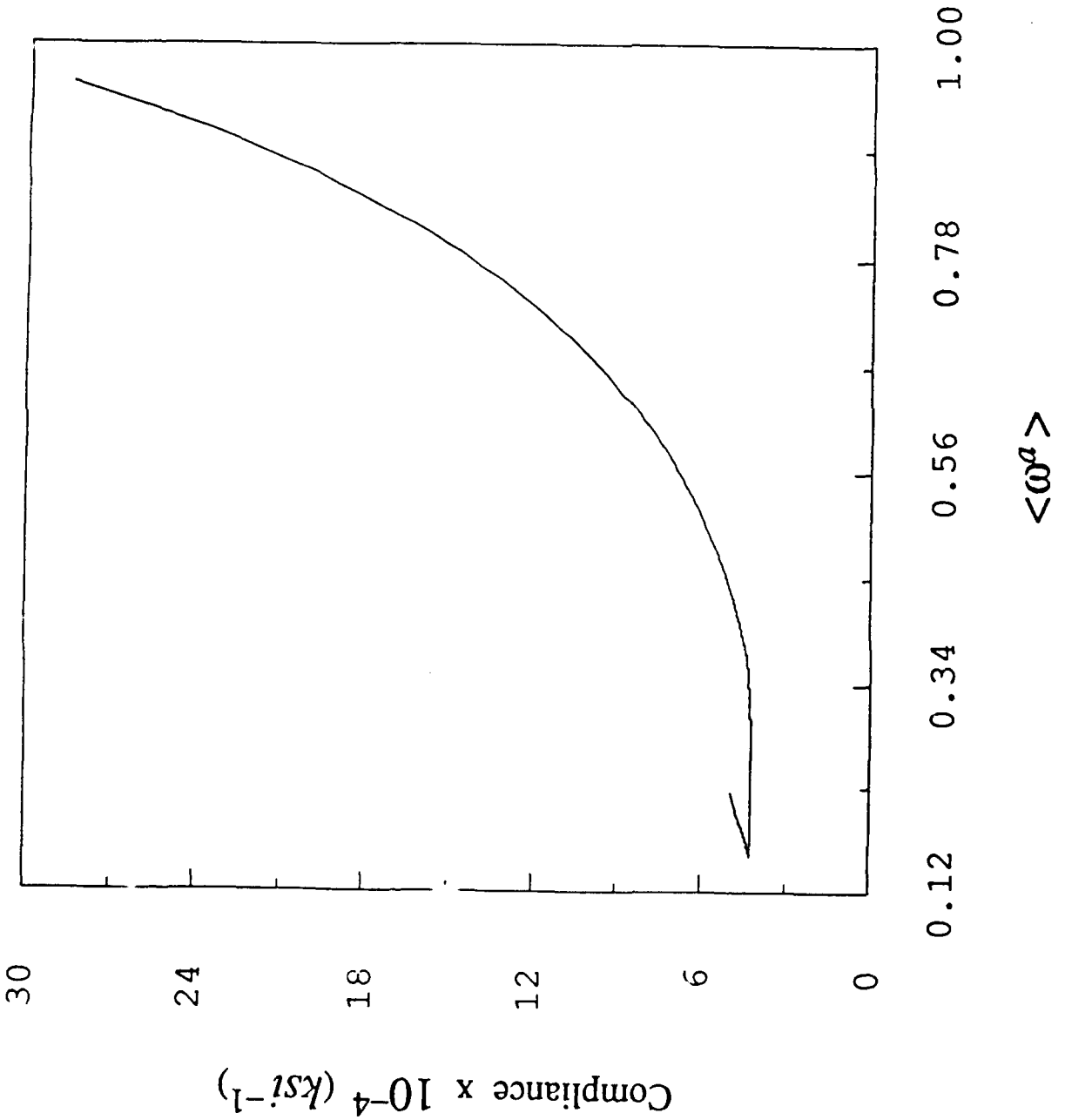

PART IV

On Three-Dimensional Self-Consistent Micromechanical Damage Models for Brittle Solids. Part I: Tensile Loadings

IV.1. Introduction

Three-dimensional micromechanical anisotropic damage models for microcrack-weakened brittle solids are presented within the framework of the self-consistent method and damage mechanics. The self-consistent method is employed in this work to account for weak or moderate interaction between flat elliptical microcracks in *fully anisotropic* media. Phenomenological (continuum) damage models are now popular and provide a convenient constitutive framework for modeling the progressive degradation of mechanical properties in solids. See Krajcinovic (1984, 1986, 1989), Bazant (1986) and Murakami (1987) for a literature review on continuum damage mechanics. However, phenomenological damage models typically can not surrender insightful descriptions of microstructural microcrack kinetics. Therefore, the underlying "damage evolution" equations are often heuristically postulated. Further, use of several (or many) fitted "material constants" in damage evolution equations is a weak link. Thus, micromechanical damage theories are desirable and warranted.

In the current literature, micromechanical "*process*" damage models are very limited. Some valuable examples are Wu (1985), Krajcinovic and Fanella (1986), Sumarac and Krajcinovic (1987, 1989), Fanella and Krajcinovic (1988), Krajcinovic and Sumarac (1989), and Ju (1991). On the other hand, micromechanical "*non-process*" damage models were proposed by Budiansky and O'Connell (1976), Hoenig (1979), Horii and Nemat-Nasser (1983), and Kachanov (1987), etc., for *stationary* microcracks. Though their methods are attractive, no microcrack growth is allowed and therefore no microcrack kinetics exists at all. It is noted that in order for a constitutive theory to possess *predictive* capability, a "process" damage model is necessary.

There are several approaches to micromechanically *derive* overall elastic-damage moduli of

microcrack-weakened brittle materials. These include the Taylor's method (e.g. Krajcinovic and Fanella (1986), Fanella and Krajcinovic (1988), and Ju (1990)), the self-consistent method (e.g. Budiansky and O'Connell (1976), Horii and Nemat-Nasser (1983), Sumarac and Krajcinovic (1987), and Ju (1991)), the differential scheme (e.g. Roscoe (1952, 1973), McLaughlin (1977), and Hashin (1988)), the Mori-Tanaka method (e.g. Mori and Tanaka (1973), Benveniste (1986), and Zhao, Tandon & Weng (1989), and the direct strong microcrack interaction method (e.g. Kachanov (1987) and his other work). In particular, the Taylor's model completely neglects the effects of microcrack interaction and assumes that a microcrack is embedded in an undamaged matrix. Clearly, the Taylor's model is applicable to dilute microcrack distribution. The self-consistent model *indirectly* considers weak microcrack interaction effects by using the (yet unknown) overall effective *anisotropic* moduli to evaluate microcrack opening displacements and damage-induced inelastic moduli. Emanating from somewhat different viewpoints, the differential scheme and the Mori-Tanaka method provide alternative avenues to accommodate weak microcrack interaction as well as microcrack-induced inelasticity and anisotropy. All effective medium methods (such as the self-consistent method, the differential scheme, and the Mori-Tanaka method) are only valid for weak or at most moderate microcrack concentrations. Furthermore, some comparisons and assessments for the self-consistent method and the differential scheme were presented by Horii and Sahasakmontri (1990), Laws and Dvorak (1987), and Nemat-Nasser and Hori (1990).

By contrast, the direct strong microcrack interaction model (Kachanov (1987)) is more desirable for higher microcrack concentrations. However, the method and required numerical computations are very involved. An effort to extend the work of Horii and Nemat-Nasser (1985) and Kachanov (1987) to account for strong microcrack interaction, microcrack growth and nucleation ("cleavage 1 and 2" *process* models (Ashby (1979)), as well as to embed statistical aspects into micro-macro constitutive theories (not random realizations or Monte-Carlo simulations) is currently undertaken by the authors. These statistical aspects include: (a) probability and conditional probability density functions of microcrack locations, orientations, lengths, and relative configurations; and (b) ensemble and volume averages of stresses and strains, etc.

For distributed three-dimensional penny-shaped flat microcracks embedded in brittle matrix, several micromechanical analyses were proposed in the literature. For instance, in the event of *stationary* elliptical (or penny-shaped) microcracks and *isotropic* damage, the self-consistent method was employed by Budiansky and O'Connell (1976), and Horii and Nemat-Nasser (1983) in deriving effective moduli. Further, for *non-stationary* penny-shaped microcracks and *anisotropic* damage, three-dimensional "cleavage 1" process models were considered by Krajcinovic and Fanella (1986) and Fanella and Krajcinovic (1988). However, the latter analyses were limited to the Taylor's model.

In the present study, three-dimensional self-consistent *process* damage models are proposed to account for weak or moderate microcrack interactions. Tensile, compressive, and combined tensile/ compressive triaxial loading/ unloading conditions are considered. Both open and closed microcracks are studied. Mode I, Mode II, and Mixed Mode microcrack growth are examined. The damaged materials are taken to be *fully anisotropic* in general (with 21 or even 36 independent compliance components); and both "cleavage 1" and "cleavage 2" deformation processes are discussed. Flat microcracks are assumed to be elliptical or circular in shape. Moreover, microcrack opening displacements in fully anisotropic solids (not transverse isotropy nor orthotropy) are evaluated by applying Hoenig's analytical solutions (Hoenig (1978,1982)). Microcrack-induced inelastic strains and compliances are subsequently derived in Sec. 3. The kinetic equations of "cleavage 1" preexisting microcrack growth in anisotropic materials are formulated based on the concept of fracture energy release rate at crack tips in Sec. 4. To reduce the complexity in evaluating the energy release rate in an anisotropic medium, a simplified formulation is developed to detect unstable microcrack growth under mixed mode condition. Simple and efficient computational algorithms for the proposed micromechanical models are given in Sec. 5. Moreover, in Sec. 6, numerical simulations are compared with the experimental data reported by Gopalaratnam and Shah (1985).

In this paper, the first part of a sequence of two, only tensile loadings and "cleavage 1" deformation processes are considered. Therefore, all microcracks are assumed to be *open* in this paper.

In the cases of uniaxial/ triaxial compression or combined compression/ tension loadings, some microcracks are *closed* (while some microcracks are open) and may experience frictional *sliding* and Mode II growth. In addition, microcrack *kinking* and new microcrack *nucleation* ("cleavage 2") are very important phenomena under compressive loadings. The self-consistent micromechanical damage models for such events are more complicated, and will be considered in detail in Part II of this work. Finally, it is noted that the proposed framework can be modified to accommodate the differential scheme (instead of the self-consistent method) to account for weak microcrack interactions and concentrations.

IV.2. A framework of micromechanical damage mechanics

In this section, a brief summary of the thermodynamic basis of damage mechanics is given. The general analysis procedure involved is subsequently presented. The virgin (undamaged) matrix material is assumed to be linearly elastic.

IV.2.1. Thermodynamic basis

There exists a one-to-one correspondence between the fourth-order elastic-damage compliance tensor $\bar{\mathbf{S}}$ and the fourth-order anisotropic damage tensor $\bar{\mathbf{D}}$; see, e.g. Simo and Ju (1987), and Ju (1989a,b). Therefore, the secant compliance $\bar{\mathbf{S}}$ can be viewed as an anisotropic damage tensor. Within the framework of the homogenization concept for inhomogeneous effective continuum medium, the volume-average complementary free energy function can be expressed as

$$\chi = \tfrac{1}{2}\bar{\boldsymbol{\sigma}} : \bar{\mathbf{S}} : \bar{\boldsymbol{\sigma}} \tag{1}$$

where $\bar{\sigma}$ is the *volume-average* stress tensor.

By applying the Coleman's method to the Clausius-Duhem inequality for isothermal process, we arrive at the following macroscopic stress-strain law and the damage dissipation inequality:

$$\bar{\boldsymbol{\epsilon}} = \bar{\mathbf{S}} : \bar{\boldsymbol{\sigma}} \quad ; \quad \tfrac{1}{2}\bar{\boldsymbol{\sigma}} : \dot{\bar{\mathbf{S}}} : \bar{\boldsymbol{\sigma}} \geq 0 \tag{2}$$

where $\bar{\epsilon}$ denotes the volume-average strain tensor. It is clear from Eq. (2) that the *evolution* of $\bar{\mathbf{S}}$ plays an essential role in the microcrack energy dissipation and the overall stress-strain response. This also constitutes a major motivation for the development of "process damage models".

Furthermore, it is assumed that the strain tensor $\bar{\epsilon}$ and the overall compliance tensor $\bar{\mathbf{S}}$ are amenable to an additive decomposition:

$$\bar{\boldsymbol{\epsilon}} = \bar{\boldsymbol{\epsilon}}^{e} + \bar{\boldsymbol{\epsilon}}^{*} \quad ; \quad \bar{\mathbf{S}} = \bar{\mathbf{S}}^{o} + \bar{\mathbf{S}}^{*} \tag{3}$$

where $\bar{\epsilon}^{e}$ and $\bar{\epsilon}^{*}$ denote the elastic and the damage-induced inelastic strains, respectively. Similarly, $\bar{\mathbf{S}}^{o}$ and $\bar{\mathbf{S}}^{*}$ signify the undamaged elastic and the damage-induced inelastic compliance, respectively.

Implicitly, it has been assumed that $\bar{\epsilon}^* \approx \mathbf{0}$ upon complete unloading; i.e. the residual strain at zero stress is negligible for brittle materials.

IV.2.2. Analysis procedure

The general analysis procedure follows the self-consistent homogenization approach outlined in Horii and Nemat-Nasser (1983). The interactions between microcracks are indirectly taken into account through *changes* in effective material properties by evaluating microcrack opening displacements over all active microcracks and by performing the volume average computations. Since microcrack growth has preferred orientations and microcrack responses vary according to external loadings, damaged materials are generally macroscopically anisotropic even though virgin materials might be initially isotropic. Therefore, the relationship between the macro-stress and macro-strain can be derived based on micromechanical analysis and the homogenization concept.

Let us start by considering a representative volume V (Hill (1966)), which contains a set of microcracks and is loaded on its external surface S. The volume average of the damage-induced inelastic strain, $\bar{\epsilon}^*_{ij}$, can be expressed by means of microcrack opening displacements $\mathbf{u}^{(k)}$ as

$$\bar{\epsilon}^*_{ij} = \frac{1}{2V} \sum_{k} \int_{S^{(k)}} (u_i n_j + u_j n_i)^{(k)} \, dS^{(k)} \tag{4}$$

where $i, j = 1, 2, 3$, and $\mathbf{n}^{(k)}$ is the unit outward normal vector at the k-th microcrack surface $S^{(k)}$. In addition, we assume in this work that the (volume averaged) macro-stress tensor $\bar{\boldsymbol{\sigma}}$ is approximately equal to the far field (applied) stress tensor $\boldsymbol{\sigma}^\infty$; i.e. $\bar{\boldsymbol{\sigma}} \approx \boldsymbol{\sigma}^\infty$. Since microcrack opening displacements are functions of externally applied stresses, Eq. (4) can be rephrased as

$$\bar{\boldsymbol{\epsilon}}^* = \bar{\mathbf{S}}^*(\bar{\mathbf{S}}) : \bar{\boldsymbol{\sigma}} \tag{5}$$

Note that the microcrack-induced inelastic compliance $\bar{\mathbf{S}}^*$ is a function of the yet unknown overall compliance $\bar{\mathbf{S}}$. The detailed derivation of these compliances will be given in Sec. 3.

Typically, the orientations and sizes of *penny-shaped* microcracks in a representative volume can be viewed as random variables and can be represented by a joint probability density function

$p(a, \phi, \theta)$. Here, a denotes the microcrack size, and (ϕ, θ) designate the two Euler angles defining the orientation of a flat penny-shaped microcrack. The probabilistic ensemble average of the inelastic compliance contribution due to a single (the k-th) microcrack can be written in the form

$$< \mathbf{S}^{*(k)} > = \int_{\Omega} \mathbf{S}^{*(k)}(a, \phi, \theta)\, p(a, \phi, \theta)\, d\Omega \tag{6}$$

where Ω is the statistical domain of active microcracks defined by (a, ϕ, θ). If the three geometric random variables, a, ϕ, and θ are statistically independent, then the joint probability density function $p(a, \phi, \theta)$ is equal to the product of three independent probability density functions as

$$p(a, \phi, \theta) = p(a)p(\phi)p(\theta) \tag{7}$$

However, care must be exercised so that the following normalization condition is met:

$$\int_{\Omega} p(a, \phi, \theta)\, d\Omega = \int_{\Omega} p(a)\, p(\phi)\, p(\theta)\, d\Omega \equiv 1 \tag{8}$$

If there are N_c microcracks in the representative volume, the total microcrack-induced inelastic compliance is as follows

$$\bar{\mathbf{S}}^{*} = N_c < \mathbf{S}^{*(k)} >= N_c \int_{\Omega} \mathbf{S}^{*(k)}(a, \phi, \theta)\, p(a, \phi, \theta)\, d\Omega \tag{9}$$

IV.3. Damage induced compliance tensor

The overall effective compliance tensor $\bar{\mathbf{S}}$ in general becomes *anisotropic* when microcracks exist. Therefore, the displacement discontinuities across microcrack surfaces in a general anisotropic elastic solid must first be evaluated in order to apply the self-consistent method (or the differential scheme). A method to determine the opening displacements of a flat elliptical microcrack in a general three-dimensional anisotropic elastic material was proposed by Hoenig (1978, 1982). Hoenig's analysis is briefly reviewed in what follows. There are, however, some misprints and minor errors in Hoenig's work (1978, 1982). These minor errors are properly corrected in this section. The results of Hoenig's analysis will subsequently be applied to obtain the inelastic compliance $\bar{\mathbf{S}}^*$ due to open microcracks. A "non-process" damage model is therefore constructed.

IV.3.1. Microcrack opening displacements in anisotropic elastic media

The underlying concept of Hoenig's analysis (1978) is to derive a relationship between the M-surface integral of a microcrack and the total work done by remote stresses acting through the microcrack opening displacements. The opening displacements can then be related to external stresses $\boldsymbol{\sigma}^{\infty}$. Let us begin by considering a single elliptical microcrack with a and b being its semi-axes, as shown in Fig. 1, in a fully anisotropic elastic body uniformly loaded at far field. The primed coordinate system is based on the elliptical microcrack orientation, with z'-axis parallel to the outward normal direction $\mathbf{n}$. The double-primed coordinate system is based on the radial plane to a typical point s on the rim Γ of the elliptical microcrack. The displacement discontinuities between surfaces of a microcrack take the form (Hoenig (1978, 1982), based on Eshelby's inclusion solutions):

$$u_i'(x', y') = 2\sqrt{ab}\,\sqrt{1 - \frac{x'^2}{a^2} - \frac{y'^2}{b^2}}\; C'^{-1}_{ik}\; \bar{\sigma}'_{3k} \tag{10}$$

where $i, k = 1, 2, 3$, C'^{-1}_{ik} is an unknown matrix which has to be determined, and $\bar{\sigma}'_{3k}$ is the remote loading stress in the elliptical microcrack coordinate system.

The work done by the applied stress through the displacement discontinuities of microcrack

surfaces can be evaluated by using Eq. (10):

$$W = \frac{1}{2}\int_{S^I} \bar{\sigma}'_{3k}\, u'_k\, dS^I = \frac{2}{3}\pi(ab)^{\frac{3}{2}} C'_{kj}\beta'_k\beta'_j \tag{11}$$

where S^I is the surface area of a microcrack, and $\beta'_k \equiv C'^{-1}_{jk}\bar{\sigma}'_{3j}$. The integration in Eq. (11) can be carried out because C'_{ij} represents material properties only and is not a function of location. As shown by Budiansky and O'Connell (1976), the M-surface integral can be expressed either in an integral form of J-integral (Rice (1968)), or by the derivative of W as

$$M = \oint_\Gamma \rho(s) \lim_{\delta\to 0} J''(s,\delta)ds = a\frac{\partial W}{\partial a} \tag{12}$$

where $\rho(s)$ is the perpendicular distance from the origin to the tangent line to curve Γ at a given point s (see Fig. 1). In addition, $J''(s,\delta)$ is the well known J-integral in two dimensional fracture mechanics. Substitution of Eq. (11) into Eq. (12) then leads to

$$2\pi a^3\gamma^{\frac{3}{2}} C'_{ij}\beta'_i\beta'_j = \oint_\Gamma \rho(s) \lim_{\delta\to 0} J''(s,\delta)ds \tag{13}$$

where $\gamma \equiv b/a$. Therefore, one has to evaluate the J-integral so that the C′-matrix can be determined.

The J-integral for a line slit in an anisotropic material can be formulated by using Lekhnitskii's theory of anisotropic elasticity (Lekhnitskii (1950)). After some straightforward but lengthy algebraic manipulations, the asymptotic solutions of related stress and displacement fields in the vicinity of microcrack tips (in the double-primed line microcrack coordinate system, Fig. 2) take the form (Hoenig (1982)):

$$\sigma''_{22} = \frac{1}{\sqrt{2\pi r''}}\mathrm{Re}\left[\sum_{i=1}^{3}\frac{N^{-1}_{ij}K_j}{\sqrt{\cos\theta'' + \mu_i\sin\theta''}}\right] \tag{14}$$

$$\sigma''_{21} = \frac{-1}{\sqrt{2\pi r''}}\mathrm{Re}\left[\sum_{i=1}^{3}\frac{\mu_i N^{-1}_{ij}K_j}{\sqrt{\cos\theta'' + \mu_i\sin\theta''}}\right] \tag{15}$$

$$\sigma''_{23} = \frac{-1}{\sqrt{2\pi r''}}\mathrm{Re}\left[\sum_{i=1}^{3}\frac{\lambda_i N^{-1}_{ij}K_j}{\sqrt{\cos\theta'' + \mu_i\sin\theta''}}\right] \tag{16}$$

$$u''_i = \sqrt{\frac{2r''}{\pi}}\mathrm{Re}\left[\sum_{j=1}^{3} p_{ij}N^{-1}_{jl}K_l\sqrt{\cos\theta'' + \mu_j\sin\theta''}\right] \tag{17}$$

Here, the subscripts $i, j, l = 1, 2, 3$, and the primed quantities are evaluated in the local line microcrack coordinate system. Moreover, μ_i are the roots of the characteristic equation

$$l_4(\mu)l_2(\mu) - l_3(\mu)l_3(\mu) = 0 \tag{18}$$

with l_i defined as

$$\begin{aligned} l_2(\mu) &\equiv M''_{55}\mu^2 - 2M''_{45}\mu + M''_{44} \\ l_3(\mu) &\equiv M''_{15}\mu^3 - (M''_{14} + M''_{56})\mu^2 + (M''_{25} + M''_{46})\mu - M''_{24} \\ l_4(\mu) &\equiv M''_{11}\mu^4 - 2M''_{16}\mu^3 + (2M''_{12} + M''_{66})\mu^2 - 2M''_{26}\mu + M''_{22} \end{aligned} \tag{19}$$

where

$$M''_{ij} \equiv \bar{S}''_{ij} - \frac{\bar{S}''_{i3}\bar{S}''_{j3}}{\bar{S}''_{33}} \tag{20}$$

Moreover,

$$\lambda_i \equiv -\frac{l_3(\mu_i)}{l_2(\mu_i)} \tag{21}$$

Eq. (18) is a sixth-order polynominal and in general has three pairs of complex conjugate roots. Only the three roots with $\mathrm{Im}[\mu_i] > 0$ are used in the analysis. Further, p_{ij} in Eq. (17) are defined as

$$\begin{aligned} p_{1i} &\equiv M''_{11}\mu_i^2 + M''_{12} - M''_{16}\mu_i + \lambda_i(-M''_{14} + \mu_i M''_{15}) \\ p_{2i} &\equiv M''_{21}\mu_i + \frac{M''_{22}}{\mu_i} - M''_{26}\mu_i + \lambda_i(-\frac{M''_{24}}{\mu_i} + M''_{25}) \\ p_{3i} &\equiv M''_{41}\mu_i + \frac{M''_{42}}{\mu_i} - M''_{46}\mu_i + \lambda_i(-\frac{M''_{44}}{\mu_i} + M''_{45}) \end{aligned} \tag{22}$$

with $i = 1, 2, 3$. The matrix $\mathbf{N}$ in Eqs. (14) through (17) is also related to the roots of Eq. (18):

$$\mathbf{N} \equiv \begin{bmatrix} -\mu_1 & -\mu_2 & -\mu_3 \\ 1 & 1 & 1 \\ -\lambda_1 & -\lambda_2 & -\lambda_3 \end{bmatrix} \tag{23}$$

Finally, the K_i in Eqs. (14) through (17) are the stress intensity factors corresponding to Mode II, I, and III as (in line microcrack coordinate system)

$$\begin{Bmatrix} K_1 \\ K_2 \\ K_3 \end{Bmatrix} \equiv \begin{Bmatrix} K_{\mathrm{II}} \\ K_{\mathrm{I}} \\ K_{\mathrm{III}} \end{Bmatrix} \tag{24}$$

On the other hand, the J-integral can be recast as (Rice (1968))

$$J'' = \lim_{\delta \to 0} \frac{1}{\delta} \int_0^{\delta} \sigma''_{2i}(\delta - r'', 0)\, u''_i(r'', \pi)\, dr'' \tag{25}$$

where $i = 1, 2, 3$, with the understanding that $1 = x'', 2 = y'', 3 = z''$. By substituting Eq. (14) through (17) into Eq. (25), we have

$$J'' = \frac{1}{2}\left\{K_{\mathrm{II}}\,\mathrm{Im}\left[p_{1j}N_{jk}^{-1}K_k\right] + K_{\mathrm{I}}\,\mathrm{Im}\left[p_{2j}N_{jk}^{-1}K_k\right] + K_{\mathrm{III}}\,\mathrm{Im}\left[p_{3j}N_{jk}^{-1}K_k\right]\right\} \tag{26}$$

From Eqs. (10) and (17), it can be shown that

$$\mathrm{Im}\left[p_{ij}N_{jk}^{-1}K_k\right] = \sqrt{\pi a}\beta_i'' \tag{27}$$

Therefore, the J-integral in the double-primed coordinate system reads

$$J'' = \frac{\pi a}{2}\left\{\mathrm{Im}\left[p_{ij}N_{jk}^{-1}\right]\right\}^{-1}\beta_i''\beta_k'' \tag{28}$$

By introducing the following transformation matrix R_{ij}, β_i'' values can be related to β_j values in terms of the elliptical microcrack coordinate system in Fig. 1:

$$\mathbf{R} \equiv (\gamma^2\cos^2\phi' + \sin^2\phi')^{-1/4}\begin{bmatrix}\gamma\cos\phi' & \sin\phi' & 0\\ 0 & 0 & \sqrt{\gamma^2\cos^2\phi' + \sin^2\phi'}\\ \sin\phi' & -\gamma\cos\phi' & 0\end{bmatrix} \tag{29}$$

$$\beta_i'' = R_{ij}\beta_j' \tag{30}$$

Substitution of Eqs. (30) and (28) into Eq. (13) then renders the final form of the C_{ij}' matrix:

$$C_{ij}' \equiv \frac{1}{\sqrt{\gamma}}\hat{C}_{ij}' = \frac{1}{\sqrt{\gamma}}\frac{1}{4}\int_0^{2\pi}\left\{\mathrm{Im}\left[p_{kl}N_{lm}^{-1}\right]\right\}^{-1}R_{ik}R_{mj}d\phi' \tag{31}$$

Consequently, the opening displacements of a flat elliptical microcrack in a general anisotropic material are now completely defined by Eqs. (10) and (31).

IV.3.2. A single microcrack induced inelastic compliance

By substituting Eqs. (10) and (31) into Eq. (4) and performing integration over the elliptical microcrack surface, we obtain the following inelastic strain components due to a single (k-th) microcrack (in **local** elliptical microcrack coordinate system):

$$V\epsilon_{ij}'^{*(k)} = \frac{2\pi}{3}a^3\gamma\left(\hat{C}_{ik}'^{-1(k)}\bar{\sigma}_{3k}'n_j' + \hat{C}_{jl}'^{-1(k)}\bar{\sigma}_{3l}'n_i'\right) \tag{32}$$

In the primed (local) coordinate system, one may choose $n_1' = n_2 = 0$ and $n_3' = 1$ for $\mathbf{n}'$ vector. In addition, the Voigt's notation is adopted for stresses and strains as $\tau_1 = \sigma_{11}$, $\tau_2 = \sigma_{22}$, $\tau_3 = \sigma_{33}$,

$\tau_4 = \sigma_{23}$, $\tau_5 = \sigma_{31}$, $\tau_6 = \sigma_{12}$, and $e_1 = \epsilon_{11}$, $e_2 = \epsilon_{22}$, $e_3 = \epsilon_{33}$, $e_4 = 2\epsilon_{23}$, $e_5 = 2\epsilon_{31}$, $e_6 = 2\epsilon_{12}$. Therefore, the non-vanishing components of inelastic strains in Eq. (32) can be rephrased as

$$Ve_3'^{*(k)} = \frac{4\pi}{3}a^3\gamma\left(\hat{C}_{33}'^{-1^{(k)}}\bar{\tau}_3' + \hat{C}_{32}'^{-1^{(k)}}\bar{\tau}_4' + \hat{C}_{31}'^{-1^{(k)}}\bar{\tau}_5'\right) \tag{33}$$

$$Ve_4'^{*(k)} = \frac{4\pi}{3}a^3\gamma\left(\hat{C}_{23}'^{-1^{(k)}}\bar{\tau}_3' + \hat{C}_{22}'^{-1^{(k)}}\bar{\tau}_4' + \hat{C}_{21}'^{-1^{(k)}}\bar{\tau}_5'\right) \tag{34}$$

$$Ve_5'^{*(k)} = \frac{4\pi}{3}a^3\gamma\left(\hat{C}_{13}'^{-1^{(k)}}\bar{\tau}_3' + \hat{C}_{12}'^{-1^{(k)}}\bar{\tau}_4' + \hat{C}_{11}'^{-1^{(k)}}\bar{\tau}_5'\right) \tag{35}$$

Consequently, the local *inelastic* compliance induced by a single elliptical open microcrack embedded in anisotropic solid takes the following matrix form:

$$\mathbf{S}'^{*(k)} = \frac{1}{V}\frac{4\pi}{3}a^3\gamma\begin{bmatrix} 0 & 0 & 0 & 0 & 0 & 0 \\ 0 & 0 & 0 & 0 & 0 & 0 \\ 0 & 0 & \hat{C}_{33}'^{-1^{(k)}} & \hat{C}_{32}'^{-1^{(k)}} & \hat{C}_{31}'^{-1^{(k)}} & 0 \\ 0 & 0 & \hat{C}_{23}'^{-1^{(k)}} & \hat{C}_{22}'^{-1^{(k)}} & \hat{C}_{21}'^{-1^{(k)}} & 0 \\ 0 & 0 & \hat{C}_{13}'^{-1^{(k)}} & \hat{C}_{12}'^{-1^{(k)}} & \hat{C}_{11}'^{-1^{(k)}} & 0 \\ 0 & 0 & 0 & 0 & 0 & 0 \end{bmatrix} \tag{36}$$

It is worth noting that in the special case of a penny-shaped microcrack embedded in an *isotropic* material, the integrand in Eq. (31) can be greatly simplified:

$$\mathrm{Im}[\mathbf{pN}^{-1}] = \begin{bmatrix} \frac{E}{2(1-\nu^2)} & 0 & 0 \\ 0 & \frac{E}{2(1-\nu^2)} & 0 \\ 0 & 0 & \frac{E}{2(1+\nu)} \end{bmatrix} \tag{37}$$

where E is the current Young's modulus and ν is the current Poisson's ratio, respectively. Hence, we obtain

$$\hat{\mathbf{C}}' = \frac{\pi}{4}\frac{E}{2(1-\nu^2)}\begin{bmatrix} 2-\nu & 0 & 0 \\ 0 & 2-\nu & 0 \\ 0 & 0 & 2 \end{bmatrix} \tag{38}$$

Further, the nonvanishing components of $\mathbf{S}'^{*(k)}$ in this case are

$$S_{33}'^{*(k)} = \frac{1}{V}\frac{16(1-\nu^2)}{3E}a^3$$

$$S_{44}'^{*(k)} = \frac{1}{V}\frac{32(1-\nu^2)}{3E(2-\nu)}a^3 \tag{39}$$

$$S_{55}'^{*(k)} = \frac{1}{V}\frac{32(1-\nu^2)}{3E(2-\nu)}a^3$$

which coincide with the solutions found by Horii and Nemat-Nasser (1983).

IV.3.3. Overall compliance due to distributed microcracks

The inelastic compliance due to a single elliptical microcrack in *global* (unprimed) coordinate system is related to that in *local* (primed) coordinates by the following transformations (see also Fig. 3):

$$S_{ij}'^{*(k)} = T_{ik}'T_{jl}'S_{kl}^{*(k)} \quad \text{and} \quad S_{ij}^{*(k)} = T_{ki}T_{lj}S_{kl}'^{*(k)} \tag{40}$$

Here, the transformation matrices $\mathbf{T}'$ and $\mathbf{T}$ are

$$\mathbf{T}' = \begin{bmatrix} \cos^2\phi & \sin^2\phi & 0 & 0 & 0 & \frac{1}{2}\sin 2\phi \\ \cos^2\theta\sin^2\phi & \cos^2\theta\cos^2\phi & \sin^2\theta & \frac{1}{2}\sin 2\theta\cos\phi & -\frac{1}{2}\sin 2\theta\sin\phi & -\frac{1}{2}\cos^2\theta\sin 2\phi \\ \sin^2\theta\sin^2\phi & \sin^2\theta\cos^2\phi & \cos^2\theta & -\frac{1}{2}\sin 2\theta\cos\phi & \frac{1}{2}\sin 2\theta\sin\phi & -\frac{1}{2}\sin^2\theta\sin 2\phi \\ -\sin 2\theta\sin^2\phi & -\sin 2\theta\cos^2\phi & \sin 2\theta & \cos 2\theta\cos\phi & -\cos 2\theta\sin\phi & \frac{1}{2}\sin 2\theta\sin 2\phi \\ \sin\theta\sin 2\phi & -\sin\theta\sin 2\phi & 0 & \cos\theta\sin\phi & \cos\theta\cos\phi & -\sin\theta\cos 2\phi \\ -\cos\theta\sin 2\phi & \cos\theta\sin 2\phi & 0 & \sin\theta\sin\phi & \sin\theta\cos\phi & \cos\theta\cos 2\phi \end{bmatrix} \tag{41}$$

and

$$\mathbf{T} = \begin{bmatrix} \cos^2\phi & \sin^2\phi & 0 & 0 & 0 & \sin 2\phi \\ \cos^2\theta\sin^2\phi & \cos^2\theta\cos^2\phi & \sin^2\theta & \sin 2\theta\cos\phi & -\sin 2\theta\sin\phi & -\cos^2\theta\sin 2\phi \\ \sin^2\theta\sin^2\phi & \sin^2\theta\cos^2\phi & \cos^2\theta & -\sin 2\theta\cos\phi & \sin 2\theta\sin\phi & -\sin^2\theta\sin 2\phi \\ -\frac{1}{2}\sin 2\theta\sin^2\phi & -\frac{1}{2}\sin 2\theta\cos^2\phi & \frac{1}{2}\sin 2\theta & \cos 2\theta\cos\phi & -\cos 2\theta\sin\phi & \frac{1}{2}\sin 2\theta\sin 2\phi \\ \frac{1}{2}\sin\theta\sin 2\phi & -\frac{1}{2}\sin\theta\sin 2\phi & 0 & \cos\theta\sin\phi & \cos\theta\cos\phi & -\sin\theta\cos 2\phi \\ -\frac{1}{2}\cos\theta\sin 2\phi & \frac{1}{2}\cos\theta\sin 2\phi & 0 & \sin\theta\sin\phi & \sin\theta\cos\phi & \cos\theta\cos 2\phi \end{bmatrix} \tag{42}$$

Let us now consider an ensemble of microcracks. The lengths and orientations of microcracks are assumed to be randomly distributed. Accordingly, the total inelastic compliance tensor $\bar{\mathbf{S}}^*$ can be determined from Eq. (9). In particular, in the special case of penny-shaped microcracks with uniformly distributed and statistically independent geometric random variables (a, ϕ and θ), the joint probability density function in Eq. (7) can be written as

$$p(a,\phi,\theta) = p(a)\,p(\phi)\,p(\theta) = \frac{1}{2\pi}\,\frac{1}{a_{0_{max}} - a_{0_{min}}} \tag{43}$$

where $a_{0_{max}}$ and $a_{0_{min}}$ are the maximum and minimum initial radii of penny-shaped microcracks, respectively. It can easily be shown that Eq. (43) indeed satisfies the normalization condition discussed in Eq. (8). Thus, $\bar{\mathbf{S}}^*$ takes the following form (for penny-shaped microcracks)

$$\bar{S}^*_{ij} = \frac{N_c}{V}\,\frac{1}{2\pi(a_{0_{max}} - a_{0_{min}})}\int_0^{\frac{\pi}{2}}\int_0^{2\pi}\int_{a_{0_{min}}}^{a_{0_{max}}} T_{ki}(\phi,\theta)\,T_{lj}(\phi,\theta)\,S'^*_{kl}(a,\phi,\theta)\,\sin\theta\,da\,d\phi\,d\theta \tag{44}$$

IV.4. A process damage model

Based on the linear elastic fracture mechanics and the self-consistent method, a micromechanical "process damage model" is proposed to analyze kinetic equations of *penny-shaped* "cleavage 1" microcrack growth under tensile loadings. At a certain stress level, some microcracks in preferred orientations become unstable and increase in size. Two simplifications of microcrack growth are made here. First, the microcrack growth process is assumed to be instantaneous (Krajcinovic and Fanella (1986)). That is, once a microcrack becomes unstable, it reaches a certain final size (corresponding to a characteristic length or an energy barrier) immediately. Second, the penny-shaped microcrack growth is assumed to be in a self-similar fashion.

IV.4.1. Fracture criterion for a microcrack

Typically, there are many pre-existing microcracks along the matrix-inclusion interfaces (or interphases) or the inter-granular planes of brittle materials, assuming that the fracture toughness of the matrix material is significantly stronger than that of the interface (or interphase). In particular, for matrix-inclusion composites, fracture criteria for interface (or interphase) microcrack growth should preferably be based on bimaterial (or interphase) properties. Although some valuable progress was recently made by Qu and Bassani (1989) and Bassani and Qu (1989), their analysis only provided necessary and sufficient condition for *non-oscillatory* two-dimensional line crack solutions on the interface between two anisotropic dissimilar materials. Therefore, non-oscillatory micromechanical bimaterial analysis is not guaranteed for a given two-dimensional interfacial microcrack (even if microcrack interaction is totally ignored). General bimaterial analysis for a three-dimensional microcrack is not yet available. Hence, in what follows, bimaterial interfacial microcrack analysis is not pursued. However, the fracture toughness at the matrix-inclusion *interface* is employed to determine the criterion of microcrack growth. An alternative choice is to use an *interphase* microcrack model; see, e.g. Achenbach and Zhu (1989) for a simple one-dimensional linear elastic extensional and shear springs numerical model for periodically spaced fibers in a matrix material. Nevertheless, very involved numerical solutions of local interphase stresses, displacements and microcrack interactions (if non-periodic fiber array) are needed to implement interphase models.

When a penny-shaped microcrack of radius a in a homogenized anisotropic body is subjected to remote loadings, the energy release rate G at each point along the edge of the microcrack (in

local or primed microcrack coordinate system) can be evaluated from Eqs. (28) and (30):

$$G'(a,\theta,\phi') = \frac{\pi a}{2}\left\{\mathrm{Im}\left[p_{ij}N_{jk}^{-1}\right]\right\}^{-1} R_{is}R_{kt}C'^{-1}_{ps}C'^{-1}_{qt}\bar{\sigma}'_{3p}\bar{\sigma}'_{3q} \tag{45}$$

We will consider triaxial loadings, with q denoting the axial tension and q^* denoting the lateral stress, respectively. The corresponding stresses in *local* coordinate system are expressed as

$$\bar{\tau}'_3 = q\cos^2\theta + q^*\sin^2\theta, \quad \bar{\tau}'_4 \equiv (q-q^*)\sin\theta\cos\theta, \quad \bar{\tau}'_5 \equiv 0 \tag{46}$$

where q and q^* are taken to be positive when they correspond to tensile stresses.

It should be pointed out that the value of energy release rate G' *varies* along the edge of a penny-shaped microcrack due to material *anisotropy*. This implies that microcrack instability starts at a certain point on the edge of the microcrack and gradually propagates from this point to other points along the edge. However, the assumptions of instantaneous and self-similar microcrack growth are introduced to simplify the process. Essentially, we assume that an microcrack starts to grow when the *average* value of G' over the microcrack edge reaches a critical value G_c^{if} (which is a material property of the matrix-inclusion interface or the inter-granular plane). Namely, the fracture criterion of a microcrack can be written as

$$G_c^{\mathrm{if}} = \frac{1}{2\pi a}\oint_\Gamma G'(a,\theta_u,\phi')ds = \frac{1}{2\pi}\oint_0^{2\pi} G'(a,\theta_u,\phi')d\phi' \tag{47}$$

where θ_u define(s) the critical orientation-bound(s) of unstable microcrack growth region for a given microcrack size a and under given stresses q and q^*. Nevertheless, if the self-consistent (yet unknown) overall moduli are involved in Eq. (47), it becomes extremely difficult to obtain solution(s) for θ_u. It is emphasized that the determination of θ_u is crucial to the integration of overall moduli $\tilde{\mathbf{S}}$ (see Eq. (44)).

Therefore, for practical applications, further simplification is introduced here. That is, the penny-shaped microcrack fracture criterion is based on the Taylor's model (no microcrack interaction). As a consequence, the average energy release rate $\tilde{G}'$ for an isotropic virgin material can be easily obtained:

$$\tilde{G}' = \frac{1-\nu^2}{E}\left[\left(2\sqrt{\frac{\pi}{a}}\bar{\tau}'_3\right)^2 + \frac{4}{2-\nu}\left(2\sqrt{\frac{\pi}{a}}\bar{\tau}'_4\right)^2\right] = \frac{1-\nu^2}{E}\left[K_{\mathrm{I}}'^2 + K_{\mathrm{II}}'^2\right] \tag{48}$$

where Mode I and II stress intensity factors K_{I} and K_{II} are defined as

$$K'_{\mathrm{I}} \equiv 2\sqrt{\frac{a}{\pi}}\,\bar{\tau}'_3 \quad ; \quad K'_{\mathrm{II}} \equiv \frac{4}{2-\nu}\sqrt{\frac{a}{\pi}}\,\bar{\tau}'_4 \tag{49}$$

Accordingly, the microcrack fracture criterion takes the form

$$G_c^{if} = \bar{G}' = \frac{1-\nu^2}{E}[K_I'^2 + K_{II}'^2] \tag{50}$$

If we are concerned with interface microcracks in brittle composites, it should be noted that the critical interfacial stress intensity factors for Mode I (K_{Ic}^{if}) and Mode II (K_{IIc}^{if}) are different in general. Therefore, it is reasonable to modify the isotropic microcrack fracture criterion Eq. (50) (corresponding to a "circle") as follows (corresponding to an "ellipse", Kanninen and Popelar (1985)):

$$\left(\frac{K_I'}{K_{Ic}^{if}}\right)^2 + \left(\frac{K_{II}'}{K_{IIc}^{if}}\right)^2 = 1 \tag{51}$$

IV.4.2. Microcrack kinetics

Under a given load level, some microcracks in preferred orientations and sizes may reach the fracture criterion (51) and start to grow. The preferred orientations can be solved in closed form as follows (see also Krajcinovic and Fanella (1986)). From Eqs. (46), (49) and (51), we arrive at

$$\left(\frac{K_{IIc}^{if}}{K_{Ic}^{if}}\right)^2 (q^* \sin^2\theta + q\cos^2\theta)^2 + \left(\frac{2}{2-\nu}\right)^2 (q-q^*)^2 \sin^2\theta\cos^2\theta = \frac{\pi}{4a}\left(K_{IIc}^{if}\right)^2 \tag{52}$$

After some derivations, the solutions of Eq. (52) can be expressed as

$$\tan^2\theta_u = \frac{-A_2 \pm \sqrt{A_2^2 - 4A_1A_3}}{2A_1} \equiv f(a, q, q^*, K_{Ic}^{if}, K_{IIc}^{if}, \nu) \geq 0 \tag{53}$$

where

$$A_1 \equiv K_{IIc}^{if}\left[\left(\frac{q^*}{K_{Ic}^{if}}\right)^2 - \frac{\pi}{4a}\right] \tag{54}$$

$$A_2 \equiv \frac{\pi}{4a}\left(K_{IIc}^{if}\right)^2 - \left(\frac{2}{2-\nu}\right)^2 (q^2 + q^{*2}) - 2\left[\left(\frac{K_{IIc}^{if}}{K_{Ic}^{if}}\right)^2 - \left(\frac{2}{2-\nu}\right)^2\right] q^* q \tag{55}$$

$$A_3 \equiv K_{IIc}^{if}\left[\left(\frac{q}{K_{Ic}^{if}}\right)^2 - \frac{\pi}{4a}\right] \tag{56}$$

Therefore, the critical angles θ_u defining the range of unstable microcracks are

$$\theta_u = \tan^{-1}\sqrt{f(a, q, q^*, K_{Ic}^{if}, K_{IIc}^{if}, \nu)} \tag{57}$$

Note that the conditions of existence of solutions θ_u are

$$A_2^2 - 4A_1A_3 \geq 0 \quad ; \quad \frac{-A_2 \pm \sqrt{A_2^2 - 4A_1A_3}}{2A_1} \geq 0 \tag{58}$$

Assuming that the lateral loading q^* is *small* such that q^* alone will not cause microcrack instability; i.e.

$$\left[q^{*2} - \frac{\pi}{4a}(K_{Ic}^{if})^2\right] < 0 \tag{59}$$

$$\left[q^{*2} - \frac{\pi}{4a}\left(\frac{2}{2-\nu}\right)^2 (K_{Ic}^{if})^2\right] < 0 \tag{60}$$

Then, f in Eq. (53) takes only the form

$$f(a, q, q^*, K_{Ic}^{if}, K_{IIc}^{if}, \nu) = \frac{-A_2 - \sqrt{A_2^2 - 4A_1A_3}}{2A_1} \geq 0 \tag{61}$$

In addition, the maximum angle $\theta_{u_{max}}$, at which microcracks with *maximum* initial size $a_{0_{max}}$ become unstable, can be evaluated as follows

$$\theta_{u_{max}} = \tan^{-1}\sqrt{f(a_{0_{max}}, q, q^*, K_{Ic}^{if}, K_{IIc}^{if}, \nu)} \tag{62}$$

Similarly, the angle $\theta_{u_{min}}$, at which *all* microcracks become unstable, is evaluated by using $a_{0_{min}}$:

$$\theta_{u_{min}} = \tan^{-1}\sqrt{f(a_{0_{min}}, q, q^*, K_{Ic}^{if}, K_{IIc}^{if}, \nu)} \tag{63}$$

Let us assume that q^* is *constant* and q is varying but *greater* than q^*. From Eq. (57), it is clear that the first microcracks to become unstable are oriented along $\theta = 0$ direction and with maximum initial size $a_{0_{max}}$. The corresponding axial threshold load is defined as q_0.

For simplicity in practical applications, we will further assume that once an *initial* interface (or inter-granular) microcrack starts to propagate, it grows along the interface (or inter-granular plane) from a_0 to a characteristic *final* size a_f (effective inclusion or grain size) instantaneously (Krajcinovic and Fanella (1986)). Microcrack kinking into the matrix material is *not* considered in Part I. In Part II of this work, however, microcrack kinking into matrix under compression will be fully accounted for. In essence, a microcrack could either have its initial size a_0 or its final size a_f in the following treatment.

Therefore, the microcrack growth kinetic sequence proceeds as follows.

(i) As $q < q_0$, all microcracks are stable and of initial sizes. The damage-induced inelastic moduli can be computed by Eq. (44).

(ii) As $q = q_0 > q^*$, those microcracks in the plane $\theta = 0$ with maximum initial size $a_{0_{max}}$ become unstable and increase in size until reaching a characteristic length a_f (e.g. the aggregate facet size). For simplicity, it is assumed that $a_f = a_0/\rho$, where ρ is a scalar between 0 and 1. In general, ρ should be a random variable.

(iii) As $q \equiv q_1 > q_0$, more microcracks become activated. The compliance contributions from stable and unstable microcracks, $\bar{S}^{*s}_{ij}$ and $\bar{S}^{*u}_{ij}$, respectively, can be computed and integrated as follows.

$$\bar{S}^{*s}_{ij} = \frac{N_c}{V}\frac{1}{2\pi(a_{0_{max}} - a_{0_{min}})}\left[\int_{\theta_{u_{max}}}^{\frac{\pi}{2}}\int_0^{2\pi}\int_{a_{0_{min}}}^{a_{0_{max}}} S^{*(k)}_{ij}(a,\phi,\theta)\sin\theta da\, d\phi\, d\theta + \int_{\theta_{u_{min}}}^{\theta_{u_{max}}}\int_0^{2\pi}\int_{a_{0_{min}}}^{a_0(\theta)} S^{*(k)}_{ij}(a,\phi,\theta)\sin\theta da\, d\phi\, d\theta\right] \tag{64}$$

$$\bar{S}^{*u}_{ij} = \frac{N_c}{V}\frac{1}{2\pi(a_{0_{max}} - a_{0_{min}})\rho^3}\left[\int_{\theta_{u_{min}}}^{\theta_{u_{max}}}\int_0^{2\pi}\int_{a_0(\theta)}^{a_{0_{max}}} S^{*(k)}_{ij}(a,\phi,\theta)\sin\theta da\, d\phi\, d\theta + \int_0^{\theta_{u_{min}}}\int_0^{2\pi}\int_{a_{0_{min}}}^{a_{0_{max}}} S^{*(k)}_{ij}(a,\phi,\theta)\sin\theta da\, d\phi\, d\theta\right] \tag{65}$$

where $S^{*(k)}_{ij}$ is given by Eq. (40), and $a_0(\theta)$ is the *minimum* microcrack size for a specified orientation θ such that a microcrack becomes unstable. Specifically, $a_0(\theta)$ can be determined from Eq. (52)

$$a_0(\theta) = \frac{\pi}{4}\frac{K^{if\,2}_{Ic}K^{if\,2}_{IIc}}{K^{if\,2}_{IIc}(q^*\sin^2\theta + q^2\cos^2\theta)^2 + K^{if\,2}_{Ic}\left(\frac{2}{2-\nu}\right)^2(q^2 - q^{*2})\sin^2\theta\cos^2\theta} \tag{66}$$

Furthermore, it is noted that $\theta_{u_{max}}$, $\theta_{u_{min}}$ and $a_0(\theta)$ are functions of applied stresses q and q^*.

(iv) As $q < q_1$, the *unloading* case is taking place. There is no further microcrack growth and $\bar{\mathbf{S}}^{*u} = \mathbf{0}$. Therefore, the elastic-damage compliance $\bar{\mathbf{S}}$ remains its previous value.

(v) As $q > q_1$, more initial microcracks are activated. The computations involved are similar to those in step (iii). "Localization modes" are not considered in this work.

IV.5. Computational algorithm

The self-consistent analysis requires the use of the yet unknown overall compliance $\bar{\mathbf{S}}$. Therefore, the proposed damage model naturally requires iterative schemes to obtain $\bar{\mathbf{S}}$ corresponding to a specified stress $\bar{\sigma}$. Efficient numerical algorithms are warranted to compute the $\mathbf{C}'$ matrix in Eq. (31) for every edge point of a microcrack, to determine stationary and unstable microcrack regions, to compute the statistical average of microcrack-induced inelastic compliance $\bar{\mathbf{S}}^*$, and to iterate and update $\bar{\mathbf{S}}^*$ until proper convergence is reached.

For numerical integrations in Eqs. (31) and (44), the Gauss quadrature formula is found to be efficient for our analysis. In addition, it is found that use of 20 Gauss points for a single integral operator is sufficiently accurate. In fact, the relative difference between using 20 and 256 Gauss points is in the order of 10^{-8}.

The computational algorithm employed in this work proceeds as follows.

(i) Determine the critical angles $\theta_{u_{max}}$ and $\theta_{u_{min}}$ at given loading stresses, q and q^*, from Eqs. (62) and (63). The unstable angle domains should be stored as *history variables*.

(ii) Compute the single microcrack-induced inelastic compliance $\bar{\mathbf{S}}^{*(k)}$ by numerical integration:

  (a) Make an initial guess for the current overall compliance. The natural guess is the *previous* overall compliance $\bar{\mathbf{S}}_n$. At the first loading step, we use the virgin elastic compliance $\bar{\mathbf{S}}^o$ as an initial guess.

  (b) For a trial $\bar{\mathbf{S}}_{n+1}$ compliance, evaluate $\mathbf{C}'$ matrix for every (discretized) microcrack orientation by using Eq. (31). This involves the numerical solution of *roots* of the sixth-order equation (18) and the numerical integration around the microcrack edge (Eq. (31)).

  (c) Obtain the single microcrack-induced compliance $\bar{\mathbf{S}}'^{*(k)}$ in local coordinate system from $\mathbf{C}'$; see Eq. (36) for details.

  (d) Perform tensor transformation to obtain $\bar{\mathbf{S}}^{*(k)}$ in global coordinate system; see Eq. (40).

(iii) Obtain the updated inelastic compliance tensor $\bar{\mathbf{S}}^*$; see Eqs. (44), (64) and (65) for details. The triple integral is computed by using the triple Gauss integration scheme.

(iv) Obtain the new trial overall compliance $\bar{\mathbf{S}}_{n+1}$ by adding $\bar{\mathbf{S}}^*$ to $\bar{\mathbf{S}}^o$. Compare this $\bar{\mathbf{S}}_{n+1}$ with the previous trial $\bar{\mathbf{S}}_n$. If the relative error is smaller than a preset tolerance, then the iterative

process is converged. Otherwise, use $\bar{\mathbf{S}}_{n+1}$ as a new estimate and go back to step (ii)-(b) to re-iterate until convergence criterion is reached. This iterative scheme leads to superlinear rate of convergence and typically requires 6 to 8 iterations. The convergence criterion employed here is based on the L_∞ norm with $TOL = 10^{-7}$:

$$\frac{\| \bar{\mathbf{S}}_{n+1} - \bar{\mathbf{S}}_n \|_\infty}{\| \bar{\mathbf{S}}_{n+1} \|_\infty} \leq TOL \tag{67}$$

(v) Apply the next loading step and go to step (i).

IV.6. Numerical results and experimental validation

As an illustration, the proposed self-consistent micromechanical damage model is applied to concrete specimens under tension loadings in this section. Three different uniaxial tension tests are considered, and the numerical predictions are compared against experimental data reported by Gopalaratnam and Shah (1985). Following Krajcinovic and Fanella (1986), the microcrack number density N_c/V needed in Eq. (44) can be expressed as

$$\frac{N_c}{V} = \frac{12 f_v}{D_{\max}^3 \alpha_v} \frac{1-\hat{\gamma}}{1-\hat{\gamma}^4} \tag{68}$$

where $D_{\max}$ is the maximum aggregate size, α_v is the volume shape factor, f_v is the volume fraction of coarse aggregates, and $\hat{\gamma} \equiv \dfrac{D_{\min}}{D_{\max}}$ (with $D_{\min}$ denoting the minimum aggregate size), respectively.

As in Krajcinovic and Fanella (1986) and Zaitsev (1983), we take $K_{IIc}^{if} = 2K_{Ic}^{if}$, $f_v = 0.33$ and $\alpha_v = 4$. In addition, the elastic Young's moduli E, Poisson's ratios ν, maximum aggregate sizes $D_{\max}$, initial and final microcrack size ratios ρ, aggregate size ratios $\hat{\gamma}$, and the critical threshold stresses q_0 for "cleavage 1" microcrack growth are given in the figure captions of Figures 4, 6 and 8. The stress-strain predictions of the self-consistent damage model are also compared with experimental data in Figures 4, 6 and 8. It is observed that model simulations agree very well with the *ascending* curves (up to the *peak* tensile strengths) of experimental data. However, because the proposed damage model is *stress-driven* (fracture mechanics based), strain softening (descending) portions of the stress-strain curves cannot be simulated. Further, axial compliances $\bar{S}_{33}$ versus axial stresses q for three tests are plotted in Figures 5, 7, and 9. The elastic compliances $\bar{S}_{33}^o$ are also appended in Figures 5, 7, and 9 for comparison purpose.

In the above three tests, microcrack concentrations are relatively low and ultimate tensile stress levels are low, too. Therefore, these are not the most ideal tensile experiments for model validation. However, these tests are the only tensile micromechanical concrete tests available to the authors at this stage. Moreover, due to the relatively low initial microcrack concentrations, the differences between the self-consistent model and the Taylor's model are relatively small in these three cases. Therefore, the (Taylor's) micromechanical damage model for concrete under tension proposed by Krajcinovic and Fanella (1986) was adequate for these tests. However, when microcrack concentration becomes moderate and ultimate stress level becomes higher for other specimens or materials, the differences between the two micromechanical damage models are more significant

(due to higher microcrack *interaction*). To illustrate this point, let us consider the fourth uniaxial tension test with moderate initial microcrack concentration and higher ultimate tensile strength. The micromechanical material properties employed together with the predictions of macroscopic stress-strain responses by the two models are shown in Fig. 10. It is observed that the damage-induced inelastic compliance $\tilde{\mathbf{S}}^*$ obtained by the self-consistent model differs significantly from that of the Taylor's model in the simulation.

In the above model predictions, only "cleavage 1" microcrack growth is considered. Microcrack *kinking* into the matrix and new microcrack *nucleation* along matrix-inclusion interfaces are not accounted for. When concrete specimens are under *compressive* loadings, however, microcrack kinking and new microcrack nucleation are important for ultimate material failure. These issues and related micromechanical damage models will be further investigated in Part II of this work.

IV.7. Conclusion

A three-dimensional self-consistent micromechanical damage model for microcrack-weakened brittle solids under *tension* is presented. The microcracks are assumed to be elliptical or penny-shaped. Their sizes and orientations are taken as random variables. The microcrack-induced inelastic compliance is derived by adopting Heonig's method to obtain microcrack opening displacements for very general anisotropic materials. Micro-macro integration procedures are also presented to obtain overall compliances and macro-strains. A process damage model is considered, which features predictive capability of macroscopic stress-strain responses. The fracture criterion for microcracks embedded in an anisotropic solid is discussed. Moreover, microcrack kinetic sequences are presented within the context of "cleavage 1" microcrack growth processes.

Efficient computational algorithms are given in detail for the proposed method. To illustrate the potential capability of the proposed model, numerical results are obtained and compared with experimental data of concrete specimens under tensile loadings. For low microcrack concentrations and low ultimate stress levels, the self-consistent model yields results similar to those of the Taylor's model. For moderate microcrack concentrations and higher ultimate strengths, nevertheless, the self-consistent damage model indirectly accounts for microcrack interaction effects and thus renders the progressive damage phenomena more appropriately. Of course, computational cost of the self-consistent damage model is also higher than that of the Taylor's model. Therefore, judgement should be exercised as to the choice of the appropriate damage model for a particular brittle material under certain loading conditions. It is emphasized that not a single fitted material parameter is employed in the proposed model. The compressive responses and underlying microcrack kinetics (including microcrack kinking and nucleation) of brittle solids within the context of the self-consistent method are the focal points of Part II of this work. More numerical results and experimental validation will also be given in Part II.

IV.8. References

1. ACHENBACH, J. D. AND ZHU, H., (1989), "Effects of Interfacial Zone on Mechanical Behavior and Failure of Fiber-Reinforced Composites", *J. Mech. Phy. Solids*, Vol. 37, No. 3, pp. 381–393.

2. ASHBY, M. F., (1979), "Micromechanisms of Fracture in Static and Cyclic Failure", In: R. A. Smith, ed., *Fracture Mechanics, Current Status, Future Prospects*, Pergamon Press, Oxford, Vol. 1, pp. 1–27.

3. BASSANI, J. L. AND QU, J., (1989), "Finite Crack on Bimaterial and Bicrystal Interfaces", *J. Mech. Phy. Solids*, Vol. 37, No. 4, pp. 435–453.

4. BAZANT, Z. P., (1986), "Mechanics of Distributed Cracking", *Appl. Mech. Rev.*, Vol. 39, No. 5, pp. 675–705.

5. BENVENISTE, Y., (1986), "On the Mori-Tanaka's Method in Cracked Bodies", *Mech. Res. Comm.*, Vol. 13, pp. 193–201.

6. BUDIANSKY, B. AND O'CONNELL, R. J., (1976), "Elastic Moduli of a Cracked Solid", *Int. J. Solids & Struct.*, Vol. 12, pp. 81–97.

7. FANELLA, D. AND KRAJCINOVIC, D., (1988), "A Micromechanical Model for Concrete in Compression", *Eng. Fract. Mech.*, Vol. 29, No. 1, pp. 49–66.

8. GOPALARATNAM, V. S. AND SHAH, S. P., (1985), "Softening Response of Plain Concrete in Direct Tension", ACI *Journal*, May–June, pp. 310–323.

9. HASHIN, Z., (1988), "The Differential Scheme and its Application to Cracked Materials", *J. Mech. Phys. Solids*, Vol. 36, pp. 719–734.

10. HILL, R., (1966), "The Essential Structure of Constitutive Laws for Metal Composites and Polycrystals", *J. Mech. Phy. Solids*, Vol. 15, pp. 79–95.

11. HOENIG, A., (1978), "The Behavior of a Flat Elliptical Crack in an Anisotropic Elastic Body", *Int. J. Solids & Struct.*, Vol. 14, pp. 925–934.

12. HOENIG, A., (1979), "Elastic Moduli of a Non-Randomly Cracked Body", *Int. J. Solids & Struct.*, Vol. 15, pp. 137–154.

13. HOENIG, A., (1982), "Near-Tip Behavior of a Crack in a Plane Anisotropic Elastic Body", *Eng. Fract. Mech.*, Vol. 16, No. 3, pp. 393–403.

14. HORII, H. AND NEMAT-NASSER, S., (1983), "Overall Moduli of Solids with Microcracks: Load-Induced Anisotropy", *J. Mech. Phy. Solids*, Vol. 31, No. 2, pp. 155–171.

15. HORII, H. AND NEMAT-NASSER, S., (1985), "Elastic Fields of Interacting Inhomogeneities", *Int. J. Solids & Struct.*, Vol. 21, No. 7, pp. 731–745.

16. HORII, H. AND SAHASAKMONTRI, K., (1990), "Mechanical Properties of Cracked Solids: Validity of the Self-Consistent Method", in *Micromechanics and Inhomogeneity*, ed. by G. J. Weng, M. Taya and H. Abe, pp. 137–159, Springer-Verlag, New York.

17. JU, J. W., (1989a), "On Energy-Based Coupled Elasto-Plastic Damage Theories: Constitutive Modeling and Computational Aspects", *Int. J. Solids & Struct.*, Vol. 25, No. 7, pp. 803–833.

18. JU, J. W., (1989b), "Energy-Based Coupled Elastoplastic Damage Models at Finite Strains", *J. Eng. Mech.*, ASCE, Vol. 115, No. 11, pp. 2507–2525.

19. JU, J. W., (1990), "A Micromechanical Damage Model for Uniaxially Reinforced Composites Weakened by Interfacial Arc Microcracks", *J. Appl. Mech.*, ASME, accepted for publication.

20. JU, J. W., (1991), "On Two-Dimensional Self-Consistent Micromechanical Damage Models for Brittle Solids", *Int. J. Solids & Struct.*, Vol. 27, No. 2, pp. 227–258.

21. KACHANOV, M., (1987), "Elastic Solids with Many Cracks: A Simple Method of Analysis", *Int. J. Solids & Struct.*, Vol. 23, No. 1, pp. 23–43.

22. KANNINEN, M. F. AND POPELAR, C. H., (1985), *Advanced Fracture Mechanics*, Oxford University Press, New York.

23. KRAJCINOVIC, D., (1984), "Continuum Damage Mechanics," *Appl. Mech. Rev.*, Vol. 37: 1–6, pp. 397–402.

24. KRAJCINOVIC, D., (1986), "Update to Continuum Damage Mechanics", *Appl. Mech. Update*, pp. 403–406.

25. KRAJCINOVIC, D., (1989), "Damage Mechanics", *Mech. Mater.*, to appear.

26. KRAJCINOVIC, D. AND FANELLA, D., (1986), "A Micromechanical Damage Model for Concrete", *Eng. Fract. Mech.*, Vol. 25, No. 5/6, pp. 585–596.

27. KRAJCINOVIC, D. AND SUMARAC, D., (1989), "A Mesomechanical Model for Brittle Deformation Processes: Part I", *J. Appl. Mech.*, Vol. 56, pp. 51–56.

28. LAWS, N. AND DVORAK, G. J., (1987), "The Effect of Fiber Breaks and Aligned Penny-Shaped Cracks on the Stiffness and Energy Release Rates in Unidirectional Composites", *Int. J. Solids & Structures*, Vol. 23, No. 9, pp. 1269–1283.

29. LEKHNITSKII, S. G., (1950), *Theory of Elasticity of an Anisotropic Elastic Body*, by the Government Publishing House for Technical-Theoretical Works, Moscow and Leningrad, 1950; and by Holden-Day, Inc., San Francisco, 1963.

30. MCLAUGHLIN, R., (1977), "A Study of the Differential Scheme for Composite Materials", *Int. J. Engng. Sci.*, Vol. 15, pp. 237–244.

31. MORI, T. AND TANAKA, K., (1973), "Average Stress in Matrix and Average Elastic Energy of Materials with Misfitting Inclusions", *Acta Metallurgica*, Vol. 21, pp. 571–574.

32. MURAKAMI, S., (1987), "Progress of Continuum Damage Mechanics", *JSME Int. J.*, Vol. 30, No. 263, pp. 701–710.

33. NEMAT-NASSER, S. AND HORI, M., (1990), "Elastic Solids with Microdefects", in *Micromechanics and Inhomogeneity*, pp. 297–320, ed. by G. J. Weng, M. Taya and H. Abe, Springer-Verlag, New York.

34. QU, J. AND BASSANI, J. L., (1989), "Cracks on Bimaterial and Bicrystal Interfaces", *J. Mech. Phy. Solids*, Vol. 37, No. 4, pp. 417–433.

35. RICE, J. R., (1968), "A Path Independent Integral and the Approximate Analysis of Strain Concentration by Notches and Cracks", *J. Appl. Mech.*, June, pp. 379–386.

36. ROSCOE, R. A., (1952), "The Viscosity of Suspensions of Rigid Spheres", *Brit. J. Apply. Phys.*, Vol. 3, pp. 267–269.

37. ROSCOE, R. A., (1973), "Isotropic Composites with Elastic or Viscoelastic Phases: General Bounds for the Moduli and Solutions for Special Geometries", *Rheol. Acta*, Vol. 12, pp. 404–411.

38. SIMO, J. C. AND JU, J. W., (1987), "Stress and Strain Based Continuum Damage Models. Part I: Formulation," *Int. J. Solids & Struct.*, Vol. 23, No. 7, pp. 821–840.

39. SUMARAC, D. AND KRAJCINOVIC, D., (1987), "A Self-Consistent Model for Microcrack-Weakened Solids", *Mech. Mater.*, Vol. 6, pp. 39–52.

40. SUMARAC, D. AND KRAJCINOVIC, D., (1989), "A Mesomechanical Model for Brittle Deformation Processes: Part II", *J. Appl. Mech.*, Vol. 56, pp. 57–62.

41. WU, C. H., (1985), "Tension-Compression Test of a Concrete Specimen via a Structure Damage Theory," in *Damage Mechanics and Continuum Modeling*, ed. by N. Stubbs and D. Krajcinovic, ASCE, pp. 1–12.

42. ZAITSEV, Y. B., (1983), "Crack Propagation in a Composite material", In: F. H. Wittmann, ed., *Fracture Mechanics of Concrete*, Elsevier, Amsterdam.

43. ZHAO, Y. H., TANDON, G. P. AND WENG, G. J., (1989), "Elastic Moduli for a Class of Porous Materials", *Acta Mechanica*, Vol. 76, pp. 105–130.

IV.9. Figure captions

Figure 1. The elliptical microcrack coordinate system.

Figure 2. The line microcrack tip coordinate system.

Figure 3. The local (primed) and global Cartesian coordinate systems.

Figure 4. The numerical results compared with experimental data (Example 1).

$E = 4952$ (ksi), $\nu = 0.3$, $D_{\max} = 0.375$ (in.), $\rho = 0.3$, $\hat{\gamma} = 0.9$, $q_0 = 400$ (psi).

Figure 5. The numerical compliance values $\bar{S}_{33}$ versus the axial stresses q for Example 1.

Figure 6. The numerical results compared with experimental data (Example 2).

$E = 5000$ (ksi), $\nu = 0.3$, $D_{\max} = 0.375$ (in.), $\rho = 0.3$, $\hat{\gamma} = 0.7$, $q_0 = 400$ (psi).

Figure 7. The numerical compliance values $\bar{S}_{33}$ versus the axial stresses q for Example 2.

Figure 8. The numerical results compared with experimental data (Example 3).

$E = 4815$ (ksi), $\nu = 0.3$, $D_{\max} = 0.375$ (in.), $\rho = 0.3$, $\hat{\gamma} = 0.9$, $q_0 = 350$ (psi).

Figure 9. The numerical compliance values $\bar{S}_{33}$ versus the axial stresses q for Example 3.

Figure 10. Comparison of numerical simulations obtained by using the self-consistent and the Taylor's models.

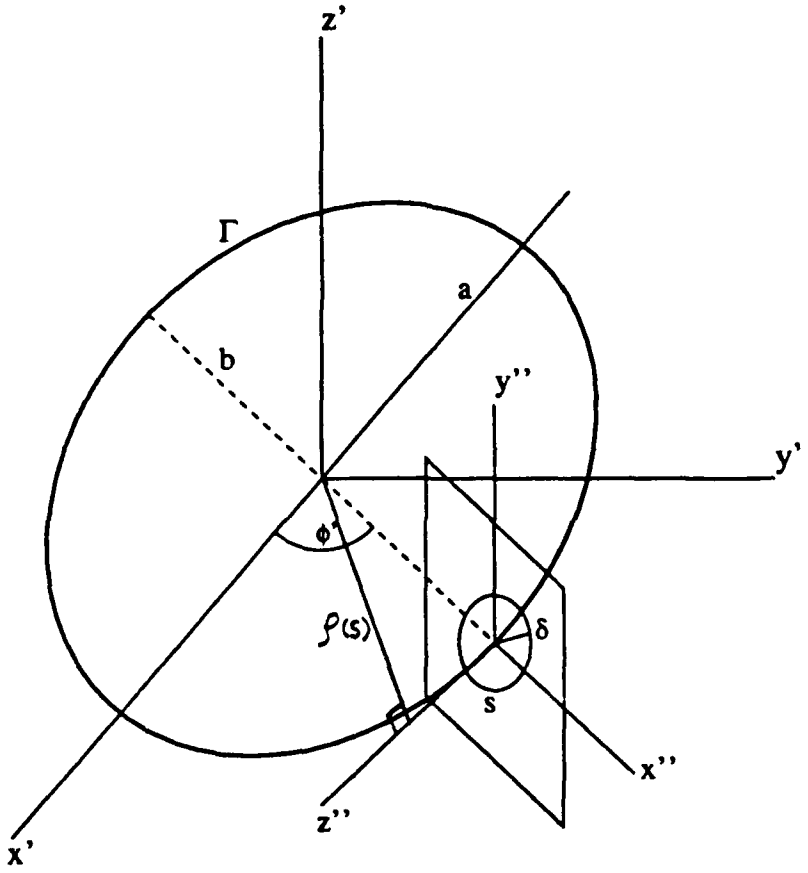

Figure 1. The elliptical microcrack coordinate system.

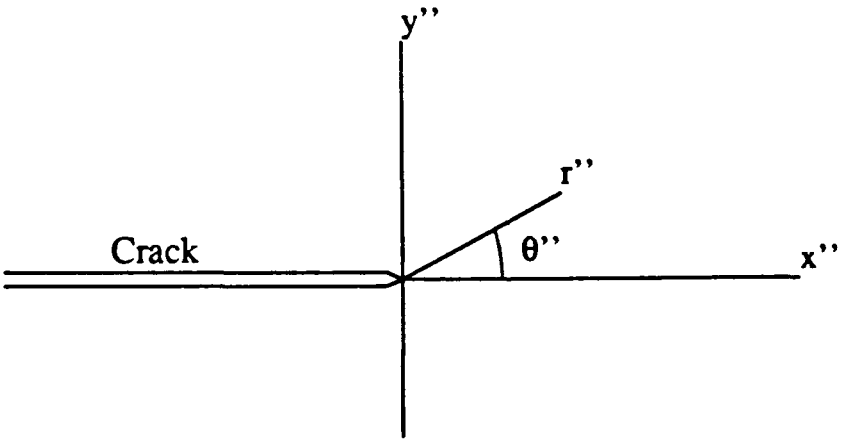

Figure 2. The line microcrack tip coordinate system.

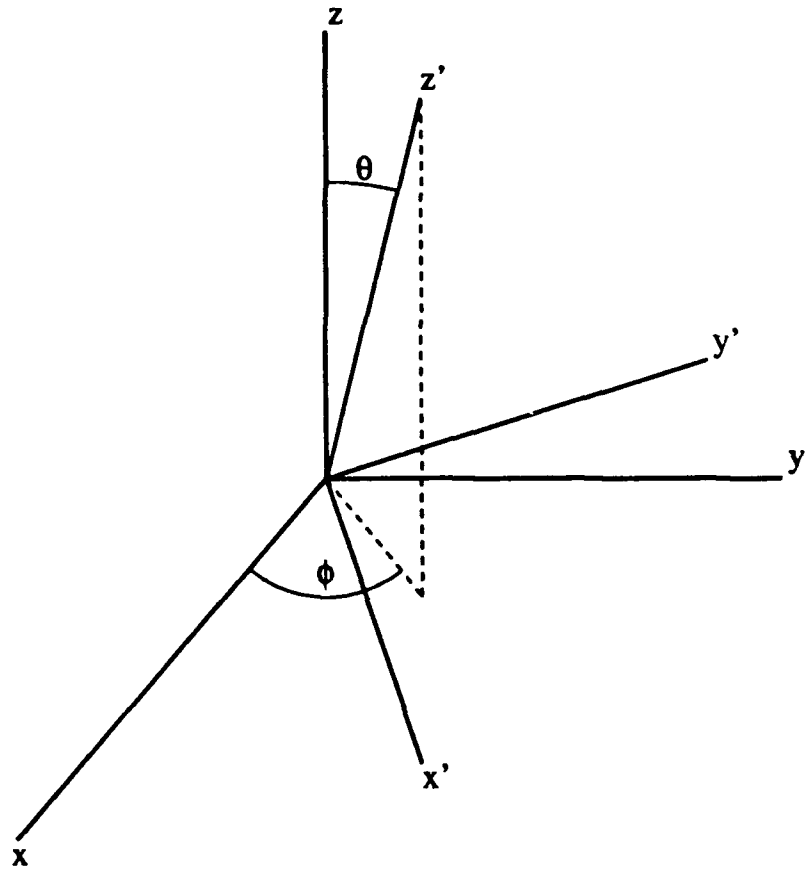

Figure 3. The local (primed) and global Cartesian coordinate systems.

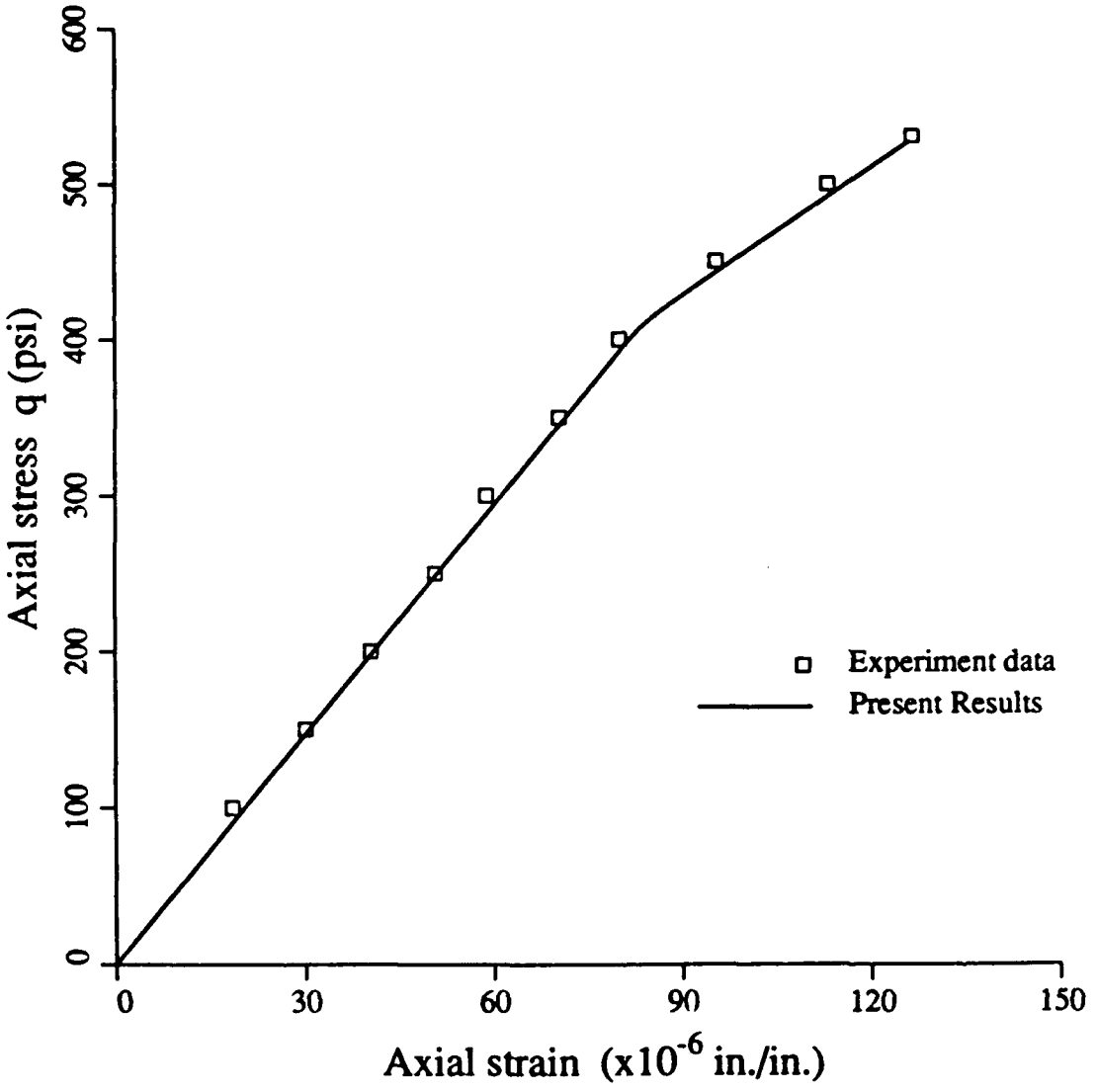

Figure 4. The numerical results compared with experimental data (Example 1). $E = 4952$ (ksi), $\nu = 0.2$, $D_{max} = 0.375$ (in.), $\rho = 0.3$, $\hat{\gamma} = 0.9$, $q_0 = 400$ (psi).

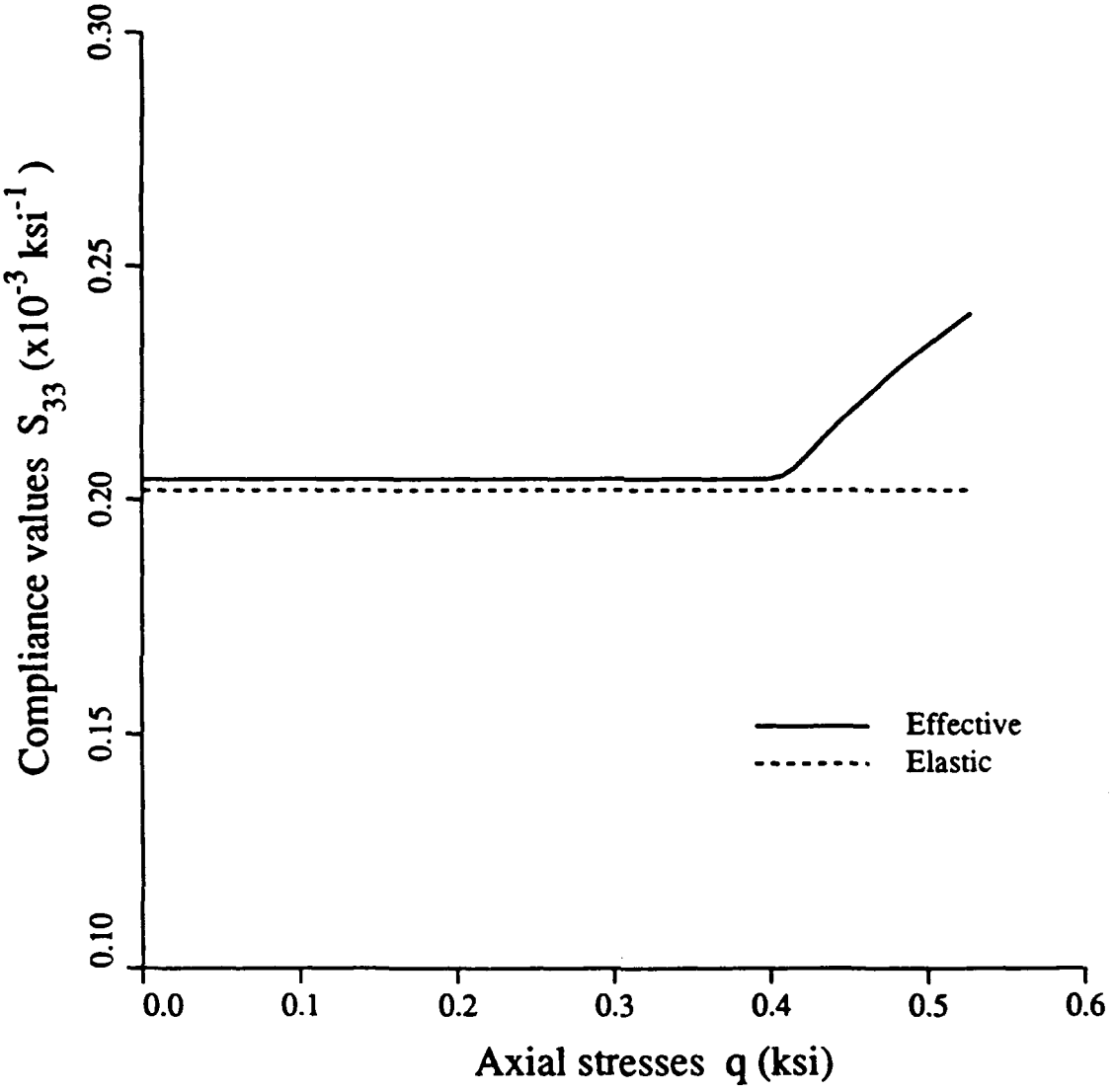

Figure 5. The numerical compliance values $\bar{S}_{33}$ versus the axial stresses q for Example 1.

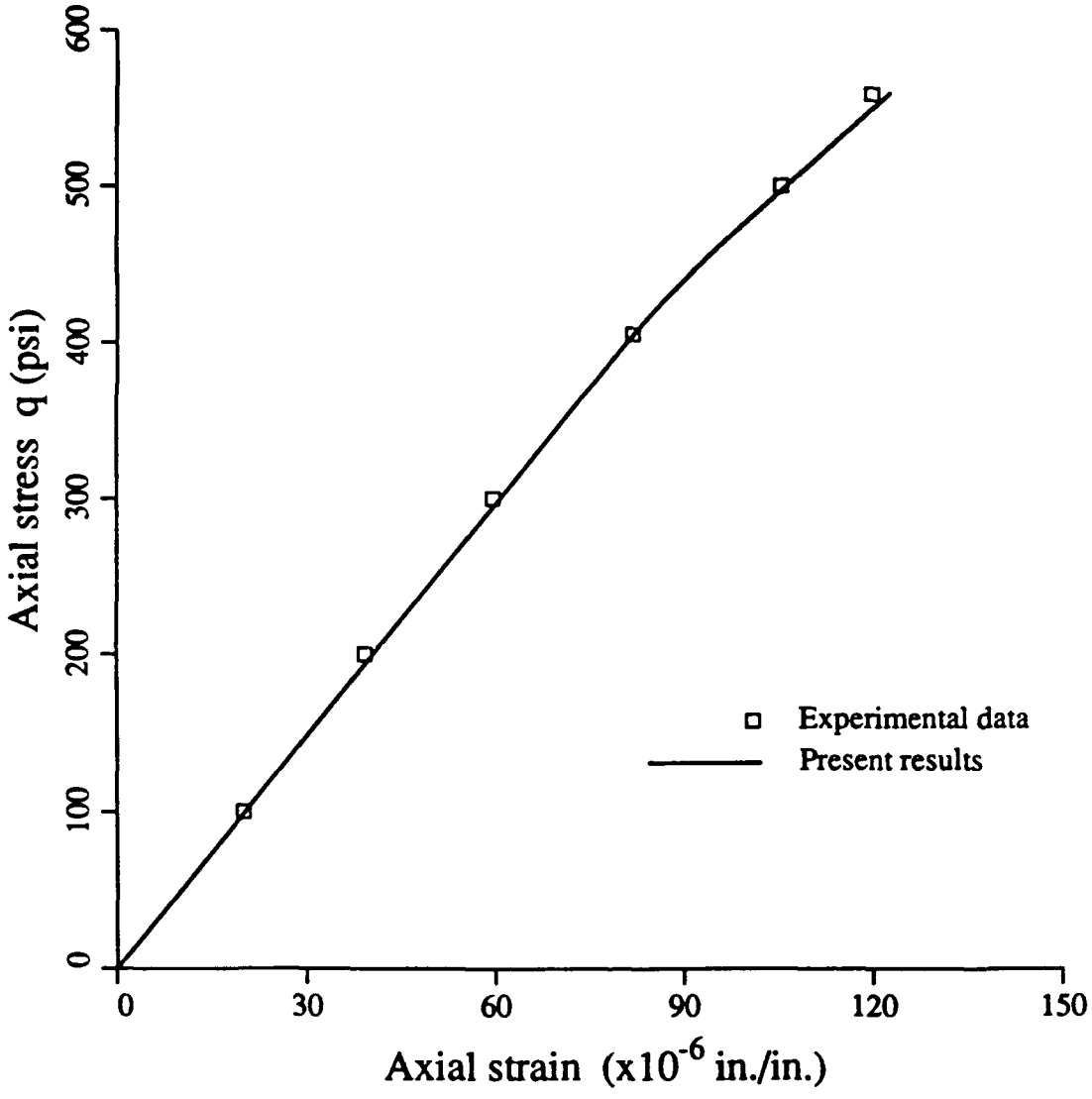

Figure 6. The numerical results compared with experimental data (Example 2). E = 5000 (ksi), ν = 0.2, D_{max} = 0.375 (in.), ρ = 0.3, $\hat{\gamma}$ = 0.7, q_0 = 400 (psi).

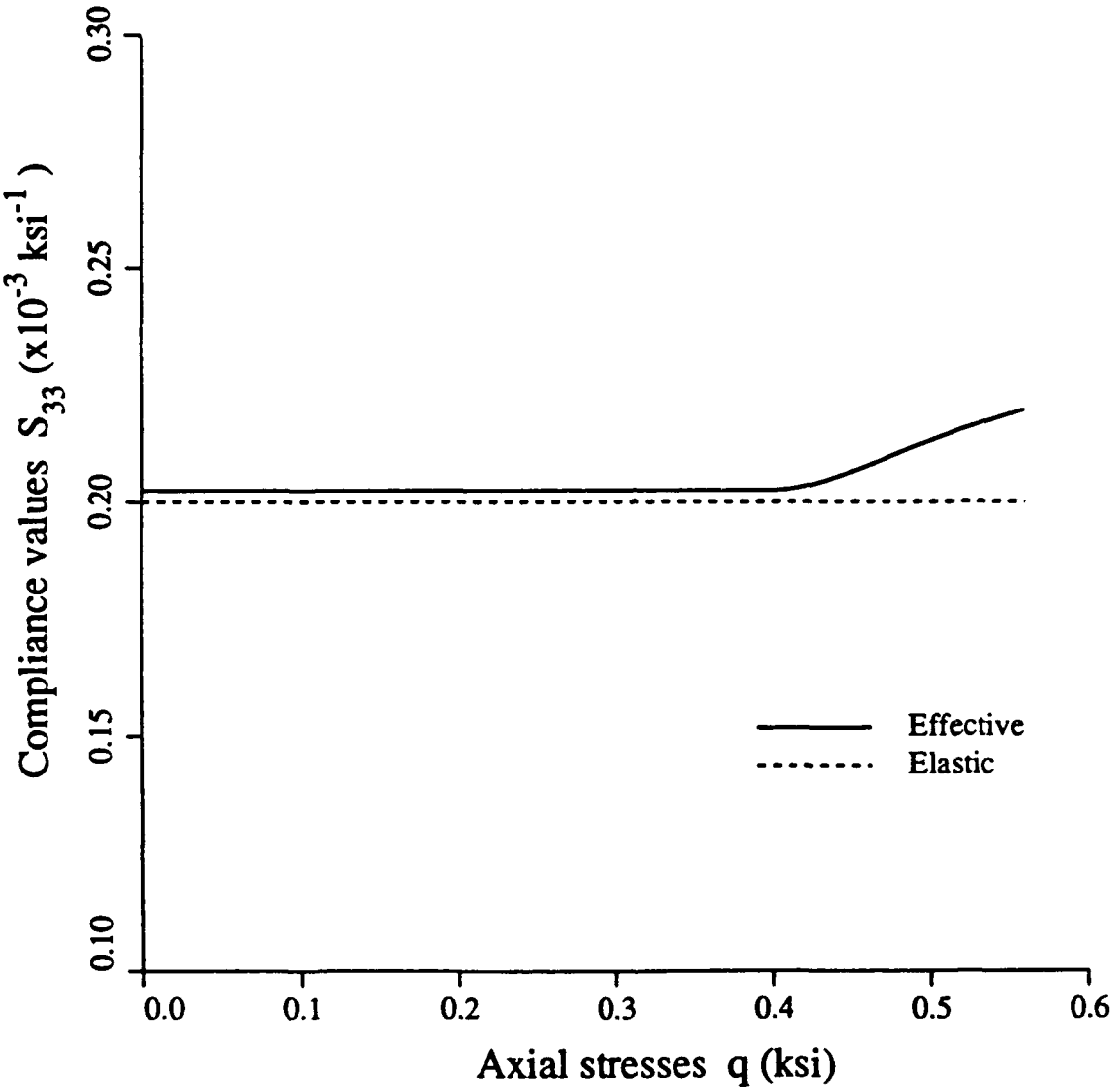

Figure 7. The numerical compliance values $\bar{S}_{33}$ versus the axial stresses q for Example 2.

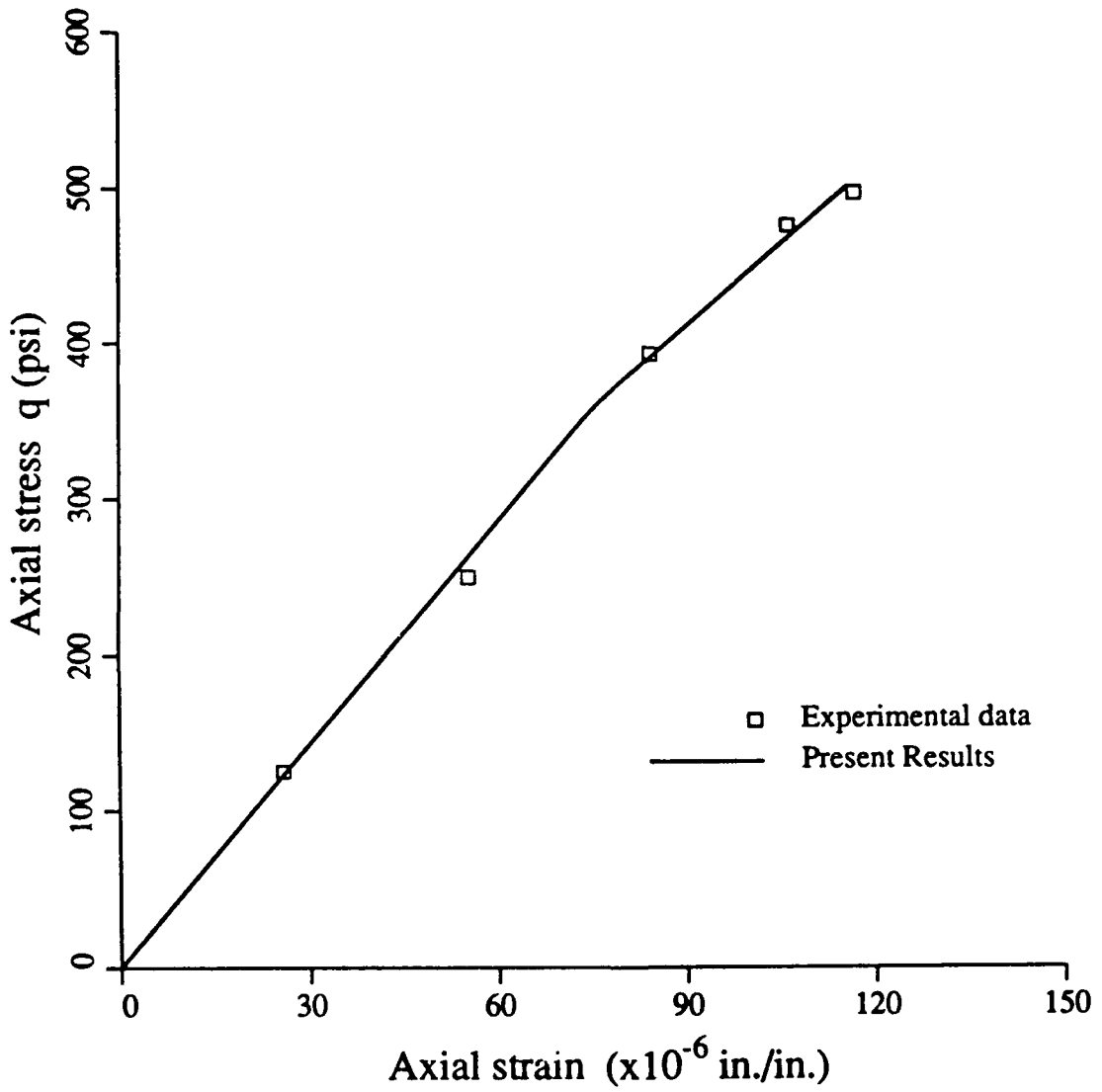

Figure 8. The numerical results compared with experimental data (Example 3).
E = 4815 (ksi), ν = 0.2, D_{max} = 0.375 (in.), ρ = 0.3, $\hat{\gamma}$ = 0.9, q_0 = 350 (psi).

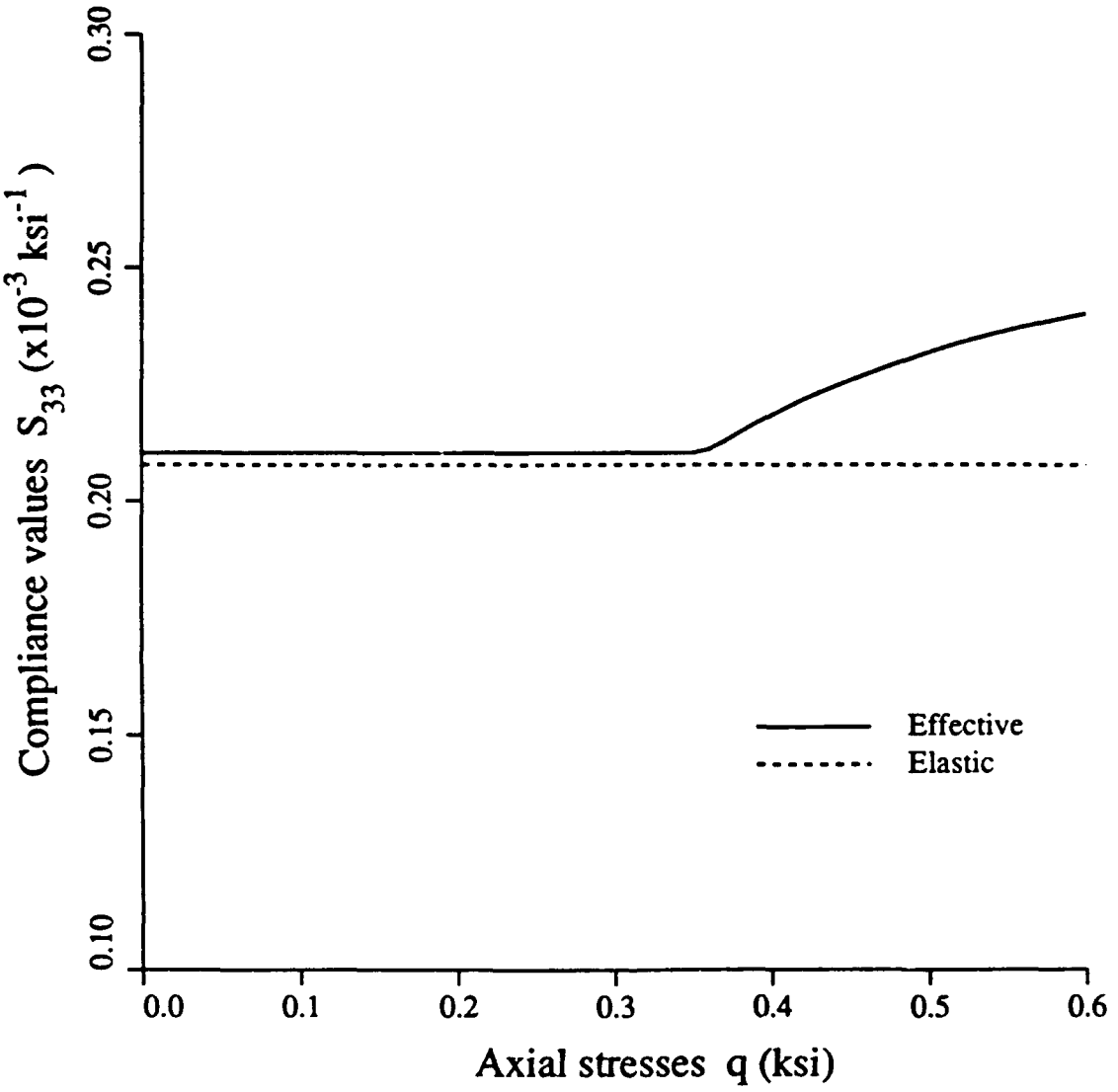

Figure 9. The numerical compliance values $\tilde{S}_{33}$ versus the axial stresses q for Example 3.

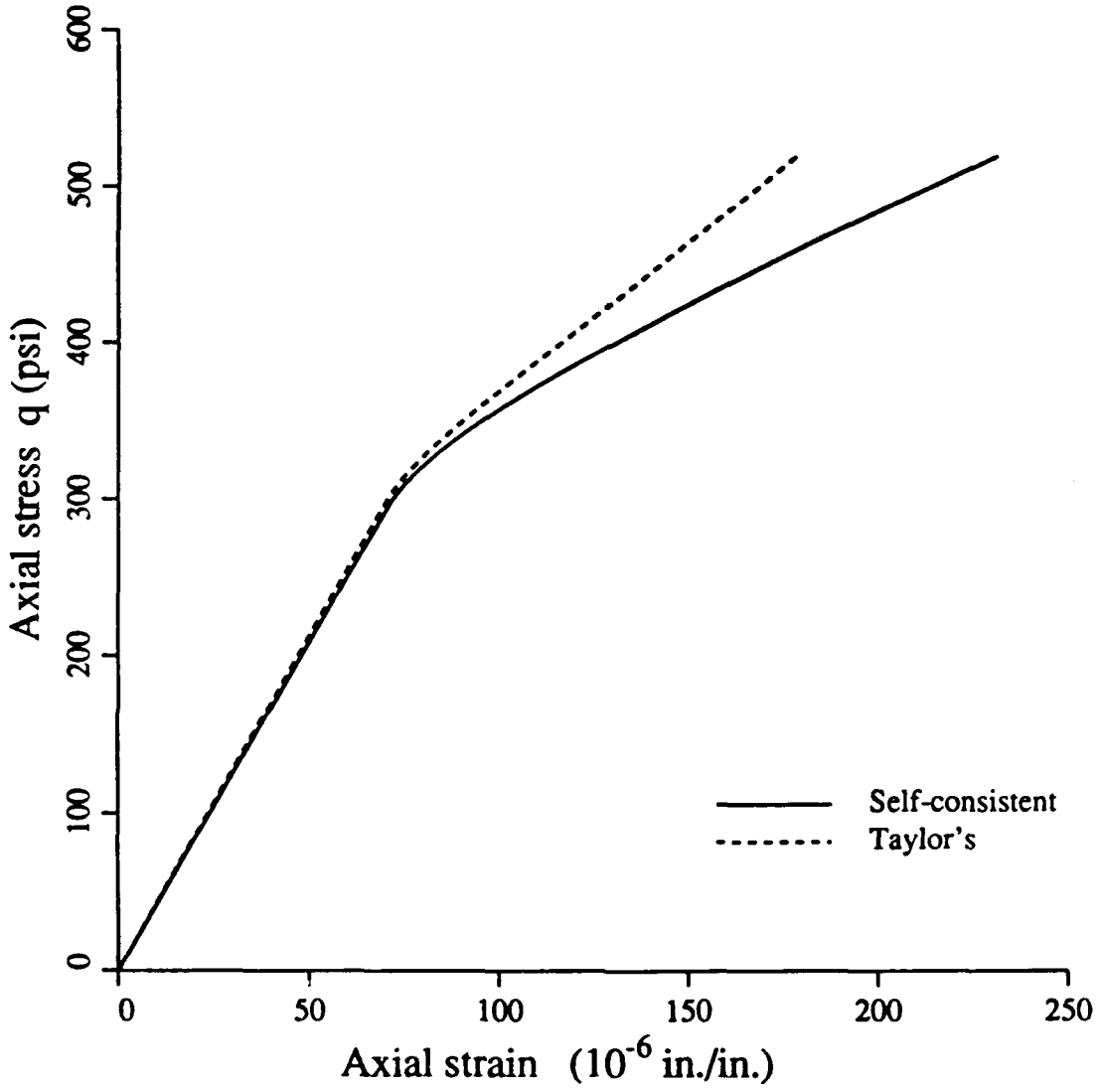

Figure 10. Comparison of numerical simulations obtained by using the self-consistent and the Taylor's models. (E = 4815 (ksi), ν = 0.2, D_{max} = 0.375 (in.), f_v = 0.4, α_v = 2, ρ = 0.5, $\hat{\gamma}$ = 0.6, q_0 = 300 (psi)).

PART V

On Three-Dimensional Self-Consistent Micromechanical Damage Models for Brittle Solids. Part II: Compressive Loadings

V.1. Introduction

In Part I of this study (PART IV of this report), a three-dimensional self-consistent micromechanical process damage model is proposed to account for "cleavage 1" microcrack deformation processes under *tensile* loadings for brittle solids (Ashby (1979)). Further, in Part I, all microcracks are assumed to be *open* and pre-existing (due to initial imperfections or previous loadings) at the matrix-inclusion interfaces of composites or at the intergranular planes of polycrystalline solids (such as ceramics). Under uniaxial or triaxial compressive loadings, however, some (or all) microcracks are *closed* and may experience frictional *sliding* and even Mode II growth ("cleavage 1" processes). In addition, under higher compressive loads, some microcracks may *kink* into the matrix or the neighboring intergranular planes, and new microcrack *nucleation* ("cleavage 2" processes) may occur for certain preferred orientations and sizes. Therefore, the self-consistent (or other effective medium theories) micromechanical process damage models for such deformation kinetics are warranted. Part II of this work is devoted to this effort.

Due to microcrack opening displacements under applied loads, inelastic strains and inelastic compliances (or stiffnesses) develop in addition to elastic material responses. The microcrack opening displacements for a single elliptical *open* flat microcrack embedded in a fully anisotropic solid (with a symmetric compliance matrix containing up to 21 independent components) have been derived in Part I of this work. Due to frictional sliding of *closed* microcracks, nevertheless, the overall moduli of brittle solids become *non-symmetric* and anisotropic (with up to 36 independent compliance components). Therefore, in this sequel, we will derive fundamental solutions of microcrack opening displacements for a single penny-shaped *closed* microcrack embedded in a *non-symmetric* anisotropic solid. This derivation is very crucial to the construction of microcrack-induced inelastic

compliances and strains.

Some relevant literatures on micromechanical damage theories are briefly reviewed in what follows. By applying the self-consistent method, Budiansky and O'Connell (1976) obtained isotropic overall moduli for microcrack-weakened solids containing open, elliptical, and perfectly randomly distributed microcracks. When some of the microcracks are closed and experience frictional sliding, Horii and Nemat-Nasser (1983) presented two-dimensional (line microcracks), self-consistent analysis for non-symmetric anisotropic solids. The foregoing work, however, are limited to non-process models; i.e. no microcrack changes its size during loading. Based on the theory of linear elastic fracture mechanics and the aforementioned work, Sumarac and Krajcinovic (1987) proposed a two-dimensional, self-consistent, anisotropic, *process* microcrack model for brittle solids under tension. Further, three-dimensional process damage models were given by Krajcinovic and Fanella (1986) for concrete under uniaxial tension, and by Fanella and Krajcinovic (1988) for concrete under uniaxial and triaxial compression. These process models, nontheless, are only "Taylor's models"; i.e. microcrack interaction effects are entirely ignored. In addition to Mode I and Mode II microcrack growth, Krajcinovic and Fanella also considered microcrack *kinking* and resulting inelastic compliances under compression. Microcrack kinking in brittle solids has been discussed in several other literatures; see, e.g. Zaitsev (1983), Nemat-Nasser and Horii (1982), Horii and Nemat-Nasser (1985, 1986).

An outline of this paper is as follows. In Section 2, we show that due to frictional sliding of *closed* microcrack faces the overall compliance matrix is inherently *non-symmetric*. It is recalled from Part I (Ju and Lee (1990)) that fundamental microcrack opening displacement solutions due to Hoenig (1978, 1982) are only valid for anisotropic solids with *symmetric* moduli. By modifying Hoenig's solutions, we re-derive relevant microcrack opening formulas presented in Part I to accommodate non-symmetry and anisotropy. This is indeed a powerful tool and therefore non-symmetric inelastic compliances can be systematically obtained. In fact, the presented framework is capable of treating combinations of open and closed microcracks under combined tensile and

compressive loads. Consequently, a self-consistent formulation of mixed loadings is rendered. Mixed Mode and Mode II microcrack growth ("cleavage 1") processes are subsequently presented in Section 3. In particular, fracture criterion for a closed sliding penny-shaped microcrack is discussed. Detailed and systematic microcrack kinetic equations for mixed open/ closed microcracks are also given.

In Section 4, microcrack *kinking* criterion under compression and approximate solutions of kinked microcrack opening displacements are given along the lines of Fanella and Krajcinovic (1988). Moreover, inelastic compliances due to kinked microcracks are derived within the framework of the self-consistent method. It is noted that "cleavage 1" process alone may not be sufficient to satisfactorily capture overall material responses and deformation processes. In fact, nucleation of new microcracks ("cleavage 2") along weak planes is an important aspect of many brittle solids under higher loadings. Therefore, a simple Zener-Stroh type microcrack nucleation model is proposed in Section 5 based on the critical shear stress nucleation criterion. Finally, numerical procedures and some experimental validations for the proposed models are presented in Section 6.

V.2. Formulation of microcrack induced inelastic compliances

The microcrack induced inelastic compliances due to *open* microcracks have been derived in Part I of this work, where inelastic compliance matrices are *symmetric* and anisotropic (with 21 independent components). When microcracks are *closed* and *sliding* under compression, effective compliances are no longer symmetric. Such non-symmetry was shown, for instance, by Horii and Nemat-Nasser (1983) for two-dimensional analysis with closed line microcracks embedded in an anisotropic body. In this section, attention is focused on the derivations of non-symmetric compliances and corresponding microcrack opening displacements for penny-shaped microcracks embedded in most general anisotropic materials (with 36 independent compliance components). The derivation of microcrack opening displacements are based on modification of Hoenig's (1978, 1982) work. In particular, the M-surface integral, the work done by external loads through opening displacements, and Lekhnitskii's (1950) theory of anisotropic elasticity are employed for this purpose.

V.2.1. Non-symmetry of compliance matrix due to closed sliding microcracks

As was discussed in Part I (Ju and Lee (1990)), the inelastic strains induced by microcrack opening displacements take the form

$$\bar{\epsilon}'^{*}_{ij} = \frac{1}{V}\sum_{k}\int_{S^{(k)}} \frac{1}{2}\left(u'_i n'_j + u'_j n'_i\right)^{(k)} dS^{(k)} \tag{1}$$

where the prime indicates that the values are evaluated in the local (microcrack) coordinate system; see Figures 1(a) and 1(b). Further, V is the volume of the representative element (unit cell), and u'_i is the opening displacement in the i-th direction. For convenience, we will use the Voigt's notation in what follows. That is,

$$\bar{e}'^{*}_{i} = \bar{S}'^{*}_{ij}\,\bar{\tau}'_j \tag{2}$$

where $e_1 = \epsilon_{11}$, $e_2 = \epsilon_{22}$, $e_3 = \epsilon_{33}$, $e_4 = 2\epsilon_{23}$, $e_5 = 2\epsilon_{31}$, and $e_6 = \epsilon_{12}$; $\tau_1 = \sigma_{11}$, $\tau_2 = \sigma_{22}$, $\tau_3 = \sigma_{33}$, $\tau_4 = \sigma_{23}$, $\tau_5 = \sigma_{31}$, and $\tau_6 = \sigma_{12}$; and $\bar{\mathbf{S}}'^{*}$ is the microcrack induced compliance matrix. As shown in Part I, the displacement jumps across the penny-shaped microcrack surfaces can be expressed as

$$u'_i(x', y') = 2\sqrt{a^2 - (x'^2 + y'^2)}\, C'^{-1}_{ij}\bar{\sigma}'_{3j} \tag{3}$$

where $C_{ij}^{\prime -1}$ is a function of components of the compliance matrix. It is recalled that $C_{ij}^{\prime -1}$ and $\bar{S}_{ij}^{\prime *}$ were given by Eqs. (31) and (36) in Part I for strictly open microcracks and symmetric compliance matrix.

Let us begin by assuming that a microcrack is subjected to (compressive) normal and shear loadings. Let η be the coefficient of friction of microcrack surfaces. Due to compressive normal stress ($\bar{\tau}_3' < 0$), the microcrack is *closed*. Moreover, the contact stresses transmitted across microcrack surfaces are presented by a vector $\bar{\tau}'^c$; i.e. $\bar{\tau}_3'^c$ is the normal contact stress, and $\bar{\tau}_4'^c$ and $\bar{\tau}_5'^c$ are the shear contact stresses, respectively. The unknown transmitted (contact) stresses, $\bar{\tau}'^c$ can be determined from the following two conditions.

(i) If the microcrack is closed and no frictional sliding occurs; i.e.

$$|\bar{\tau}_4'| \leq -\eta \bar{\tau}_3' \quad \text{and} \quad |\bar{\tau}_5'| \leq -\eta \bar{\tau}_3' \tag{4}$$

then

$$u_i' \equiv 0\,; \quad \bar{\tau}_3'^c = \bar{\tau}_3'\,, \quad \bar{\tau}_4'^c = \bar{\tau}_4'\,, \quad \bar{\tau}_5'^c = \bar{\tau}_5' \tag{5}$$

(ii) If the microcrack is closed and experiencing frictional *sliding*; i.e.

$$\text{either} \quad |\bar{\tau}_4'| > -\eta \bar{\tau}_3'^c \quad \text{or} \quad |\bar{\tau}_5'| > -\eta \bar{\tau}_3'^c \tag{6}$$

then

$$u_3' \equiv 0\,; \quad \bar{\tau}_4'^c = -\text{sgn}(\bar{\tau}_4')\eta \bar{\tau}_3'^c \quad \text{and} \quad \bar{\tau}_5'^c = -\text{sgn}(\bar{\tau}_5')\eta \bar{\tau}_3'^c \tag{7}$$

where $\text{sgn}(\bar{\tau}') = -1,\ 0,$ or 1, depending on whether $\bar{\tau}'$ is negative, zero, or positive.

When the first condition (i) is met, there is no displacement jump across microcrack surfaces. Therefore, no microcrack induced inelastic compliance matrix exists. On the other hand, when microcrack surfaces undergo frictional sliding, there is no normal displacement jump ($u_3' \equiv 0$), and Eq. (3) leads to

$$C_{31}^{\prime -1}(\bar{\tau}_5' - \bar{\tau}_5'^c) + C_{32}^{\prime -1}(\bar{\tau}_4' - \bar{\tau}_4'^c) + C_{33}^{\prime -1}(\bar{\tau}_3' - \bar{\tau}_3'^c) \equiv 0 \tag{8}$$

Thus, the normal contact stress $\bar{\tau}_3'^c$ is compressive and equal to

$$\bar{\tau}_3'^c = \frac{C_{33}^{\prime -1}\bar{\tau}_3' + C_{32}^{\prime -1}\bar{\tau}_4' + C_{31}^{\prime -1}\bar{\tau}_5'}{C_{33}^{\prime -1} - \text{sgn}(\bar{\tau}_4')\eta C_{32}^{\prime -1} - \text{sgn}(\bar{\tau}_5')\eta C_{31}^{\prime -1}} < 0 \tag{9}$$

By choosing the local microcrack coordinate system to be $n_1' = n_2' = 0$ and $n_3' = 1$ and integrating Eq. (1) over microcrack surfaces, the only two *non-vanishing* strain components are (for a single penny-shaped microcrack contribution)

$$e_4'^* = \frac{1}{V}\frac{4\pi}{3}a^3\left[C_{21}'^{-1}(\bar{\tau}_5' - \bar{\tau}_5'^c) + C_{22}'^{-1}(\bar{\tau}_4' - \bar{\tau}_4'^c) + C_{23}'^{-1}(\bar{\tau}_3' - \bar{\tau}_3'^c)\right] \tag{10}$$

and

$$e_5'^* = \frac{1}{V}\frac{4\pi}{3}a^3\left[C_{11}'^{-1}(\bar{\tau}_5' - \bar{\tau}_5'^c) + C_{12}'^{-1}(\bar{\tau}_4' - \bar{\tau}_4'^c) + C_{13}'^{-1}(\bar{\tau}_3' - \bar{\tau}_3'^c)\right] \tag{11}$$

From Eqs. (2), (10) and (11), the only *non-vanishing* components of a single *closed* microcrack induced inelastic compliance matrix are

$$S_{43}'^* = \frac{1}{V}\frac{4\pi}{3}a^3\left[C_{23}'^{-1} - C_{33}'^{-1}H_1'\right] \quad ; \quad S_{44}'^* = \frac{1}{V}\frac{4\pi}{3}a^3\left[C_{22}'^{-1} - C_{32}'^{-1}H_1'\right] \tag{12}$$

$$S_{45}'^* = \frac{1}{V}\frac{4\pi}{3}a^3\left[C_{21}'^{-1} - C_{31}'^{-1}H_1'\right] \quad ; \quad S_{53}'^* = \frac{1}{V}\frac{4\pi}{3}a^3\left[C_{13}'^{-1} - C_{33}'^{-1}H_2'\right] \tag{13}$$

$$S_{54}'^* = \frac{1}{V}\frac{4\pi}{3}a^3\left[C_{12}'^{-1} - C_{32}'^{-1}H_2'\right] \quad ; \quad S_{55}'^* = \frac{1}{V}\frac{4\pi}{3}a^3\left[C_{11}'^{-1} - C_{31}'^{-1}H_2'\right] \tag{14}$$

where

$$H_1' \equiv \frac{C_{23}'^{-1} - \mathrm{sgn}(\bar{\tau}_4')\eta C_{22}'^{-1} - \mathrm{sgn}(\bar{\tau}_5')\eta C_{21}'^{-1}}{C_{33}'^{-1} - \mathrm{sgn}(\bar{\tau}_4')\eta C_{32}'^{-1} - \mathrm{sgn}(\bar{\tau}_5')\eta C_{31}'^{-1}} \tag{15}$$

$$H_2' \equiv \frac{C_{13}'^{-1} - \mathrm{sgn}(\bar{\tau}_4')\eta C_{12}'^{-1} - \mathrm{sgn}(\bar{\tau}_5')\eta C_{11}'^{-1}}{C_{33}'^{-1} - \mathrm{sgn}(\bar{\tau}_4')\eta C_{32}'^{-1} - \mathrm{sgn}(\bar{\tau}_5')\eta C_{31}'^{-1}} \tag{16}$$

The other components $S_{ij}'^* = 0$. Therefore, it is clear that the inelastic compliance matrix $S_{ij}'^*$ and the overall compliance matrix $\bar{S}_{ij}$, in general, do not remain symmetric when frictional slidings occur on closed microcrack surfaces. It is noted that when microcracks experience frictionless sliding, i.e. $\eta = 0$, Eqs. (12) to (16) show that $S_{34}'^* = 0$, $S_{53}'^* = 0$, and $S_{45}'^* = S_{54}'^*$ and the symmetry of $S_{ij}'^*$ recovers. It can be easily shown that the inelastic compliance matrix, $S_{ij}'^*$, reduces to Horii and Nemat-Nasser's (1983) solutions if two-dimensional analysis is performed.

V.2.2. Solution of a single microcrack opening displacements

The *non-symmetry* of overall compliance matrices has been shown in the previous section when some microcracks are closed and undergo frictional sliding. Therefore, the method of obtaining

microcrack opening displacements (or simply C'_{ij} components) in anisotropic materials as described in Part I of this work (Ju and Lee (1990)) cannot be directly applied. Certain modifications have to be made to accommodate the non-symmetry of compliance matrix. It is emphasized that the framework developed in this section is valid for *both* open and closed penny-shaped microcracks.

The solution procedure outlined in what follows is based on Lekhnitskii's (1950) theory of anisotropic elasticity. Once the *characteristic equation* to the *non-symmetric* compliance is obtained, Hoenig's solutions (1978, 1982) for analyzing displacements and stress fields of penny-shaped microcracks can be modified to evaluate microcrack induced inelastic compliance.

We shall consider a general anisotropic linear elastic body under equilibrium conditions in the absence of body forces. Assume that the generalized plane deformation condition, defined by Lekhnitskii (1950), is met. Hence, equations of equilibrium in the two-dimensional line crack coordinate system, Fig. 1(c), are (in Voigt's notations):

$$\begin{aligned} \frac{\partial \bar{\tau}''_1}{\partial x''} + \frac{\partial \bar{\tau}''_6}{\partial y''} &= 0 \\ \frac{\partial \bar{\tau}''_6}{\partial x''} + \frac{\partial \bar{\tau}''_2}{\partial y''} &= 0 \\ \frac{\partial \bar{\tau}''_5}{\partial x''} + \frac{\partial \bar{\tau}''_4}{\partial y''} &= 0 \end{aligned} \tag{17}$$

with

$$\bar{\tau}''_3 = -\frac{\left(\bar{S}''_{31}\bar{\tau}''_1 + \bar{S}''_{32}\bar{\tau}''_2 + \bar{S}''_{34}\bar{\tau}''_4 + \bar{S}''_{35}\bar{\tau}''_5 + \bar{S}''_{36}\bar{\tau}''_6\right)}{\bar{S}''_{33}} \tag{18}$$

Further, the constitutive equations for the line crack are

$$\bar{e}''_i = \bar{S}''_{ij}\bar{\tau}''_j \tag{19}$$

where $\bar{S}''_{ij} \neq \bar{S}''_{ji}$ in general. We introducing two stress functions, $F(x'', y'')$ and $\Psi(x'', y'')$, such that stresses are

$$\bar{\tau}''_1 = \frac{\partial^2 F}{\partial y''^2}, \qquad \bar{\tau}''_2 = \frac{\partial^2 F}{\partial x''^2} \tag{20}$$

$$\bar{\tau}''_6 = -\frac{\partial^2 F}{\partial x'' \partial y''}, \quad \bar{\tau}''_5 = \frac{\partial \Psi}{\partial y''}, \quad \bar{\tau}''_4 = -\frac{\partial \Psi}{\partial x''} \tag{21}$$

By substituting Eqs. (20) and (21) into the constitutive equations (19) and then utilizing compatibility conditions, we obtain the following two differential equations:

$$\begin{aligned} L_3^{(2)} F(x'', y'') + L_2 \Psi(x'', y'') &= 0 \\ L_4 F(x'', y'') + L_3^{(1)} \Psi(x'', y'') &= 0 \end{aligned} \tag{22}$$

where L_i are the i-th differential operators defined by

$$L_2 \equiv M''_{44}\frac{\partial^2}{\partial x''^2} - (M''_{45} + M''_{54})\frac{\partial^2}{\partial x'' \partial y''} + M''_{55}\frac{\partial^2}{\partial y''^2} \tag{23}$$

$$L_3^{(1)} \equiv -M''_{24}\frac{\partial^3}{\partial x''^3} + (M''_{25} + M''_{64})\frac{\partial^3}{\partial x''^2 \partial y''} - (M''_{14} + M''_{65})\frac{\partial^3}{\partial x'' \partial y''^2} + M''_{15}\frac{\partial^3}{\partial y''^3} \tag{24}$$

$$L_3^{(2)} \equiv -M''_{42}\frac{\partial^3}{\partial x''^3} + (M''_{52} + M''_{46})\frac{\partial^3}{\partial x''^2 \partial y''} - (M''_{41} + M''_{56})\frac{\partial^3}{\partial x'' \partial y''^2} + M''_{51}\frac{\partial^3}{\partial y''^3} \tag{25}$$

$$L_4 \equiv M''_{22}\frac{\partial^4}{\partial x''^4} - (M''_{26}+M''_{62})\frac{\partial^4}{\partial x''^3 \partial y''} + (M''_{12}+M''_{21}+M''_{66})\frac{\partial^4}{\partial x''^2 \partial y''^2} - (M''_{16}+M''_{61})\frac{\partial^4}{\partial x'' \partial y''^3} + M''_{11}\frac{\partial^4}{\partial y''^4} \tag{26}$$

The newly introduced coefficient matrix M''_{ij} is defined as

$$M''_{ij} \equiv \bar{S}''_{ij} - \frac{\bar{S}''_{i3}\bar{S}''_{3j}}{\bar{S}''_{33}}, \qquad \text{for} \quad i, j = 1, 2, 4, 5, 6 \tag{27}$$

After some simple algebraic manipulations to Eqs. (22), two independent sixth-order partial differential equations of the stress functions, $F(x'', y'')$ and $\Psi(x'', y'')$, respectively, can be written as

$$\begin{aligned} \left(L_4 L_2 - L_3^{(1)} L_3^{(2)}\right) F(x'', y'') &= 0 \\ \left(L_4 L_2 - L_3^{(1)} L_3^{(2)}\right) \Psi(x'', y'') &= 0 \end{aligned} \tag{28}$$

The characteristic equation of these two differential equations is given by (with μ denoting the roots)

$$l_4(\mu)\, l_2(\mu) - l_3^{(1)}(\mu)\, l_3^{(2)}(\mu) = 0 \tag{29}$$

where $l_i(\mu)$ functions are

$$l_2(\mu) \equiv M''_{55}\mu^2 - (M''_{45} + M''_{54})\mu + M''_{44} \tag{30}$$

$$l_3^{(1)}(\mu) \equiv M''_{15}\mu^3 - (M''_{14} + M''_{65})\mu^2 + (M''_{25} + M''_{64})\mu - M''_{24} \tag{31}$$

$$l_3^{(2)}(\mu) \equiv M''_{51}\mu^3 - (M''_{41} + M''_{56})\mu^2 + (M''_{52} + M''_{46})\mu - M''_{42} \tag{32}$$

$$l_4(\mu) \equiv M''_{11}\mu^4 - (M''_{16} + M''_{61})\mu^3 + (M''_{12} + M''_{21} + M''_{66})\mu^2 - (M''_{26} + M''_{62})\mu + M''_{22} \tag{33}$$

Notice that Eqs. (30) – (33) are the non-symmetric counterparts of Eqs. (19) in Part I for symmetric compliance. In addition, Eq. (29) is a sixth-order polynomial equation and has six roots. These roots μ_i govern the structure of stress functions. The theorems in Lekhnitskii (1950), defining the nature of these six roots, are valid even for a non-symmetric compliance matrix $\tilde{\mathbf{S}}''$. Accordingly, these roots μ_i are always complex and occur as three pairs of complex conjugates. By taking the three distinct roots μ_i ($i = 1, 2, 3$) with *positive* imaginary parts ($\mathrm{Im}(\mu_i) > 0$), the stress functions can be expressed as

$$F(x'', y'') = 2\,\mathrm{Re}\left[\sum_{i=1}^{3} F(z_i'')\right] \tag{34}$$

$$\Psi(x'', y'') = 2\,\mathrm{Re}\left[\sum_{i=1}^{3} \lambda_i \frac{dF(z_i'')}{dz_i''}\right] \tag{35}$$

where

$$z_i'' \equiv x'' + \mu_i\, y'', \quad \text{and} \quad \lambda_i \equiv -\frac{l_3^{(2)}(\mu_i)}{l_2(\mu_i)} \tag{36}$$

The equilibrium and compatibility conditions are automatically satisfied if these two equations, (34) and (35) are used to represent stresses in Eqs. (20) and (21). It can be shown that the p_{ij} matrix takes the following form:

$$\begin{aligned} p_{1i} &= M_{11}''\mu_i^2 + M_{12}'' - M_{16}''\mu_i + \lambda_i(-M_{14}'' + M_{15}''\mu_i) \\ p_{2i} &= M_{21}''\mu_i + \frac{M_{22}''}{\mu_i} - M_{26}'' + \lambda_i\left(-\frac{M_{24}''}{\mu_i} + M_{25}''\right) \\ p_{3i} &= M_{41}''\mu_i + \frac{M_{42}''}{\mu_i} - M_{46}'' + \lambda_i\left(-\frac{M_{44}''}{\mu_i} + M_{45}''\right) \end{aligned} \tag{37}$$

It is observed that Eqs. (37) are the same as Eqs. (22) in Part I (Ju and Lee (1990)). Consequently, similar to Part I of this work, the C_{ij}'-matrix can be derived as

$$C_{ij}' = \frac{1}{4}\int_0^{2\pi} \left\{\mathrm{Im}\left[p_{kl}N_{lm}^{-1}\right]\right\}^{-1} R_{ki}R_{mj}\,d\phi' \tag{38}$$

where N_{ij} and R_{ij} are

$$\mathbf{N} \equiv \begin{bmatrix} -\mu_1 & -\mu_2 & -\mu_3 \\ 1 & 1 & 1 \\ -\lambda_1 & -\lambda_2 & -\lambda_3 \end{bmatrix} \tag{39}$$

$$\mathbf{R} \equiv (\gamma^2\cos^2\phi' + \sin^2\phi')^{-1/4} \begin{bmatrix} \gamma\cos\phi' & \sin\phi' & 0 \\ 0 & 0 & \sqrt{\gamma^2\cos^2\phi' + \sin^2\phi'} \\ \sin\phi' & -\gamma\cos\phi' & 0 \end{bmatrix} \tag{40}$$

Therefore, the inelastic compliance matrix S'^{*}_{ij} induced by a single *closed sliding* microcrack (embedded in an anisotropic solid with non-symmetric overall compliance) is now completely defined by substituting Eq. (38) into Eqs. (12)–(14). If some microcracks are open while others are closed (such that the overall compliance is still non-symmetric), then the inelastic compliance matrix S'^{*}_{ij} induced by a single *open* microcrack is completely defined by Eqs. (31) and (36) in Part I of this work, with the understanding that the characteristic equation (29) in Part II should be employed instead of Eq. (18) in Part I. Of course, if *all* microcracks are *open* and therefore the overall compliance is symmetric, then Eqs. (31) and (36) in Part I together with Eq. (18) in Part I can be employed to evaluate the inelastic compliance matrix S'^{*}_{ij}, as outlined in Part I of this work. In fact, if the overall compliance is symmetric, then $l_3^{(1)}$ and $l_3^{(2)}$ are equal and hence the derivations in this section yield exactly the same results as in Part I.

Finally, the inelastic compliance matrix $\tilde{\mathbf{S}}^{*}$ due to many distributed microcracks can be obtained by using Eqs. (40)–(44) in Part I. Therefore, the overall compliance matrix is obtained by simply adding $\tilde{\mathbf{S}}^{*}$ to the elastic compliance $\tilde{\mathbf{S}}^{o}$. A "non-process" micromechanical damage model is hence completed. Extensions to account for microcrack kinetics (i.e. "process damage models") will be discussed in the following sections.

V.3. Cleavage 1 microcrack growth

As discussed in Part I of this work, if fracture criterion is met for some microcracks under certain loadings, then those microcracks will grow in size. This is precisely the "cleavage 1" deformation process and is certainly different from non-process damage models. As in Part I, it is assumed that microcrack growth along the weak plane (an interface or inter-granular plane) is instantaneous (from its initial size a_0 to a final size a_f) and is in a self-similar fashion. Microcrack kinking into the matrix material will be considered in Section 4. Further, as noted in Section 4.1 of Part I, the Mixed Mode fracture criterion is defined by comparing the average value of the energy release rate G' over the entire edge of a penny-shaped microcrack against a critical value. The difficulty in determining the average value of G' in self-consistent analyses is also stated in Part I. For simplicity, the following Mixed Mode fracture criterion is used:

$$\left(\frac{K_{\mathrm{I}}'}{K_{\mathrm{Ic}}^{\mathrm{if}}}\right)^2 + \left(\frac{K_{\mathrm{II}}'}{K_{\mathrm{IIc}}^{\mathrm{if}}}\right)^2 = 1 \tag{41}$$

where $K_{\mathrm{Ic}}^{\mathrm{if}}$ and $K_{\mathrm{IIc}}^{\mathrm{if}}$ are the Mode I and Mode II critical stress intensity factors at the interface (or other weak plane), respectively.

For open microcracks under tensile loadings, microcrack growth kinetics has been outlined in Section 4.2 in Part I. In the following sections, we consider a Mode II fracture criterion for closed sliding microcracks under compression and mixed open/ closed microcrack growth kinetics under various loading conditions. The derivations basically follow the work of Fanella and Krajcinovic (1988).

V.3.1. Fracture criterion for a closed sliding microcrack

When a microcrack is closed and undergoes frictional sliding, there is no Mode I component and therefore Eq. (41) reduces to the Mode II fracture criterion:

$$K_{\mathrm{II}}' = K_{\mathrm{IIc}}^{\mathrm{if}} \tag{42}$$

For a penny-shaped microcrack, the Mode II stress intensity factor can be calculated from shear

stress as

$$K'_{II} = \frac{4}{2-\nu}\sqrt{\frac{a}{\pi}}\,|\bar{\tau}'_4 + \mathrm{sgn}(\bar{\tau}'_4)\,\eta\bar{\tau}'_3| \tag{43}$$

Attention is focused on triaxial loadings, with q denoting the axial compression and q^* denoting the lateral stress, respectively. Compression is taken as *negative* here. Thus, the normal stress $\bar{\tau}'_3$ and the shear stress $\bar{\tau}'_4$ can be calculated from loading stresses as

$$\bar{\tau}'_3 = q^* \sin^2\theta + q\cos^2\theta \tag{44}$$

$$\bar{\tau}'_4 = (q - q^*)\sin\theta\cos\theta \tag{45}$$

where θ defines the microcrack orientation. As previously indicated, the normal stress $\bar{\tau}'_3$ must be in compression if a microcrack is closed. Moreover, the sliding condition requires that

$$|\bar{\tau}'_4| \geq |\eta\ \bar{\tau}'_3| \tag{46}$$

By substituting Eqs. (44) and (45) into Eq. (43) and letting $K'_{II} = K^{if}_{IIc}$, we arrive at

$$K^{if}_{IIc} = \frac{4}{2-\nu}\sqrt{\frac{a}{\pi}}\,\left|(q - q^*)\sin\theta\cos\theta + \mathrm{sgn}(\bar{\tau}'_4)\eta(q^*\sin^2\theta + q\cos^2\theta)\right| \tag{47}$$

Since microcrack sizes randomly vary within the range $\left[a_{0_{min}}, a_{0_{max}}\right]$, the maximum microcrack size $a_{0_{max}}$ should be used in Eq. (47) instead of a in order to determine the critical domain of unstable microcrack growth. Therefore, Eqs. (42) and (47) render the orientations θ_u at which the largest microcracks become unstable (under Mode II) and increase in size:

$$\theta_{u_{1,2}} = \tan^{-1}\left[\frac{-(q-q^*) \pm \sqrt{(q-q^*)^2 - 4\left(K^{if}_{IIc}\frac{(2-\nu)}{4}\sqrt{\frac{\pi}{a_{0_{max}}}} - \eta q^*\right)\left(K^{if}_{IIc}\frac{(2-\nu)}{4}\sqrt{\frac{\pi}{a_{0_{max}}}} - \eta q\right)}}{2\left(K^{if}_{IIc}\frac{(2-\nu)}{4}\sqrt{\frac{\pi}{a_{0_{max}}}} - \eta q^*\right)}\right] \tag{48}$$

The above equation is exactly the same as Eq. (15) in Fanella and Krajcinovic (1988). As they pointed out, the unstable microcrack growth begins at a preferred orientation θ_{u_0}, which is determined by minimizing the axial compression q in Eq. (47):

$$\theta_{u_0} = \tan^{-1}\left[\eta + \sqrt{\eta^2 + 1}\right] \tag{49}$$

The corresponding axial compressive stress is denoted by q_0. The q value in Eq. (48) is assumed to be greater than q_0.

In addition, at a specified microcrack orientation θ within the range $[\theta_{u_1}, \theta_{u_2}]$, the minimum microcrack radius $a_0(\theta)$ required to activate Mode II growth can be evaluated from Eq. (48):

$$a_0(\theta) = \frac{\pi \left(\frac{2-\nu}{4} K_{II}^{cf}\right)^2}{\left[|q - q^*| \sin\theta\cos\theta + \eta(q^* \sin^2\theta + q\cos^2\theta)\right]^2} \tag{50}$$

V.3.2. Mixed open/ closed microcrack kinetics

"Cleavage 1" open microcrack kinetics under tensile loadings within the context of three-dimensional self-consistent analysis has been presented in detail in Part I. When combined triaxial compressive/ tensile loadings are applied, microcrack kinetic equations are more complicated. In particular, under combined compressive/ tensile loadings, some microcracks are open (in Mixed Mode) while others are closed (either undergoing frictional sliding or frictional sticking– no discontinuities). In this section, we investigate microcrack kinetics in various loading conditions. It is assumed that the lateral stress q^* is held constant while the axial stress q varies.

Case I. If the axial loading q and the lateral confinement q^* are both tensile (positive), we refer to Section 4.2 of Part I for the appropriate microcrack kinetics.

Case II. If both the axial and lateral stresses are compressive ($q \leq 0$ and $q^* \leq 0$), the normal stress $\tilde{\tau}_3'$ is always negative for any orientation and therefore all microcracks are *closed*. The sliding condition, Eq. (46), then leads to

$$|q - q^*| \sin\theta\cos\theta + \eta(q^* \sin^2\theta + q\cos^2\theta) = 0 \tag{51}$$

The angles $\theta_{s_{1,2}}$ defining the sliding domain are obtained by solving the above equation (51)

$$\theta_{s_{1,2}} = \tan^{-1}\left[\frac{(q - q^*) \pm \sqrt{(q - q^*)^2 - 4\eta^2 q^* q}}{2\eta q^*}\right] \tag{52}$$

Eq. (51) can be recast in the following form:

$$q = q^* \frac{\tan\theta(\eta\tan\theta + 1)}{\tan\theta - \eta} \tag{53}$$

The minimum value of q is obtained at $\theta_0 = \tan^{-1}[\eta + \sqrt{\eta^2 + 1}]$, at which frictional sliding of microcrack faces first begins. Clearly, this angle θ_0 is exactly the same as θ_{u_0} in Eq. (49). This implies that both sliding and Mode II growth of the largest microcracks begin from the same orientation θ_0. Furthermore, there are three different possibilities (domains) regarding microcrack states (see previous equations for definitions of various angles):

(i) Microcracks are closed, *without* frictional sliding, and *stationary* (no growth) if $0 \leq \theta \leq \theta_{s_1}$ or $\theta_{s_2} \leq \theta \leq \frac{\pi}{2}$. Microcrack sizes are irrelevant in this case. These microcracks have no contribution whatsoever to inelastic strain or compliance.

(ii) Microcracks are closed, *with* frictional sliding, and *stationary* if $\theta_{s_1} \leq \theta \leq \theta_{u_1}$, $\theta_{u_2} \leq \theta \leq \theta_{s_2}$ (sizes irrelevant), *or* $\theta_{u_1} \leq \theta \leq \theta_{u_2}$ and $a \leq a_0(\theta)$. The inelastic compliances due to these microcracks can be easily evaluated by using Eqs. (12), (13), (14), and (38). One should employ the initial microcrack sizes a_0 in the aforementioned equations. Specifically, one needs to perform the following integrations (assuming uniform probability):

$$\bar{S}_{ij}^{*s} = \frac{N_c}{V} \frac{1}{2\pi(a_{0_{\max}} - a_{0_{\min}})} \left[\int_{\theta_{s_1}}^{\theta_{u_1}} \int_0^{2\pi} \int_{a_{0_{\min}}}^{a_{0_{\max}}} S_{ij}^{*(k)}(a, \phi, \theta) \sin\theta da\, d\phi\, d\theta \right.$$

$$\left. + \int_{\theta_{u_2}}^{\theta_{s_2}} \int_0^{2\pi} \int_{a_{0_{\min}}}^{a_{0_{\max}}} S_{ij}^{*(k)}(a, \phi, \theta) \sin\theta da\, d\phi\, d\theta + \int_{\theta_{u_1}}^{\theta_{u_2}} \int_0^{2\pi} \int_{a_{0_{\min}}}^{a_0(\theta)} S_{ij}^{*(k)}(a, \phi, \theta) \sin\theta da\, d\phi\, d\theta \right] \quad (54)$$

(iii) Microcracks are closed, *with* frictional sliding, and undergoing Mode II *growth* if $\theta_{u_1} \leq \theta \leq \theta_{u_2}$ and $a \geq a_0(\theta)$. Similar to (ii), The inelastic compliances due to these unstable microcracks can be integrated by using Eqs. (12), (13), (14), and (38). Nevertheless, one should employ the final microcrack sizes a_f in those equations ($a_f = a_0/\rho$, see Part I). Specifically, one needs to perform the following integration:

$$\bar{S}_{ij}^{*u} = \frac{N_c}{V} \frac{1}{2\pi(a_{0_{\max}} - a_{0_{\min}})\rho^3} \left[\int_{\theta_{u_1}}^{\theta_{u_2}} \int_0^{2\pi} \int_{a_0(\theta)}^{a_{0_{\max}}} S_{ij}^{*(k)}(a, \phi, \theta) \sin\theta da\, d\phi\, d\theta \right] \quad (55)$$

See Fig. 2(a) for a schematic representation. To obtain the overall compliance matrix, simply add $\bar{\mathbf{S}}^{*s}$ and $\bar{\mathbf{S}}^{*u}$ to the elastic compliance $\bar{\mathbf{S}}^{o}$.

Case III. If the axial stress q is compressive (negative) and the lateral stress q^* is tensile (positive, but relatively *small*), then the condition $\bar{\tau}_3' = 0$ yields

$$\theta_m = \tan^{-1}\sqrt{-\frac{q}{q^*}} \tag{56}$$

If $\theta_m \leq \theta \leq \frac{\pi}{2}$, Eq. (44) indicates that the normal stresses are tensile and therefore microcracks are open. On the other hand, if $0 \leq \theta \leq \theta_m$, then microcracks are closed. As a consequence, we have mixed open/ closed microcracks in a representative volume element.

For *closed* microcracks, the frictional sliding condition (46) yields the critical sliding angle bound:

$$\theta_s = \tan^{-1}\left[\frac{(q-q^*)+\sqrt{(q-q^*)^2+4\eta^2 q^* q}}{2\eta q^*}\right] \tag{57}$$

There is only one solution for θ_s since we require $\theta_s > 0$. This θ_s value is in fact the *lower* angle bound for closed microcrack sliding under combined compression/ tension loading. The *upper* angle bound for frictional sliding is simply θ_m given in (56). The Mode II fracture criterion and stable/ unstable microcrack domains of closed microcracks are similar to previous formulas. For *open* microcracks, similarly, the Mixed Mode fracture criterion and stable/ unstable domains are previously given in Section 4 of Part I.

Moreover, there are five different possibilities (domains) regarding microcrack states (see previous equations for definitions of various angles):

(i) Microcracks are *closed*, *stick* and *stationary* if $0 \leq \theta \leq \theta_s$. These microcracks have no contribution to $\tilde{\mathbf{S}}^*$ at all.

(ii) Microcracks are *closed*, *sliding* and *stationary* if $\theta_s \leq \theta \leq \theta_{u_1}, \theta_{u_2} \leq \theta \leq \theta_m$ (sizes irrelevant), *or* $\theta_{u_1} \leq \theta \leq \theta_{u_2}$ and $a \leq a_0(\theta)$ (see Eq. (50)). The inelastic compliances due to these microcracks can be evaluated by using Eqs. (12), (13), (14), and (38). The initial microcrack sizes a_0 should be used in the aforementioned equations. In particular, one needs to perform the following integrations:

$$\tilde{S}_{ij}^{*sII} = \frac{N_c}{V}\frac{1}{2\pi(a_{0_{max}} - a_{0_{min}})}\left[\int_{\theta_s}^{\theta_{u_1}}\int_0^{2\pi}\int_{a_{0_{min}}}^{a_{0_{max}}} S_{ij}^{*(k)}(a,\phi,\theta)\sin\theta da\, d\phi\, d\theta\right.$$

$$+\int_{\theta_{u_2}}^{\theta_m}\int_0^{2\pi}\int_{a_{0_{\min}}}^{a_{0_{\max}}} S_{ij}^{*(k)}(a,\phi,\theta)\sin\theta da\, d\phi\, d\theta + \int_{\theta_{u_1}}^{\theta_{u_2}}\int_0^{2\pi}\int_{a_{0_{\min}}}^{a_0(\theta)} S_{ij}^{*(k)}(a,\phi,\theta)\sin\theta da\, d\phi\, d\theta\Bigg] \quad (58)$$

(iii) Microcracks are *closed, sliding* and *unstable* if $\theta_{u_1} \le \theta \le \theta_{u_2}$ and $a \ge a_0(\theta)$ (see Eq. (50)). The inelastic compliances due to these unstable microcracks can be again integrated by using Eqs. (12), (13), (14), and (38). The final microcrack sizes a_f should be adopted. In particular, one needs to perform the integration in Eq. (55).

(iv) Microcracks are *open* and *stationary* if $\theta^m_{u_{\max}} \le \theta \le \frac{\pi}{2}$, *or* $\theta^m_{u_{\min}} \le \theta \le \theta^m_{u_{\max}}$ and $a \le a_0^m(\theta)$ (see Eqs. (62), (63) & (66) in Part I). The inelastic compliances due to these microcracks can be evaluated by using Eq. (36) of Part I and Eq. (38) of Part II. The initial microcrack sizes a_0 should be used. We need to perform the following integrations:

$$\bar{S}_{ij}^{*sm} = \frac{N_c}{V}\frac{1}{2\pi(a_{0_{\max}} - a_{0_{\min}})}\Bigg[\int_{\theta^m_{u_{\max}}}^{\frac{\pi}{2}}\int_0^{2\pi}\int_{a_{0_{\min}}}^{a_{0_{\max}}} S_{ij}^{*(k)}(a,\phi,\theta)\sin\theta da\, d\phi\, d\theta + \int_{\theta^m_{u_{\min}}}^{\theta^m_{u_{\max}}}\int_0^{2\pi}\int_{a_{0_{\min}}}^{a_0^m(\theta)} S_{ij}^{*(k)}(a,\phi,\theta)\sin\theta da\, d\phi\, d\theta\Bigg] \quad (59)$$

(v) Microcracks are *open* and *unstable* if $\theta_m \le \theta \le \theta^m_{u_{\min}}$, *or* $\theta^m_{u_{\min}} \le \theta \le \theta^m_{u_{\max}}$ and $a \ge a_0^m(\theta)$ (see Eq. (66) in Part I). The inelastic compliances due to these microcracks can be evaluated by using Eq. (36) of Part I and Eq. (38) of Part II. The final microcrack sizes a_f should be used. The following integrations should be performed:

$$\bar{S}_{ij}^{*um} = \frac{N_c}{V}\frac{1}{2\pi(a_{0_{\max}} - a_{0_{\min}})\rho^3}\Bigg[\int_{\theta^m_{u_{\min}}}^{\theta^m_{u_{\max}}}\int_0^{2\pi}\int_{a_0^m(\theta)}^{a_{0_{\max}}} S_{ij}^{*(k)}(a,\phi,\theta)\sin\theta da\, d\phi\, d\theta + \int_{\theta_m}^{\theta^m_{u_{\min}}}\int_0^{2\pi}\int_{a_{0_{\min}}}^{a_{0_{\max}}} S_{ij}^{*(k)}(a,\phi,\theta)\sin\theta da\, d\phi\, d\theta\Bigg] \quad (60)$$

See Fig. 2(b) for a schematic representation. To obtain the overall compliance matrix, simply add up all inelastic compliances and the elastic compliance $\bar{\mathbf{S}}^o$.

V.4. Microcrack kinking under compression

In Section 3, "cleavage 1" microcrack growth along certain weak planes are presented for brittle solids such as concrete, rocks, and ceramics. Those microcracks (with lengths a_f) are assumed to be *arrested* at the edge of inclusion particles (or grains) due to higher energy barriers offered by the matrix material or grains along different orientations. Under higher compression, however, it has been experimentally observed that those arrested microcracks may resume to propagate (kink) into the matrix material in a non-self-similar fashion. In particular, for concrete and rocks, microcrack kinking under compression were investigated by Nemat-Nasser and Horii (1982), Horii and Nemat-Nasser (1985, 1986), and Zaitsev (1983), etc. These kinked microcracks tend to line up in the direction parallel to the axial compression. Further, they typically grow gradually with increasing axial compression in a stable manner until certain lengths are attained, at which unstable growth begins and results in ultimate failure of the material.

The difficulties involved in analyzing kinked microcracks in three-dimension were discussed in detail by Fanella and Krajcinovic (1988). As they pointed out, there are no closed form solutions available for sliding and opening displacements for either three-dimensional or two-dimensional problems. Instead, approximate "equivalent two-dimensional microcrack systems" are available in the literature; see, Horii and Nemat-Nasser (1986), Zaitsev (1983), and Fanella and Krajcinovic (1988), etc. In particular, Fanella and Krajcinovic (1988) assume that a three-dimensional kinked microcrack can be approximated by a series of two-dimensional kinked cross-sections. The sliding and opening displacements of a three-dimensional kinked microcrack are approximately determined by averaging two-dimensional solutions along the rim of a 3-dimensional microcrack, Fig. 3(a) & 3(b) (see also Kachanov (1982)). The inelastic compliances induced by microcrack kinking can then be derived. In this section, we follow the procedures outlined in Fanella and Krajcinovic (1988) as well as the self-consistent framework.

V.4.1. Microcrack kinking criterion and approximate openings

For completeness, we summarize the relevant kinking equations given by Fanella and Krajci-

novic (1988) in what follows. By minimizing the sliding shear stress acting on any cross-section located at an angle β' (see Fig. 3(a) and 3(b)), it is found that the *onset* of kinking occurs when $\beta' = 0$, $\theta = \theta_0 = \theta_{u_0}$ and $a_f = a_{f_{max}}$ (the largest microcrack radius). The corresponding axial (compressive) kinking threshold stress q_0^k is

$$q_0^k = -\frac{(2-\nu)\sqrt{3\pi}K_{Ic}^c - 8\sqrt{a_f}\,q^*(\sin\theta_0\cos\theta_0 + \eta\sin^2\theta_0)}{8\sqrt{a_f}\,(\sin\theta_0\cos\theta_0 - \eta\cos^2\theta_0)} \tag{61}$$

where K_{Ic}^c is the critical Mode I stress intensity factor of the matrix material. It is assumed that the entire penny-shaped microcrack rim will start to kink once Eq. (61) is satisfied at $\beta' = 0$.

The orientation bounds for which the largest microcracks kink can be obtained from

$$\theta_{k_{1,2}} = \tan^{-1}\left[\frac{-(q-q^*) \pm \sqrt{(q-q^*)^2 - 4(A_1 - \eta q^*)(A_1 - \eta q)}}{(A_1 - \eta q^*)}\right] \tag{62}$$

where

$$A_1 \equiv \frac{\sqrt{3}(2-\nu)K_{Ic}^c}{8}\sqrt{\frac{\pi}{a_{f_{max}}}} \tag{63}$$

Moreover, the minimum microcrack size needed to activate kinking for a specified loading and orientation θ (between θ_{k1} and θ_{k2}) is given by

$$a_k(\theta) = \frac{3\pi}{64}\left[\frac{(2-\nu)K_{Ic}^c}{(q-q^*)\sin\theta\cos\theta - \eta(q^*\sin^2\theta + q\cos^2\theta)}\right]^2 \tag{64}$$

Instead of modeling the shear stress induced kink opening load as a concentrated load, Fanella and Krajcinovic (1988) assume that the tension is uniformly distributed on the equivalent 2-dimensional microcrack surface over a length of $2\alpha_k a_f \sin\theta$ (see (Fig. 3(c)) such that displacement singularities due to the point load is eliminated. The value α_k is determined by matching the Mode I stress intensity factor of the equivalent microcrack to the one numerically computed in Horii and Nemat-Nasser (1985). The average 2-dimensional kink microcrack opening (due to shear induced tensile load only) for an arbitrary cross-section at an angle β' is (Tada (1973), Fanella and Krajcinovic (1988))

$$\bar{v}'^k(\beta') = -\frac{4.8(1-\nu^2)}{\pi E}F_1(a_f, \theta, l)(\bar{\tau}_4' - \bar{\tau}_4'^c)\cos\beta' \tag{65}$$

where ν and E are the Poisson's ratio and Young's modulus of the *matrix* material, respectively; l is the kinked length which will be given later; and F_1 is defined as

$$F_1(a_f,\theta,l) \equiv \frac{\sin^{-1}\left(\frac{\alpha_k a_f \sin\theta}{\alpha_k a_f \sin\theta + l}\right)\sqrt{(\alpha_k a_f \sin\theta + l)^2 - (\alpha_k a_f \sin\theta)^2} + (\alpha_k a_f \sin\theta)\ln\left(\frac{\alpha_k a_f \sin\theta}{\alpha_k a_f \sin\theta + l}\right)}{\alpha_k \tan\theta} \tag{66}$$

Notice that only elastic material properties of the matrix are employed to evaluate the 2-dimensional average kink opening in Eq. (65) since kinked microcracks exist in the matrix only. However, within the context of the self-consistent method (at variance with Fanella and Krajcinovic (1988)), the microcrack-induced *anisotropy* of overall moduli does *indirectly affect* the kink opening because the shear stress $\bar{\tau}_4'^c$ transmitted across interface microcrack surfaces is a function of overall moduli; see Eqs. (7) and (9) for details. In addition, the sliding shear stress $[\bar{\tau}_4' - \bar{\tau}_4'^c]$ varies along the interface microcrack rim, too. Finally, the *average* 3-dimensional displacement components along the interface microcrack rim can be shown to be (in the interface microcrack coordinate system)

$$\begin{aligned}
\bar{u}_1'^k &= 0 \\
\bar{u}_2'^k &= \frac{9.6(1-\nu^2)}{\pi^2 E} F_1(a_f,\theta,l)\cos\theta(\bar{\tau}_4' + \mathrm{sgn}(\bar{\tau}_4')\eta\bar{\tau}_3'^c) \\
\bar{u}_3'^k &= -\frac{9.6(1-\nu^2)}{\pi^2 E} F_1(a_f,\theta,l)\sin\theta(\bar{\tau}_4' + \mathrm{sgn}(\bar{\tau}_4')\eta\bar{\tau}_3'^c)
\end{aligned} \tag{67}$$

V.4.2. Inelastic compliance due to kinked microcracks

In order to derive the kinked microcrack induced inelastic compliance, the shape of kinked microcrack has to be determined so that the integration of microcrack opening over the entire microcrack surface can be performed. *Since the kink length varies along the rim of the interface* penny-shaped microcrack, it is impossible to determine the 3-dimensional kinked microcrack shape in closed form. Therefore, in the present study, it is assumed that kinked microcracks are elliptical in shape. The two axes of an ellipse are taken as a_f and l (at $\beta = 0$) of a particular kinked microcrack. The loadings acting on a kinked microcrack surfaces actually have two components – (a) the normal tensile force due to frictional shear stress $[\bar{\tau}_4' - \bar{\tau}_4'^c]$, and (b) the lateral confinement loading

q^*. Specifically, the normal tension P at $\beta' = 0$ is evaluated from the shear stress as

$$P = -2a_f(\bar{\tau}_4' - \bar{\tau}_4'^c)\cos\theta \tag{68}$$

where $\bar{\tau}_4'$ and $\bar{\tau}_4'^c$ are previously given in Eqs. (45) and (7), respectively.

The solution of stress intensity factor of a line crack subjected to a concentrated load P acting at the center of the crack was given by Tada (1973). Assuming stable kinked microcrack growth, the Mode I critical stress intensity factor (of the matrix) at the kinked microcrack tip under the concentrated force P and uniform lateral loading q^* can be obtained as follows

$$K_{I_c}^c = -\frac{2a_f(\bar{\tau}_4' - \bar{\tau}_4'^c)\cos\theta}{\sqrt{\pi l}} + \sqrt{\pi l}q^* \tag{69}$$

Consequently, the kink length l (at $\beta' = 0$) can be derived from Eq. (69):

$$l = \frac{1}{\pi}\left(\frac{K_{I_c}^c + \text{sgn}(q^*)\sqrt{(K_{I_c}^c)^2 + 8q^* a_f(\bar{\tau}_4' - \bar{\tau}_4'^c)\cos\theta)}}{2q^*}\right)^2 \tag{70}$$

where $\text{sgn}(q^*) = -1$ or 1, depending on whether $q^* < 0$ or $q^* > 0$. If there is no confinement loading ($q^* = 0$), the kink length is re-derived from Eq. (69):

$$l = \frac{1}{\pi}\left(\frac{2a_f(\bar{\tau}_4' - \bar{\tau}_4'^c)\cos\theta}{K_{I_c}^c}\right)^2 \tag{71}$$

The inelastic compliance components induced by a kinked microcrack under loading P only are now derivable from Eqs. (67) and (70) or (71): (in the local interface microcrack coordinate system)

$$\mathbf{S}_p'^{*k} = A'^* \begin{bmatrix} 0 & 0 & 0 & 0 & 0 & 0 \\ 0 & 0 & \eta B_1'^* \cos^2\theta & -B_2'^* \cos^2\theta & 0 & 0 \\ 0 & 0 & \eta B_1'^* \sin^2\theta & -B_2'^* \sin^2\theta & 0 & 0 \\ 0 & 0 & -\eta B_1'^* \sin 2\theta & B_2'^* \sin 2\theta & 0 & 0 \\ 0 & 0 & 0 & 0 & 0 & 0 \\ 0 & 0 & 0 & 0 & 0 & 0 \end{bmatrix} \tag{72}$$

where

$$A'^* \equiv \frac{1}{V}\frac{4.8a_f l(1-\nu^2)}{\pi E} F_1(a_f, \theta, l) \tag{73}$$

and

$$B_1'^* \equiv \frac{C_{33}'^{-1}}{C_{33}'^{-1} - \eta C_{32}'^{-1}}, \qquad B_2'^* \equiv 1 - \frac{\eta C_{32}'^{-1}}{C_{33}'^{-1} - \eta C_{32}'^{-1}} \tag{74}$$

On the other hand, the inelastic compliance components induced by a kinked microcrack due to lateral load q^* only should be accounted for, too. To this end, we first note that the normal displacement jump of an elliptical shaped crack embedded in an isotropic matrix under uniform normal load is available from Budiansky and O'Connell (1976, p. 86): (in the kinked microcrack coordinate system)

$$u_3^{*k} = \frac{4(1-\nu^2)}{E}\frac{b}{\mathrm{E}(\bar{\mathrm{k}})}\sqrt{1-\frac{x^2}{a^2}-\frac{y^2}{b^2}}\,q^* \tag{75}$$

where $\mathrm{E}(\bar{\mathrm{k}})$ is the complete elliptic integral of the second kind; and $\bar{\mathrm{k}}$, a and b are defined as

$$\bar{\mathrm{k}} \equiv \sqrt{1-\frac{b^2}{a^2}}\,, \qquad \begin{cases} a = a_f, \quad b = l, & \text{if } l < a_f\,; \\ a = l, \quad b = a_f, & \text{if } l > a_f\,. \end{cases} \tag{76}$$

Therefore, the only non-zero component of the inelastic compliance matrix induced by a kinked microcrack under the load q^* is (in the kinked microcrack coordinate system):

$$S^{*k}_{33_c} = \frac{1}{V}\frac{16(1-\nu^2)}{3E}\frac{ab^2\pi}{\mathrm{E}(\bar{\mathrm{k}})} \tag{77}$$

It is emphasized that the inelastic compliance in Eq. (77) is evaluated in a *different* coordinate system from those in Eq. (72). Therefore, a proper coordinate transformation must be performed before these two inelastic compliances can be summed up. The kinked microcrack induced inelastic compliance matrix is

$$\bar{S}^{*k}_{ij} = \frac{N_c}{V}\frac{1}{2\pi(a_{0_{\max}}-a_{0_{\min}})}\int_{\theta_{k_1}}^{\theta_{k_2}}\int_0^{2\pi}\int_{a_k(\theta)}^{a_{0_{\max}}} S^{*k}_{ij}(l, a/\rho, \phi, \theta)\sin\theta\, da\, d\phi\, d\theta \tag{78}$$

where S^{*k}_{ij} is the sum of $S^{*k}_{ij_p}$ and $S^{*k}_{ij_c}$ in the global coordinate. Furthermore, the normal displacement of a kinked microcrack must retain a positive value since it is in an opening mode. The inelastic compliances due to many distributed kinked microcracks can be integrated straightforwards based on single microcrack expressions. It is noted that the procedures presented in this section are at variance with those presented in Fanella and Krajcinovic (1988).

V.5. A simple process model for microcrack nucleation

Our presentation so far is limited to the "cleavage 1" microcrack growth and kinking processes. Many brittle solids (such as concrete, rocks and ceramics), however, exhibit the "cleavage 2" microcrack nucleation phenomenon under higher loadings. That is, in addition to the growth and kinking of pre-existing microcracks, brittle solids may experience nucleation of *new* microcracks along preferred orientations, depending on the externally applied loads. These newly nucleated microcracks, of course, may grow in size later under higher loads.

To accommodate the foregoing mixed "cleavage 1" and "cleavage 2" deformation processes, a simple Zener-Stroh type microcrack nucleation mechanism under compressive loadings is incorporated into the proposed micromechanical process models. We refer to Stroh (1954, 1955) as well as Smith and Barnby (1967) for details. It is noted that a dilute (non-interactive) micromechanical microcrack nucleation model was proposed by Stojimirovic et al. (1987) for polycrystalline MgO ceramics.

The proposed "cleavage 2" model is based on the "critical shear stress criterion" of the Zener-Stroh type (under compression). It is assumed that the failure (debonding) stress τ_{bond} of the interfacial (or inter-granular) bond between the matrix and the inclusion (or between crystalline grains) is *lower* than failure stresses of the matrix and inclusion materials. That is, new microcracks are assumed to nucleate only at the interfaces (or inter-granular planes). The sizes of newly nucleated microcracks are proportional to the inclusion (grain) sizes (Ashby (1979)). Due to lack of a precise micromechanism to determine sizes of nucleated microcracks, it is further assumed that nucleated microcracks have the same initial sizes as pre-existing microcracks with the same statistical size distribution. The shear stress $\bar{\tau}_4'$ has previously been given in Eq. (45). By letting $\bar{\tau}_4' = \tau_{bond}$, the domain $[\theta_{n_1}, \theta_{n_2}]$, in which shear stresses exceed the critical debonding stress, is determined:

$$\theta_{n_{1,2}} = \tan^{-1}\left(\frac{-(q-q^*) \pm \sqrt{(q-q^*)^2 - 4\tau_{bond}^2}}{2\tau_{bond}}\right) \tag{79}$$

From Eq. (79), it is observed that microcrack nucleation first starts along the preferred orientation $\theta_{n_0} = 45°$, and that the nucleation domain later expands from the 45° line. Once these new

microcracks are generated, they are immediately checked against the criterion for frictional sliding. It is noted that, for any coefficient of friction $\eta > 0$, we have $\theta_{s_0} = \tan^{-1}[\eta + \sqrt{\eta^2 + 1}] > \theta_{n_0}$ (θ_{s_0} = the first sliding orientation). Therefore, nucleated microcracks are initially in frictional *stick* (no-slip) until the loading further increases so that the frictional sliding domain overlaps the microcrack nucleation domain. That is,

$$\theta_{s_1} < \theta_{n_2} = \tan^{-1}\left(\frac{-(q-q^*) + \sqrt{(q-q^*)^2 - 4\tau_{\text{bond}}^2}}{2\tau_{\text{bond}}}\right) \tag{80}$$

where θ_{s_1} is the lower angle limit of the frictional sliding domain. Subsequently, the microcrack fracture (growth) criterion and kinking criterion are applied to those newly nucleated (sliding) microcracks to check their stability. Accordingly, depending on the loading levels, the states and the corresponding domains of newly nucleated (sliding) microcracks are (assume $\theta \le \theta_{n_2} \le \theta_0$): (a) frictional sliding with initial sizes a_0 for $\theta_{s_1} \le \theta < \theta_{u_1}$, *or* $\theta_{u_1} \le \theta \le \theta_{n_2}$ and $a \le a_0(\theta)$; (b) frictional sliding with Mode II growth ($a = a_f$, the inclusion facet sizes) for $\theta_{u_1} \le \theta \le \theta_{k_1}$ and $a \ge a_0(\theta)$, *or* $\theta_{k_1} \le \theta \le \theta_{n_2}$ and $a_0(\theta) \le a \le a_k(\theta)$; and (c) microcrack kinking for $\theta_{k_1} \le \theta \le \theta_{n_2}$ and $a \ge a_k(\theta)$, etc.

In addition, the inelastic compliances induced by the newly nucleated microcracks are

$$\tilde{\mathbf{S}}^{*n} = \tilde{\mathbf{S}}^{*sn} + \tilde{\mathbf{S}}^{*un} + \tilde{\mathbf{S}}^{*kn} \tag{81}$$

where the superscripts s, u and k indicate the compliance contributions from the sliding microcracks ($a = a_0$), the Mode II growth microcracks ($a = a_f$), and the kinked microcracks, respectively. More specifically, we have

$$\tilde{S}_{ij}^{*n} = \frac{N_n}{V}\frac{1}{2\pi(a_{0_{\max}} - a_{0_{\min}})}\left[\int_{\theta_{s_1}}^{\theta_{n_2}}\int_0^{2\pi}\int_{a_{0_{\min}}}^{a_{0_{\max}}} S_{ij}^{*sn}(a,\phi,\theta)\sin\theta\, da\, d\phi\, d\theta + \int_{\theta_{u_1}}^{\theta_{n_2}}\int_0^{2\pi}\int_{a_{0_{\min}}}^{a_0(\theta)} S_{ij}^{*sn}(a,\phi,\theta)\sin\theta\, da\, d\phi\, d\theta\right.$$
$$\left. + \int_{\theta_{u_1}}^{\theta_{n_2}}\int_0^{2\pi}\int_{a_0(\theta)}^{a_{0_{\max}}} S_{ij}^{*un}(a/\rho,\phi,\theta)\sin\theta\, da\, d\phi\, d\theta + \int_{\theta_{k_1}}^{\theta_{n_2}}\int_0^{2\pi}\int_{a_k(\theta)}^{a_{0_{\max}}} S_{ij}^{*kn}(l,a/\rho,\phi,\theta)\sin\theta\, da\, d\phi\, d\theta\right] \tag{82}$$

Moreover, the average number (or density) of nucleated microcracks is needed. Obviously, the total number of pre-existing and nucleated microcracks is related to the total number of inclusions

(or grains) and their shapes. Therefore, the number of nucleated microcracks N_n has to be within the range

$$0 \leq N_n \leq (N_f N_a - N_c) \frac{\theta_{n_2} - \theta_{n_1}}{\pi/2} \tag{83}$$

where N_f, N_a, and N_c are the average number of facets on each inclusion (or grains), the average number of inclusions (or grains), and the average number of pre-existing microcracks, respectively. For instance, if $N_f = 7$ and $N_c = 3N_a$ (Krajcinovic and Fanella (1986)), then the number of nucleated microcracks obeys $0 \leq N_n \leq \frac{4N_a(\theta_{n_2} - \theta_{n_1})}{\pi/2}$.

V.6. Numerical procedures and experimental validation

In this section, we address the numerical procedures and computational algorithms involved in the proposed micromechanical models. Further, some comparisons of model predictions against experimental data are performed.

V.6.1. Numerical procedures

The computational algorithm needed to carry out the proposed micromechanical models under compressive loads is similar to that presented in Section 5 of Part I of this work. However, some modifications are warranted to implement the proposed models in Part II. Basically, at each loading step, the domains (angle bounds) defining various states of microcracks (e.g. frictional sliding, Mode II growth, Mixed Mode growth, kinking, and nucleation, etc.) must be determined and stored as *history variables*. Then, one needs to compute various microcrack-induced inelastic compliances by numerical integrations. Namely, one has to compute the inelastic compliance contributions from open (stable or mixed mode growth, $\bar{\mathbf{S}}^{*o}$), closed (sliding or Mode II growth, $\bar{\mathbf{S}}^{*c}$), kinked ($\bar{\mathbf{S}}^{*k}$), and nucleated ($\bar{\mathbf{S}}^{*n}$) microcracks. The sum of individual inelastic compliances in global coordinates is then added to the elastic compliance $\bar{S}^0_{ij}$. That is,

$$\bar{\mathbf{S}} = \bar{\mathbf{S}}^0 + \bar{\mathbf{S}}^{*o} + \bar{\mathbf{S}}^{*c} + \bar{\mathbf{S}}^{*k} + \bar{\mathbf{S}}^{*n} \tag{84}$$

where $\bar{\mathbf{S}}^{*o}$ is the sum of $\bar{\mathbf{S}}^{*sm}$ in (59) and $\bar{\mathbf{S}}^{*um}$ in (60); $\bar{\mathbf{S}}^{*c}$ is the sum of $\bar{\mathbf{S}}^{*sII}$ in (58) and $\bar{\mathbf{S}}^{*uII}$ in (55); $\bar{\mathbf{S}}^{*k}$ is given in (78); and $\bar{\mathbf{S}}^{*n}$ is given in (82).

Subsequently, an iterative procedure to find the overall compliance is performed as outlined in Part I.

V.6.2. Experimental validation

In this section, the proposed self-consistent micromechanical damage models are applied to concrete specimens under compressive loadings. In particular, three model simulations are carried out; i.e. a uniaxial compression test, a triaxial compression test, and an axial compression with small tensile lateral confinement. The Taylor's model analyses are also performed and compared with the proposed models under same loadings. Further, model predictions of uniaxial and triaxial compression tests are compared with available experimental data (Newman and Newman (1972)). The material properties used in these simulations are: the maximum and minimum aggregate sizes

= 0.75 in. (1.905 cm) and 0.19 in. (0.4826 cm), respectively; the initial microcrack size ratio $\rho = 0.72$; the volume fraction of coarse aggregates $f_v = 0.39$; the shape factor of aggregate $\alpha_v = 5$; the Young's modulus of virgin material $E = 5,800$ ksi (40,020 MPa) and Poisson's ratio $\nu = 0.2$; the critical stress intensity factors of the interface and matrix (K_{IIc}^{if}, K_{Ic}^{if} and K_{Ic}^{c}) = 300 psi$\sqrt{\text{in}}$ (0.33 MN/m$^{3/2}$), 150 psi$\sqrt{\text{in}}$ (0.165 MN/m$^{3/2}$), and 450 psi$\sqrt{\text{in}}$ (0.495 MN/m$^{3/2}$), respectively. Most of these values are taken from Newman and Newman (1972), Fanella and Krajcinovic (1988) and the references therein.

Figure 4 exhibits the experimental data of a uniaxial compression test (no post-peak curve) and model predictions (stress-strain curves) of both the present and the Taylor's models. It is observed that the analytical results agree well with experimental data (up to the peak strength point). The difference between the Taylor's and the present models is small because the initial microcrack density parameter $\omega_i \equiv \frac{N_c}{V} < a_i^3 >= 10.3\%\omega_c$ (Budiansky and O'Connell (1976), $\omega_c = 0.5625$ – the maximum allowable density for the self-consistent method) is relative small. When the initial microcrack density parameter ω_i increases, the differences between the two analytical results become more significant; see Fig. 5 for the case of $\omega_i = 14.70\%\omega_c$. In addition, Fig. 6 depicts the results of the proposed model for three different ω_i values. To further demonstrate the differences between the self-consistent and the Taylor's models, the overall compliance components $\bar{S}_{33}$, $\bar{S}_{13}$, and $\bar{S}_{31}$ (normalized by the corresponding elastic compliance components) are plotted against the normalized microcrack density parameters ω_i/ω_c in Figs. 7, 8 and 9, respectively.

To illustrate the effects of microcrack nucleation under uniaxial compression, the self-consistent prediction in Fig. 4 (with nucleation mechanism) is re-computed without nucleation mechanism; see Fig. 10 for details. The critical debonding shear stress τ_{bond} is taken as 3.0 ksi (20.67 MPa). The density of newly nucleated microcracks is taken as 50% of the initial microcrack density. It is seen that microcrack nucleation is important in the higher loading regions.

For triaxial compression test (with compressive lateral confinement $q^* = -0.5$ ksi, the results of the self-consistent model, the Taylor's model (both with nucleation mechanism), and experimental data are displayed in Figure 11. It is observed that the present model renders good agreement with the experimental data.

On the other hand, if a very small tensile lateral stress ($q^* = 0.1$ ksi or 0.689 MPa) is applied in addition to axial compression, the model predictions are very different from those of uniaxial and triaxial compression tests. See Fig. 12 for detailed stress-strain curves. In fact, by examining

the model predictions of three loading conditions in Figs. 4, Fig. 11, and Fig. 12, the effects of lateral confinement to material responses become apparent. This is primarily due to the Mode II microcrack growth and kinking mechanisms presented earlier. That is, the Mode II fracture and kinking threshold stresses and the kink lengths are quite different in uniaxial compression, triaxial compression, and axial compression with a small lateral tensile stress. As a consequence, the peak strengths and stress-strain curves (no post-peak portions) are significantly different in three loading cases. See also the discussions in Fanella and Krajcinovic (1988).

V.7. Conclusion

Within the framework of the self-consistent method, three-dimensional micromechanical damage models are presented for brittle solids under compressive loadings. Due to frictional sliding of closed microcracks, the damaged overall compliance matrices are non-symmetric in nature. The solutions of microcrack opening displacements in non-symmetric anisotropic solids are constructed. In addition to "cleavage 1" Mode II microcrack growth under compressive loadings, microcrack kinking and microcrack nucleation ("cleavage 2") mechanisms are also incorporated into the proposed models. Therefore, the proposed micromechanical damage models are physically meaningful. Moreover, experimental validation confirms the applicability of the proposed models to a class of brittle cementitious composite materials.

As commented in Part I, the differences between the self-consistent and Taylor's models are small for relatively low microcrack densities. At moderate microcrack density levels, however, the differences between the two models become more significant. Therefore, we conclude that Taylor's model is acceptable for low microcrack density levels, and the self-consistent model is more desirable for moderate microcrack concentrations.

V.8. References

1. ASHBY, M. F. , (1979), "Micromechanisms of Fracture in Static and Cyclic Failure", In: R. A. Smith, ed., *Fracture Mechanics, Current Status, Future Prospects*, Pergamon Press, Oxford, Vol. 1, pp. 1–27.

2. BUDIANSKY, B. AND O'CONNELL, R. J., (1976), "Elastic Moduli of a Cracked Solid", *Int. J. Solids & Struct.*, Vol. 12, pp. 81–97.

3. FANELLA, D. AND KRAJCINOVIC, D., (1988), "A Micromechanical Damage Model for Concrete in Compression", *Eng. Fract. Mech.*, Vol. 29, No. 1, pp. 49–66.

4. HOENIG, A., (1978), "The Behavior of a Flat Elliptical Crack in an Anisotropic Elastic Body", *Int. J. Solids & Struct.*, Vol 14, pp. 925–934.

5. HOENIG, A., (1982), "Near-Tip Behavior of a Crack in a Plane Anisotropic Elastic Body", *Eng. Fract. Mech.*, Vol. 16, No. 3, pp. 393–403.

6. HORII, H. AND NEMAT-NASSER, S., (1983), "Overall Moduli of Solids with Microcracks: Load-Induced Anisotropy", *J. Mech. Phy. Solids*, Vol. 31, No. 2, pp.155–171.

7. HORII, H. AND NEMAT-NASSER, S., (1985), "Compression-Induced Microcrack Growth in Brittle Solids: Axial Splitting and Shear Failure", *J. Geophy. Res.*, Vol. 90, No. B4, pp. 3105–3125.

8. HORII, H. AND NEMAT-NASSER, S., (1986), "Brittle Failure in Compression: Splitting, Faulting and Brittle-Ductile Transition", *Phil. Trans. Royal Soc. London*, Series A, Vol. 319, pp. 337–374.

9. JU, J. W. AND LEE, X., (1990), *On Three-Dimensional Self-Consistent Micromechanical Damage Models for Brittle Solids. Part I: Tensile Loadings*, submitted to *Journal of Engineering Mechanics*, ASCE, June 1990.

10. KACHANOV, M., (1982), "A Microcrack Model of Rock Inelasticity", *Mech. Mater.*, Vol. 1, pp. 19–27, 29–40.

11. KRAJCINOVIC, D. AND FANELLA, D., (1986), "A Micromechanical Damage Model for Concrete", *Eng. Fract. Mech.*, Vol. 25, No. 5/6, pp. 585–596.

12. LEKHNITSKII, S. G., (1950), *Theory of Elasticity of an Anisotropic Elastic Body*, by the Government Publishing House for Technical-Theoretical Works, Moscow and Leningrad, 1950; and by Holden-Day, Inc., San Francisco, 1963.

13. NEMAT-NASSER, S. AND HORII, H., (1982), "Compression-Induced Nonplanar Crack Extension with Application to Splitting, Exfoliation, and Rockburst", *J. Geophy. Res.*, Vol. 87, No. B8, pp. 6805–6821.

14. NEWMAN, J. B. AND NEWMAN, K., (1972), "The Cracking and Failure of Concrete under Combined Stresses and its Implications for Structural Design" in *The Deformation and Rupture of Solids Subjected to Multiaxial Stresses*, Vol. 1, Int. Symp. of RILEM, Cannes, pp. 149–168.

15. SMITH, E. AND BARNBY, J. T., (1967), "Crack Nucleation in Crystalline Solids", *Metal Science Journal*, Vol. 1, pp. 56–64.

16. STOJIMIROVIC, D., KRAJCINOVIC, D. AND SADOWSKI, T., (1987), "Constitutive Model for Polycrystalline MgO Ceramics", in *Constitutive Modeling for Nontraditional Materials*, Ed. by V. Stokes and D. Krajcinovic, AMD–Vol. 85, ASME, pp. 175–187.

17. STROH, A. N., (1954), "The Formation of Cracks as a Result of Plastic Flow", *Proc. Roy. Soc.*, [A], Vol. 223, pp. 404–414.

18. STROH, A. N., (1955), "The Formation of Cracks in Plastic Flow. II.", *Proc. Roy. Soc.*, [A], Vol. 232, pp. 548–560.

19. SUMARAC, D. AND KRAJCINOVIC, D., (1987), "A Self-Consistent Model for Microcrack-Weakened Solids", *Mech. Mater.*, Vol. 6, pp. 39–52.

20. TADA, H., (1973), *The Stress Analysis of Cracks handbook*, Del Research, Hellertown, PA.

21. ZAITSEV, Y. B., (1983), "Crack Propagation in a Composite Material", In: F. H. Wittmann, ed., *Fracture Mechanics of Concrete*, Elsevier, Amsterdam.

V.9. Figure captions and figures

Figure 1. (a) The local (primed) and global Cartesian coordinate systems, (b) the elliptical microcrack coordinate system, (c) the line microcrack tip coordinate system.

Figure 2. (a) Domains of sliding, Mode II growth, and kinking of microcracks under triaxial compression, (b) domains of open, mixed mode growth, sliding, Mode II growth, and kinking of microcracks under combined compression/ tension.

Figure 3. (a) 3-dimensional kinked microcrack, (b) 2-dimensional kinked microcrack system, (c) approximate equivalent 2-dimensional microcrack system.

Figure 4. Comparison of the self-consistent, the Taylor's, and experimental stress-strain curves for a uniaxial compression test; $\omega_i = 10.3\%\omega_c$.

Figure 5. Comparison of the self-consistent and the Taylor's simulated stress-strain curves for a uniaxial compression test; $\omega_i = 14.7\%\omega_c$.

Figure 6. Three simulated stress-strain curves for uniaxial compression by using the self-consistent method.

Figure 7. The normalized compliance $\bar{S}_{33}/\bar{S}^o_{33}$ vs. the normalized microcrack density parameter ω_i/ω_c.

Figure 8. The normalized compliance $\bar{S}_{13}/\bar{S}^o_{13}$ vs. the normalized microcrack density parameter ω_i/ω_c.

Figure 9. The normalized compliance $\bar{S}_{31}/\bar{S}^o_{31}$ vs. the normalized microcrack density parameter ω_i/ω_c.

Figure 10. Comparison of simulated responses by using the self-consistent method with and without, respectively, the microcrack nucleation mechanism for a uniaxial compression test; $\omega_i = 10.3\%\omega_c$.

Figure 11. Comparison of the self-consistent, the Taylor's, and experimental stress-strain curves for a triaxial compression test; $\omega_i = 10.3\%\omega_c$; $q^* = -0.5$ ksi.

Figure 12. Comparison of the self-consistent and the Taylor's simulated stress-strain curves for axial compression with very small tensile lateral stress; $\omega_i = 10.3\%\omega_c$; $q^* = 0.1$ ksi.

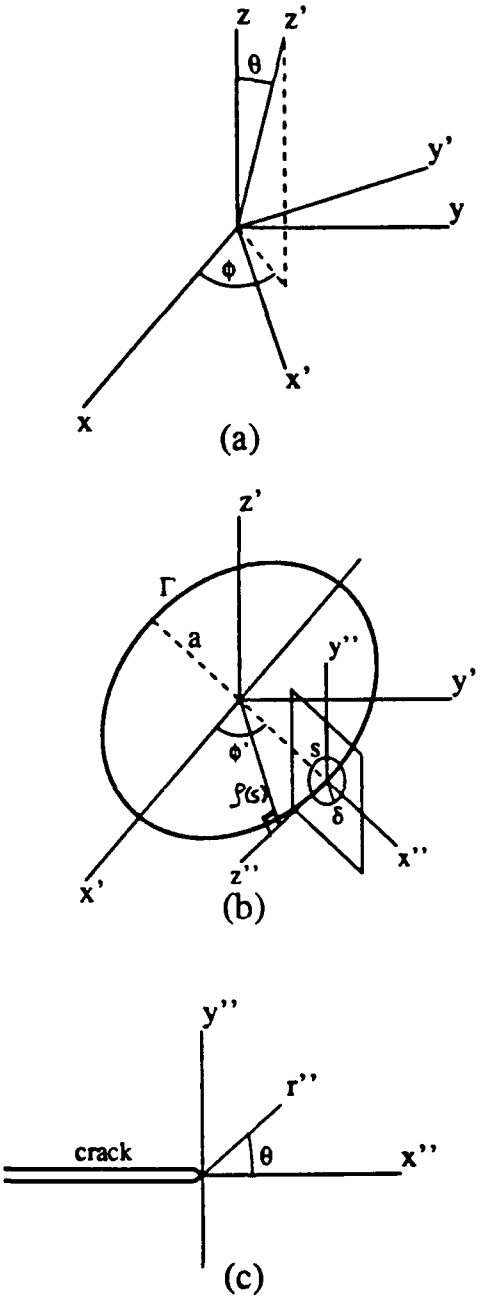

Figure 1. (a) The local (primed) and global Cartesian coordinate systems,
(b) the elliptical microcrack coordinate system,
(c) the line microcrack tip coordinate system.

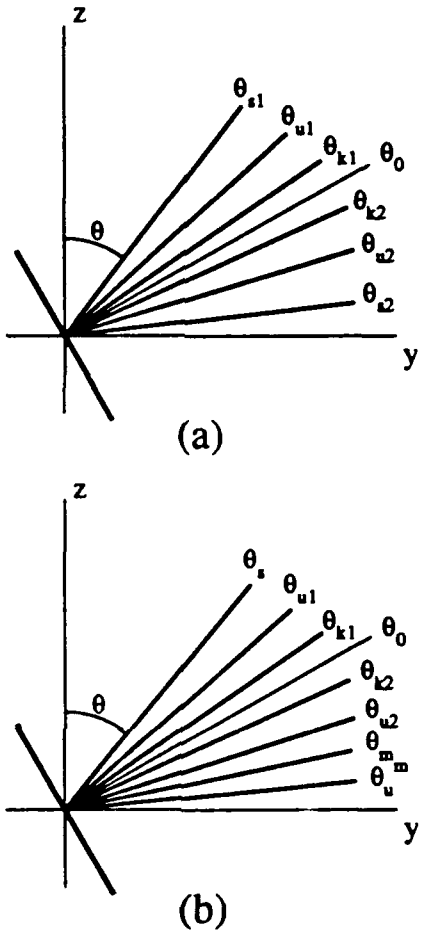

Figure 2. (a) Domains of sliding, Mode II growth, and kinking of microcracks under triaxial compression, (b) domains of open, mixed mode growth, sliding, Mode II growth, and kinking of microcracks under combined compression/ tension.

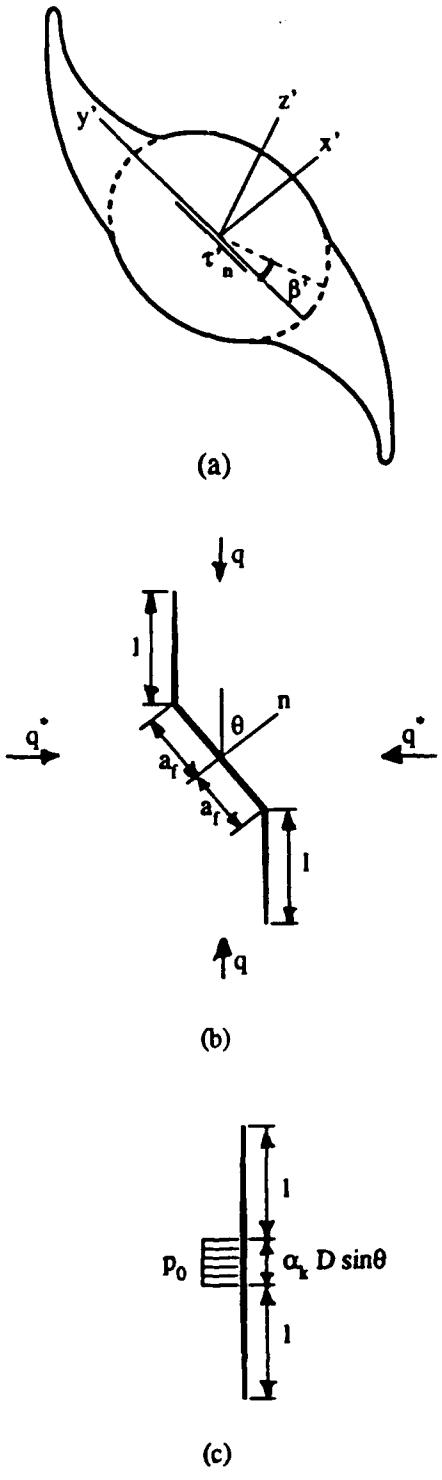

Figure 3. (a) 3-dimensional kinked microcrack, (b) 2-dimensional kinked microcrack, (c) approximate equivalent 2-dimensional microcrack ($D \equiv 2a_f$).

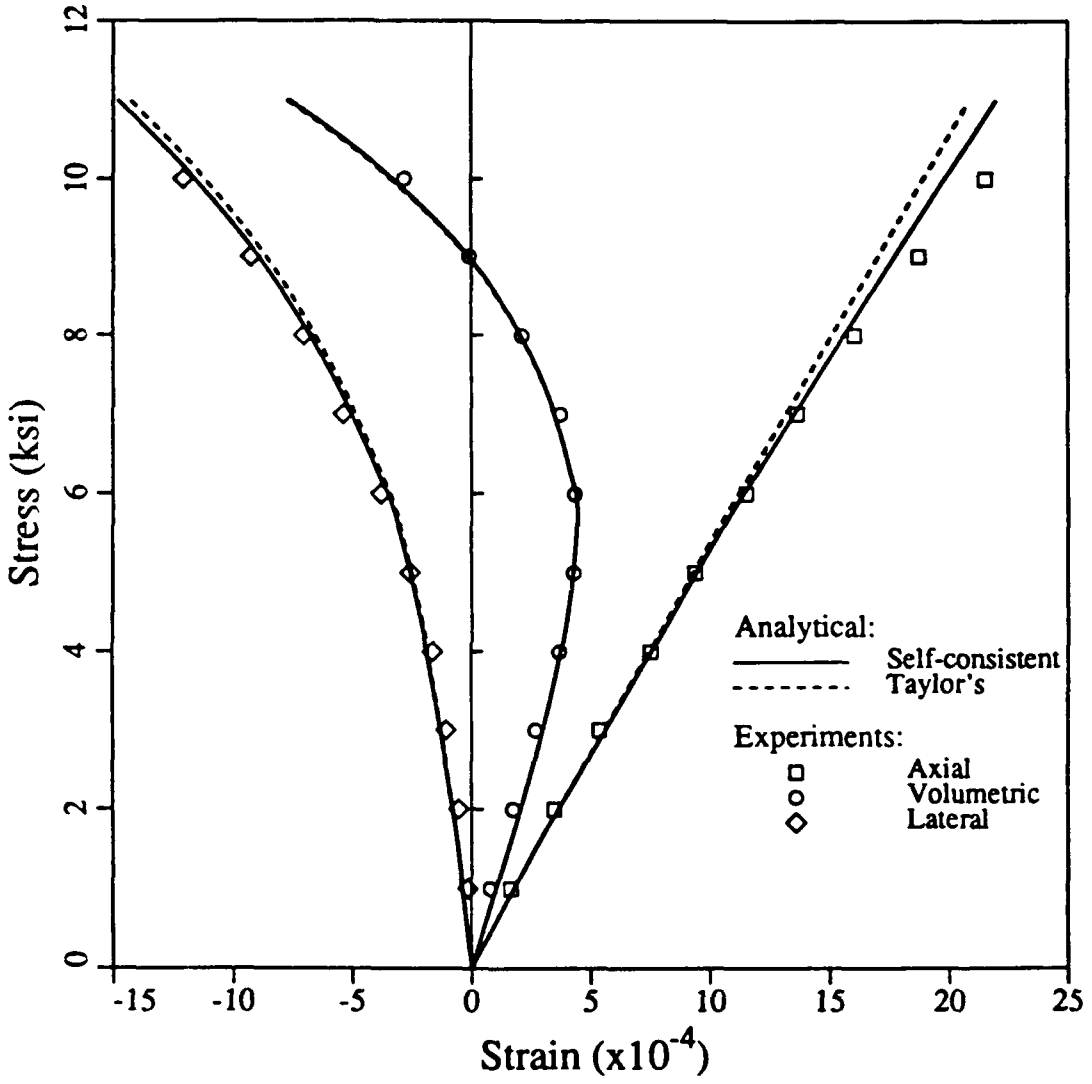

Figure 4. Comparison of the self-consistent, the Taylor's, and experimental stress-strain curves for a uniaxial compression test; $\omega_i = 10.3\%\omega_c$.

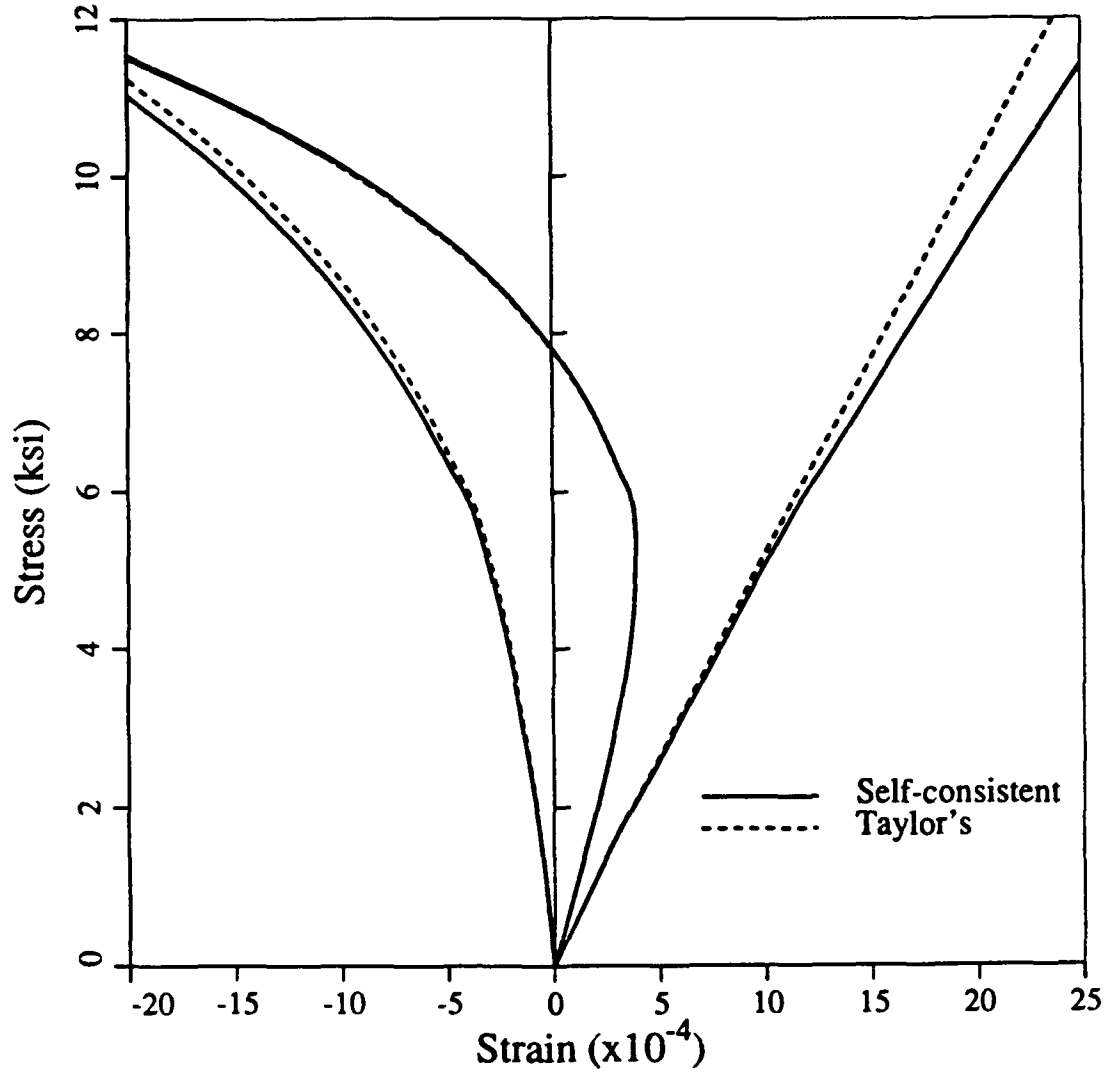

Figure 5. Comparison of the self-consistent and the Taylor's simulated stress-strain curves for a uniaxial compression test; $\omega_i = 14.7\%\omega_c$.

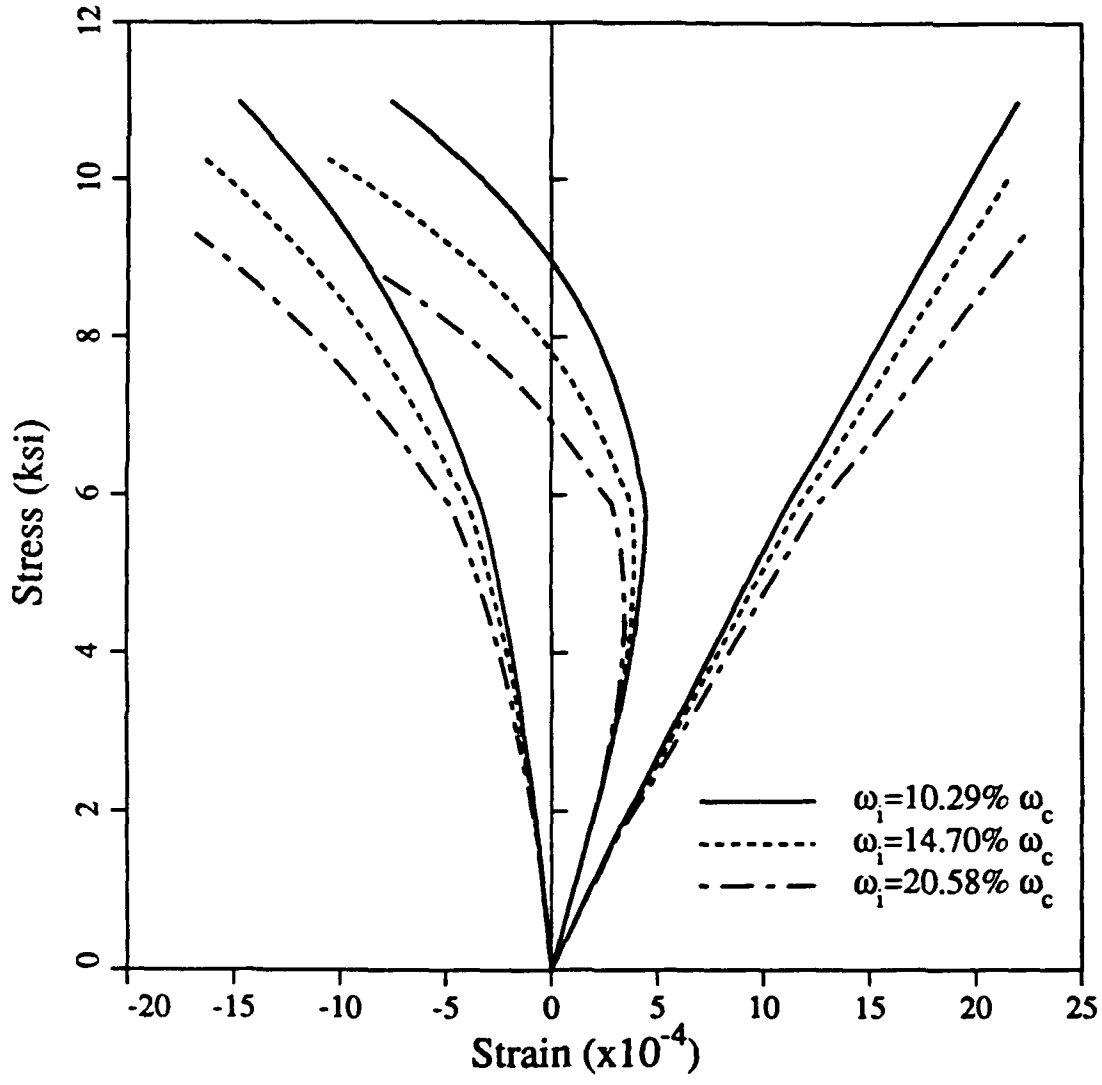

Figure 6. Three simulated stress-strain curves for uniaxial compression by using the self-consistent method.

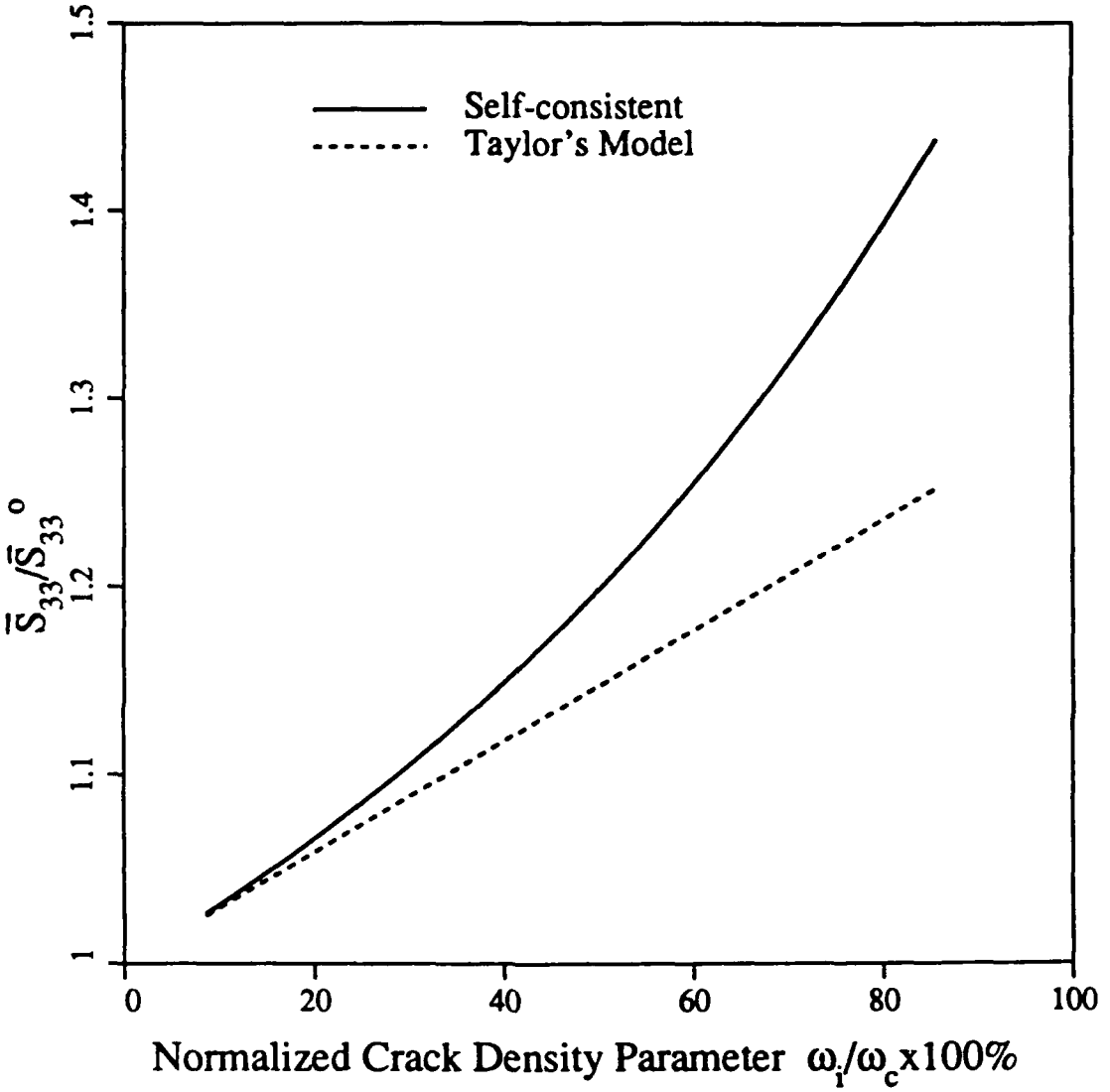

Figure 7. The normalized compliance $\bar{S}_{33}/\bar{S}^{o}_{33}$ vs. the normalized microcrack density parameter ω_i/ω_c.

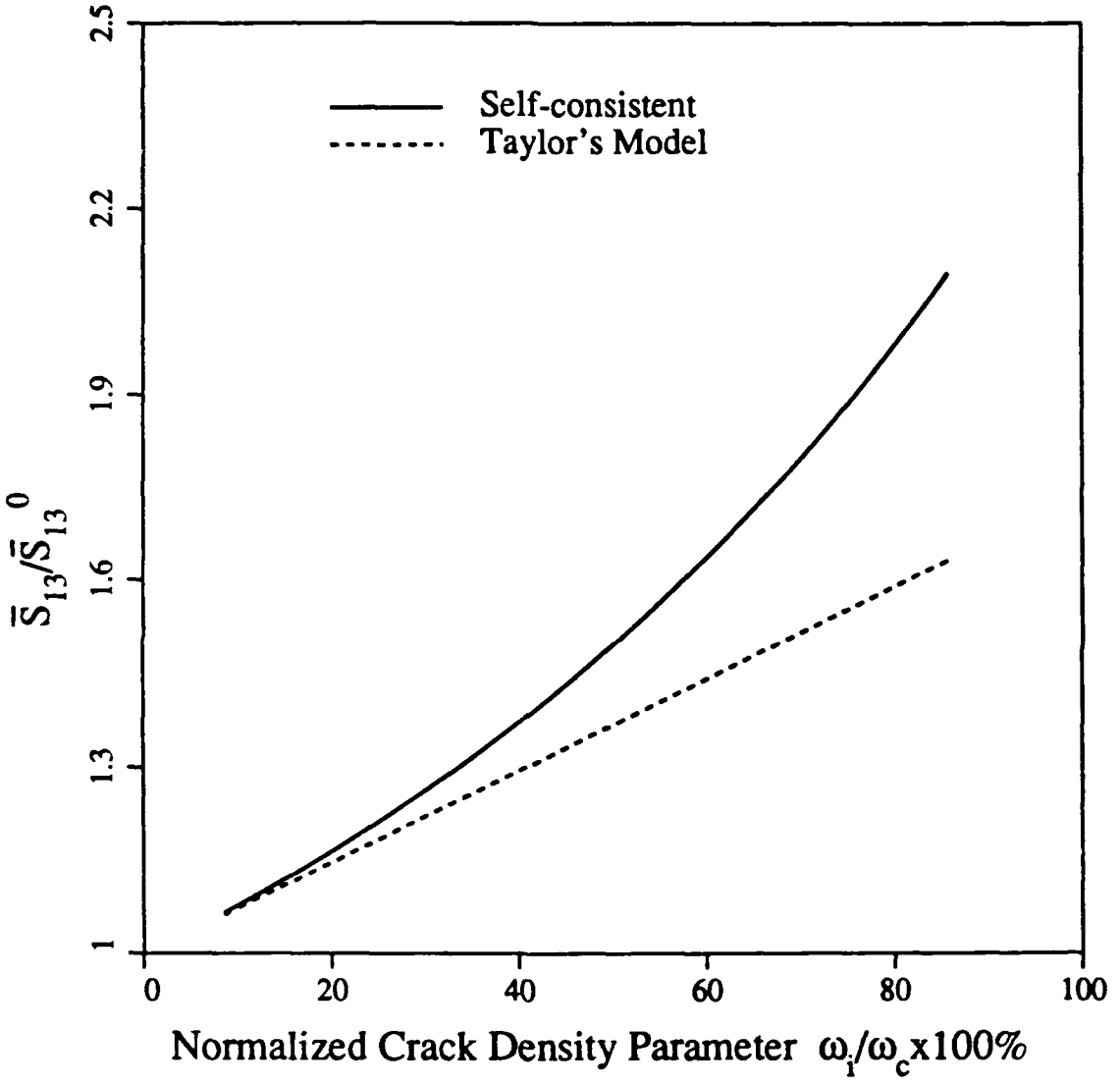

Figure 8. The normalized compliance $\bar{S}_{13}/\bar{S}_{13}^{o}$ vs. the normalized microcrack density parameter ω_i/ω_c.

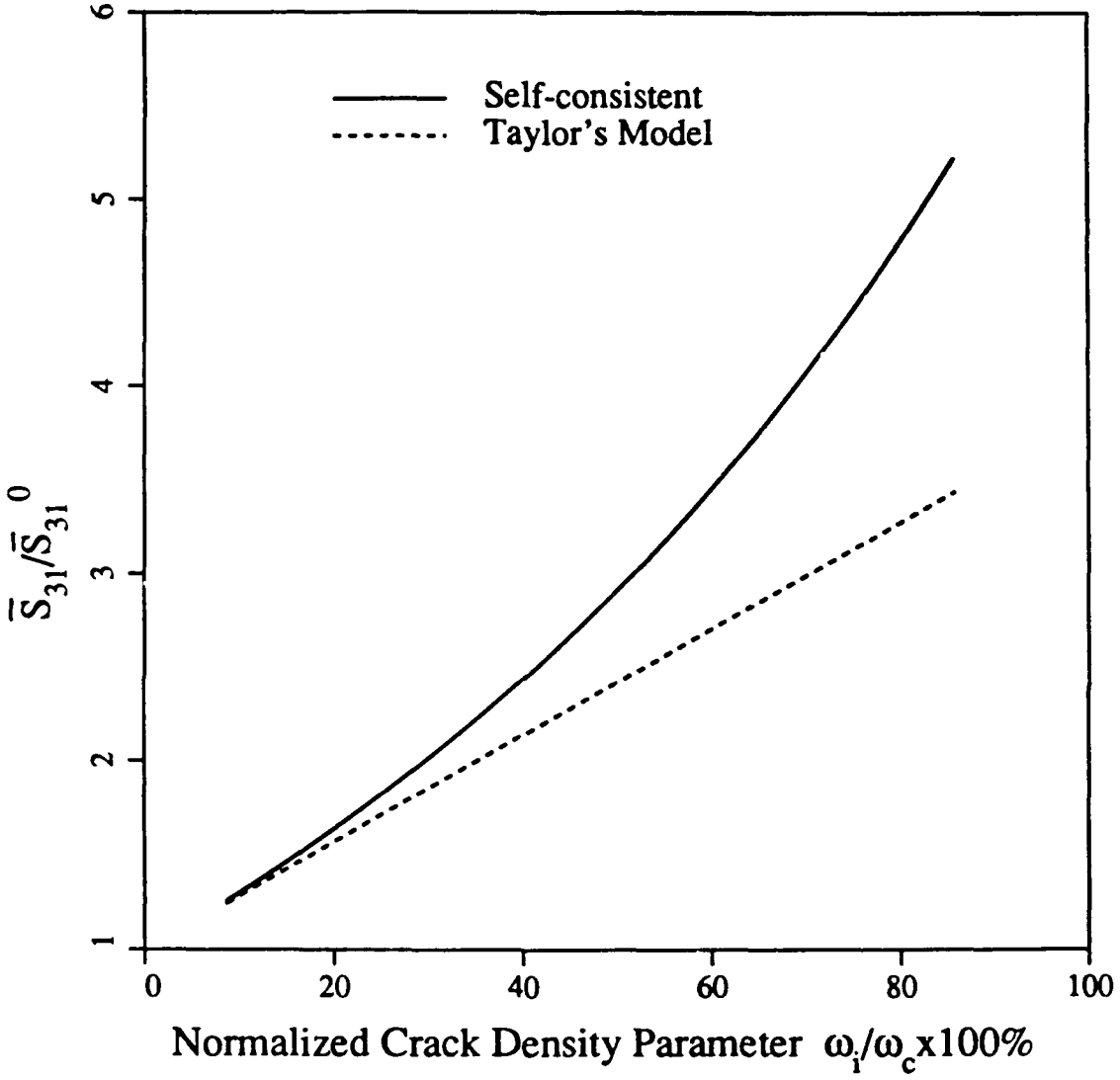

Figure 9. The normalized compliance $\bar{S}_{31}/\bar{S}^o_{31}$ vs. the normalized microcrack density parameter ω_i/ω_c.

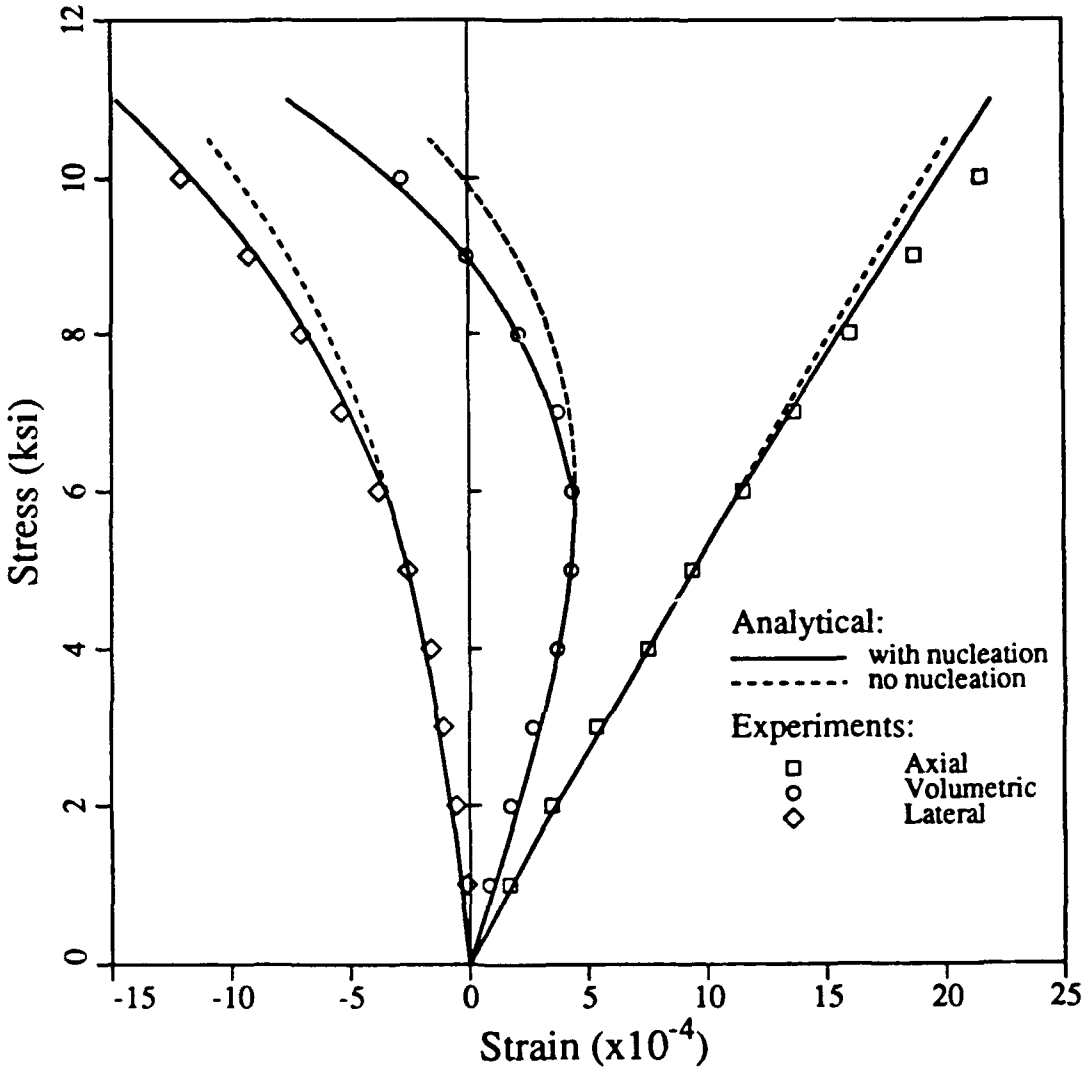

Figure 10. Comparison of simulated responses by using the self-consistent method with and without, respectively, the microcrack nucleation mechanism for a uniaxial compression test; $\omega_i = 10.3\%\omega_c$.

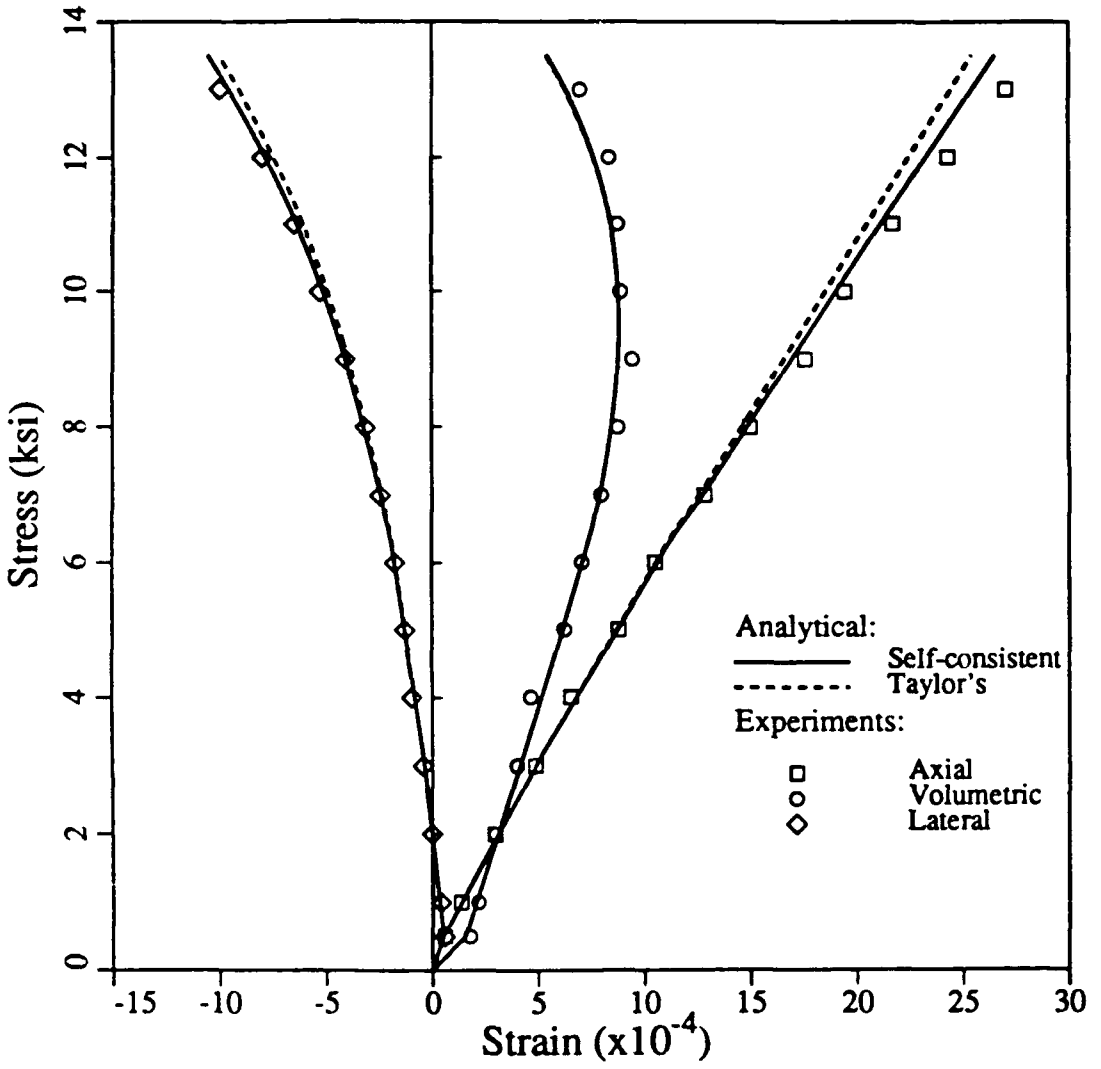

Figure 11. Comparison of the self-consistent, the Taylor's, and experimental stress-strain curves for a triaxial compression test; $\omega_i = 10.3\%\omega_c$; $q^* = -0.5$ ksi.

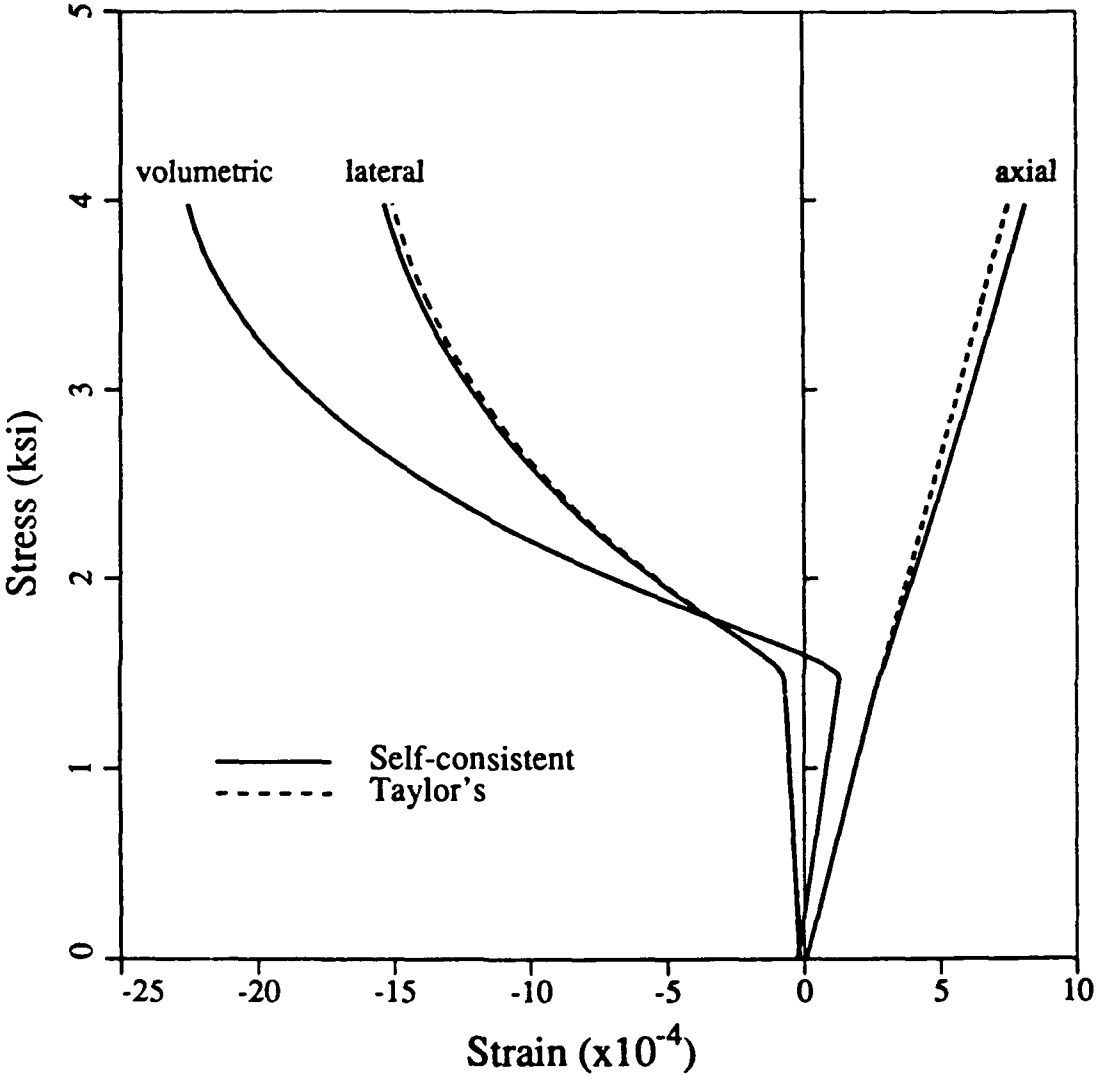

Figure 12. Comparison of the self-consistent and the Taylor's simulated stress-strain curves for axial compression with very small tensile lateral stress; $\omega_i = 10.3\%\omega_c$; $q^* = 0.1$ ksi.